CORROSION OF STEEL IN CONCRETE:

CEMENT MATRIX VARIABLES

by

GEORGE SERGI

A Thesis
Submitted for the Degree of
Doctor of Philosophy
of the
University of Aston in Birmingham

June 1986

THE UNIVERSITY OF ASTON IN BIRMINGHAM

"CORROSION OF STEEL IN CONCRETE: CEMENT MATRIX VARIABLES"

George SERGI Doctor of Philosophy 1986

SUMMARY

Properties of cements influencing chloride ingress or egress in concretes and the neutralization of the cement matrix were investigated. Electrochemical studies were then carried out on steel embedded in hardened cement pastes or concrete in order to relate such properties to the behaviour of steel reinforcement in concrete.

The behaviour of chloride in concrete and its effect on the corrosion of the embedded steel was thought to be strongly influenced by the presence and mobility of other ionic species in the pore electrolyte. Diffusion coefficients for a number of ions were, therefore, determined for a selection of cements by either a quasi-steady state technique or by the analysis of ionic concentration profiles in semi-infinite solids. The latter was achieved by extracting the pore liquid of cylindrical hardened cement pastes at increasing depths from the surface. This technique enabled also a more detailed study of ionic interrelation during diffusion. An activation energy for the diffusion process of OH^- in an OPC was also obtained.

The effect of carbonation on the pore solution chemistry of hardened portland cement paste was studied. Ionic diffusion characteristics in such cement pastes were also investigated.

Powdered samples of a selection of hardened cement pastes were systematically neutralized by the addition of nitric acid, in order to observe pH arrests associated with different hydration phases and study buffering characteristics.

The electrochemical studies carried out were of two types. Firstly, anodic potentiostatic polarization scans were used to investigate the pitting behaviour of iron embedded in a selection of cement pastes with a specifically controlled pore electrolyte.

Secondly, corrosion intensities of steel embedded in carbonated concrete during wet/dry cycles were monitored by the techniques of linear polarization and a.c. impedance.

KEY WORDS cements, chlorides, diffusion, corrosion, carbonation

To my daughter Elena Christina

ACKNOWLEDGEMENTS

I am deeply indebted to Dr. C.L. Page, my supervisor over the whole period of the research. His knowledge, expertise and guidance were invaluable.

I am grateful also to the Building Research Establishment for the provision of funds for the research; in particular to Mr. K.W.J. Treadaway who also acted as my external supervisor. I appreciate his helpful comments.

I wish to thank Dr. K. Starzewski for arranging joint funds with the BRE for my visit to the Instituto Eduardo Torroja in Madrid. Dr. Mª Carmen Andrade and Miss Mª Cruz Alonso of the institute were particularly helpful to me in the areas of carbonation and corrosion monitoring for which I am very grateful.

I am grateful also to Mr. C.J. Thompson for his generous help and advice throughout the period and to Dr P. Lambert for his valuable expertise on graph drawing.

I appreciate also the work carried out by Mr. S.A. Mbogo on the corrosion monitoring of steel in carbonated concrete.

Also I wish to thank my friend Mr. M. Maleki for our many stimulating discussions.

I remain indebted to Dr. D.J. Arrowsmith who has taught me most of what I know on corrosion and encouraged me in my early student days.

To my sisters and all my other relatives and friends who stood by me and encouraged me at difficult times, and to my parents in-law a very special thankyou for their support.

I will always remain deeply indebted to my parents for their love and understanding throughout my life and for their encouragement and financial support during my student years.

Finally, but more importantly, I am eternally grateful to my darling wife Chrys for her immaculate typing, but above all her love, understanding, support, and encouragement, without which this work would not have been completed.

LIST OF CONTENTS

LIST OF FIGURES

Figures in appendices

LIST OF TABLES

Table no.

CHAPTER 1 INTRODUCTION

The value of embedding steel bars in concrete to form reinforced concrete was realised during the second half of the nineteenth century and as its properties began to be appreciated, application of the composite material grew rapidly.

Since the start of this century reinforced concrete has been used extensively for a variety of building and civil engineering work, thus becoming the most versatile constructional material available.

Concrete and steel complement each other. The resistance to compression of well-mixed and hardened concrete combines well with the tensile strength of steel. Furthermore concrete offers good physical and chemical protection to the steel reinforcement. The chemical protection is provided by the highly alkaline environment of the hydrated cement matrix which induces the formation of a thin continuous passive ferric oxide film on the surface of the steel.

Aided by such a protection mechanism the performance of reinforced concrete in relation to durability and need for maintainance is generally good [1]. There are still, however, a few examples of early deterioration mainly caused by reinforcement corrosion [2]. Bursting forces owing to the expansive nature of the corrosion products lead to cracking of the concrete cover, rust staining and subsequently to spalling [3]. Maintainance can be very expen-

sive but lack of it could lead to structural weakening and possibly to failure [4].

There are two common ways of steel reinforcement depassivation viz, the loss of alkalinity in the pore solution and the attack of the steel by aggressive ions. Loss of alkalinity is the result of a reaction between the basic cement components and acidic gases in the atmosphere [5], or in rarer cases, by the leaching of hydroxyl ions from the cement matrix [6]. Once neutralization occurs, provided the electrolyte around the steel is maintained by moisture, corrosion of the reinforcement is possible [7] because the passive film is no longer stable.

The most aggressive ion with regards to steel reinforcement corrosion is the chloride. When present in sufficient quantities in the pore solution, it destroys the passive film, often causing severe localised corrosion in the form of pits [8]. A combination of both depassivating methods can be very dangerous as the level of chloride required to cause corrosion decreases with decreasing pH [9].

A thick depth of cover and a good compact concrete should achieve sufficient protection against corrosion as the environmentally affected zone may never reach the steel. Controls in this country with regards to the introduction of chlorides at the mixing stage [10] -compatible with economy in the use of indigenous materials - have reduced the

risk of such contamination considerably.

It is mainly for instances where an adequate depth of cover is difficult to achieve owing to design considerations, particularly where high outside chloride levels are expected as for bridge decks and offshore structures, or in cases where low levels of chloride in concreting materials have to be accepted for economic reasons, that improved ways of protection are desirable.

Alternative ways of protection have been looked at extensively by researchers. Coating the steel with epoxy resin [11] or zinc [12,13], or applying an extra physical barrier by impregnating the concrete with polymer [14-16] are ideas put forward and to some extent tested. Not enough supporting evidence has been produced however. Research into the use of zinc coated steel reinforcement bars has, for instance, shown conflicting results [17]. Recent published work by the author [18] and other researchers [19] have provided some evidence against such a treatment. Added costs make most of these methods of protection even less attractive. The only real alternative must be to achieve protection by exploiting to the full useful properties offered by the cement. To accomplish such a goal, these properties must first be fully understood.

1.1 PROPERTIES OF CEMENTS

A portland cement consists basically of the following com-

pounds.

$3CaO.SiO_2$	(C_3S)*
$2CaO.SiO_2$	(C_2S)
$3CaO.Al_2O_3$	(C_3A)
$4CaO.Al_2O_3.Fe_2O_3$	(C_4AF)
$CaSO_4.2H_2O$	Gypsum

When water is added to the cement, several complicated reactions are initiated which finally lead to the formation of a hardened mass. The calcium silicates are the most important constituents, forming the strength bearing calcium silicate hydrate gel (an amorphous mass) and $Ca(OH)_2$. Diamond [20] estimated that the C-S-H gel forms 70% (by weight) of the fully hydrated cement paste and $Ca(OH)_2$ about 20%. Other phases produced by the remaining compounds are calcium aluminate trisulphate hydrate (ettringite) and calcium aluminate monosulphate.hydrate (about 7% in total); tricalcium aluminate hydrate, unhydrated clinker residue and other minor constituents making up the remainder.

Sodium and potassium sulphates present in the cement react to form mainly ettringite causing the release of the alkali ions into the pore solution. It is the balancing of these

---

* Cement Chemist's Shorthand notations.
ie $CaO=C$, $SiO_2=S$, $H_2O=H$.

cations in solution by hydroxyl ions that enables high pH values to be reached. The composition of the pore solution of cement pastes has been shown to be practically concentrated sodium and potassium hydroxides the concentration increasing with hydration time as the alkalies are continually liberated [21,22].

The C_3A phase is the other important constituent with regards to corrosion properties. It can react with free chloride in the water forming tricalcium chloroaluminate hydrate a complex insoluble salt, thus removing the aggressive ionic species from the pore solution.

There are however special cases where low C_3A content cements are preferred because of their resistance to sulphate attack. When sulphate ions penetrate the structure they react with the C_3A in the same way as the chlorides to form expansive calcium sulphoaluminates thus increasing the risk of cracking [23]. Sulphate resisting portland cements (SRPC) as they are known, may therefore offer less protection to the steel reinforcement in the presence of chloride ions, as their chloride complexing capacity is lower [24].

There are suspicions that carbonation (the neutralization of concrete by CO_2 in the atmosphere) may cause the release of the bound chloride back into the pore solution as the calcium chloroaluminate phase is unstable in the pre-

sence of carbonic acid [25]. The complications would then be that an apparently low risk of chloride attack, is greatly increase, especially as the hydroxyl concentration is lowered. A high $[Cl^-]/[OH^-]$ ratio in the pore solution is considered detrimental for obvious reasons [9].

According to Page [26] a layer of portlandite ($Ca(OH)_2$) is formed on the surface of steel cast in portland cement paste which may *act both as a physical barrier to chloride* penetration and as a hydroxyl ion replenisher at potential corrosion sites. The amount of $Ca(OH)_2$ produced during hydration may, therefore, have a direct bearing on the ability of the cement to provide such protective characteristics.

There are special cements that owing to their pozzolanic nature do not allow very much $Ca(OH)_2$ to remain as free in the hydrated cement matrix [27] thus minimising the above-mentioned protection offered to steel. A counter effect may however be achieved in pozzolanas where the diffusion of ions, like chlorides, from an outside source is often much slower than in most ordinary cements [28], so that the critical chloride level for corrosion to take place could take longer to be reached.

In summarising, the main properties of the cement that appear to influence corrosion of steel are, the ability of the cement,

(i) to delay or prevent the penetration of

chloride ions from an outside source,

(ii) to complex and hence remove from the pore solution chloride ions, a property mainly related to the C_3A content,

(iii) to produce $Ca(OH)_2$ or similar phases which can act both as a buffer and maintain the pH of the pore solution to high values and as a protective barrier round the steel,

(iv) to delay acidic gases such as CO_2 from entering the pores and neutralizing the cement matrix, or delay the neutralization process itself.

Such properties were investigated for a selection of cements and were related to the corrosion of the steel reinforcement in order to improve the knowledge and understanding of the corrosion processes involved in concrete construction. This thesis reports on the findings of the investigation.

1.2 PLAN OF PRESENTATION

The thesis is divided into seven chapters. Following the introduction (chapter 1), chapter 2 describes the materials, specimen preparation and experimental techniques used throughout the investigation. The experimental work is contained in the next four chapters (3 to 6). Each experimental chapter starts with a general introduction of the topic

which is divided into two interrelated but separate and self-containing parts. In each part an introduction and, where applicable a review of the relevant literature precedes the experimental procedure which in turn is followed by the results and discussion. At the end of each part there is a summary of the results and conclusions.

Finally chapter 7 contains the general discussion and conclusions drawn from the whole investigation followed by suggestions for future work aimed at generating new research.

More specifically, chapters 3 and 4 look at the cement properties of ionic diffusion and chloride complexation which relate mainly to chloride induced corrosion. In chapter 3 diffusion of hydroxyl and chloride ions in cement pastes is studied making use of two alternative techniques for the determination of effective diffusion coefficient values for a selection of cements.

Results of chapter 3, suggesting an interrelation of diffusing ions, prompted the work which is reported in chapter 4. Novel techniques were developed in this case to study the apparently complex diffusion mechanism and to develop the diffusion theory.

Chapter 5 is concerned mainly with the other main depassivating mechanism of steel reinforcement, that induced by carbonation. Results obtained from pore solution and other analyses of carbonated OPC pastes are related to the corrosion

of steel reinforcement. In part II of this chapter, a more systematic neutralization process is described, used mainly to study the property of buffering for a number of cements.

Chapter 6 attempts to relate the properties studied in the previous chapters to results obtained from electrochemical studies; namely "pitting" experiments applied to steel wires embedded in well-characterised cement pastes and corrosion measurements applied to steel reinforcement embedded in carbonated concrete specimens obtained from an existing building.

CHAPTER 2 MATERIALS AND EXPERIMENTAL TECHNIQUES

In this chapter the materials used, the preparation of specimens, and the subsequent experimental techniques used for investigation are described in some detail.

2.1 MATERIALS

In order for the results to be comparable to work previously carried out on chloride diffusivities in cement pastes, the five cements used in the present work, were those originally used by Page et al [28] and Holden et al [9] and were kept in air-tight bins until needed. There were two varieties of Portland Cement (OPC-A and OPC-B) two cements with OPC-B substituted by either 65% by weight Blast Furnace Slag (BFS) or 30% Pulverised Fuel Ash (PFA) and a Sulphate Resisting Portland Cement (SRPC). Their oxide and Bogue compositions are shown in table 2.1.

When the original batch of OPC-B had been exhausted, it was replaced by a new one of a similar composition denoted by OPC-B'. This was used for specimens prepared for the work described in chapters 4 (part II), 5 and 6 (part I).

2.1.1 Sulphate-Resisting Portland Cements

As mentioned in the introduction, when sulphates penetrate a cement from an outside source, they react with the calcium aluminates present in the cement, to form fresh expansive calcium sulphoaluminates. The resultant expansion can cause

TABLE 2.1a Chemical Analysis of Cements and Blending Agents.

MATERIAL	CaO	SiO_2	Al_2O_3	Fe_2O_3	SO_3	MgO	Na_2O	K_2O	IGNITION LOSS
OPC-A	62.8	20.8	5.1	3.4	2.9	1.3	—	0.96	1.6
OPC-B	63.0	20.3	7.1	2.7	3.3	1.3	0.47	0.60	0.8
OPC-B'	63.4	20.2	7.3	2.3	3.1	1.2	0.40	0.50	0.9
SRPC	64.0	20.2	4.1	5.3	2.6	1.4	0.28	0.39	1.1
PFA	2.9	46.6	24.0	9.5	0.9	2.1	2.00	3.80	3.3
BFS	42.4	33.3	10.8	0.3	-	8.7	0.37	0.50	-

TABLE 2.1b Bogue Oxide Compositions of Cements.

CEMENT	C_3S	C_2S	C_3A	C_4AF
OPC-B	41.3	27.0	14.2	8.2
OPC-B'	43.4	25.2	15.5	7.0
OPC-A	50.2	21.7	7.8	10.4
SRPC	64.5	9.3	1.9	16.1

the gradual disintegration of the structure. To resist such an attack, it is necessary to formulate a cement with a low C_3A content; such cements are called sulphate-resisting portland cements.

It is important to know to what extent, the low C_3A contents of this cement could affect the ability of the cement to protect the steel reinforcement.

2.1.2 Pulverised Fuel Ash

Pulverised Fuel ash is ash precipitated electrostatically from exhaust fumes of coal-fired power stations and is the most common artificial pozzolana.

A pozzolana is a natural or artificial material, containing silica in a reactive form. The ASTM specification C618-78 describes it as "a siliceous or siliceous and aluminous material which in itself possesses little or no cementitious value but will, in finely divided form and in the presence of moisture, chemically react with calcium hydroxide at ordinary temperatures to form components possessing cementitious properties".

Pozzolanas, such as PFA, are mixed with portland cements which provide the necessary $Ca(OH)_2$ as it liberates during hydration. Their ability to combine with and remove the $Ca(OH)_2$ improves the cement's ability to resist chemical attack caused by reactions with $Ca(OH)_2$. On the other hand

as will be discussed in chapter 5 and 6, such a removal of $Ca(OH)_2$ may be detrimental to the structure's ability to protect steel reinforcement.

2.1.3 Blast Furnace Slag

Blast furnace slag is a waste product obtained in the manufacture of pig-iron in the blast furnace. It is formed by the combination of the iron ore with the limestone flux and has essentially the same main oxides as a portland cement, namely lime, silica and alumina, but in different proportions.

Ground granulated slag is either mixed with a suitable proportion of limestone, which can then be used as a raw material for the manufacture of portland cement, or straight with a portland cement. On hydration, as happens with pozzolanas, BFS removes the $Ca(OH)_2$ formed. High BFS content cements often have no free $Ca(OH)_2$ left after complete hydration [29] possibly leading to a diminished protection of the steel reinforcement.

2.2 PREPARATION OF MATERIALS

All materials were sieved through a 150μm mesh in order to produce a consistent fineness of powder. Each individual cement was then weigh ed and if required, mixed with the right proportion of BFS or PFA, before the correct amount of deionised water was added to produce a 0.5 w/c (water to ce-

ment ratio) paste. If NaCl was to be included in the mix, this was dissolved in the water prior to the addition.

The mixture was then mixed thoroughly by hand for 5 minutes with a wooden rod. It was then poured into cylindrical PVC containers, 49mm diameter by 75mm in height, which were vibrated for a further 4 minutes on a vibrating table for better compactness.

On at least two occasions, the "foamy" layer that had accumulated on the surface was removed and replaced by fresh cement paste. A polythene sheet was then placed on top of each of the containers, to prevent the entrapment of air by the cap which was subsequently fitted on top.

The cylinders were then rotated top to bottom at a speed of 8rpm for 24 hours, in order to minimise segregation and enable the production of uniform cement pastes. The specimens were finally stored in a high humidity store room at 22°C for the required time before demoulding.

If discs were required, the cement pastes were cut using the Cambridge micro-slice-2 which is an accurate diamond wheel saw, working on the principle of a carefully counterbalanced "see-saw". Deionised water was used a a lubricant. The discs were then lightly ground on 600 grade carbide paper and stored as required for their specific applications (see individual chapters).

2.3 EXPRESSION OF PORE SOLUTIONS

A development by Longuet et al [21] who had pressed water from 300 gramme specimens of hardened cement paste, the pore solution expression device is perhaps the most important item used in this investigation. Its ability to remove capillary pore solutions by pressure has facilitated the accurate and easy determinations of levels of ionic constituents in pastes, mortars and concretes.

It is a purpose-built pressure vessel, consisting of four main sections, as shown in figure 2.1. After assembly the specimen, in the form of either a hardened cement paste cylinder or, in most cases in the present work, as a series of cement paste discs piled together, was positioned on the platten, encased by the die body. A slowly increasing pressure was then applied on the piston, reaching a maximum of 375 Mpa and the PTFE disc inserted between the specimen and the piston, spread to seal the whole diameter of the die body, preventing liquid from escaping other than through the fluid drain via a circular groove on the platten. The solution was then drawn into a syringe through a drain hole lined with PTFE and stored in sealed plastic vials to prevent unnecessary exposure to air.

The separate parts of the press were thoroughly cleaned with water and acetone and the connecting surfaces were sprayed with a PTFE non-stick spray for lubrication and protection ready for the next specimen.

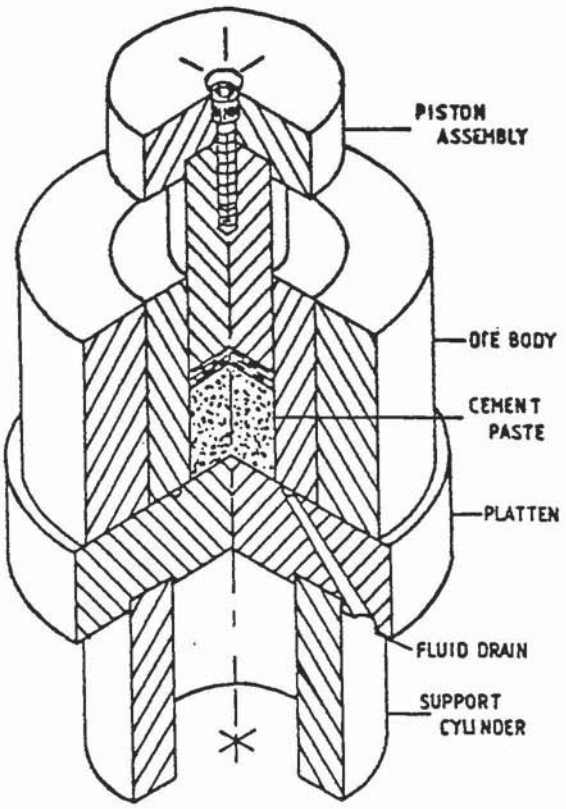

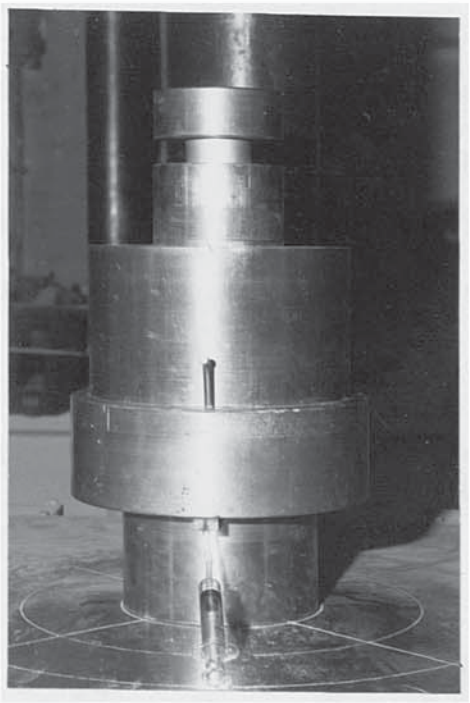

FIGURE 2.1 The Pore Solution Expression Device.

Normally 2-3ml of solution was extracted from the paste. It is shown in chapter 6 that the "squeezed" liquid is a true representative of the solution in the pores.

2.4 SOLUTION ANALYSIS

In most cases 100 microlitre aliquots taken with a standard micropipette were sufficient for the analysis of most ions ie OH^-, Cl^-, Na^+ and K^+ using standard methods. On occasions where the concentrations were very small and where the amount of solution permitted it, larger aliquots of up to 10ml were taken for analysis. In such cases the methods will be described in the appropriate chapters. On all occeasions at least duplicate tests were performed and an average taken.

2.4.1 Hydroxyl Ion

The 100µl aliquots made up to 1ml with deionised water, were titrated using a standard 0.01 or 0.001 molar nitric acid solution with phenolphthalein as the indicator. The acid was dispensed from a 10µl graduated microburette.

If the pH of the solution was required, it was calculated from the hydroxyl concentration as follows:

$$pH = -\text{Log}_{10}\ (H^+)$$

$$pOH = -\text{Log}_{10}\ (OH^-)$$

$$pH+pOH = 14$$

$$pH = 14 + \text{Log}_{10}(OH^-)$$

(After Sorensen)

2.4.2 pH METER

Where the pH value of the solution was about 10 or less, a Pye Unicam pH electrode in conjunction with a Philips digital pH meter was used instead of titration. It was necessary to calibrate the pH meter with buffers at pH 4, 7 and 9. This method of determination gives results, at intermediate values, accurate to within 0.01 of a pH unit.

2.4.3 CHLORIDE ION

Chloride ions displace thiocyanate ions which, in the presence of iron (III) ions form a highly coloured complex.

$$2Cl^- + Hg(SCN)_2 + 2Fe^{3+} \longrightarrow HgCl_2 + 2Fe(SCN)^{2+} \quad \text{(ref. 30)}$$

As the intensity of the colour is related to the original chloride ion concentration, this can be determined on a spectrophotometer which measures the absorption of light at a specific wavelength. Such a technique was used for the present investigation in order to determine chloride concentrations of the solutions, by employing a Beckman model-24 spectrophotometer.

An addition of 9.9ml of deionised water was made to each 0.1ml aliquot of solution, into which 2ml of 0.25 molar ferric ammonium sulphate ($Fe(NH_4)(SO_4)_2.12H_2O$) in 9 molar nitric acid, and 2ml of saturated mercuric thiocyanate in ethanol were added.

Two glass cells, one containing the coloured solution and

the other water, were placed next to each other in a special enclosure inside the spectrophotometer. A beam of light was passed through the cells, whose wavelength was selected by a prism (460nm for this analysis) onto a photoelectric device. The difference in absorption between the two cells was an indication of the amount of chloride as stated by the Beer-Lambert law:

$$It = I_o.10^{-ect}$$

where:

It = intensity of transmitted light

I_o = intensity of incident light

e = molecular extinction coefficient

c = concentration of solution

t = thickness of solution

The intensity of a beam of monochromatic light is thus related to the concentration of the absorbing substance it passes through (31).

Chloride concentrations were estimated from a calibration curve constructed by plotting a curve of concentration of standard chloride solutions against absorption (appendix 1).

2.4.4 SODIUM AND POTASSIUM IONS

Analysis of sodium and potassium ions was made using a Flame photometer. After the solutions were diluted by 500 or by 1000 in deionised water, depending on the expected concen-

tration, the solution was drawn through a thin tube into the flame photometer which atomised and sprayed the liquid over a flame.

When an ionic species is burned in a flame, it glows transmitting a light of a specific set of wavelengths.

A filter placed in front of the flame, which allowed only light of the required wavelength to pass through, enabled the estimation of the concentration of each ionic species by relating the intensity of the light to the ionic concentration.

2.4.5 CALCIUM IONS

The analysis of solutions for Ca^{++} ions was performed on a "Corning" calcium analyser (model 940). This is a fluorometer which measures the emitted fluorescence of excited molecules. Excitation is achieved by the addition of "calcein" to the solution, an indicator which forms an intensely fluorescent nondissociated complex with Ca^{++} ions in an alkaline medium. The analytical procedure incorporated in the instrument is based on the quenching of this fluorescence by chelating the Ca^{++} ions with the titrant EGTA (Ethylene glycol bis(β-aminoethyl ether) N,N'-tetra-acetic acid).

A 50µl aliquot of the solution to be analysed was added to a cuvette which was partly filled with 1M KOH and contained 1ml of the indicator. At the end of the titration the Ca^{++}

concentration was displayed in mM/litre on a digital meter. Calibration was achieved by titrating a calcium standard solution.

2.5 EVAPORABLE AND NON EVAPORABLE WATER

Ionic species can be expressed as free amounts present in the pore solution or as total present in the paste as a fraction of the unhydrated cement. In order for this to be possible it is necessary to determine the bound and free amounts of water present in the cement.

Various methods have been employed for the evaluation of the two types of water[32] but the di stinction between free and bound water is always somewhat arbitrary.

The method adopted in this work assumes that the water driven off at 105°C is mainly the evaporable or free water and that the remaining non-evaporable or bound water is lost at ignition of the cement at 950°C. It is inevitable that there must be some degree of overlap but the results obtained suggest a reasonable accuracy.

About 2 grammes of hydrated cement, broken into small fragments, was weigh ed in a platinum crucible immediately after crushing. It was then heated in an oven at 105°C until a steady weight was obtained. Finally the cement was ignited for 30 minutes at 950°C and the final weight recorded.

At 950°C the cement also loses some mass termed the ignition

loss, which has to be determined. This was done by following the method given in British Standards [33]. About 1 gramme of unhydrated cement was weigh ed in a platinum crucible before and after heating for 30 minutes at 950°C. The lost mass was converted into a percentage "loss-on-ignition".

The amounts of evaporable and non-evaporable water were then calculated in grammes of water per gramme of unhydrated cement after correction for ignition loss, and for admixtures, as was the case when NaCl was added in the mix, by the following equations:

$$E.W(\%) = \frac{W_0 - W_{105}}{W_{950}} \times (100-i+a)$$

$$N.E.W(\%) = \frac{W_{105}\,(100-i+a) - W_{950}(100+a)}{W_{950}}$$

(After Lambert)

where

E.W. = evaporable water (% gms/gm of cement)

N.E.W. = non-evaporable water (% gms/gm of cement)

W_0 = weight of hydrated cement (gms)

W_{105} = weight at 105°C (gms)

W_{950} = weight at 950°C (gms)

i = loss-on-ignition (% gms/gm of cements)

a = total admixtures (% gms/gm of cement).

The derivations of the formulae and a worked example are given in Appendix 2.

2.6 CARBON DIOXIDE

Cements which were carbonated, when heated to 950°C had lost not only their water but also the bound CO_2 from the breakdown of the carbonate phases. It was therefore necessary to determine the amount of CO_2 released at ignition, firstly in order to calculate the free and bound water and secondly to determine the degree of carbonation of the cement.

A small amount of the hydrated cement was ground to powder using a pestle and mortar, passed through a 150μm sieve and heated to 105°C until a constant weight was obtained. The sample was then placed in a lightweight tin container and dropped into a vertical quartz tube of an Elemental Analyser (model 1106) maintained at 1030°C, through which a constant flow of helium was run. The helium stream was temporarily enriched with pure oxygen after which flash combustion took place, primed by the oxidation of the container.

Quantitative combustion was then achieved by passing the mixture of gases over Cr_2O_3. The mixture of combustion gases then passed over copper at 650°C to remove the excess of oxygen. The individual components were then separated and eluted as CO_2-H_2O. They were measured by a thermal conductivity detector, whose signal fed a potentiometric recorder. Calibration of the instrument was achieved by combustion of standard compounds. The amount of CO_2 was then subtracted from the total weight loss at 950°C to enable the calculation of the bound and free water.

2.7 TOTAL CHLORIDE

When cement pastes contained chlorides, it was necessary to determine their total amounts of chloride. This was achieved by a method similar to that used by Lambert [34] which is a development of Berman's technique [35].

A small amount of the cement paste was ground to a powder in a pestle and mortar and passed through a 150μm sieve. One gramme of the powder was then placed in a glass vessell and dried to 105°C prior to an addition of 10ml off deionised water. The mixture was thoroughly shaken to "wet" all the cement powder and attached to a condenser needed to avoid evaporation of the solution. Three millilitres of concentrated nitric acid were then added from the top of the condenser and the mixture was placed over a flame to encourage the dissolution of all the chloride by the acid (fig 2.2).

Once the solution had cooled and settled leaving a clear solution on top, a 100μl aliquot was withdrawn and analysed for chloride as described in section 2.4.3. The total chloride was then calculated as follows:

$$\text{Total Chloride } (\text{mM } Cl^-/\text{g cem.}) = \frac{\text{Conc. of } Cl^- \text{ in solution (mM/litre)} \times 113}{\text{Weight of sample at 950°C (g)} \times 1000}$$

The weight of the sample at 105°C needed to be corrected to that at 950°C by means of the evaporable and non-evaporable water data, as shown in section 2.5. A worked example is

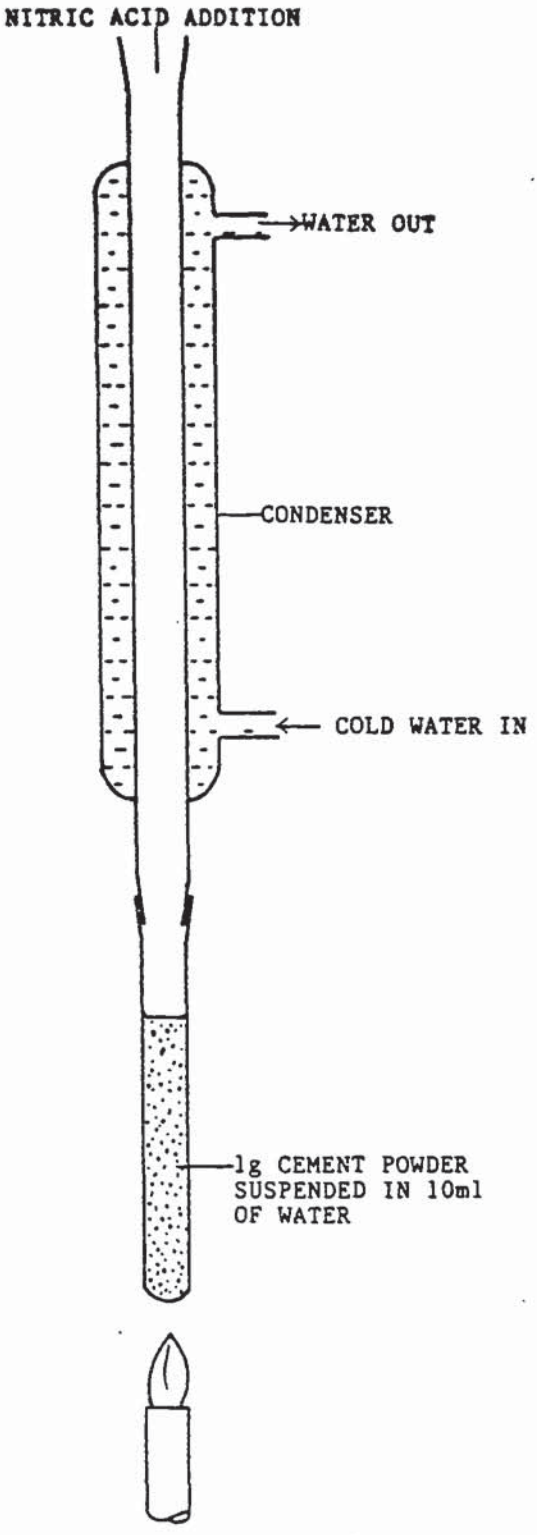

FIGURE 2.2 Apparatus set-up for the determination of total chloride in cement pastes.

shown in Appendix 3.

2.8 IDENTIFICATION OF CEMENT PHASES

Two main techniques used extensively by cement chemists, were adopted for the identification of the different phases present in cements, viz, the Differential thermal analyser and the X-Ray Diffraction techniques.

2.8.1 DIFFERENTIAL THERMAL ANALYSIS

The Differential Thermal Analyser (DTA) consists of two small Rhodium-Platinum crucibles, situated over two thermocouples inside a furnace (see figure 2.3). A small amount of powdered cement, dried in a desiccator, is placed in the one crucible and an equal amount of calcined alumina, acting as an inert reference, in the other. Both are heated at a slow rate of 20°C per minute up to a maximum of 950°C. If there is no thermal change in the cement, its temperature would be the same as that of the alumina so the temperature difference would be zero. If there is a thermal change, either an absorption or evolution of heat, the temperature of the sample would become higher or lower than that of the reference and this can be plotted on a chart recorder as temperature of the furnace against the differential temperature.

In cements the dehydration of the various phases is normally accompanied by characteristic endothermic reactions at spe-

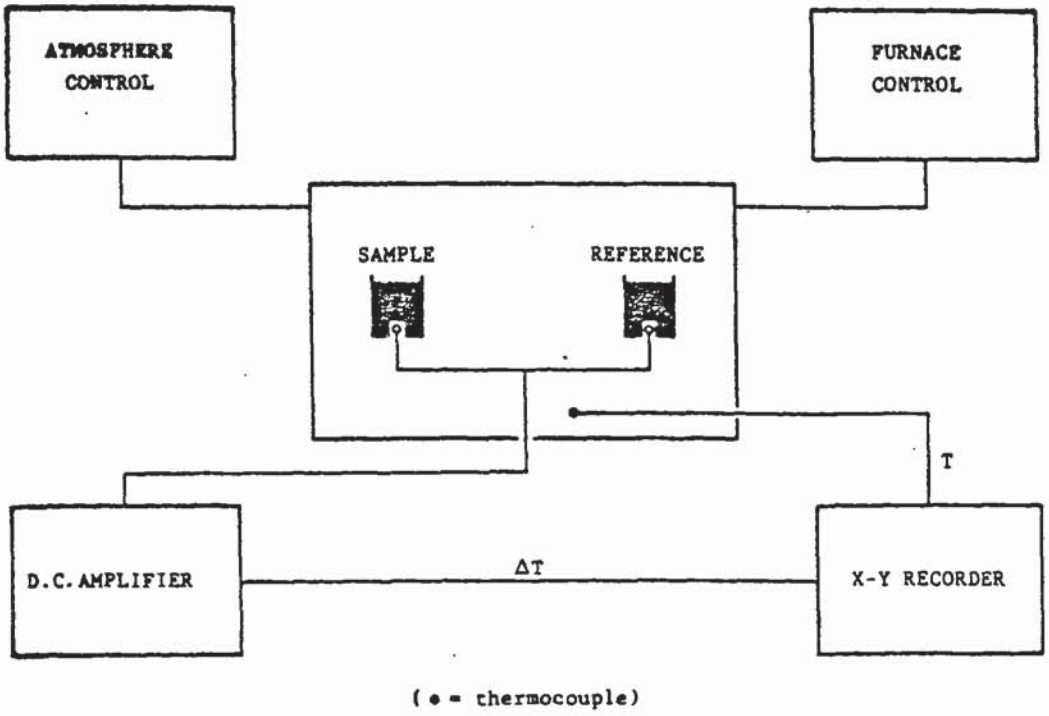

FIGURE 2.3 Schematic representation of the Differential Thermal Analyser.

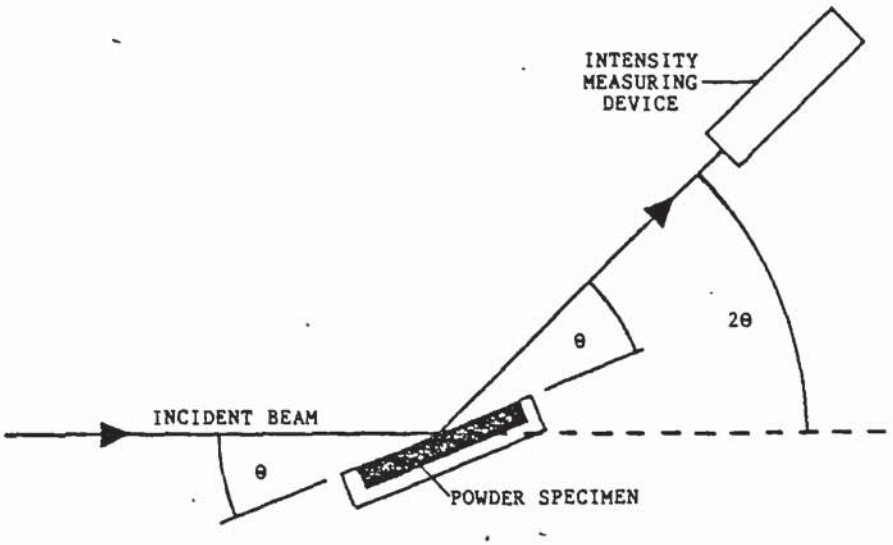

FIGURE 2.4 Geometric arrangement of the X-ray Diffractometer.

cific temperatures, so it is possible to detect the presence of most hydrated compounds in the cement.

It was convenient in this work to represent the traces as peaks rather than the troughs normally shown for endothermic reactions. Peaks found in the present work are represented diagramatically in appendix 4 with an indication of the references from which information on each peak was extracted.

2.8.2 X-RAY DIFFRACTION ANALYSIS

The conditions that need to be satisfied for the reflection of x-rays of a specific wavelenght are given by Bragg's law [36] which states that:

$$n\lambda = 2d \sin \Theta$$

where

- n = the order of reflection (1,2,etc)
- λ = the wavelength of the X-rays
- d = the spacing of the crystal planes
- Θ = the angle of incidence or reflection of the x-ray beam.

It is therefore possible, for a given wavelength and angle of incidence to calculate the atom spacing.

A "Philips" X-ray diffractometer (with Cu Kα radiation) was used for the analysis of powdered specimens which uses an electronic counter tube to measure the intensity of the X-ray reflections. The counter tube is rotated at twice the

speed of the specimens in order to receive the reflected rays (see figure 2.4). A trace of intensity against Bragg angle is recorded on a chart recorder from which values of d can be determined and compared to standard data [37]. An example of cement phase identification can be seen in appendix 5.

2.9 PORE SIZE DISTRIBUTION DETERMINATIONS

As a means of determining the pore-size distribution of different cements, the "Micrometrics Instrument Corporation" porosimeter (model 900/910) was employed.

A three millimetre thick disc of a cement paste was broken into small platelets , which were dried at 105°C for two days. Afterweighing, the sample was placed in a glass cell which was fixed into the porosimeter allowing it to be evacuated, for removal of any remaining moisture and gases. The vessel was then filled with mercury, a non wetting liquid, which was subjected to increasing pressures. The amount of mercury needed to refill the vessel was taken as that which had penetrated a certain size of pores. As the pressure was increased, the quantity of liquid forced into the pores increased in proportion to the differential pore volume, the size of the pores corresponding to the instantaneous pressure.

The pressure at which mercury enters pores of a given size may be calculated from the Washburn equation [38]

$$P = \frac{-4\gamma \cos \theta}{d}$$

where

P = the applied pressure (P.S.I.)

d = the pore diameter (microns)

γ = the surface tension of the mercury (N/m)

θ = the contact angle between mercury and the material (degrees).

As pressure could be translated into pore diameter by assuming an appropriate value for the contact angle (117° in this case following the work of Winslow and Diamond [39]) it was possible to plot the penetration volume versus the pore diameter for the cement paste.

Results do not represent exactly the pore-size distribution of the cement paste as it is necessary to dry the specimens prior to the test, which may influence the pores, and because of the uncertainty in the value of the contact angle. The technique is however useful in terms of comparing different cements, or similar specimens but of varying conditions of exposure and curing.

Appendix 6 shows an example calculation of pore size distribution.

2.10 CORROSION MONITORING TECHNIQUES

The more conventional and proven [40,41] linear polarisa-

tion technique used extensively by other workers [42,43], was employed for measuring corrosion intensities of embedded steel in cement or concrete. The A.C. Impedance technique, which is still in its development stage in the field of corrosion in concrete, was used only in a small comparative study against the linear polarisation technique (Chapter 6 part II). An essential feature for both methods is that the cement or concrete has at least a second electrode either embedded in it, or, in the case of fully or partly submerged structures, immersed in the solution. Both methods are essentially non-destructive.

2.10.1 LINEAR POLARISATION

Linear polarisation as applied in the present work, involves the determination of a plot of applied potential (ΔE) against current density (ΔI) for each steel electrode. Values of ΔE are in the order of a few millivolts about the zero point, corresponding to E_{corr} (rest potential). The polarisation resistance (Rp) is the slope of the plot and is related to the corrosion intensity I_{corr} by the Stern and Geary equation [44,45].

$$Rp = \frac{\Delta E}{\Delta I} = \frac{\beta a . \beta c}{2.3\ (I_{corr})(\beta a + \beta c)}$$

where βa and βc are the anodic and cathodic Tafel constants.

The Tafel constants are characteristic of a particular corroding system and can be determined from a separate scan of

several hundred millivolts either side of E_{corr}. Such a large shift in potential can alter the electrochemical state of the steel, so it is common to assume the value of the Tafel constants. In the present work these were taken as 0.12 Volts/decade which gives a value for the constant B of 26mV, where

$$I_{corr} = \frac{B}{Rp} \quad \text{and}$$

$$B = \frac{\beta a \, \beta c}{2.3(\beta a + \beta c)}$$

Andrade and Gonzalez [40] had found that for a corroding steel in concrete a value of B = 26mV gives corrosion rates similar to those obtained by gravimetric weight loss methods.

Two linear polarisation techniques were employed in the present work. The first involved the use of an "E.G.&G./P.A.R. model 350" microprocessor. It was programmed to carry out a slow potentiodynamic scan between E_{corr}-20mV to E_{corr} + 20mV at a scan rate of 10mV/min. The results were then displayed by means of an integral "x-y" plotter (see figure 2.5)[46]. Rp, I_{corr} and E_{corr} values were automatically determined and printed on the graph. The microprocessor had an I-R compensation module attached to it which automatically compensated for the Ohmic drop between the working and reference electrodes.

The second technique made use of the "AMEL model 551" potentiostat. In this case the potential was shifted manually to

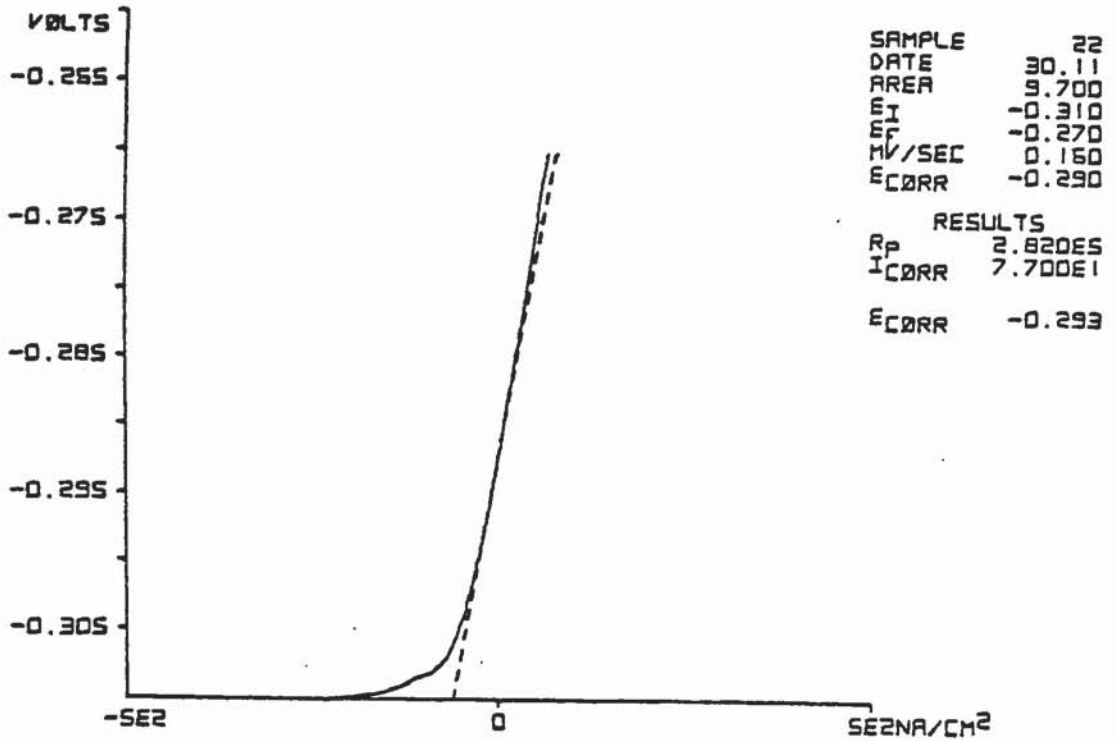

FIGURE 2.5 Typical linear polarisation plot of the "PAR" microprocessor.

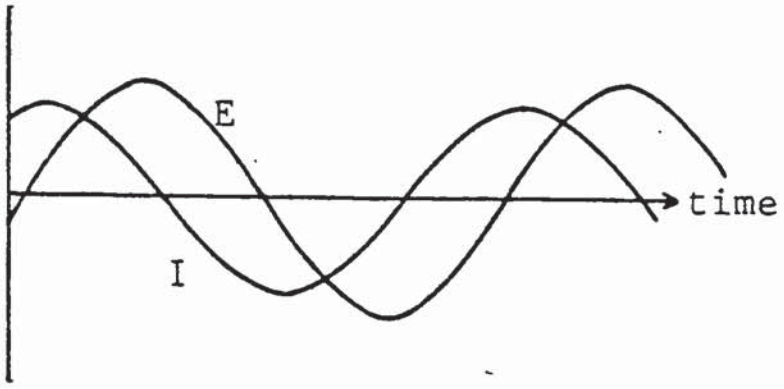

FIGURE 2.6 A.C. waveforms for an applied potential and a resultant current.

10mV above the rest potential and the resultant current recorded after 30 seconds by which time it had reached a near-steady condition. In order to avoid errors arrising from the misdetermination of the actual E_{corr} value, it was necessary to move the potential back to the assumed rest potential, allow 30 seconds for stabilisation and then shift it in the negative direction by 10mV, again recording the current after a 30 second period. ΔI was then taken as the average of the modulus of the two readings. The "AMEL" potentiostat was fitted with positive feed-back which could be used for compensation of the I.R. drop.

The two techniques had been shown to produce almost identical results by Gonzalez et al [47] and by Lambert [34].

An example of a calculation of I_{corr} using the "manual" method can be found in Appendix 7.

2.10.2 A.C. IMPEDANCE

The A.C. Impedance technique for studying corrosion phenomena and monitoring corrosion rates has been used in special applications such as in polymer coated steels or painted systems [48] with good success. Recently the technique has been applied to corroding steel electrodes in concrete [49,50] but difficulties in interpretations have not been completely overcome.

An attempt was made in this work to evaluate its usefulness

as a tool for measuring corrosion rates of steel in concrete by carrying out a small comparative study between corrosion intensities obtained by either the linear polarization or the A.C. impedance techniques.

2.10.2a The Theory of A.C. Impedance (51,52)

The electrode interface during an electrochemical reaction can be thought of as analogous to an electronic circuit consisting of an array of resistors and capacitors. The simplest system representing steel in an electrolyte is the Randles circuit (figure 2.8).

The resistance R_Ω represents the solution resistance and is equivalent to the Ohmic drop encountered in linear polarisation, Rt is the charge transfer resistance, equivalent to Rp and Cdl is the electrochemical double layer capacity resulting from absorbed ions and water molecules.

In the case of linear polarisation the resistance is defined by Ohms law:

$$E = IR \quad .....(1)$$

If an "alternating" potential is applied the analogous equa-

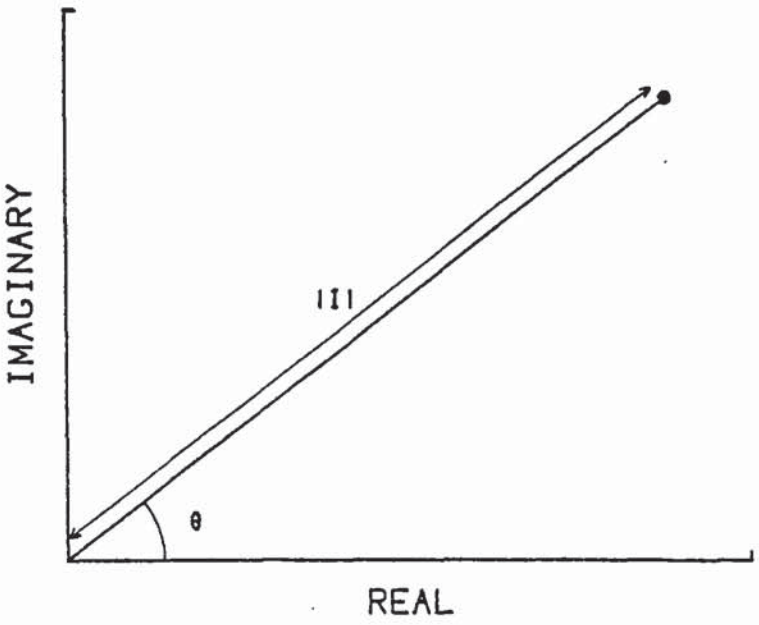

FIGURE 2.7a Vector in terms of angle θ and magnitude I.

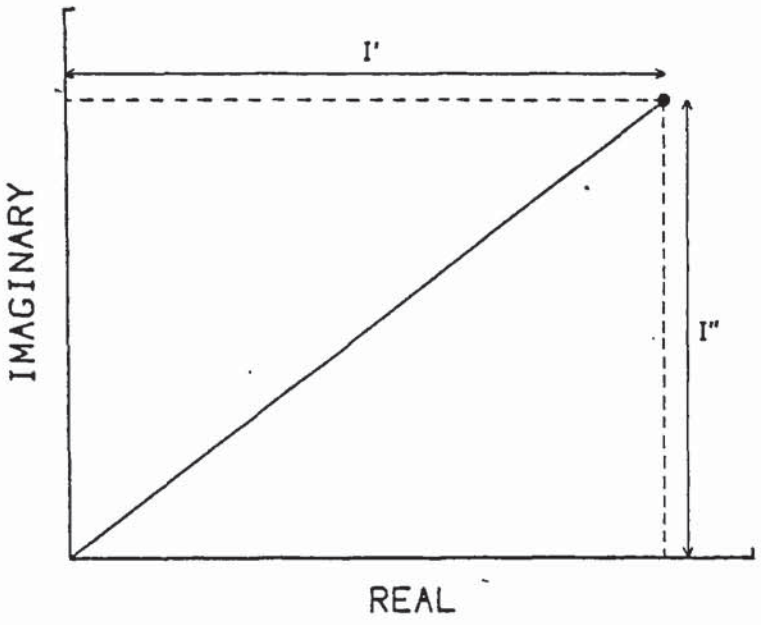

FIGURE 2.7b Vector in terms of coordinates real (I') and imaginary (I'').

tion is:

$$E = IZ \quad .....(2)$$

where E and I are waveform amplitudes for potential and current respectively (figure 2.6) and Z is the "impedance" which is the a.c. equivalent of resistance. It is an obstruction to current which in the case of a.c. can be achieved by capacitors and inductors as well as resistors. This phenomenon can produce an a.c. waveform as in figure 2.6 where not only the amplitude of the two waveforms is affected but also the phase.

One method of describing the wave in terms of its amplitude and its phase characteristics is by vector analysis. It is possible to represent the vector by an angle θ and a magnitude $|I|$ (figure 2.7a) or by its real and imaginary components I' and I'' (figure 2.7b).

In a similar way, the potential waveform can be expressed in real and imaginary components. The two components are defined with respect to some reference waveform, which allows expression of the current and voltage waveforms as vectors with respect to the same coordinate axes. This in turn facilitates the calculation of the impedance vector from equation (2) which can also be defined in terms of the same coordinate axes.

For each excitation frequency, a real and imaginary component of impedance exists which can be plotted on a complex

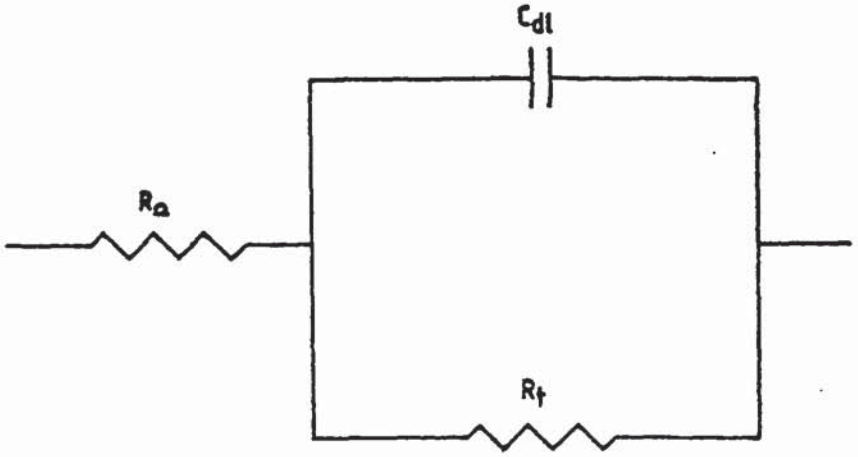

FIGURE 2.8 Randles Circuit. The simplest system representing steel in an electrolyte.

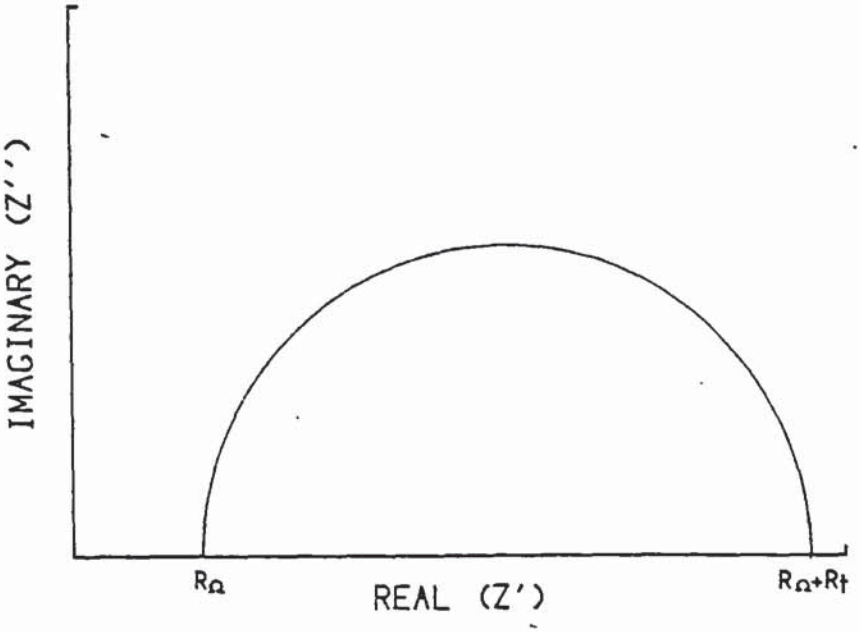

FIGURE 2.9 Complex impedance plane diagram for the simple Randles electrochemical system.

impedance plane diagram, more commonly known as a Nyquist Plot. Over a range of frequencies, this would look something like figure 2.9 which is the equivalent plot for the circuit in figure 2.8. It is therefore theoretically possible to determine Rt values which are equivalent to Rp and can be used in the Ste rn and Geary equation for the calculation of I_{corr} (see 2.10.1).

2.10.2b The Fast Fourier Transform (FFT)

As it is unrealistic to apply a full range of separate frequencies of potential waveforms to obtain enough data for sensible extrapolation, the Fast Fourier Transform (FFT) technique is used for producing a mixture of excitation waveforms of varying frequencies. This complex waveform can be thought of as the algebraic sum of many individual waveforms of equal amplitude, but each with a different frequency and phase characteristic. Figure 2.10 shows a typical excitation waveform that contains twenty frequencies from 0.05Hz to 5Hz.

2.10.2c Equipment set-up

For the present work a "Hewlett Packard model 3582A" spectrum analyser was used, capable of covering a range of 0.02Hz to 25.6KHz. The equipment set-up was as that used by Andrade and Castelo [53] and is shown in figure 2.11. The potentiostat used was the "AMEL-551" which had the dual function of a potentiostat, enabling the cycling of the potential

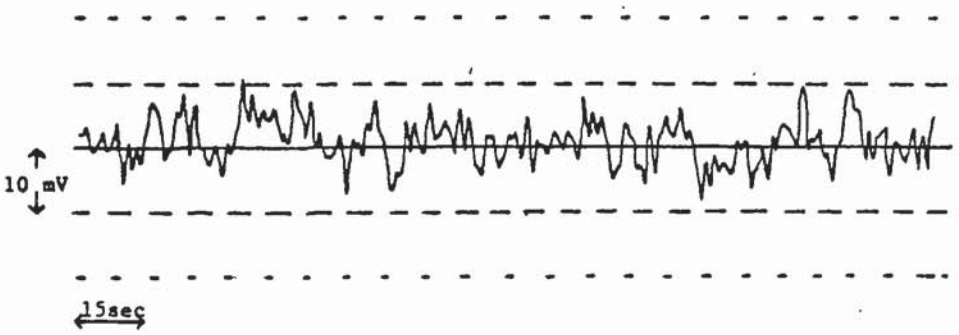

FIGURE 2.10 A Fast Fourier Transform (FFT) waveform for a base frequency of 50Hz and maximum amplitude of 10mV.

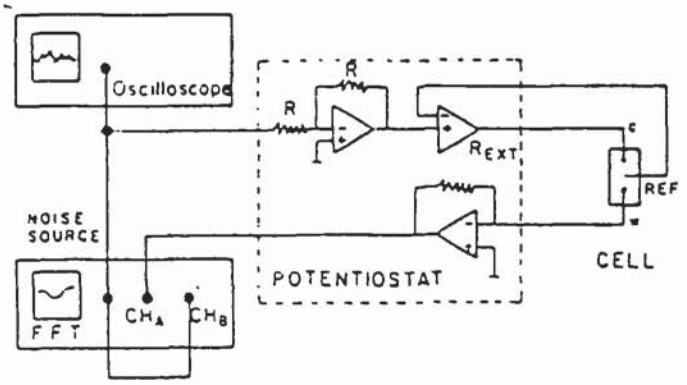

FIGURE 2.11 Set-up used for A.C.Impedance measurements by means of a spectrum analyser (After Andrade and Castelo).

about E_{corr}, and an amplifier of the output by making use of an internal variable resistor.

A frequency range was selected, normally 2.5Hz giving a set of frequencies up to 2.5Hz. The "noise" generated was then fed to the specimen via the potentiostat, to channel B of the analyser and to an oscilloscope, to ensure that the amplitude was in the order of 10-15mV. The resultant output from the potentiostat was fed to channel A which, in combination with the variable resistor of the potentiostat, was set for the lowest sensitivity range which ensured a correct coherence function of 1 for the majority of frequencies, as read off the analyser screen.

An average value of 4 runs was normally taken for this frequency range, and on completion, data were recorded. These were in the form of frequency, modulus of impedance $|Z|$ and phase angle θ. It was possible to collect them manually by moving a marker along the curves of the plots of modulus and phase angle versus frequency on the screen.

The procedure was then repeated for higher frequency ranges, typically 50Hz and 250Hz, with an average of 32 runs, until the phase angle was zero.

The results were then represented on graphs (see chapter 6 part II) after the amplification factor of the internal resistor of the potentiostat was taken into account. (For an example see appendix 8).

2.11 POTENTIOSTATIC POLARIZATION

Potentiostatic Polarization scans, using the "AMEL 551" potentiostat, were performed on iron wires embedded in cement pastes in order to study their pitting characteristics. Full details of the experimental procedure and equipment set-up can be found in chapter 6 part I.

CHAPTER 3 THE DIFFUSION OF CHLORIDE AND HYDROXYL IONS IN CEMENT PASTES

3.1 INTRODUCTION

Of the two major depassivating mechanisms for steel reinforcement in concrete mentioned in chapter 1, the commonest in this country is that caused by aggressive ions, the most important of which are chlorides.

According to Kay et al [54] there are three possible ways for chlorides to enter a structure. These are classified by them as:

(i) Primary chloride entry
(ii) Secondary chloride entry
and (iii) Tertiary chloride entry

Primary chlorides, are chlorides introduced at the mixing stage, mainly from contaminated aggregates, sand or water. Secondary chlorides are those penetrating from a concrete surface inwards, sometime after the casting of the structure and tertiary chlorides are those that reach the steel interface through cracks which have occurred from such causes as shrinkage and thermal expansion.

The first category is only a serious problem in countries where there are no stringent controls such as those experienced in the U.K. [10], so that for a concrete structure with small and insignificant cracks, the only way for

chloride ingress is by category (ii)

Chloride penetration in such structures is primarily controlled by the process of diffusion. This was shown to be true by Sorensen and Maahn [55] who had studied the penetration of chloride in many 15-20 years old concrete structures on the Danish coast. They had taken out cores of concrete perpendicular to the surface, at varying heights above the water level. Their results showed that the chloride penetration profile for each condition had obeyed Ficks 2nd law of diffusion to a good approximation.

Once sufficient quantities of chloride reach the steel reinforcement, provided there is a supply of oxygen the process of corrosion begins. The threshold concentration of chloride required to initiate corrosion depends primarily on the relative concentration of hydroxyl ions.

Attempts have been made to determine the threshold chloride to hydroxyl ratio for corrosion initiation. Hausman [56] found that, in alkaline solutions in the pH range of 11.6 - 13.2, chloride can be tolerated by steel up to a concentration where the ratio of $[Cl^-]$ to $[OH^-]$ reaches about 0.61 (see fig. 3.1).

Tuutti [57] had reported similar results for simulated high pH pore solutionsof concrete. Gouda [58] obtained the relationship,

$$pH = n\log C_{Cl^-} + K$$

where,

n & K are constants

and C_{Cl^-} is the highest concentration of Cl^- that can be tolerated.

Her relationship was obeyed between the pH values of 11.75 and 13.5.

These observations are all however for steel in alkaline solutions at equilibrium with the air. Steel in concrete is now normally accepted to tolerate much higher thresholds of relative concentrations of the ions [59,60]. According to Gouda and Halaka [59] the reason for this, is the part removal of the chloride by the C_3A phase, as will be discussed later in the chapter. There is also the suggestion put forward by Page [26] that portlandite formation around the steel reinforcement, can act both as a physical barrier to chloride penetration and as a local hydroxyl ion replenisher so that while the chloride has a greater diffusional path to traverse, the hydroxyl ions are readily available at the interface (see fig. 6.9). The concept of easy hydroxyl replenishment to the steel surface will be discussed further in chapters 4 and 5.

Certain cements containing slags and pozzolanas, may reduce the effectiveness of the portlandite barrier as they remove $Ca(OH)_2$ during hydration. In such cases, the value of $[Cl^-]/[OH^-]$ may be nearer to that reported for normal alkaline solutions. Furthermore, the diffusional length for hydroxyl

ions would also be longer, so the relative migration of the two anions to the corrosion site would become significant with regards to the dual ionic replenishment.

In the case of the partial neutralization of portland cement concrete, either by carbonation or to a lesser extent by the leaching action of water on calcium hydroxide, the effectiveness of the portlandite layer may be reduced so that again the relative migration of Cl^- and OH^- ions to the site may be of significance.

In view of the importance of the relative ionic mobilities mentioned, work was carried out to determine effective diffusion coefficients for both chloride and hydroxyl ions in hardened cement pastes. This chapter reports on the results and is divided into 2 parts. Part I contains work on the relative migration of the two ionic species in OPC pastes and part II on the diffusion of hydroxyl ions through a selection of hardened cement pastes.

PART I THE RELATIVE MIGRATION OF HYDROXYL AND CHLORIDE IONS IN CEMENT PASTE

3.2 INTRODUCTION AND LITERATURE REVIEW

An obvious way of studying the penetration mechanism of chloride into cement pastes, mortars or concretes, is by exposing one flat surface of the material to a chloride solution for a length of time and determining the concentration of the investigated ionic species at increasing depths. It is possible to vary such parameters as type of cement, water to cement ratio, temperature and concentration of the chloride solution in order to study their effect on chloride penetration.

Researchers have used this experimental technique extensively [61-64] as it closely resembles many real life situations such as offshore structures exposed to seawater.

Traetteberg [61] studied the effect of maturity of portland cement paste on the penetration rate of chloride, by determining total amounts of chloride at increasing depths. She concluded that penetration depths decreased with increasing maturity of the paste. She also observed the formation of calcium chloroaluminate. She believed that Friedel's salt, as it is commonly referred to, is formed by transformation of ettringite accompanied by precipitation of calcium sulphate.

Similar studies by Midgley and Illston however [62,63]

showed that Friedel's salt is not formed at the expense of other calcium aluminate hydrates, but only by reaction with anhydrous C_3A. They concluded also that a substantial proportion of chloride is not locked up in the crystalline form but is present in another form mainly as free ions in solution.

Their work involved exposing the one surface of portland cement paste cylinders protected by rubber sheaths to NaCl solutions and chemically analysing the cements at increasing depths for chloride and other phases after six months of exposure.

Translating penetration rates to numerical values is of high importance to researchers. A direct comparison of a range of cements in terms of their resistance to chloride penetration can then be made and a structure's ability to protect steel reinforcement in terms of avoiding or reducing chloride ingress can be evaluated.

If the process of ionic migration is diffusion controlled, it can be shown that for a given temperature, the mobility of the ions in concrete is directly proportional to the diffusion coefficient [65] as stated by the Nernst-Einstein relationship.

$$D = ukT$$

where

D = the coefficient of diffusion

u = the mobility of the "particles"

k = the Boltzmann constant

and T = the temperature

so calculated values of the diffusion coefficient D, would be representative of the ionic mobilities.

An attempt to obtain such values for various ions in cement pastes, was made as long ago as 1952 by Spinks et al[66] who used solutions labelled with radioactive isotopes (^{45}Ca, ^{35}S, ^{131}I or ^{22}Na). After exposing the one side of cylindrical OPC or SRPC pastes for a length of time, they measured the radiation at different depths of the pastes and translated their readings into concentrations of the particular ion under investigation. They observed that penetration of ions into cement pastes followed Fick's second law of diffusion into a semi-infinite solid, so they were able to calculate diffusion coefficients for each of the ions, which ranged in the order of 10^{-11} to 10^{-9} cm^2s^{-1}. Generally speaking "D" values were higher for the anions than the cations (see also part II of this chapter). No mention was made however of curing conditions or W/C ratios of the cement pastes.

Collepardi et al [67 - 69] used the same technique for their diffusivity determinations. After exposure of the cement pastes of w/c 0.4 to 0.6 to various solutions, the specimens were sliced into discs at increasing depths which were then subjected to specific chemical analysis to deter-

mine the total concentrations of the ions under investigation. A solution to Fick's 2nd law (see appendix 9) was then used to calculate values of D. Diffusion coefficients for chloride were in the order of 10^{-8} cm^2s^{-1} and did not depend on the concentration of the solution.

In view of the earlier mentioned importance of hydroxyl ionic diffusion, it is perhaps surprising that no literature has as yet been published on the subject. The work described in this chapter attempts to rectify that to some extent. In this part of the chapter the method used by Collepardi is developed further, in order to enable the calculation of the diffusion coefficients for both chloride and hydroxyl ions for the same portland cement, but by taking into account free amounts of the ionic species as well as the total chloride concentration. It is ofcourse the free amounts present in the pore solutions that mainly affect the passivity of the steel. Their determination has been facilitated by the pore expression device, which is proving to be a very useful tool for diffusion work as well as for cement chemistry in general.

3.3 EXPERIMENTAL PROCEDURE

Cylindrical specimens made from OPC-B as described in chapter 2 (para. 2.2) were demoulded after 90 days of storage in saturated air at 22±2°C, ensuring a near maximum hydration. About 1cm was sliced off the one end of each cylinder

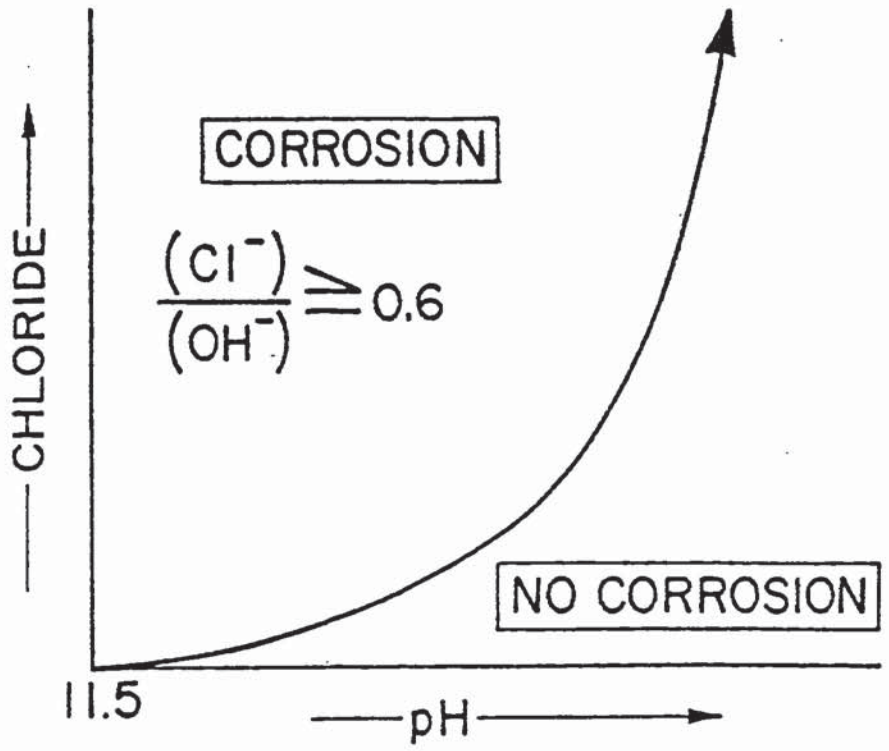

FIGURE 3.1 Threshold chloride ion concentration for corrosion to occur as a function of alkalinity (after Hausman).

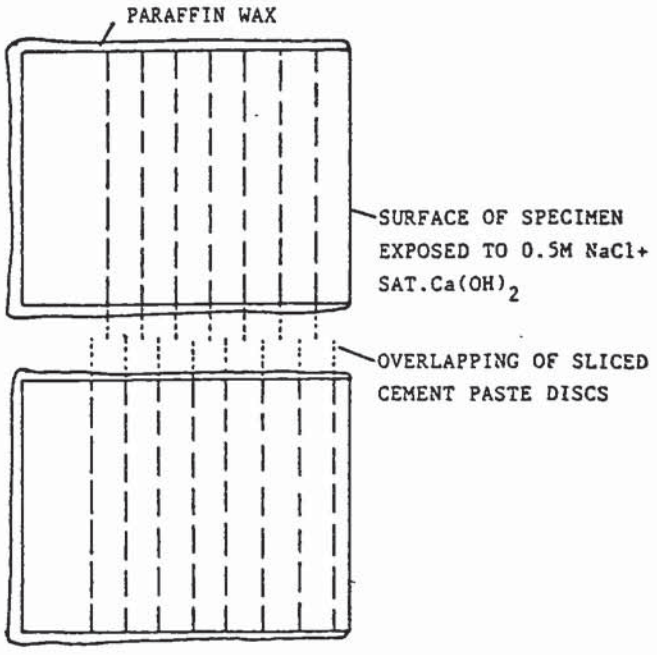

FIGURE 3.2 Specimens exposed to solution for the diffusion experiments.

using the microslice (chapter 2, para. 2.2) and the fresh surface was lightly ground on 600 grade carbide paper. The remaining area of the specimen was masked-off with paraffin wax painted on by brush, building up a thickness of a few millimetres (see fig. 3.2). Thirty six such cylinders were prepared and positioned with the axes horizontal in groups of 12 in three large sealed containers each filled with 5 litres of saturated $Ca(OH)_2$ plus 1M NaCl solution. The containers were finally placed inside an incubator maintaining a constant temperature of 25±2°C. The large volume of solution compared to the exposed surfaces of the cement pastes was necessary in order to avoid excessive changes in the concentration.

After an exposure period of 100 days, the cylinders were removed from the solution and a group of ten specimens were cut into 7mm discs up to a depth of 52.5mm using a dry diamond blade. A second set of 10 were again sliced at 7mm intervals but with the first disc cut at 3.5mm so that an "overlapping" effect could be achieved (see fig. 3.2). Between 6 and 8 discs from the same depth were grouped together and kept in polythene bags inside air-tight containers for the minimum possible time, ready for pressing in the pore-expression device (see chapter 2 para. 2.3).

The solutions expressed from the cement discs were quickly analysed first for OH^- and then for Cl^- ions as described in chapter 2 (para. 2.4) so as to minimise changes in con-

centrations such as those caused by CO_2 absorption.

Total chloride concentrations were also determined for each set of unpressed discs by the method described in chapter 2 (para. 2.7). To express the values of free and total chloride in terms of mM/g of cement it was necessary to know the amounts of evaporable and non-evaporable water and these were determined by the technique described in chapter 2 (para. 2.5).

Samples from the discs were also subjected to differential thermal analysis (see chapter 2 para. 2.8.1) so that any changes in the hydrates present in the pastes could be detected.

3.4 RESULTS

3.4.1 Ionic Concentrations

The chloride and hydroxyl concentrations of the pressed solutions are tabulated in table 3.1 along with the equivalent chloride to hydroxyl ratios. Figures 3.3 and 3.4 represent the Cl^- and OH^- concentration profiles respectively.

Different solutions to Fick's 2nd law of diffusion allow the determination of the diffusion coefficients for each ionic species by knowing the concentration at increasing depths from the surface. (For the derivation of the equations see appendix 9). For the case of chloride penetration, the solution is,

TABLE 3.1 Concentration of Cl^- and OH^- with depth into cement paste.

DEPTH x (cm)	Cl^- mM/l	OH^- mM/l	$\frac{[Cl^-]}{[OH^-]}$
0.175	991	104	9.53
0.350	838	112	7.48
0.700	670	134	5.00
1.050	572	171	3.35
1.400	366	219	1.67
1.750	292	257	1.14
2.100	135	274	0.49
2.450	59	319	0.18
2.800	39	335	0.12
3.150	24	351	0.07
3.500	14	364	0.04
3.850	15	355	0.04
4.200	7	375	0.02
4.550	2	388	0.00
4.900	1	384	0.00

TABLE 3.2 Diffusion coefficient values for Cl^- and OH^- in OPC-B.

ION	$D(x10^9)cm^2/s$	r	c(cm)	b(cm)	95% conf. int. D-range $(x10^9)cm^2/s$
OH^-	212.4	0.997	0.015	2.710	183.2-244.0
Cl^-	118.8	0.991	0.000	2.026	98.7-140.7
FREE Cl^-	118.9	0.991	-0.002	2.027	98.4-141.3
TOTAL Cl^-	180.3	0.995	0.008	2.496	146.4-217.7

r=Correlation Coefficient

c=Intercept

b=slope

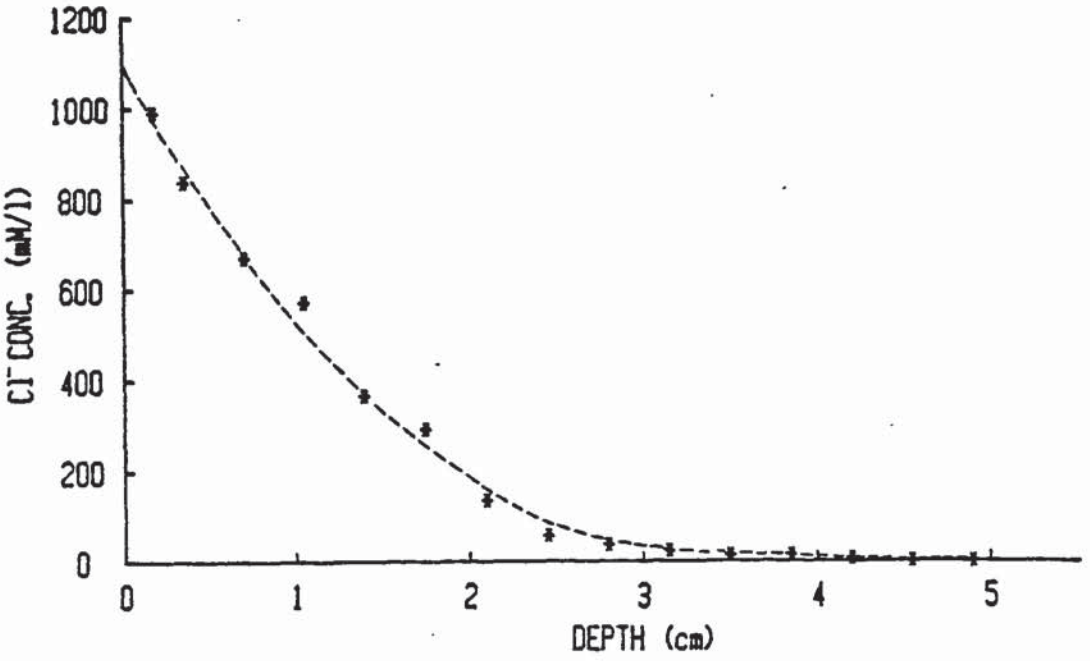

FIGURE 3.3 Concentration profile of Cl^- in OPC-B exposed to 1M NaCl in sat. $Ca(OH)_2$ for 100 days.

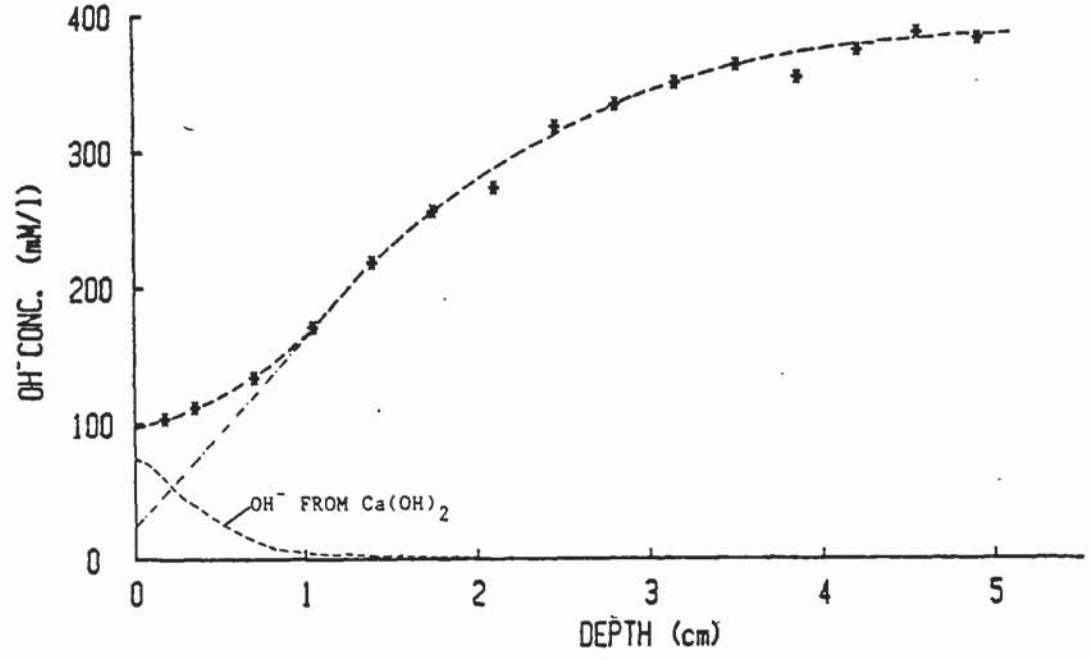

FIGURE 3.4 Concentration profile of OH^- in OPC-B exposed to 1M NaCl in sat. $Ca(OH)_2$ for 100 days.

$$C_x = C_o[1\text{-erfy}] \quad \text{(ref. 70)}$$

where $y = \frac{x}{2\sqrt{Dt}}$

for the boundary conditions,

$C_x = C_o$ for x=o for all t

C_x = o at x>o and t=o

$C_x = C_{(x,t)}$ at x>o and t>o

where,

C_o = the concentration at the surface (ie at x=o)

C_x = the concentration at a depth x from the surface

x = the depth into the specimen (cm)

D = the diffusion coefficient (cm^2s^{-1})

t = the duration of exposure (sec)

As the dimensions of D are independent of the units of concentrations C_o and C_x, these can be of any units such as mM/litre or mM/g.

For the oppositely diffusing hydroxyl ions, the concentration profile can be assumed to be half the curve of that considered in chapter 4 part I and provided the concentration at the surface remains effectively constant throughout the exposure period ie

$C_x = \frac{C_o}{2}$ at t=o for any t,

then the equation is obeyed [70] (see also equation 1 in chapter 4 para. 4.2).

Values of erfy are tabulated against y in mathematical tables [71] so that it is possible to obtain a specific value of y for any concentration along the depth of the specimen which depends on the ratio of the two concentrations C_x and C_o and is dimensionless. From the expression

$$y = \frac{x}{2\sqrt{Dt}}$$

a graph of x v's y would theoretically result in a linear plot with an intercept at zero (see fig. 3.5). It is then possible to calculate values of the gradient of the plot B, the correlation coefficient r and the intercept C, by regression analysis and hence determine the diffusion coefficient from $B = 2\sqrt{Dt}$ (For a full calculation of D see appendix 10). A correlation coefficient close to unity and an intercept close to zero would signify that ionic migration is by the mechanism of diffusion obeying Ficks 2nd law.

The diffusion coefficients of the two sets of ions thus determined are shown in table 3.2 together with the 95% confidence intervals. The theoretical concentration profiles obtained from the calculated coefficients, are those shown by broken lines over the plotted points, on figures 3.3 and 3.4 verifying the good correlation obtained. Diffusion

coefficients for chloride are similar to those reported in the literature [55,67].

The deviation of the hydroxyl concentration profile away from the normal near the surface is caused by the $Ca(OH)_2$ in solution, which increases with the lowering of the pH. This increase is represented in figure 3.4. The extrapolated line to x=o shows a "background" hydroxyl concentration of about 30mM/litre indicating a slow rise from zero over the 100 days. This rise is however too small to significantly affect the diffusion of hydroxyl ions, and the subsequent calculations.

3.4.2 Evaporable and Non-Evaporable Waters

The two components of water together with the total amounts, are represented in table 3.3. The average values are as follows.

We = 29.71%

Wn = 18.85%

Total water = 48.56%

It can be seen that a small amount of water has been lost almost certainly owing to the particular dry-cutting technique employed, which tended to raise the temperature of the discs slightly on slicing. An alternative cutting method described in chapter 4, reduced the amount of lost water considerably for later experiments.

In view of the somewhat inconsistent cutting method, it is

TABLE 3.3 Evaporable and non-evaporable water contents with depth into cement.

DEPTH x (cm)	We (%)	Wn (%)	TOTAL WATER (%)
0.175	29.03	17.64	46.67
0.350	32.12	18.10	50.22
0.700	30.18	17.91	48.09
1.050	30.94	18.64	49.58
1.400	29.32	18.73	48.05
1.750	30.46	19.21	49.67
2.100	29.89	18.56	48.45
2.450	29.84	19.74	49.58
2.800	33.04	19.44	52.48
3.150	28.63	19.12	47.75
3.500	29.90	18.96	48.86
3.850	27.53	18.92	46.45
4.200	28.57	19.58	48.15
4.550	27.25	18.89	46.14
4.900	28.89	19.33	48.22

TABLE 3.4 Free, Bound and Total amounts of chloride with depth into cement.

DEPTH x cm	FREE Cl^- mM/g	BOUND Cl^- mM/g	TOTAL Cl^- mM/g	FREE / TOTAL
0.175	0.288	0.372	0.660	0.436
0.350	0.269	0.330	0.599	0.449
0.700	0.202	0.236	0.438	0.461
1.050	0.177	0.247	0.424	0.417
1.400	0.107	0.238	0.345	0.310
1.750	0.089	0.093	0.182	—
2.100	0.041	0.158	0.199	0.206
2.450	0.018	—	0.018	—
2.800	0.013	0.065	0.078	0.167
3.150	0.007	0.010	0.017	—
3.500	0.004	0.027	0.031	0.129
3.850	0.004	—	0.002	—
4.200	0.002	0.002	0.004	—
4.550	0.001	0.001	0.002	—
4.900	0.000	0.004	0.004	—

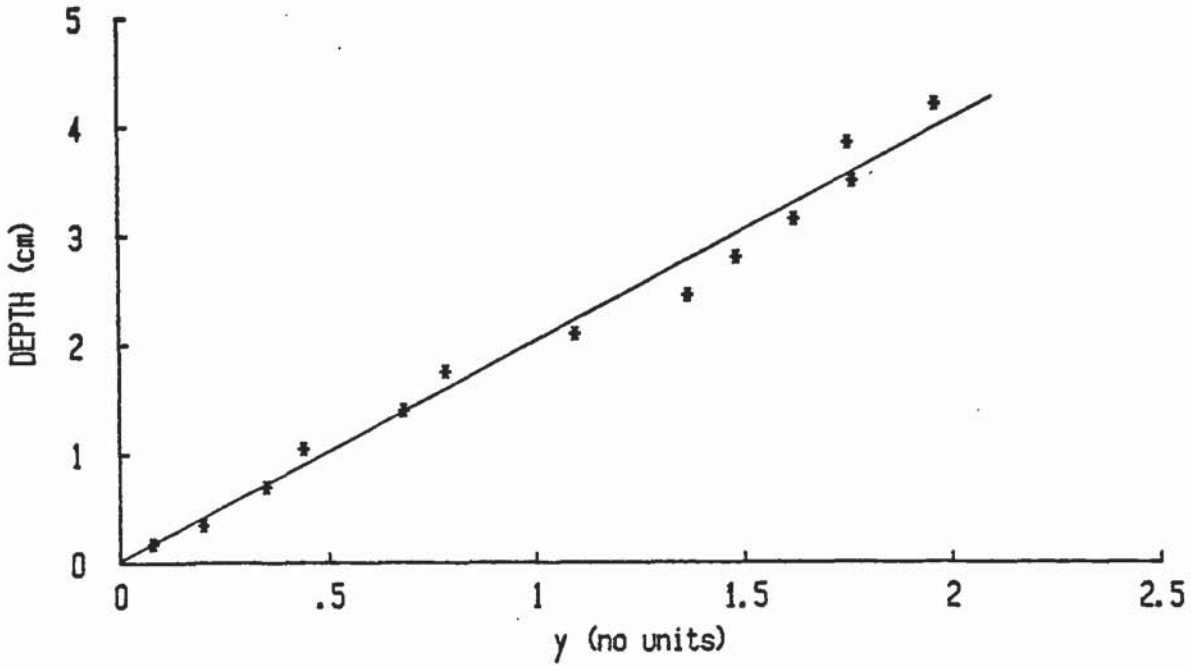

FIGURE 3.5 Plot of depth into cylindrical specimen versus the calculated value of y for the Cl^- concentration profile.

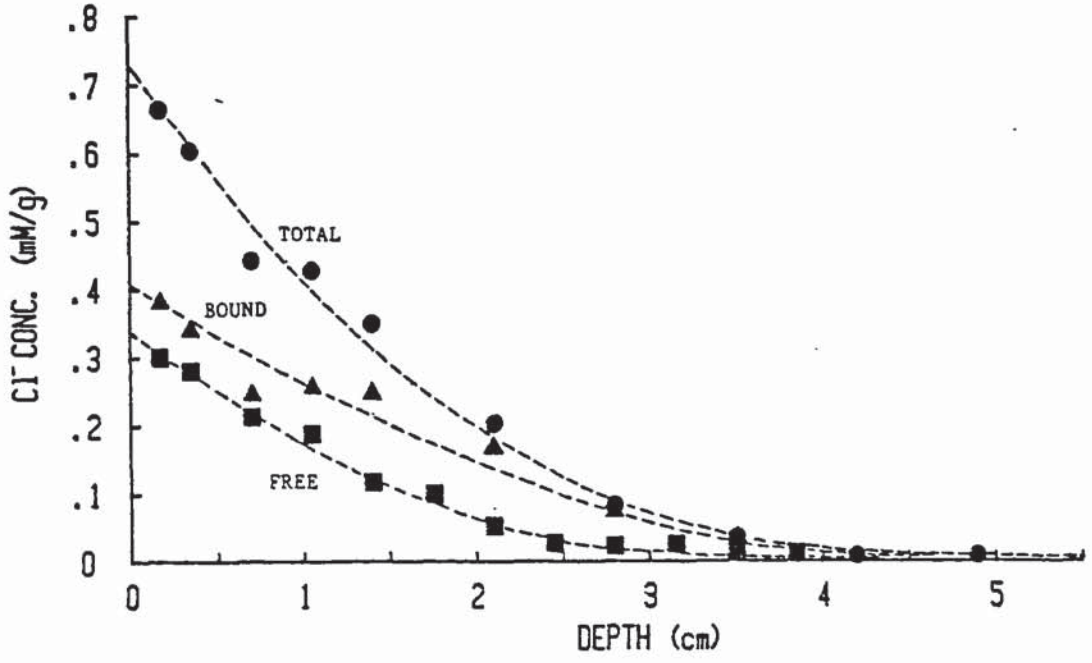

FIGURE 3.6 Concentration profiles of total, free and bound chlorides in OPC-B after 100 days of exposure in 1M NaCl in sat. $Ca(OH)_2$.

not surprising that some scatter exists in these results so no meaningful trend is evident

3.4.3 Total and Free Chloride

Table 3.4 represents the free total and bound amounts of chloride, as well as the free to total ratios. (Examples of the free and total chloride determinations are shown in appendix 3). Those figures underlined in table 3.4 are considered unreliable because they were determined by an apparently less accurate method as follows. After the mixture of cement powder water and acid was warmed to allow the dissolution of the cement, as described in chapter 2 (para. 2.7), the mixture was filtered, unlike the later established normal method described and the clear solution analysed for chloride. It is believed therefore that an amount of chloride may have been retained on the filter reducing the actual concentration measured.

The free, total and bound amounts of chloride are represented also in figure 3.6. The diffusion coefficients calculated for both total and free chlorides are shown in table 3.2 with the concentration profiles determined by these diffusivities superimposed over the equivalent sets of points for the two types of chloride; their difference giving the superimposed bound chloride line.

3.4.4 Differential Thermal Analysis

The change in hydrate composition of the cement paste with

the penetration of chloride is best summarised by figure 3.7. The formation of the calcium chloroaluminate phase can be seen clearly up to a depth of at least 1.05cm. This phase was not detectable beyond that depth owing, primarily, to the low sensitivity of the DTA for the chloroaluminate phase.

3.5 DISCUSSION OF RESULTS

From the diffusion coefficient values (table 3.2) it appears that hydroxyl ions migrating outwards move at a faster rate than the incoming chloride ions giving a value for the ratio $D[OH^-]/D[Cl^-]$ of 1.79. If the total chloride is considered however with a diffusion coefficient of $180.3 \times 10^{-9} cm^2 s^{-1}$, the ratio $D[OH^-]/D[Cl^-]_{TOTAL}$ is only 1.18 and judging by the 95% confidence ranges (table 3.2) the two values are not significantly different.

The apparent depth of penetration of the "total" chloride is therefore approximately the same as the apparent depth affected by the leaching action of hydroxyl ions, ie about 4.5 to 5cm as seen on the respective graphs (fig. 3.4 & 3.6). The fact that free chloride appears to be diffusing at a slower rate ($D[Cl^-]_{FREE}/D[Cl^-]_{TOTAL} = 0.65$) is due to the part removal of the chloride from the pore solution by the C_3A phase, forming insoluble calcium chloroaluminates. The removed chloride, which is in fact the bound chloride shown

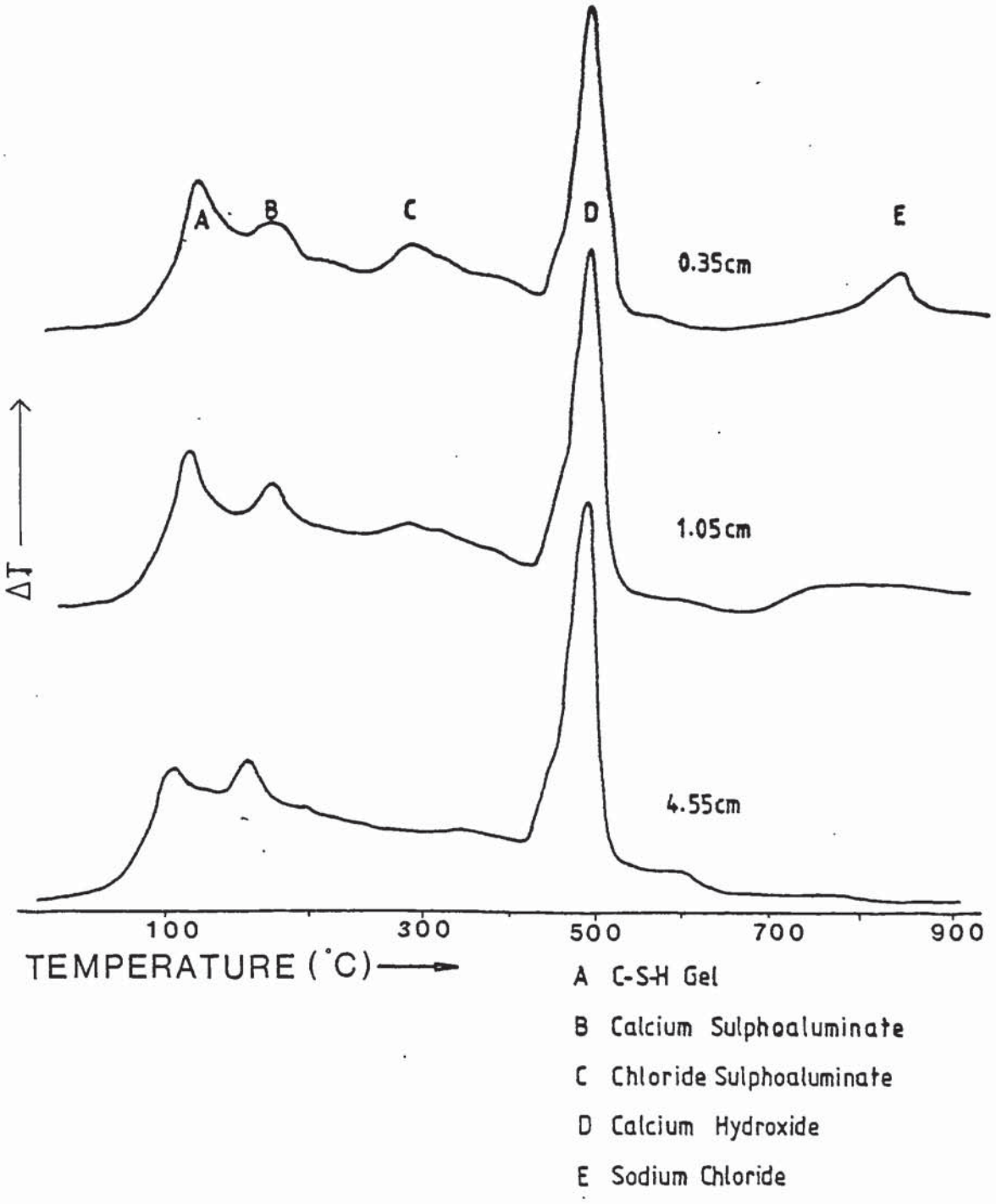

FIGURE 3.7 DTA thermographs of OPC-B at increasing depths after exposure to 1M NaCl in sat. $Ca(OH)_2$ for 100 days.

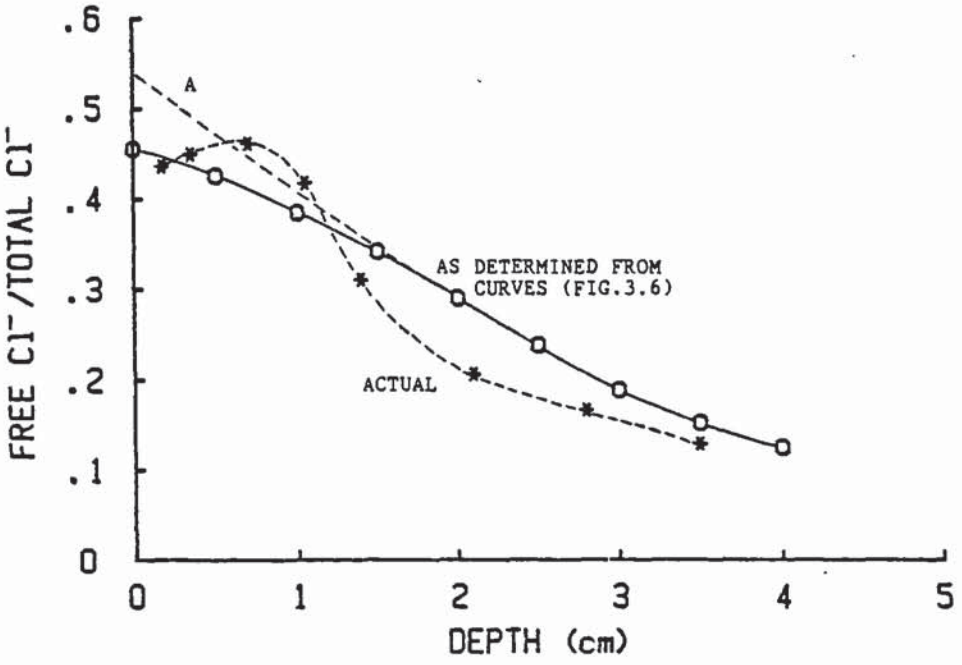

FIGURE 3.8 Variation of the free to total chloride ratio with depth into OPC-B paste.

in figure 3.6, appears to be concentration dependent, a fact reported also by Sorensen and Maahn [55]. They concluded that free to total chloride ratios of concretes exposed to seawater were lower for low total chloride levels and higher for high total chloride levels. They suggested that "this indicates that the concrete attains saturation in chemically bound chloride and further chloride will remain in dissolved or soluble form".

Figure 3.8 shows the variation of free to total chloride with depth graphically. The solid line was determined by considering the calculated penetration profiles of the two types of chloride and may be more representative as the broken line, which represents actual values, includes the errors encountered on the determination of both the free and the total chlorides.

Basically the observation by Sorensen and Maahn [55] is verified but with a slight deviation at the high chloride levels. Theoretically the curve should follow the broken line marked A in figure 3.8. The fact that the curve actually begins to "even out" near the surface, suggests a counter-effect process, possibly caused by a lower stability of the ettringite phase near the surface, releasing "new" C_3A to react with more chloride. The DTA thermographs (fig. 3.7) indicate a possible decrease in the ettringite phase near the surface but as this particular DTA set-up does not allow quantitative analysis it is only possible to speculate

at this stage.

The amount of calcium chloroaluminate formation is known to be closely related to the C_3A content of the cement[24,72]. Roberts [72] demonstrated that as higher C_3A content cements were effective in removing more of the added chloride, they were able to reduce the risk of corrosion of steel reinforcement. His experiments comprised of embedding steel wires in calcium chloride containing portland cement concretes with C_3A contents of 1% or 9%.

As suggested by Verbeck, [73] in the case of chloride penetrating from an outside source, cements with a high C_3A content could delay the penetration of the chloride to the steel interface by modifying the penetration profile as in figure 3.9. Furthermore, as was described earlier (fig. 3.6) the free chloride would have an even lower apparent diffusivity than the total chloride caused by the near complete complexation of the chloride by the C_3A at low concentrations.

Steel embedded in high C_3A cement concretes exposed to chloride solutions should therefore be better protected against corrosion than steel in low C_3A concretes. This fact was demonstrated by Verbeck [74] (as cited by Popovics et al [3] who exposed reinforced concrete piles made from 22 different portland cements of various compositions and studied the cracking of the concrete structures caused by steel

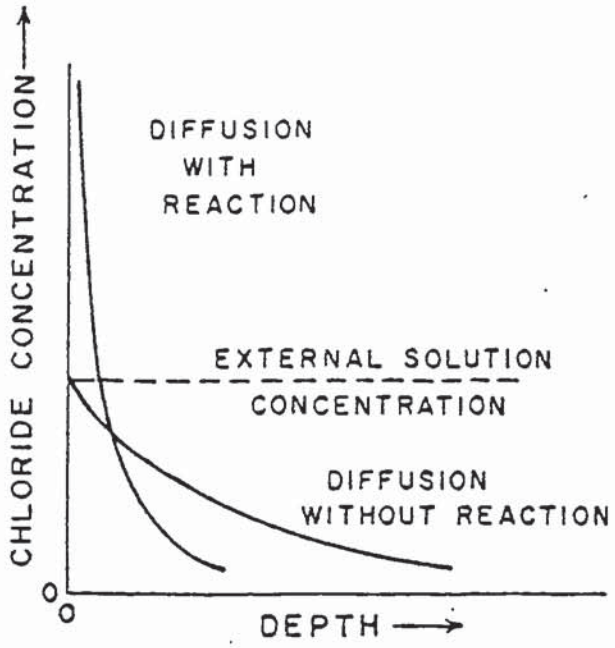

FIGURE 3.9 Effect of chemical reaction of penetrating chloride on the concentration profile of total chloride (After Verbeck).

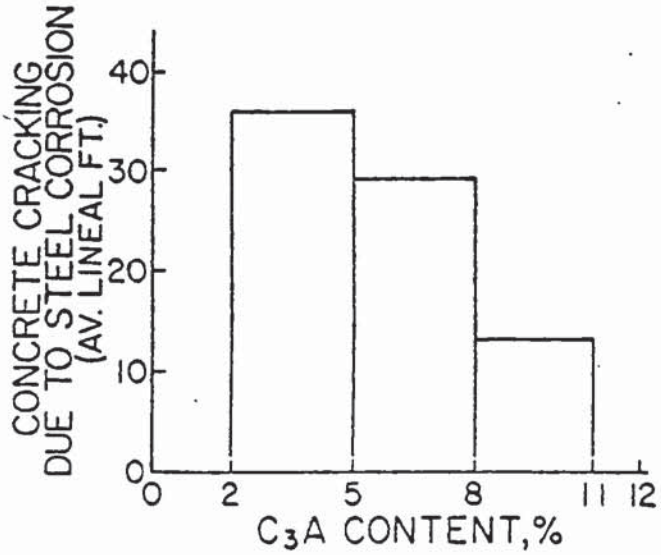

FIGURE 3.10 Effect of C_3A content on concrete cracking due to steel corrosion in marine environment (After Verbeck).

corrosion. His results are summarised in figure 3.10 and illustrate that higher C_3A content concretes reduce the likelihood of corrosion.

No other work has however been cited on the effect of C_3A content of cements on the corrosion of the reinforcement, so it may be unwise to draw strong conclusions on the evidence of one publication. Other workers[75 - 76] had suggested for instance that the role of C_3A on chloride diffusion is minimal when compared to other parameters such as porosity, w/c ratio and fineness of cement. This will be discussed further in subsequent chapters.

One further point to be considered, is the effect the counterdiffusing hydroxyl ions may have on the corrosion of steel. If a critical chloride to hydroxyl ratio does exist for corrosion initiation to be possible, then the double effect of hydroxyl ion decrease and chloride ion increase with time of exposure would lead to the critical ratio being reached earlier than if the hydroxyl concentration had remained constant throughout. As an indication of the principle, an arbitrary depth can be chosen from table 3.1, i.e 1.05cm. At that depth the actual chloride to hydroxyl ratio is 3.35, but if the hydroxyl concentration had remained at around 390mM/litre, the ratio would have had a lower value of 1.47.

In summarising the results the following points arise:

(i) Free and total chloride ingress obeys Fick's 2nd law of diffusion to a good approximation, enabling a diffusion coefficient to be calculated for each.

(ii) The C_3A phase present in portland cement paste, by reacting with part of the chloride, causes some reduction in the penetration rate of free chloride as compared to total chloride.

(iii) A ratio of the two diffusivities ($D[Cl^-]FREE/D[Cl^-]TOTAL$ = 0.65 for this cement) may be taken as an indication of the cement's ability to remove chloride from solution.

(iv) The ratio of free to total chloride is concentration dependent and increases as the total amount of chloride increases. This means that for higher chloride levels a lower proportion of the chloride is present in the "bound" form because the paste approaches its saturation point in chemically bound chloride allowing more of the chloride to remain soluble.

(v) Counter-diffusing hydroxyl ions also obey Ficks 2nd law of diffusion to a good approximation. Hydroxyl ions appear to diffuse at a faster rate in this OPC compared to free chloride.

As migration of OH^- and Cl^- ions obey the diffusion laws, it should be possible to determine diffusion coefficients for a variety of cements with their respective $D[OH^-]/D[Cl^-]$ ratios. Where applicable, the relative diffusivities and hence ease

of reprenishment of chloride and hydroxyl ions to the corrosion sites, may give an indication of the cements ability to sustain a corrosion pit and encourage corrosion propagation.

It is mainly this last point that prompted the determination of hydroxyl diffusion coefficients for a variety of cements whose chloride diffusivities were already known. This work is reported in part II of this chapter.

PART II THE DIFFUSION OF HYDROXYL IONS IN HARDENED CEMENT PASTE.

3.6 INTRODUCTION AND LITERATURE REVIEW

Diffusion of ions in hardened cement pastes is a relatively slow process and often excessively long exposure periods are necessary to enable the accurate calculation of diffusion coefficients with the method described in part I. An alternative experimental technique is therefore necessary for the speedier determination of the coefficients.

Such a technique was developed [28,77,78] on the basis of Fick's 1st law of diffusion, viz ,

$$J = -D \frac{dc}{dx}$$

where J = the amount of substance passing perpendicularly through a surface of unit area during unit time.

D = the diffusion coefficient

and $\frac{dc}{dx}$ = the concentration gradient of the diffusing substance in the direction of diffusion.

For a thin disc of cement paste, it is possible to find the diffusion coefficient D, by knowing the flux J, while keeping the unequal concentrations on either side of the disc effectively constant.

The most usual way to achieve this, is to have the cement

disc "sandwiched" between two compartments, one containing a solution of a high concentration of the investigated ionic species and the other, a much lower concentration of the same solution so that any small increase in the latter, although detectable, is insignificant compared to the difference in the concentration of the two cells (see fig. 3.11). This increase in concentration with time is linear and represents the amount of diffused substance per unit area of the disc, ie the flux, which is proportional to the diffusion coefficient. (A full explanation of the technique and the theory behind it can be found in paragraph 3.7.2 and 3.8).

Atkinson and Nickerson[79] termed their diffusivities found in this way the intrinsic diffusion coefficients because they do not represent the flux flowing through a cross-sectional area of the liquid, but that through the area of the medium. Consequently, the calculated values of D would be underestimated by a proportion related to the porosity. They were also critical of this type of set-up for the fact that if a high concentration of a solution is in contact with the one surface of the disc and a solution of low concentration with the other, an osmotic flow of liquid may result from the low to the high concentration side.

A further criticism of the technique is that it does not resemble any real life situation, but despite its limitations, the speed, non-destructive nature, and small specimen requirement justify its use in obtaining effective diffusion

TABLE 3.5 Activation energies for diffusion of chloride ions in OPC-B pastes.[ref. 28]

TABLE 3.6 Effective diffusion coefficients of chloride ions at 25°C in various cement pastes of w/c 0.5 [ref.28]

coefficients for the purpose of comparison, between cement types or of other variables.

It is the speed and simplicity of the technique that enabled the comprehensive study on the diffusion of chloride through a portland cement at various temperatures and w/c by Page et al [28]. For each w/c they obtained a linear relationship between the reciprocal of the absolute temperature and the logarithms of the effective diffusivity enabling the calculation of activation energies (table 3.5). The fact that they were able to do so suggested, as they pointed out, that a single dominant process controlled the diffusion of the ions. The activation energy for each of the three w/c were in excess of values characteristic of the diffusion of chloride ions in normal electrolyte solutions, which are typically in the region of 17.6 kJ/mole [80]. They concluded from this that a form of surface interaction between the diffusing ions and the cement paste particles might be the rate-limiting process, but were unable to suggest the precise nature of the interaction. They speculated that it may involve "desorption of the diffusing ions from binding sites on the pore walls and/or structural rearrangements necessary to accomodate ion migration through surface bound water".

Additions of PFA and particularly BFS to the OPC resulted in a considerable decrease in the mobility of the chloride ions through the pastes (table 3.6). They assumed that,

since these reductions could not be attributed solely to the respective pore size distributions, different mechanisms of diffusion rate control must be involved.

Japanese researchers [77, 81 - 83] carried out a lot of work using the same techniques, determining effective diffusion coefficients for a variety of ionic species. The results of Kondo et al [77] for a 0.4 w/c portland cement paste cured for 28 days in saturated lime, are summarised in table 3.7. Their calculated diffusion coefficients of the various ions were in the decreasing order of D_{Cl^-}, D_{K^+}, D_{Na^+}, D_{Li^+} but all were in the order of 10^{-7}-10^{-8} cm^2s^{-1}.

They had also found that the diffusion of the chloride ions was greatly affected by the co-diffusing cations and decreased in the order, $MgCl_2$, $CaCl_2$, LiCl , KCl, NaCl. The faster chloride diffusion compared to that of the accompanying cation, was explained by the authors by the counter-diffusion of hydroxyl ions.

It is evident from the above results that effective diffusion coefficients of ions through cement paste are reduced by several orders of magnitude as compared to their diffusivities in infinitely diluted bulk solutions, with values for, D_{Li^+}, D_{Na^+}, D_{K^+}, D_{Cl^-}, of 1.04, 1.35, 1.98 and 2.03 x 10^{-5} cm^2s^{-1} respectively [80]. The most interesting aspect of these results is the degree of reduction with ratios of D bulk/D cement paste, of 717, 608, 600 and 263 respectively (in the same order as above).

TABLE 3.7 Effective diffusion coefficients of various ions in OPC pastes of w/c 0.4.[ref. 77]

TABLE 3.8 Effective diffusion coefficients of OH^- in OPC-B pastes at different temperatures.

TEMP. (°C)	$Dx10^9$ (cm^2s^{-1})
9	40.2
15	77.3
25	112.6
35	184.7
45	334.0

Clearly, the effect is more prominent for the cations than for the chloride anion, perhaps indicating some form of electropositive interaction with the cement particle surfaces.

An explanation for this effect was put forward by Takagi et al [83] who had determined diffusion coefficients for Na^+ and I^- using the same technique through a selection of cements. They suggested that the reason why the cation diffused faster than the anion was because of the electric double layer. The surface of cement hydrates are, according to them, positively charged because of the adsorption of Ca^{++} ions. The resultant electric double layer [84] attracts the anions towards the surface enabling them to enter the micro-pores and hence diffuse easier, whereas the repelled cations are reluctant to do so.

As was also shown by Page et al [28] for chloride diffusivities, the addition of fly-ash to their portland cement decreased the effective diffusion coefficients of both Na^+ and I^- ions, but unlike Page et al, they explained the effect purely by the lowering of the pore volume of pores smaller than 20Å in radius. Although their reasoning was not clear, the implication is that for ionic diffusion to occur, ions must penetrate such small pores at some stage.

Uchikawa et al [82] confirmed the reduction of the mobility of Na^+ ions in fly-ash cements and observed a similar

reduction, though to a lesser extent, with slag cements. Contrary to Takagi et al [83] they attributed this reduction, at least partly, to the increase in zeta potentials [84] of the "pozzolanic" cements. They suggested that the higher zeta potentials of these cements are caused by more easily adsorbed Na^+ ions onto the C-S-H gel decreasing their mobility.

Despite the reviewed extensive studies on diffusion of ions in cements, a large gap still exists with regards to the hydroxyl ions. The importance of the migration of hydroxyl ions in cement matrices and particularly their relation to chloride mobility for steel reinforcement corrosion, as mentioned earlier, prompted the work reported in this part of chapter 3, in an attempt to "plug" the existing gap. It describes work involving the determination of effective diffusion coefficients of hydroxyl ions in the cements previously used by Page et al [28] and Holden et al [9] for chloride diffusivity calculations, with an adaptation of their "thin-disc" technique.

3.7 EXPERIMENTAL PROCEDURE

3.7.1 Specimen Preperation

Five types of cement pastes used previously at Aston [9,28] namely OPC-A, OPC-B, SRPC, OPC-B/30% PFA and OPC-B/65% BFS (see chapter 2 para. 2.1) were prepared as described in

chapter 2 (para. 2.2). After an initial 3-day curing period in their moulds, they were demoulded and their middle sections sliced into 3mm discs as described in chapter 2 (para. 2.2). The discs were then stored in a solution of 0.032 molar NaOH, or in one occasion in a solution of 0.032 molar KOH, for a period of 60 days at a temperature of 22±2°C. The pH of the solution was monitored daily with a pH electrode (see chapter 2 para. 2.4.2) and replaced when it approached pH 12.9. A minimum pH of 12.5 was chosen for the curing solutions in order to minimise the leaching of $Ca(OH)_2$ from within the cement pastes.

Three OPC-B' paste specimens after their initial 1 year curing period in their moulds at 22±2°C, were sliced in 3mm discs as above and stored in a saturated $Ca(OH)_2$ solution for a further 2 months.

The variety of cements and curing conditions were chosen so that the following factors could be investigated for their effect on diffusion.

(i) Temperature for specimens of constant cement composition and curing condition,

(ii) Curing condition and accompanying cation for specimens of fixed cement composition at constant temperature.

(iii) Variations in cement composition for

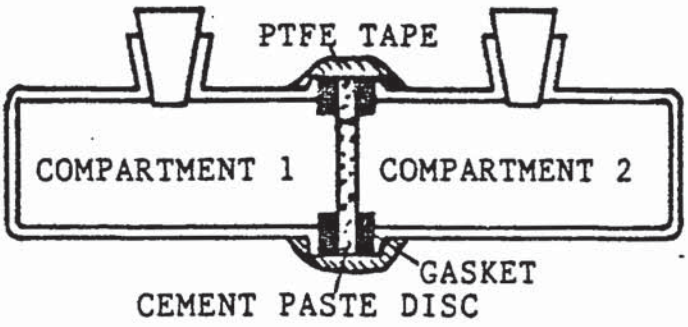

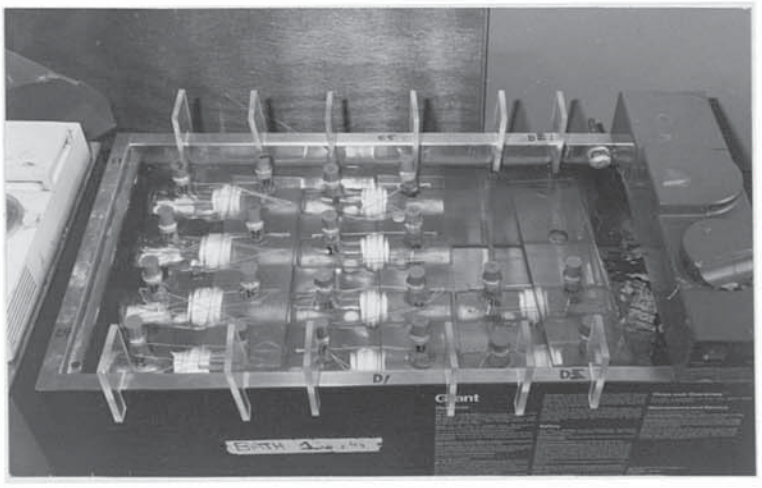

FIGURE 3.11 Diffusion cell and set-up.

specimens at constant curing condition and temperature.

3.7.2 Experimental Set-Up

Figure 3.11 depicts the cell used for the diffusion experiments and is the same as that used by Page et al [28]. For factors (i) and (iii) (see above) compartment 1 of the cell was filled with a 1M NaOH solution and compartment 2 with a known volume (normally 80ml) of 0.032M NaOH. The controlling parameter for the "background" solution used in the diffusion cells was the curing solution, as the two had to be identical in order to avoid leaching of other ions which could interfere with diffusion. For factor (ii) therefore, a known volume of one of the three types of solution required for the curing of the OPC-B discs, namely 0.032M NaOH, 0.032M KOH or saturated $Ca(OH)_2$, was used for compartment 2 of the cell, with 1M NaOH, 1M KOH or saturated $Ca(OH)_2$ + 1M NaOH respectively filling compartment 1.

Either 5 or 6 cells were set-up for each condition which were placed in a water bath of the required constant temperature (fig. 3.11). On a regular basis, 100µl aliquots of the compartment 2 solutions were withdrawn and analysed for hydroxyl and-in the case of the discs in $Ca(OH)_2$ - for sodium concentrations by the methods described in chapter 2 (para. 2.4). The withdrawn solution was not replaced as the overall reduction in volume was negligible.

The experiments were terminated before the concentration of the solution in compartment-2 had reached 0.1 molar, after at least 5 readings had been recorded. This normally required a period of 1 to 3 weeks but in the case of BFS based cement pastes, periods of up to 3 months were necessary. At termination, the average thickness of the discs was determined with the use of a micrometer.

3.7.3 DTA and MIP Investigations

Selected cement paste discs were analysed by DTA (see chapter 2 para. 2.8.1) both before and after being subjected to diffusion to detect any possible changes in the hydrates.

In order to determine whether the curing condition had any effect on the porosity and hence diffusion rate, cement discs from each condition were subjected to MIP as described in chapter 2 (para. 2.9). The results were then compared to those obtained by Page et al [28] for the same cements cured in limewater for 60 days.

3.8 RESULTS

Figure 3.12 represents a typical plot of concentration in compartment 2 of the cell versus time of diffusion. It can be seen that after a period when diffusion becomes established across the disc, the rise in concentration C_1 is linear with time-the concenctration C_1 remaining effectively constant. If it is assumed that conditions of quasi-steady-state diffusion are operating across the disc, then the

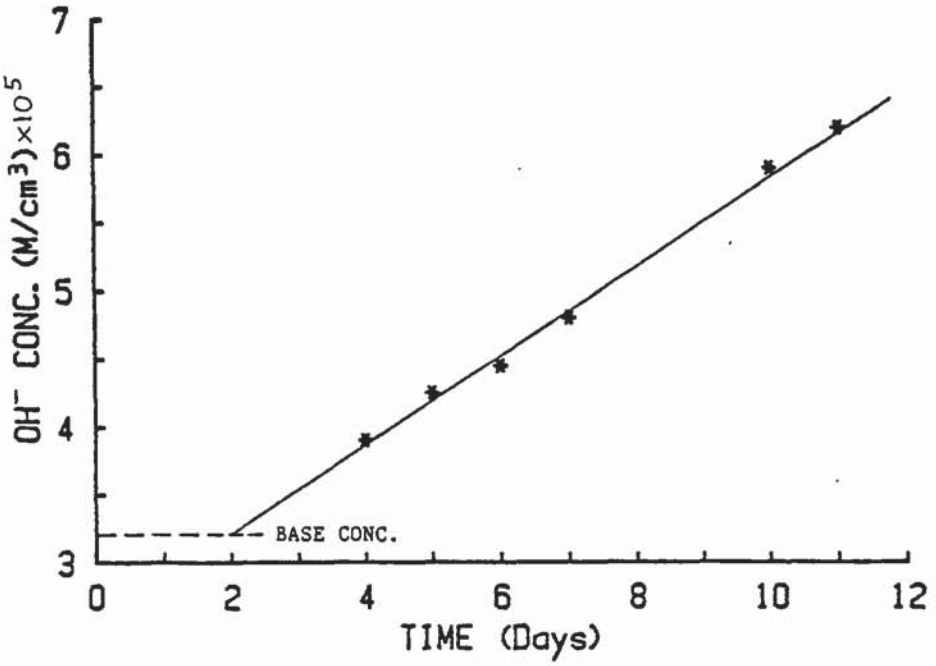

FIGURE 3.12 Typical plot of rise of ionic concentration in compartment 2 of the diffusion cell with time.

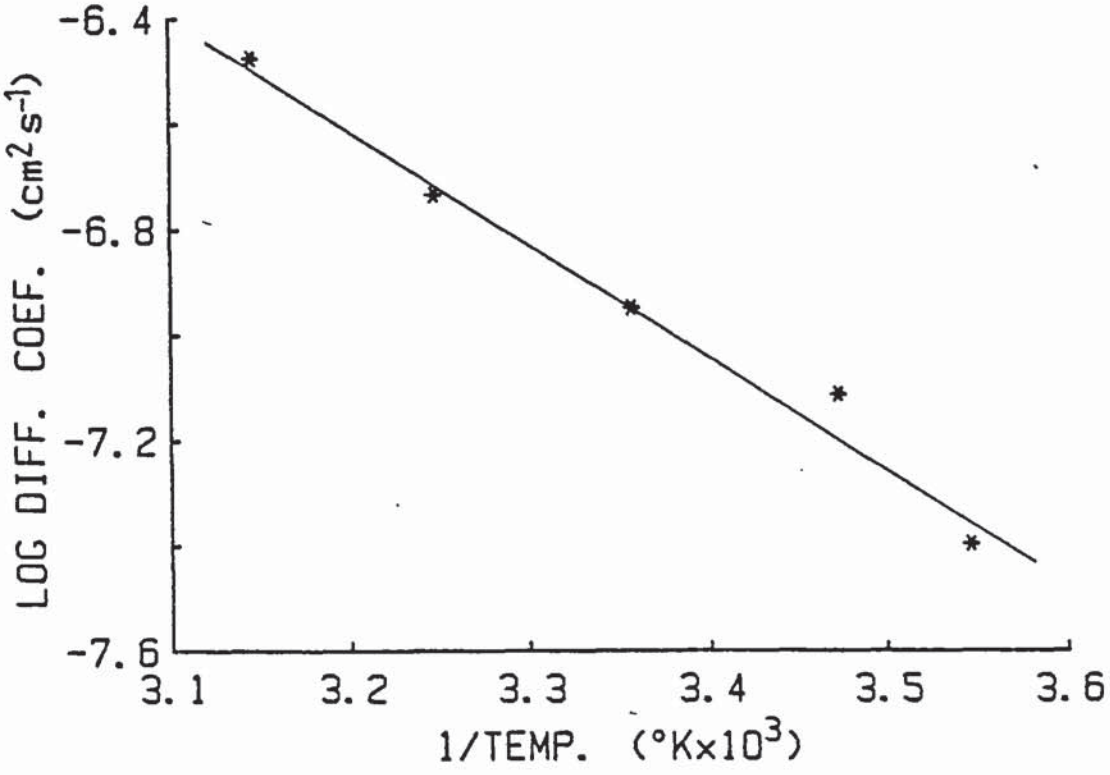

FIGURE 3.13 Arrhenius plot for hydroxyl diffusion in OPC-B.

flux and activity of the diffusing ion remain effectively unchanged throughout the disc.

From Fick's 1st law (see para. 3.6) the flux (J) in moles $cm^{-2}s^{-1}$ of the ion entering compartment 2 is given by:

$$J = \frac{V}{A}\frac{dC_2}{dt} = -D\frac{(C_1-C_2)}{l}$$

where, V = the volume of compartment 2 (cm^3)

A = the cross-sectional area of the disc (cm^2)

C_1 = the concentration of the ionic species in compartment 1 ($mole/cm^3$).

C_2 = the concentration of the ionic species in compartment 2 ($mole/cm^3$)

t = the time (sec)

l = the thickness of the disc (cm)

D = the Diffusion Coefficient (cm^2s^{-1})

This can be simplified to:

$$D = \frac{SVl}{A(C_1-C_2)}$$

where, S = the gradient of the rectilinear plot C_2 v's t (see appendix 11)

Values of D can thus be easily calculated (see appendix 11). The full values of the calculated effective diffusivities are tabulated in appendix 12.

The average effective diffusion coefficients of hydroxyl ions in OPC-B cement paste at individual temperatures are

tabulated in table 3.8. From the results an Arrhenius plot of log D versus the reciprocal of absolute temperature (fig. 3.13) was constructed by means of linear regression analysis (see appendix 13). Its correlation coefficient was calculated to be -0.965. The activation energy for diffusion of hydroxyl ions in OPC-B paste was calculated by the slope of the resultant linear plot (see appendix 13) and had a value of 41.3 ± 4.5kJ/mole (95% confidence limits).

Table 3.9 represents the effective diffusion coefficients for hydroxyl ions for the same cement but subjected to varying curing conditions or exposed to different cationic species. The effective diffusivity of the accompanying sodium ions for the cement exposed to a saturated $Ca(OH)_2$ solution is also shown in the same table.

The influence of variation in cement composition on the effective diffusion coefficient of hydroxyl ions can be clearly seen in table 3.10. The equivalent chloride effective diffusivities calculated by Page te al [28] and Holden et al [9] are shown in the same table together with the ratio $D[OH^-]/D[Cl^-]$ for each cement. This is a parameter which may be important to an extent, for the evaluation of the degree of corrosion susceptibility of the steel reinforcement surrounded by the cement matrix, a point which will be discussed later.

The MIP results are summarised in figure 3.14 and have simi-

TABLE 3.9 Effective diffusion coefficients of Na^+ and OH^- in OPC-B for different curing conditions at 25°C.

CURING CONDITION	$Dx10^9$ (cm^2s^{-1}) OH^-	Na^+
60 DAYS IN 0.032M NaOH	112.6	——
60 DAYS IN 0.032M KOH	127.4	——
360 DAYS IN SAT. AIR + 60 DAYS IN SAT.$Ca(OH)_2$	90.1	84.3

TABLE 3.10 Effective diffusion coefficients of OH^- and Cl^- at 25°C in various cement pastes of w/c 0.5.

TYPE OF CEMENT	$Dx10^9$ (cm^2/s^1) OH^-	Cl^-	$\frac{D[OH^-]}{D[Cl^-]}$
OPC-A	34.1	31.5+	1.1
OPC-B	112.6	44.7*	2.5
SRPC	83.2	100.0*	0.8
OPC-B/30% PFA	37.3	14.7*	2.5
OPC-B/65% BFS	5.7	4.1*	1.4

+ Ref. 9

* Ref. 28

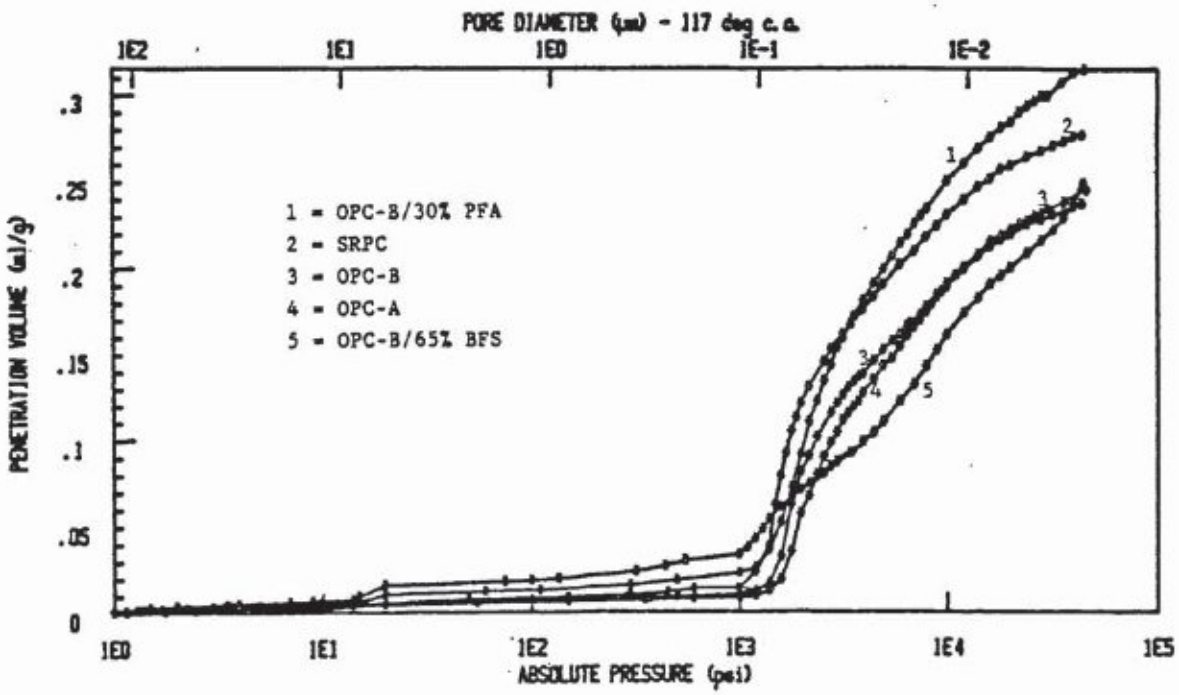

FIGURE 3.14 Pore size distribution curves of cement pastes after curing in 0.032M NaOH for 60 days.

FIGURE 3.15 Pore size distribution curves of cement pastes after curing in sat.$Ca(OH)_2$ for 60 days [ref 28]

lar pore size distributions to those determined by Page et al [28] (fig. 3.15) for 4 of the cements cured in saturated lime. NaOH curing has however resulted in slight and fairly consistent increases in the total porosities of all the cements, but these alone can only cause small changes in the effective diffusion coefficients (see also discussion of results later).

DTA thermographs of the cements before and after diffusion did not show any significant changes (see for example Fig. 3.16) indicating that the diffusion of hydroxides through the cement pastes did not alter their hydrated phases.

3.9 DISCUSSION OF RESULTS

As can be deduced from table 3.9 the effect of the co-diffusing cation on the effective diffusion coefficient of hydroxyl ions is minimal. Statistically there is no significant difference at the 5% level between the calculated diffusivities whether the accompanying cations were Na^+ or K^+ (for the full calculation see appendix 14). There is however a small but significant reduction when the curing condition is altered. This change can be wholly attributed to the porosity of the two samples, as the longer curing period and different curing condition of the saturated air/limewater cured specimen caused a reduction in the total porosity (see fig. 3.17).

From the same table (3.9) it can also be seen that Na^+ and

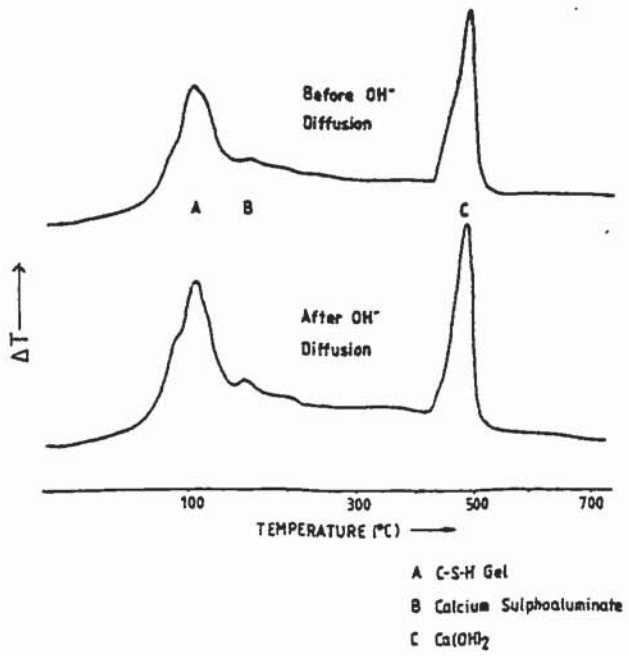

FIGURE 3.16 DTA thermographs of OPC-A pastes before and after being subjected to OH^- diffusion.

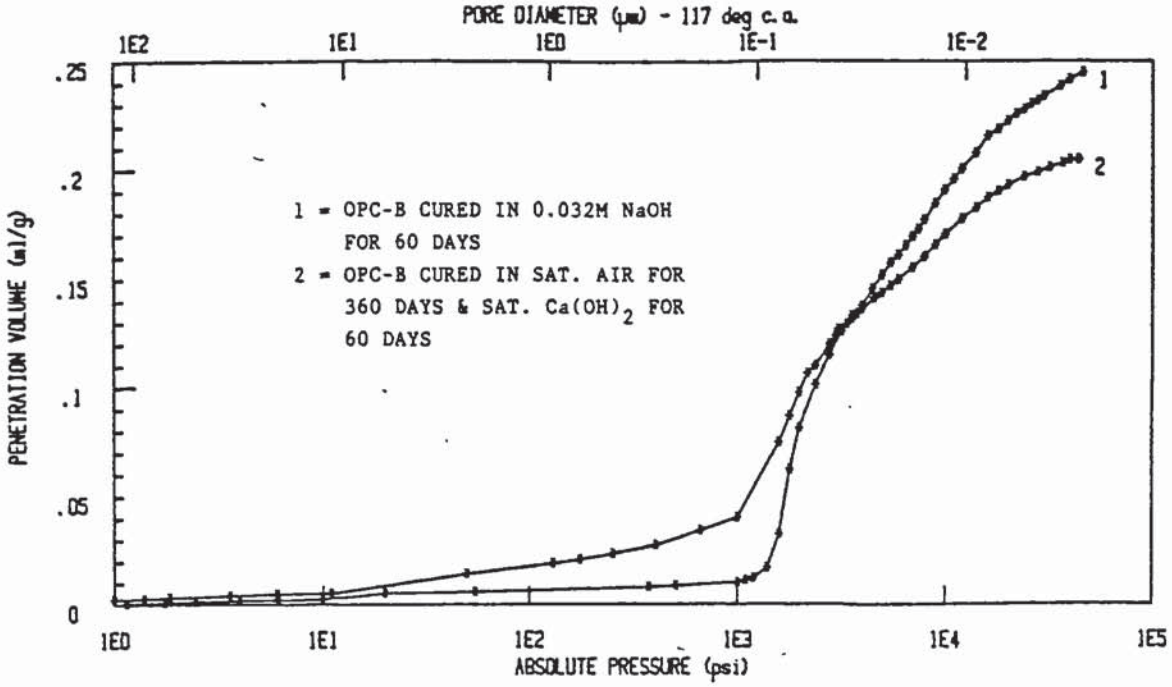

FIGURE 3.17 Pore size distribution curves of OPC-B pastes subjected to different curing conditions.

OH^- ions, for the condition studied had diffused at the same rate*. This is not consistent with the observations of others [77,83,85] that anions are more mobile than the accompanying cations. The explanation offered by Kondo et al [77] (see also intro. part II) was that the higher rate of chloride diffusion in their experiments is caused by the counter-diffusion of hydroxyl ions.

This concept is verified in chapter 5 part I where it is shown that the excess in Cl^- compared to Na^+ ions in compartment 2 of the diffusion cell is consistent with an equivalent increase of the OH^- concentration in compartment 1. In the case of hydroxyl diffusion, as there is no other available anionic species, no counter diffusion effect is possible. For a "charge" balance to be maintained across the disc and in the two cells, hydroxyl ions can only diffuse at the same rate as the sodium ions.

At first sight it may be assumed that the hydroxyl ions in this diffusion situation are controlled entirely by the Na^+ ions and that their diffusion rate is reduced to that of the cations. The effective diffusion rate of Na^+ shown in table 5.7 (chapter 5), however, suggests otherwise. There, the diffusivity is $50.6 \times 10^{-9} cm^2 s^{-1}$ for the same cement paste and curing condition with NaCl as the diffusant, a much lower value than the present $84.3 \times 10^{-9} cm^2 s^{-1}$. The

* All comparisons are made statistically and an example is shown in appendix 14.

actual mechanism may therefore, be one of a mutual influence. The cation slows down the anion to an extent so that both end up diffusing at the same "compromised" rate. As far as chloride diffusion is concerned, its naturally faster rate is, at least partly, satisfied by counter-diffusing anions.

The ratio of $D[OH^-]/D[Cl^-]$ (table 3.10) may not therefore represent a true parameter for each cement as the diffusion mechanisms of the two sets of anions in the separate diffusion experiments are not essentially the same. The concept is further complicated by the apparent sensitivity of the chloride effective diffusion coefficient to the original curing of the cement [28], an effect which does not appear to influence hydroxyl diffusion (table 3.9).

The ratio is still useful, however, for the direct comparison of different types of cements. The known individual influences on diffusion rates in these experiments are, an increase of chloride diffusivity caused by counter-diffusion of hydroxyl ions and a small increase of the hydroxyl diffusivity from a slightly increased porosity; both effects can be assumed for all cements. In addition chloride diffusion may be influenced by the amount of C_3A present in the cement as shown in part I.

The cements can then be ranked according to their $D[OH^-]/D[Cl^-]$ ratio and related to their C_3A contents and ability

to bind chloride (table 3.11). The cement's chloride binding capacity is represented in the last column of table 3.11 (taken from table 6.3) which shows each cement's free to total chloride ratios of 6mm thick discs exposed to a solution of saturated $Ca(OH)_2$ + 0.5M NaCl for 314 days.

It appears from table 3.11 that the C_3A content of the cement, or its chloride binding capacity are the most influential parameters on the diffusivity ratios. One exception is the BFS but as diffusion through this cement was extremely slow, the resultant larger error involved in the calculations may justify the deviation.

As mentioned earlier, this ranking order would apply to situations where little hydroxyl replenishment exists near the corrosion site either because phases such as calcium hydroxide are reduced to minimal values from the pozzolanic action of cements (ie BFS and PFA), or because of the unavailability of such phases caused by either partial neutralization of the cement matrix or by possible chemical attacks on them. In such situations the higher the $D[OH^-]$ to $D[Cl^-]$ ratio, the better the protection offered to the steel, as there will always be a tendency for increasing hydroxyl/rather than chloride concentrations near the pit site.

Perhaps a more important parameter in designing against corrosion from chloride ingress, is the actual effective

TABLE 3.11 Rank order of $D[OH^-]/D[Cl^-]$ for various cements against their C_3A contents and Free/Total chloride ratios.

CEMENT	$D[OH^-]/D[Cl^-]$	C_3A(%)	FREE/TOTAL Cl^-
OPC-B	2.5	14.2	0.290
OPC-B/30% PFA	2.5	—	0.337
OPC-B/65% BFS	1.4	—	0.233
OPC-A	1.1	7.8	—
SRPC	0.8	1.9	0.405

TABLE 3.12 Effective diffusion coefficients after "correction" as determined by two different techniques.

	EFFECTIVE DIFFUSIVITIES x 10^9 (cm^2s^{-1})					
	PART II				PART I	
	ACTUAL		CORRECTED			
CURING CONDITION	OH^-	Cl^-	OH^-	Cl^-	OH^-	Cl^-
60 days in 0.032M NaOH	112.6		261.9			
360 days in sealed moulds +60 days in sat.$Ca(OH)_2$	90.1		209.5			
60 days in sat.$Ca(OH)_2$		44.7		104.0		
90 days in sealed moulds					212.4	118.8

diffusion coefficient values. It is obvious from table 3.10 that additions of PFA, and particularly BFS to OPC has decreased the mobility of both hydroxyl and chloride ions. Others [82,83,85] have shown this to be true for a variety of ionic species.

As mentioned by Page et al [28] the slower diffusion by these cements cannot be explained by differences in their porosities (fig. 3.15). As an example, the two OPC's have nearly identical pore-size distributions (fig. 3.14) but their hydroxyl effective diffusivities are dissimilar. The differences in the diffusion coefficients can only be caused therefore by variable degrees of surface interactions between the diffusing ions and the cement particles.

Differences in positive zeta potentials were the reason given by Uchikawa et al [82] for the reduction in sodium mobility in BFS and PFA based cement pastes. As hydroxyl diffusion is greatly influenced by the diffusivity of sodium ions the same apparent effect would be observed for the hydroxyl ions.

This general ionic mobility reduction caused by the addition of BFS or PFA to OPC would increase the protection offered to the steel reinforcement, by reducing the penetration rate of aggressive ions such as chlorides.

Comparing the activation energies obtained for OH^- and Cl^-

ionic diffusion in the same cements, it is evident that there is no significant difference between the two, both giving a value of about 41-45kJ/mole. The same rate limiting mechanism of surface interaction mentioned by Page et al [28] (see earlier) for chloride diffusion, may also apply therefore to hydroxyl diffusion.

If an assumption is made that Na^+ and OH^- ions diffuse through OPC-B at the same rate at all temperatures, which should be true as no other ions are involved, the activation energy of sodium diffusion is also that calculated for hydroxyl and consequently the same as for chloride.

If the effect of the electric double layer described earlier [83] is accepted, then it can be assumed that it is the reluctance of the accompanying cationic species to diffuse ie the Na^+, which is mostly responsible for the high activation energies of both chloride and hydroxyl diffusion. In other words, it is the accompanying cations that mostly control the diffusion of the anions. An indication of this concept is found in the results of Kondo et al [77] which were discussed earlier, showing a dependence of chloride diffusion on the accompanying cation.

Effective diffusion coefficients determined by the steady-state method, described in this part of the chapter, were consistently lower than those obtained in part I. This is not altogether suprising if it is remembered that, as sug-

gested by Atkinson and Nickerson [79], the cross-sectional area of the cement paste disc is not representative of the "true" cross-sectional area. If an assumption is made that ionic diffusion occurs only in the pore solution through "continuous" pores, the "pore" cross-sectional area of the disc as a fraction to the total area can be estimated from the result of a typical pore-size distribution curve for the particular type of cement. (For the calculation see appendix 18). For OPC-B the "correction" factor would thus be 0.43, giving comparable diffusivities for both OH^- and Cl^- as calculated by either method (see table 3.12).

The results may finally be summarised as follows:

(i) As was shown by one test condition, OH^- ions diffuse through non-contaminated cement paste at the same rate as Na^+ ions because there is no possible anionic exchange capacity as exists with chloride diffusion.

(ii) Diffusivity of hydroxyl ions, as is the case for chlorides, is lowered by the addition of PFA and particularly BFS, to OPC. The reduction cannot be attributed to the differences in pore size distributions. It may be explained by differing surface interactions caused possibly by changing zeta potentials.

(iii) It is possible to rank cements according to their $D[OH^-]$ to $D[Cl^-]$ ratios, a parameter which for the limited number of cements studied in this work appears to be related to the C_3A content of the cement and hence its chloride binding capacity. In certain conditions, this parameter may signify the cements ability to protect steel reinforcement.

(iv) The activation energy for hydroxyl and presumably for sodium diffusion through OPC-B cement is the same as for chloride, pointing to the same rate limiting mechanism. The mechanism may be one of anionic migration control by the slower diffusing cations whose diffusion is hampered by a surface interaction with cement particles such as that caused by an electric double layer.

It appears obvious from results in this chapter, that the migration of ions in cement paste is influenced considerably by other co-or counter-diffusing ions. For a better understanding of the mechanism of diffusion of ions in cements, it is necessary therefore to study the migration of all the relevant ions as a whole and not separate each individual ionic species. It was with this in mind that the novel techniques described in chapter 4 were developed. These were designed to study in more detail the diffusion of a set of co-diffusing ions in portland cement.

CHAPTER 4 NOVEL DIFFUSION TECHNIQUES - DEVELOPMENT OF THE IONIC DIFFUSION THEORY

4.1 INTRODUCTION

A substantial amount of work has been carried out in the field of diffusion of chloride in cements, mortars or concretes [28,55,86] (see also chapter 3) because of its importance with regards to steel reinforcement corrosion. In some cases, tentative suggestions were made [28,67] that a form of surface interaction between the chlorides as an ionic species and the cement particles alters diffusion rates in different cements, a phenomenon not found in the case of diffusion of undissociated molecules such as urea [67].

In the majority of cases however, chloride was looked at as an entity diffusing through the cement matrix and no real consideration was made of the accompanying cation. As already mentioned (chapter 3), Kondo et al [77] found a definite dependence of chloride diffusion on the type of the co-diffusing cation. It was also suggested by Takagi et al [83] that it is the positive electric double layer of the cement particles that delays cationic diffusion which in turn influences the mobility of the anions.

The apparent rate dependance of the diffusing chlorides on the accompanying cations and, as mentioned in chapter 3, a relationship between counter-diffusing anions, points to a

complex mechanism of chloride diffusion in cements.

A lack of appreciation of the complexity of the mechanism has witheld the development of the general ionic diffusion theory in cement pastes and cement-based materials; a theory that can be useful not only in the construction industry but also as mentioned by Atkinson and Nickerson [79], in other diverse areas, as in the nuclear industry for the construction of such structures as trenches for low-level waste disposal. It is essential therefore, that the ionic diffusion theory is developed, both on the actual surface interaction mechanism mentioned earlier and on the interrelation between mobile or soluble ions within the cement paste, so that any misinterpretation of experimental results is avoided.

An attempt to assist in the development of the ionic diffusion theory with regards to ionic interrelation was made and the results are reported in this chapter, which is divided into two parts. In part I diffusion of ions from chloride-rich to chloride-free cement pastes is described. This may be found in practice in concrete repair work or modular construction where one part, or "module" of the structure, may contain higher concentrations of ions than another with which it is in contact. It is however of more value as a controlled laboratory technique for the investigation of the theory of diffusion and the associated cement chemistry.

Similarly, work in part II was designed to broaden the knowledge of unidirectional diffusion of several ionic species from within cement pastes to an outer near neutral solution. This method also enabled the development of a third technique for the calculation of effective diffusion coefficients of ions in cements, by monitoring the change in concentration of the outer solution. It is a set-up which can easily be adopted for mortars and concretes and requires relatively short periods of exposure.

PART I IONIC DIFFUSION WITHIN CEMENT PASTES.

4.2 INTRODUCTION

In a simple situation when two semi-infinite solids A and B (figure 4.1) are joined together and a diffusing species C of concentration C_o on side A diffuses into side B of concentration 0, provided the two solids are of approximately the same composition, the species C would diffuse according to Fick's 2nd law of diffusion and its diffusion coefficient could be calculated from the following solution to the equation [70] (see appendix 9):

$$C_x = \frac{C_o}{2}\,[1-\text{erf}y] \quad \text{for } x > o \quad \ldots.(1)$$

$$\text{and } C_x = \frac{C_o}{2}\,[1+\text{erf}y] \quad \text{for } x < o \quad \ldots.(2)$$

$$\text{where } y = \frac{x}{2\sqrt{Dt}} \text{ and}$$

x = the distance from the interface-cm (+ve towards B and -ve towards A)

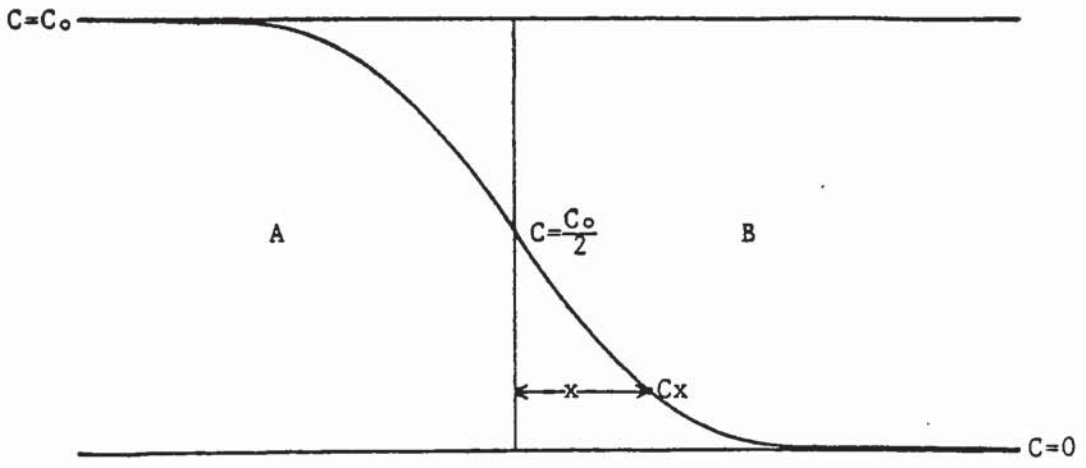

FIGURE 4.1 Diffusion of species C from a semi-infinite solid A to a semi-infinite solid B according to Fick's 2nd law of diffusion.

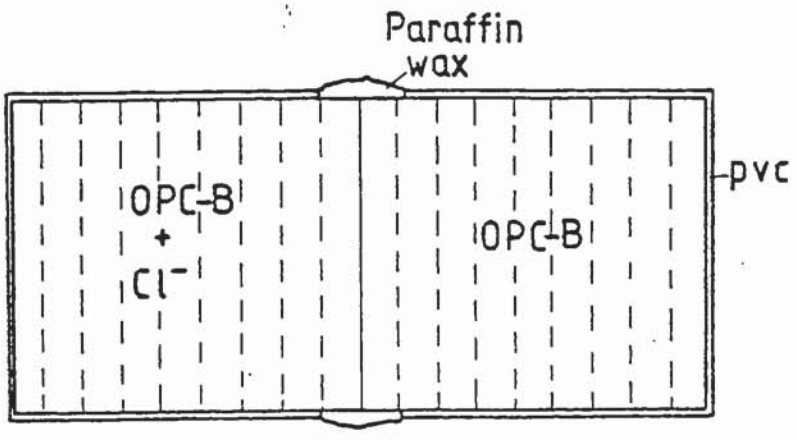

FIGURE 4.2 Specimen set-up for the diffusion of chloride from contaminated to uncontaminated OPC-B paste.

t = time-seconds

C_x = concentration at a distance x (of any units such as mM/litre but the same as C_o).

D = the Diffusion Coefficient-cm^2s^{-1}

When part removal of the diffusing species occurs inside B, such as the complexing of the chloride by the C_3A phase, the above consideration may no longer be applicable. Added to that the necessity of an ionic charge balance along the diffusing path when other ions are involved and an electropositive cement particle surface interaction with the diffusing ions, as suggested in chapter 3 and the complexity of the mechanism becomes apparent.

The better analytical techniques developed for the work in chapter 3 part I involving the pore solution expression device (chapter 2 para. 2.3), enabled the study of this diffusion mechanism and the results are reported in this part of chapter 4.

4.3 EXPERIMENTAL SET-UP

The OPC-B cement paste preparation was essentially the same as that described in chapter 3 part I. Further cylinders were also prepared with an addition of 2% Cl^- by weight of cement as NaCl (see chapter 2 para.2.2). Two specimens one of which contained the NaCl, after the initial 90 day curing period were cemented together forming a larger cylindrical

specimen. The cementing was achieved by applying a thin layer of an OPC-B cement slurry on both freshly cut and lightly ground flat surfaces and carefully sliding them together, so preventing the entrapment of air bubbles.

Thirty-six such specimens were produced and positioned with axes vertical in a 100% RH environment at 22±2°C for 24 hours. They were then enclosed in a "case" made out of 2PVC tight-fitting containers and paraffin wax, as shown in figure 4.2. Finally all 36 cylinders were positioned with axes horizontal in an incubator maintaining a constant temperature of 25±2°C until they were required.

After 100 days, 6 such specimens were "opened-up" and sliced into discs at 7mm intervals (figure 4.7) using a "donkey" saw, a mechanical hacksaw, carefully cleaning the steel blade inbetween cuts in order to prevent chloride transfer. This new dry-cutting technique did not raise the temperature of the discs as much as the original method described in chapter 3 part I. The subsequent procedure was then the same as that described in chapter 3 part I, expressing the pore solution from groups of discs and analysing them for Cl^-, OH^- as well as Na^+ with the techniques described in chapter 2 (para. 2.4).

After 225 days, a further set of cylinders were subjected to the same procedure, this time aiming for the "overlapping" effect explained in chapter 3 (para. 3.3). The expressed pore

solution at each depth was then analysed for K^+ ions as well as Cl^-, OH^- and Na^+ (chapter 2 para. 2.4).

Free and total chloride and evaporable and non-evaporable water content determinations and phase composition analysis with the use of the DTA, were carried out in the same way as that described in chapter 3 (para. 3.3). Additionally in order to substantiate the results of the DTA, discs at different "depths" were subjected to X-ray diffraction analysis (chapter 2 para. 2.8.2).

4.4 RESULTS

The concentration profiles of Na^+ and K^+ ions at 225 days as well as that of Na^+ at 100 days are shown in figure 4.3. The depth (in cm) is as measured from the interface of the two half-cylinders, negative values indicating the depth into the part-specimen containing the original NaCl addition (side A).

In the same way, the concentration profiles of both Cl^- and OH^- at the two exposure periods are represented in figures 4.4 and 4.5 respectively. (The full tables representing the numerical values of each concentration with depth can be found in appendix 15).

Where possible, diffusion coefficients for the different ionic species were calculated by the method described in chapter 3 (para. 3.4.1) using equations 1 and 2 (para. 4.2). These are shown in table 4.1 together with their correlation

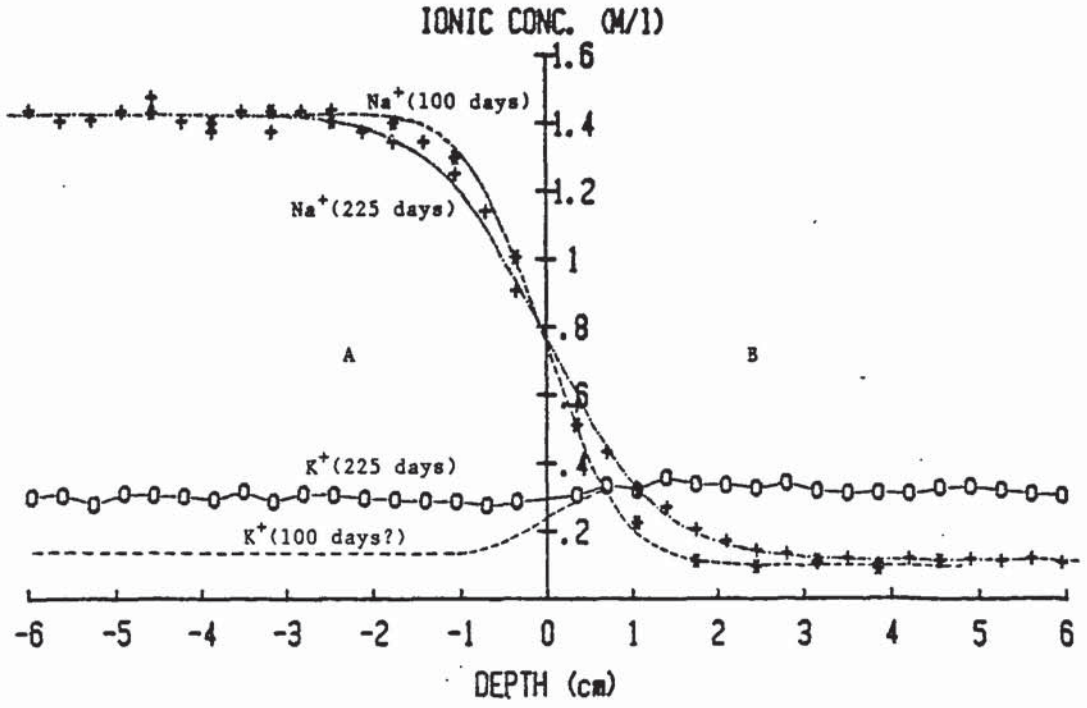

FIGURE 4.3 Na^+ and K^+ concentration profiles in OPC-B.

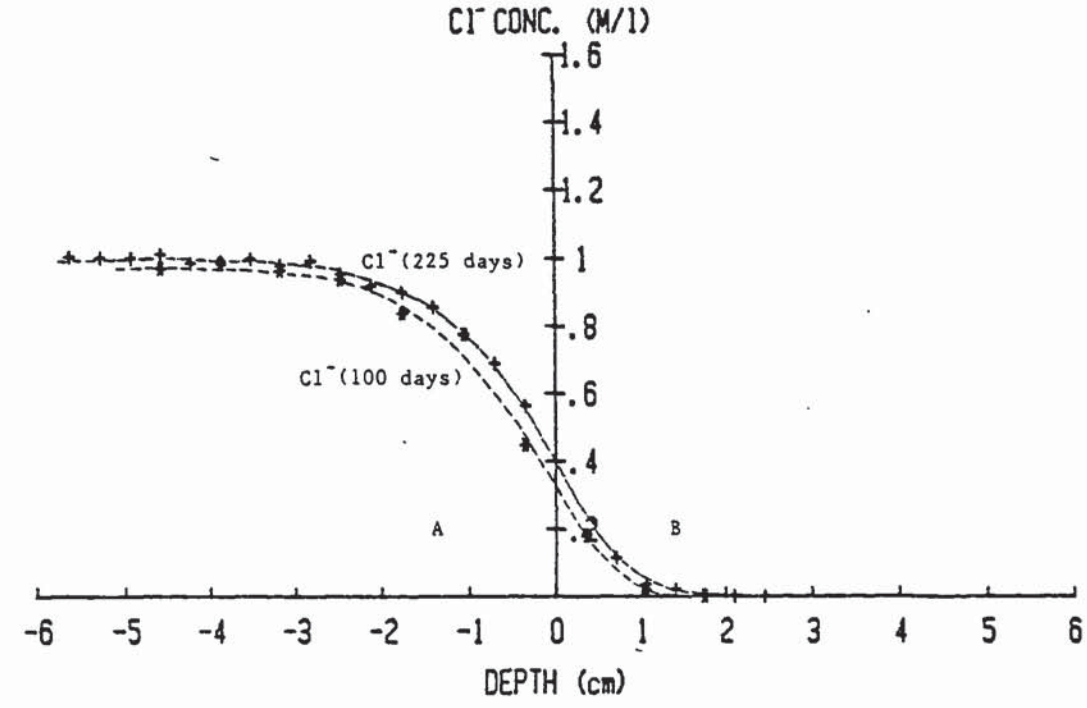

FIGURE 4.4 Cl^- concentration profile in OPC-B.

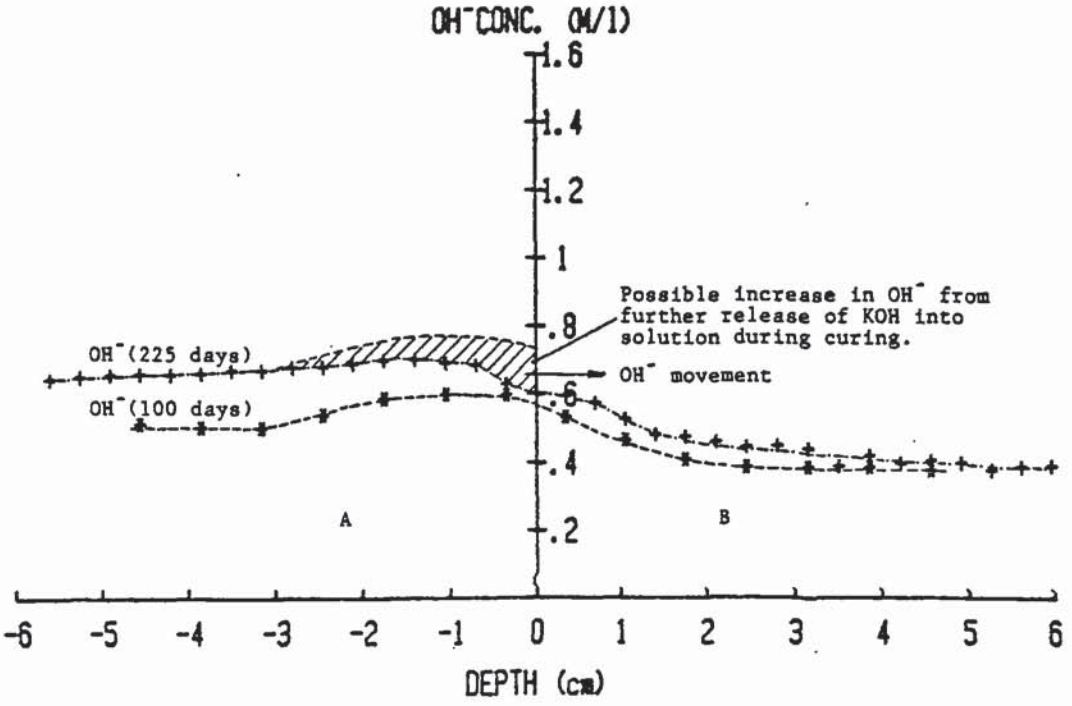

FIGURE 4.5 OH^- concentration profile in OPC-B.

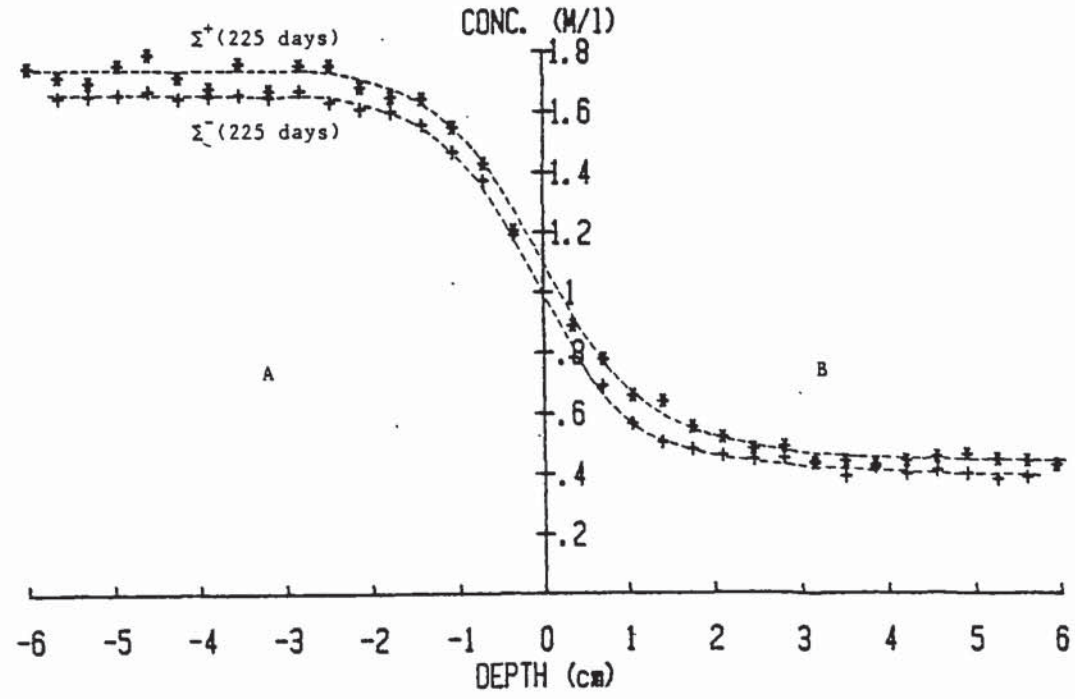

FIGURE 4.6 Σ^+ and Σ^- concentration profiles in OPC-B after 225 days.

TABLE 4.1 Diffusion coefficients of various ions in OPC-B paste as determined by concentration profiles at 100 and 225 days.

IONS	r	c (cm)	$D(x10^9)$ cm^2s^{-1}	95% conf. int. D-range $(x10^9)cm^2s^{-1}$
100 DAYS				
Σ^+	–	—	—	—
Σ^-	0.994	-0.061	36.6	29.1- 45.1
Na^+	0.999	-0.036	35.5	31.7- 39.6
Cl^-_A	0.991	-0.091	89.8	51.6-138.7
Cl^-_B	0.997	-0.049	23.9	- 98.8
TOTAL Cl^-_B	–	—	—	—
225 DAYS				
Σ^+	0.996	0.052	35.2	31.0- 39.6
Σ^-	0.994	-0.019	30.6	28.6- 32.7
Na^+	0.995	0.095	34.5	30.3- 39.1
Cl^-_A	0.995	0.257	54.5	43.2- 67.0
Cl^-_B	0.985	-0.048	12.3	5.8- 21.4
TOTAL Cl^-_B	0.991	-0.045	24.6	17.4- 33.1

r=Correlation Coefficient

c=Intercept

coefficients, intercepts C and 95% confidence intervals.

For the purpose of obtaining some diffusivity values for the chloride penetration profiles these were considered as two separate sets of curves on either side of the interface. Although not strictly true, an assumption was made here that the chloride concentration at the interface (ie at x=0) had remained effectively constant throughout most of the "exposure" period [70]. These calculated values are also tabulated in table 4.1. The sum of anions and cations at 225 days are represented in figure 4.6 (the table of values can be found in appendix 15). As these curves were typical of "diffusion" profiles, it was possible to calculated diffusion coefficients for each set and these together with that of Σ^- at 100 days are represented in table 4.1.

As mentioned in chapter 3 (para. 3.4.1), for a good fit of experimental results to the theoretical concentration profile, a correlation coefficient close to unity is required as well as an intercept of nearly zero. If the intercept differs too much from zero, then the curve deviates from the theoretical one as the interface is approached even if a good correlation is found. This is evident in the determination of the diffusivity for chloride at 225 days in side A (see also discussion later). All other penetration profiles appear to obey Fick's 2nd law of diffusion to a good approximation.

Evaporable (We) and non-evaporable (Wn) water contents with distance are tabulated in table 4.2 and are represented graphically in figure 4.7. It can be seen that We is considerably higher on side A as compared to side B even though the non-evaporable water content is essentially the same throughout. There appears therefore to have been some moisture movement from side B to the high chloride content side A, induced by the imbalance of the NaCl concentration, suggesting an osmotic effect similar to that pointed out by Atkinson and Nickerson [79] in the "thin- disc" diffusion method.

Table 4.3 represents the total, free and bound amounts of chloride in mM/g of cement, as well as the free to total ratio. The different forms of chloride are shown graphically in figure 4.8. It appears that the bound chloride (difference between the total and free amounts of chloride) remains constant throughout side A even though the free chloride concentration falls as the interface is approached. In view of the very high free/total chloride ratio throughout side A (up to 0.7) it seems that the amount of bound chloride reaches a maximum level above which any added chloride remains as free (see also chapter 7). The chloride in the bound form does not appear to diffuse into side B, so in this respect it does not significantly contribute to the overall diffusion of chloride.

Chloride concentration profiles for side B (fig. 4.8) are very similar to those obtained in chapter 3 (see figure 3.6)

TABLE 4.2 Evaporable and non-evaporable water contents with depth into OPC-B paste at 225 days.

DEPTH x (cm)	We%	Wn%	TOTAL WATER
-5.25	33.06	19.91	52.97
-4.55	31.89	19.95	51.84
-3.85	31.55	20.00	51.55
-3.15	32.03	19.48	51.51
-2.45	31.63	19.68	51.31
-1.75	32.07	20.06	52.13
-1.05	30.43	19.73	50.16
-0.35	26.60	20.13	46.73
0.35	25.61	20.78	46.39
1.05	26.13	20.97	47.10
1.75	26.15	21.30	47.45
2.45	26.19	20.79	46.98
3.15	25.45	20.68	46.13
3.85	25.42	20.60	46.02
4.55	24.51	20.62	45.13

TABLE 4.3 Total, free and bound chloride with depth into OPC-B paste at 225 days.

DEPTH x (cm)	TOTAL (mM/g)	FREE (mM/g)	BOUND (mM/g)	FREE / TOTAL
-5.60	0.513	0.332	0.181	0.647
-5.25	0.503	0.331	0.173	0.657
-4.90	0.465	0.325	0.140	0.699
-4.55	0.473	0.322	0.151	0.699
-4.20	0.491	0.313	0.178	0.637
-3.85	0.452	0.313	0.139	0.692
-3.50	0.507	0.317	0.190	0.625
-3.15	0.433	0.314	0.119	0.725
-2.80	0.451	0.316	0.135	0.701
-2.45	0.458	0.302	0.156	0.659
-2.10	0.453	0.292	0.160	0.647
-1,75	0.436	0.289	0.147	0.663
-1.40	0.404	0.267	0.137	0.661
-1.05	0.364	0.236	0.128	0.648
-0.70	0.443	0.196	0.247	0.442
-0.35	0.326	0.149	0.177	0.457
0.35	0.172	0.047	0.125	0.273
0.70	0.113	0.030	0.083	0.265
1.05	0.073	0.010	0.063	0.137
1.40	0.024	0.006	0.018	0.250
1.75	0.015	0.001	0.014	0.067
2.10	0.010	—	—	—
2.45	0.003	—	—	—
2.80	0.003	—	—	—
3.15	0.002	—	—	—

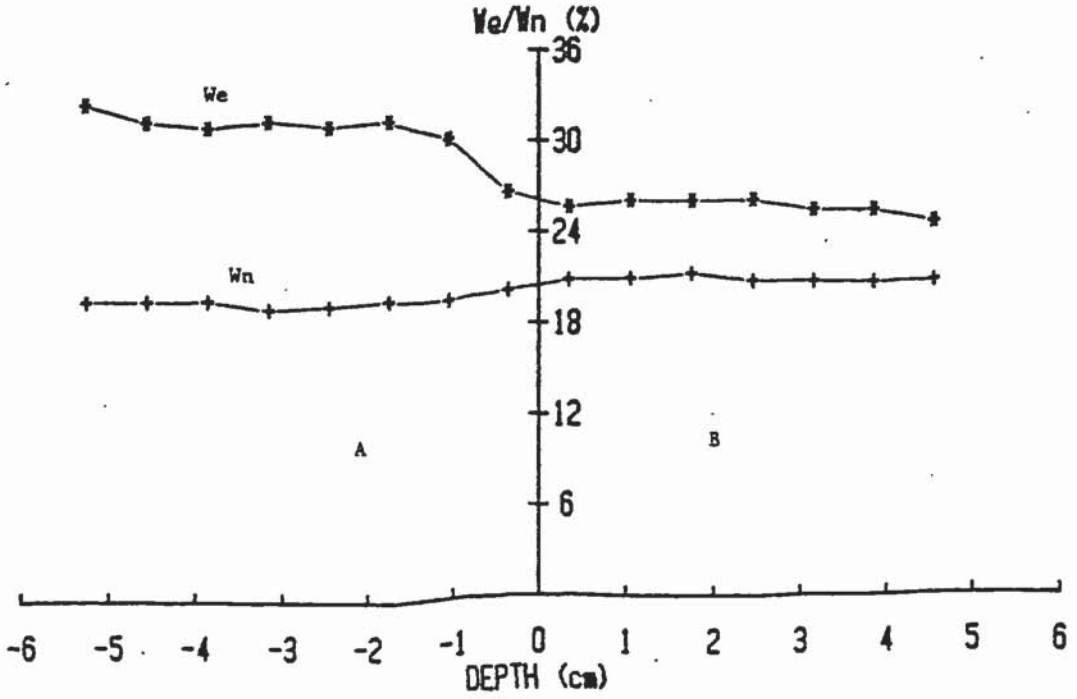

FIGURE 4.7 Evaporable and non-evaporable water content variation with depth in OPC-B after 225 days.

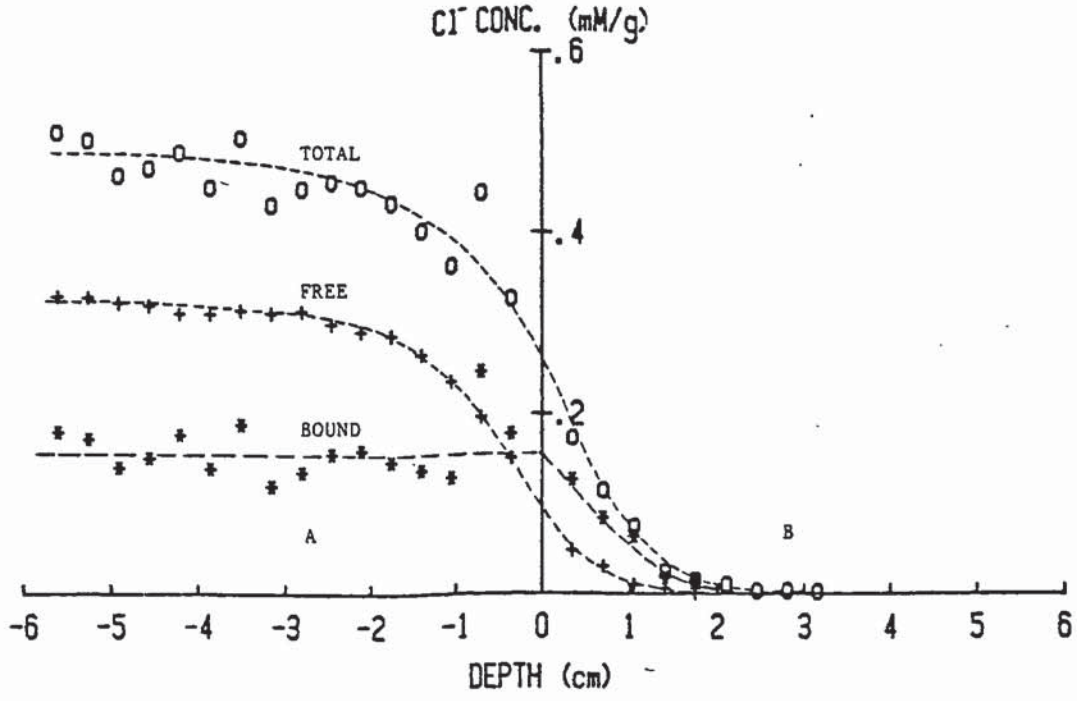

FIGURE 4.8 Total, free & bound Cl^- concentration profiles in OPC-B after 225 days.

indicating essentially the same chloride diffusion behaviour as that described in chapter 3 part I but with considerably lower diffusion coefficients. The slower overall diffusion was caused by the fewer water-filled continuous pores since the specimens were not immersed in solution, as was the case earlier (chapter 3).

DTA and X-ray diffraction analysis taken collectively (figures 4.9 & 4.10), show lowering amounts of NaCl (DTA) and calcium chloroaluminate with distance from the interface into side B up to 1.75cm. Beyond this it is difficult to detect any sign of chloride by either method. Both analytical methods indicate essentially equal amounts of the chloroaluminate phase for all depths into side A with NaCl starting to decrease appreciably at 0.35cm into A. These results which are summarised in figures 4.9 and 4.10 appear to be consistent with the actual concentration profiles.

4.5 DISCUSSION OF RESULTS

The first observation from the solution analysis results is that Na^+ ions have diffused at a constant rate of between 35 and 36 x $10^{-9}cm^2s^{-1}$ (table 4.1) giving concentration profiles very close to the theoretical ones shown by the broken lines in figure 4.3. Chloride and hydroxyl anions did not at first appear to follow suit with widely dissimilar concentration profiles (figures 4.4 and 4.5).

If however the two sets of anions are taken collectively as a

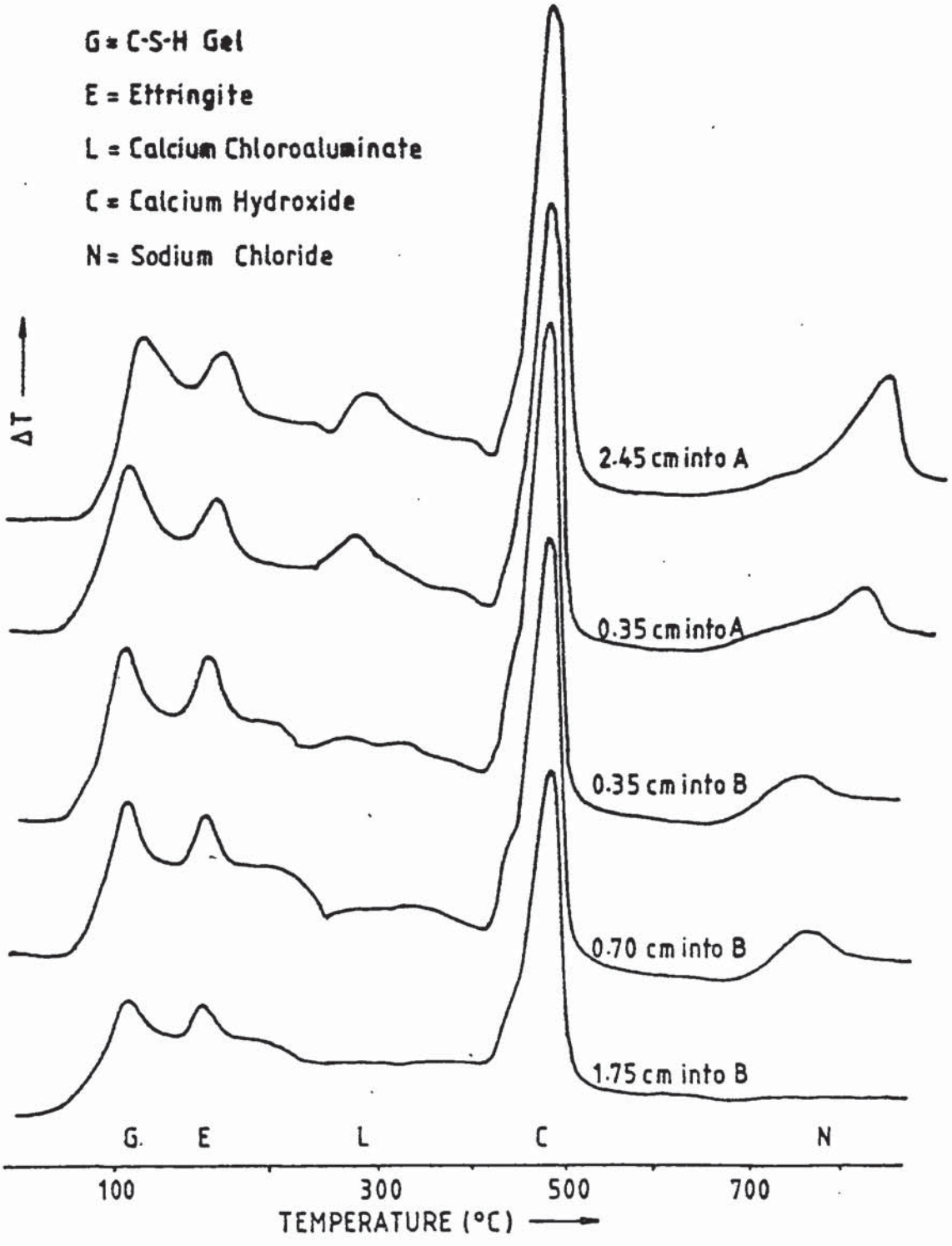

FIGURE 4.9 DTA thermographs of OPC-B samples taken at various depths after 225 days.

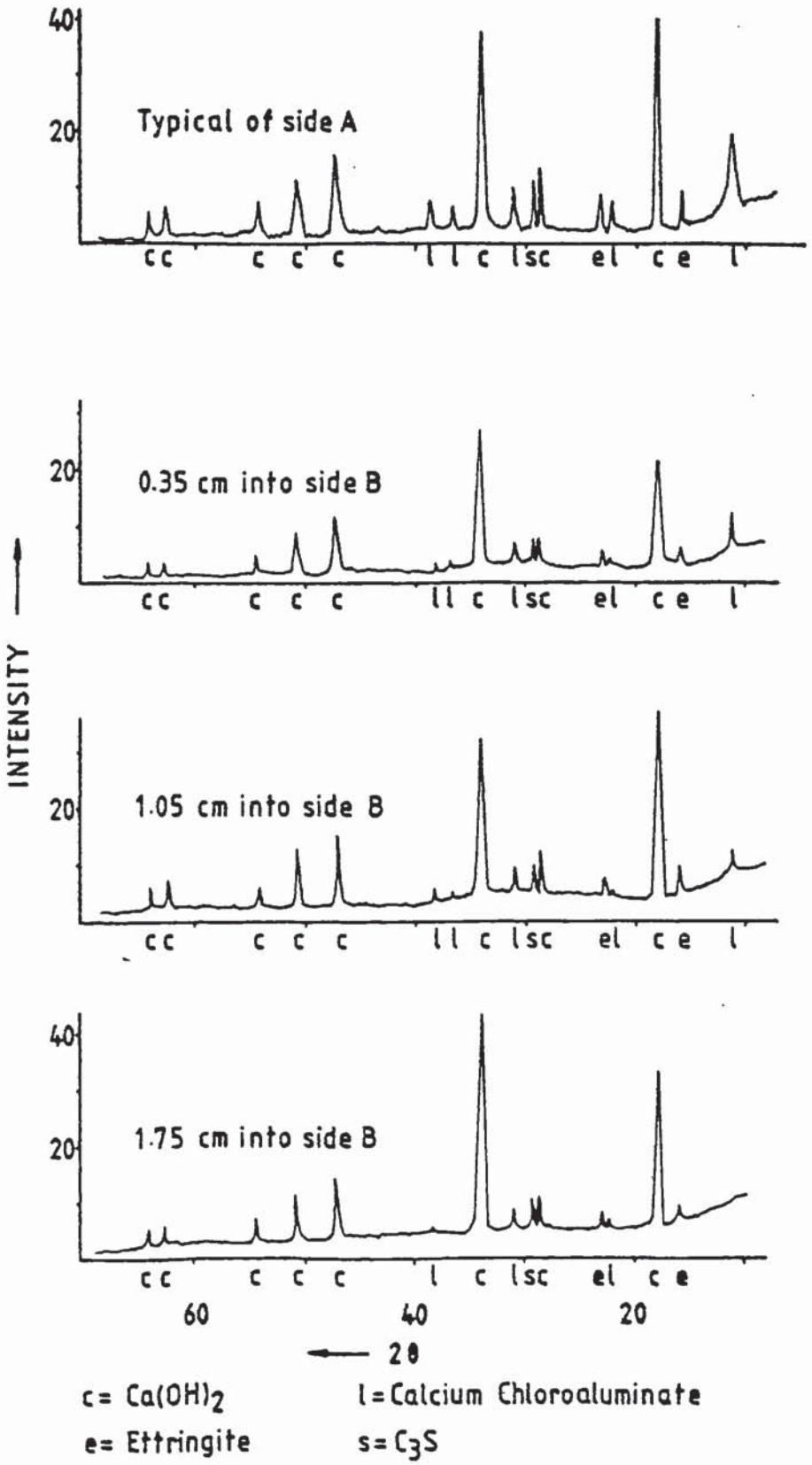

FIGURE 4.10 XRD traces of OPC-B samples taken at various depths after 225 days.

unit (Σ^-) then the resultant concentration profile is consistent with that of the Na^+ ions (fig.4.6). In addition a diffusion coefficient can be calculated which is very similar to that of the sodium (table 4.1). The same applies to Σ^+ (cations) and when the two sets of ions are plotted together (fig. 4.6) it seems likely that, in the case of the unidirectional diffusion of several ionic species as encountered in this experiment two conditions must be met.

(i) The sum of cations must equal the sum of anions at any one point along the cement paste (the slight apparent excess of Σ^+ ions is almost certainly due to the sulphate ions).

(ii) The sum of similarly charged ions diffuse as a unit at a constant rate according to Fick's 2nd law and its "apparent" diffusion rate is equal to that of the oppositely charged ions and of the same directionality.

By studying the chloride concentration profile (fig. 4.4), it becomes apparent that the free amount of chloride gained in side B is less than that "lost" in side A. This suggests that part of the free chloride which had entered side B must have been removed out of solution (see fig. 4.8), presumably by the C_3A phase, as discussed in chapter 3.

In order to investigate how the complexing of some of the free chloride may influence its diffusion and that of other

co-diffusing anions, a simple model needs to be developed. First the case of "no-complexation" of chloride will be considered with the following assumptions.

(i) The specimen arrangement is as described earlier, with initial ionic concentrations on either side of the interface as shown in table 4.4.

(ii) No K^+ diffusion takes place, as its ionic concentration is constant throughout the specimen but the concentration imbalance of the other species causes their diffusion into side B.

(iii) All three ionic species, ie Na^+, Cl^- and OH^- diffuse at the same rate of about 3×10^{-8} cm^2 s^{-1}, roughly the value determined earlier (table 4.1).

The resultant calculated concentrations at various depths along the specimen after an assumed exposure time of 225 days are tabulated in table 4.5 and the concentration profiles of the individual ions represented by figure 4.11. The above assumptions are shown to be reasonable by the fact that a charge balance is maintained along the whole specimen (fig. 4.5).

A further assumption will now be made that part of the chloride entering side B is complexed by the C_3A phase causing the release of an equivalent amount of hydroxyl ions by the

TABLE 4.4 Original ionic concentrations of model.

ION	SIDE A (M/l)	SIDE B (M/l)
Na^+	1.40	0.10
K^+	0.30	0.30
Σ^+	1.70	0.40
Cl^-	1.10	0.00
OH^-	0.60	0.40
Σ^-	1.70	0.40

TABLE 4.5 Calculated ionic concentrations of model at 225 days.

DEPTH x (cm)	Na^+	K^+	Cl^-	OH^-	Σ^+	Σ^-
-2.0	1.36	0.30	1.07	0.59	1.66	1.66
-1.5	1.29	0.30	1.00	0.58	1.59	1.58
-1.0	1.16	0.30	0.90	0.57	1.46	1.47
-0.5	0.98	0.30	0.74	0.54	1.28	1.28
0.0	0.76	0.30	0.55	0.50	1.06	1.05
0.5	0.51	0.30	0.35	0.47	0.81	0.82
1.0	0.34	0.30	0.20	0.44	0.64	0.64
1.5	0.21	0.30	0.09	0.42	0.51	0.51
2.0	0.14	0.30	0.04	0.41	0.44	0.45

TABLE 4.6 Calculated ionic concentrations of model at 225 days assuming a free/total chloride ratio in side B of 0.4.

DEPTH x (cm)	Σ^-	TOTAL Cl^-	FREE Cl^-	RELEASED OH^-	TOTAL OH^-
0.0	1.05	0.55	0.22	0.33	0.83
0.5	0.82	0.35	0.14	0.21	0.68
1.0	0.64	0.20	0.08	0.12	0.56
1.5	0.51	0.09	0.04	0.05	0.47
2.0	0.45	0.04	0.02	0.02	0.43

following possible reaction,

$$3CaO.Al_2O_3 + 2Cl^- + 10\ H_2O + Ca(OH)_2 \longrightarrow$$

$$3CaO.Al_2O_3.CaCl_2.\ 10\ H_2O + 2OH^-.$$

For the sake of simplicity the complexing ability of the cement will be assumed constant at all chloride concentrations so that the free to total chloride ratio is maintained at an arbitrary value of 0.4.

The modified chloride and hydroxyl ionic concentrations will now be as tabulated in table 4.6 and shown in figure 4.11. The buildup of hydroxyl ions in side B will cause their "back-diffusion" into A, countered by an equal amount of chloride ions moving in the opposite direction, as indicated by the arrows in figure 4.11, so that the charge balance can be maintained throughout. This anionic movement would alter the concentration profiles of the two species to roughly those shown by the solid lines in figure 4.11. The result would be that chloride anions would cross the interface at a faster rate than the sodium cations thus lengthening the "affected" depth of side A for chloride (see fig. 4.11).

If finally the variable chloride complexing capacity of the cement paste with increasing amount of chloride is also considered, the concentration profiles arrived at will be very similar to the actual results obtained (see earlier), indicating that the assumed model is a fair representation of the diffusion mechanism in such a system.

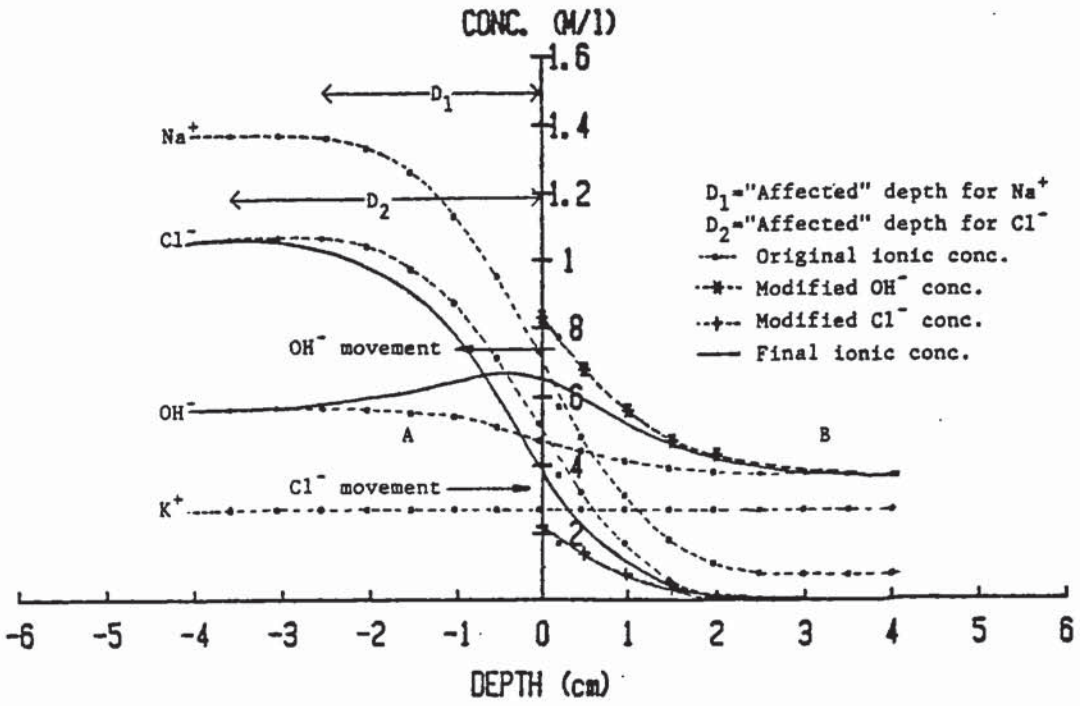

FIGURE 4.11 Model ionic concentrations at 225 days assuming a diffusion coefficient of $3x10^{-8}cm^2s^{-1}$.

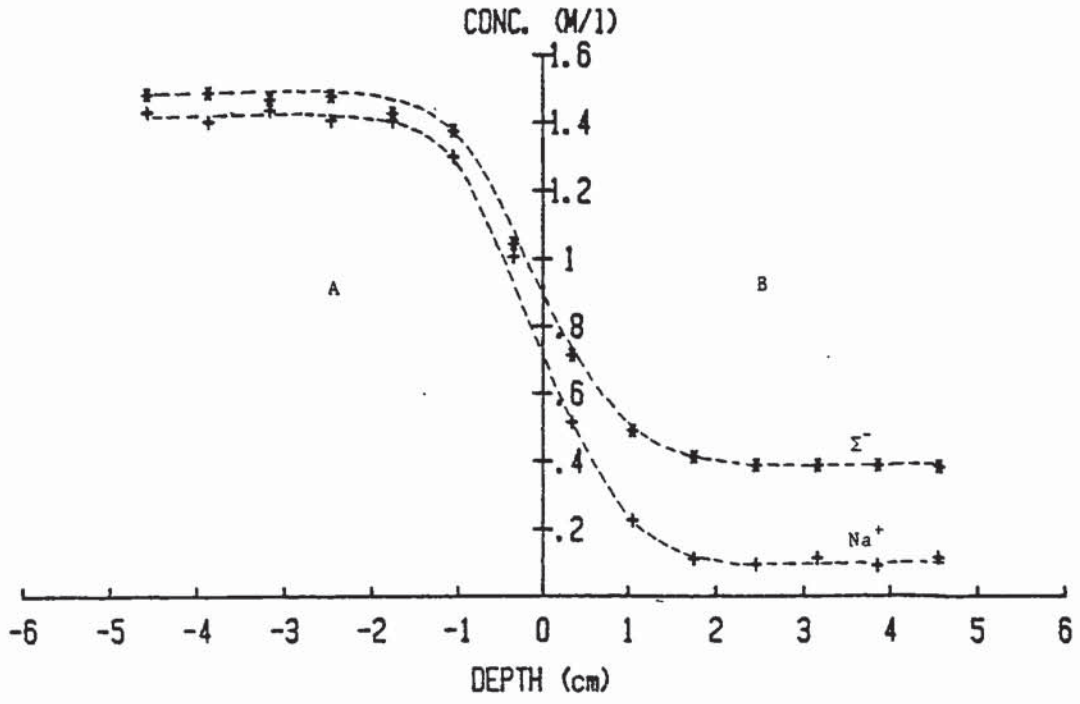

FIGURE 4.12 Σ^- and Na^+ concentration profiles in OPC-B after 100 days.

There are however slight discrepancies such as the fact that Cl^- diffusion appeared to have slowed down almost to a standstill with time, so that the concentration profiles at 100 days and 225 days appear to be almost identical (fig.4.4). The slowing down effect can be borne out of the values of the diffusivity D and intercept C for chloride in side A (table 4.1). At 225 days the intercept is unusually high and suggests a deviation of the concentration profile from the normal. The curve (fig. 4.4) is typical of a situation where diffusion of the ionic species is restricted as it approaches the surface - or in this particular case the interface - as will be shown in part II of this chapter.

The main factor for the apparent slowing down of Cl^- penetration is most probably the effect of K^+ ions. Even though the concentrations of these were not determined at 100 days, by making some assumptions they can be estimated. Figure 4.12 shows the concentration profiles of Σ^- ions and Na^+ ions. If it is assumed that the difference between the two is the missing K^+ ions then it can be seen that on side A their concentration is much lower than on side B. If this is correct, then a large amount of K^+ ions would have been released from the cement paste into the pore solution between 100 days and 225 days in order for the levels of the latter to be reached. It is not clear why this should happen but it may be due to the large amountof NaCl added to side A causing the delay of the normal release of such alkali ions

as there is an already high ionic concentration in the pore solution. The above mentioned increase in KOH is represented by the shaded area in figure 4.5. It can be seen from the figure that a large amount of OH^- ions must have diffused from A to B between 100 and 225 days instead of chloride. In other words Na^+ ions were accompanied mostly by OH^- anions during the later stages of the experiment causing the observed retardation in the chloride migration.

Evidently from the results, the migration of chloride ions in cement paste cannot be considered as a single diffusing substance but only as a part of a multitude of mobile ions which depend on each other's physical and chemical interactions with the cement particles. It is also clear, as suggested by others [77,83] that anions are more mobile in cement pastes than cations but, in the case of unidirectional diffusion, it appears that they can only penetrate the structure as far as the accompanying cations.

Finally in summarising the results it is evident that,

(i) Migration of chloride ions in cements is only a part of a complex diffusion mechanism involving all mobile ions,

(ii) An ionic charge balance must be maintained throughout the cement paste,

(iii) At least in the case of unidirectional diffusion, if the sum of similarly charged ions

is taken as a unit, this obeys Fick's 2nd law of diffusion to a good approximation, but ionic species separately may show deviation from the law when part complexing is encountered provided the charge balance can be maintained.

(iv) Anions in portland cement are more mobile than cations, pointing to a stronger cement particle surface interaction with cations.

(v) Free chloride "penetration" of the cement paste, as was also shown in chapter 3, appears to be reduced slightly by the reaction with the C_3A phase and its part removal, because at low chloride levels most of it is present in the bound form.

(vi) A maximum chloride binding capacity seems to exist for a cement, above which all added chloride remains as free in the pore solution.

PART II IONIC DIFFUSION OUT-OF CEMENT PASTES

4.6 INTRODUCTION

In the preceding sections it has been shown that ionic migration obeys the diffusion laws to a good approximation in well characterised and essentially uniform cement pastes. Normally the diffusion work has been carried out in solutions of pH values of at least 12.5. This was necessary primarily in order to avoid the leaching of the $Ca(OH)_2$ from within the cements and hence risk altering the diffusion rates of the investigated ions, either by the structural or physical alteration of the cements or by the interference of further diffusing ions.

In reality, this rarely is the case. A structure exposed to seawater for example, is constantly in contact with a near neutral solution so that $Ca(OH)_2$, as well as other soluble substances, are unavoidably being progressively removed from the structure [6]. It is essential therefore, to investigate the possible effects that the leaching of $Ca(OH)_2$ and other phases, whose stability may be affected at such low pH's, may have on the ionic diffusion mechanism in cements. This would assist in an overall better understanding of the ionic diffusion theory in cement pastes.

Continuing on the concept of unidirectional diffusion, well characterised portland cement pastes with NaCl additions were exposed to deionised water of effectively zero ionic

concentration in order to encourage the diffusion of all ions out of the cements and hence be in a position to study their interrelation. The work which was carried out along similar lines to the preceding diffusional work in the first part of chapters 3 and 4, is described here, in part II of this chapter.

4.7 EXPERIMENTAL PROCEDURE

The preparation of OPC-B' cement pastes was the same as that described earlier (para. 2.2, 3.7 and 4.3) but with an increased curing period of 12 months as opposed to the earlier mentioned 90 days. The prolonged curing was carried out in an attempt to reduce the likelihood of ionic release in the pore-solution during the "diffusion" period as was experienced earlier (para. 4.5) and also to ensure the formation of uniform "fully-cured" cement pastes.

After demoulding, 24 cylinders were prepared and masked with paraffin wax as described in chapter 3 (para. 3.3) and depicted in figure 3.2. These were then separated into two groups of 12 and immersed in 5 litres of deionised water, in two separate sealed containers, maintained at a temperature of 22±2°C.

The solution of each container was then monitored on a regular basis, determining the concentrations of Na^+, K^+, Ca^{++}, OH^-, and Cl^- ions by the methods described in chapter 2 (para. 2.4). As the ionic concentrations of the solutions

were very small and the volume large, it was possible to carry out the analyses on undiluted larger amounts of withdrawn solution (up to 10ml) hence eliminating errors involved in the process of dilution. The removed solution was always replaced by an equal volume of deionised water.

In order to maintain the leaching of $Ca(OH)_2$ from within the cement pastes, the pH of the outer solution was not allowed to increase beyond 12. Each of the 5 litres of solution was hence replaced by fresh deionised water whenever pH-12 was approached.

After 165 days of exposure to the solution, the cylinders were removed and dry-cut into 7mm discs by a mechanical hacksaw in the same way as was described in chapter 4 (para. 4.3) aiming for the overlapping effect shown in chapter 3 (fig. 3.2) so as to achieve an improved resolution.

Equidistant discs were grouped together and pressed as normal with the use of the pore-expression device (chapter 2 para. 2.3). The expressed solution was then analysed for the ionic concentrations of Na^+,K^+,Ca^{++}, OH^- and Cl^- ions as described in chapter 2 (para. 2.4).

As usual, other discs were also subjected to DTA and X-ray diffraction analyses, evaporable and non-evaporable water content and free and total chloride determinations. Additionally, in order to determine any effects that the leaching may have had on the porosity of the pastes, thin discs sli-

ced from one cylinder at various depths were subjected to MIP investigations (chapter 2 para. 2.9).

A further 2 cement pastes of the same original composition were subjected to pore solution analysis, after a 530 day (ie 365 + 165) curing period in their sealed moulds at 22± 2°C so that any possible changes in the pore solution chemistry during diffusion could be detected.

4.8 RESULTS

The average increase in ionic concentrations of the solutions in the two containers with time are represented by figures 4.13 4.14 and 4.15 (for the full values see table 4.7). These are in the form of accumulated totals versus the square root of time. The intervals of solution replacement are marked on the same graphs by broken vertical lines.

The amount of "substance" diffusing out of the one flat surface of a "semi-infinite" cement paste is related to time by the following solution to Fick's 2nd law of diffusion (87).

$$Mt = 2C_o\sqrt{\frac{Dt}{\pi}} \quad \ldots (1)$$

where: Mt = Amount of total diffused "substance" per unit area ($mMcm^{-2}$)

C_o = Original concentration of the "substance" in the cement paste ($mMcm^{-3}$)

TABLE 4.7 Accumulated ionic concentrations in solution with time.

TIME (Days)	Na^+	K^+	Ca^{2+}	Σ^+	OH^-	Cl^-	Σ^-	$(OH^-)^*$
5	2.60	1.39	3.62	11.23	10.60	0.69	11.29	3.36
6	2.87	1.40	4.12	12.51	11.25	0.79	12.04	3.01
7	3.44	1.65	4.06	13.21	12.15	0.82	12.97	4.03
8	3.64	1.76	4.91	15.22	14.15	0.89	15.04	4.33
11	4.23	2.08	6.17	18.65	17.30	1.05	18.35	4.96
12	4.42	2.14	6.46	19.48	18.13	1.10	19.23	5.21
13	4.59	2.23	6.81	20.44	19.05	1.17	20.22	5.43
18	5.08	2.41	7.70	22.89	22.17	1.40	23.57	6.77
20	5.35	2.53	8.69	25.26	24.75	1.49	26.24	7.37
22	5.61	2.64	9.28	26.81	26.22	1.57	27.79	7.66
29	6.42	3.01	10.66	30.75	29.97	1.82	31.79	8.65
43	7.87	3.67	13.49	38.52	37.45	2.25	39.70	10.47
53	8.82	4.07	15.57	44.03	42.90	2.53	45.43	11.76
61	9.42	4.38	16.42	46.64	45.33	2.74	48.07	12.49
77	10.70	4.98	18.98	53.64	52.16	3.16	55.32	14.20
95	11.92	5.55	21.28	60.03	58.36	3.51	61.87	15.80
105	12.65	5.87	22.88	64.28	62.49	3.71	66.20	16.73
112	13.08	6.08	23.36	65.88	64.09	3.85	67.94	17.37
132	14.26	6.63	25.41	71.71	69.69	4.18	73.87	18.87
150	15.27	7.08	27.15	76.65	74.54	4.44	78.98	20.24

*OH^- concentration excluding $Ca(OH)_2$

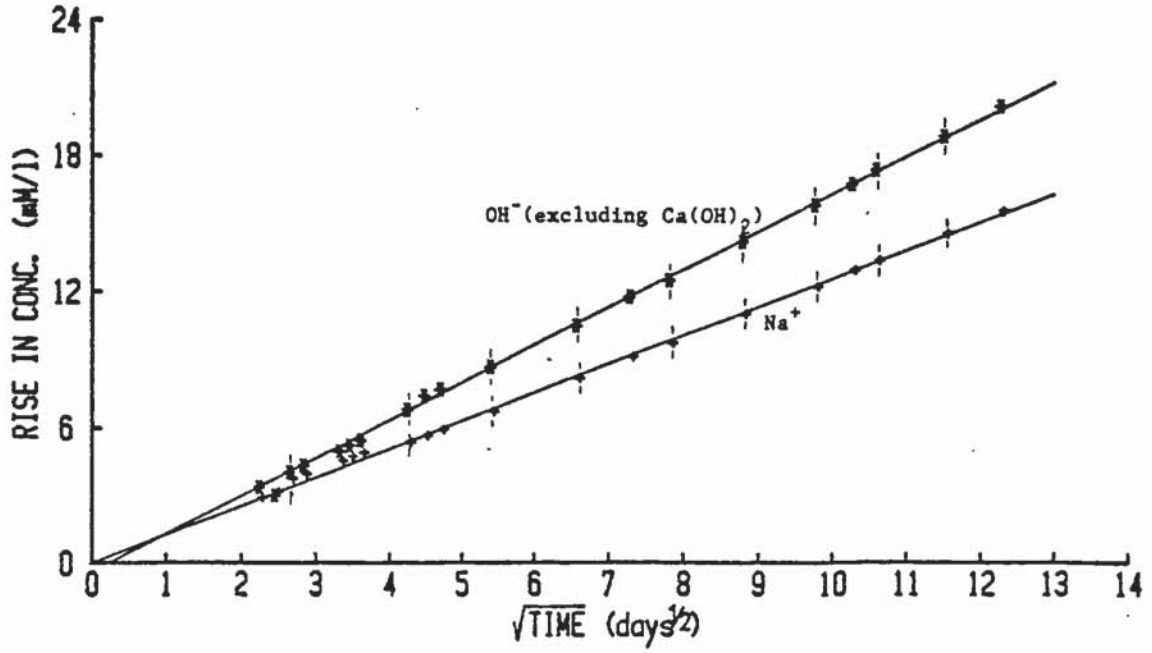

FIGURE 4.13 Rise in ionic concentration with $\sqrt{time}$ in the external solution due to leaching from OPC-B' paste.

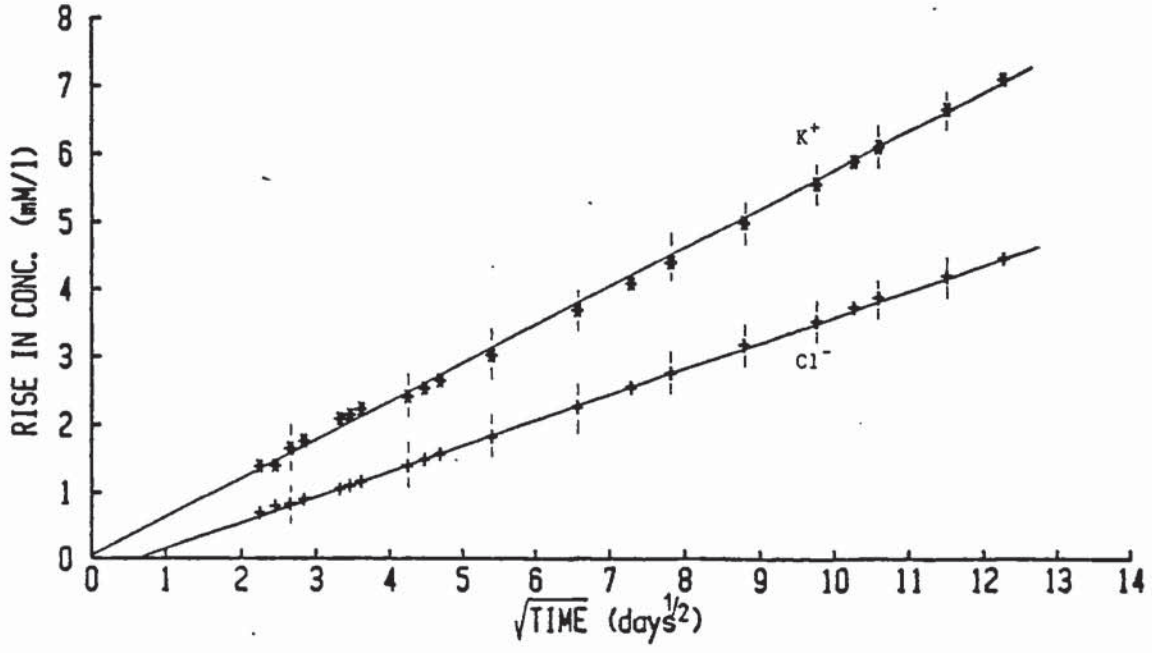

FIGURE 4.14 Rise in ionic concentration with $\sqrt{time}$ in the external solution due to leaching from OPC-B' paste.

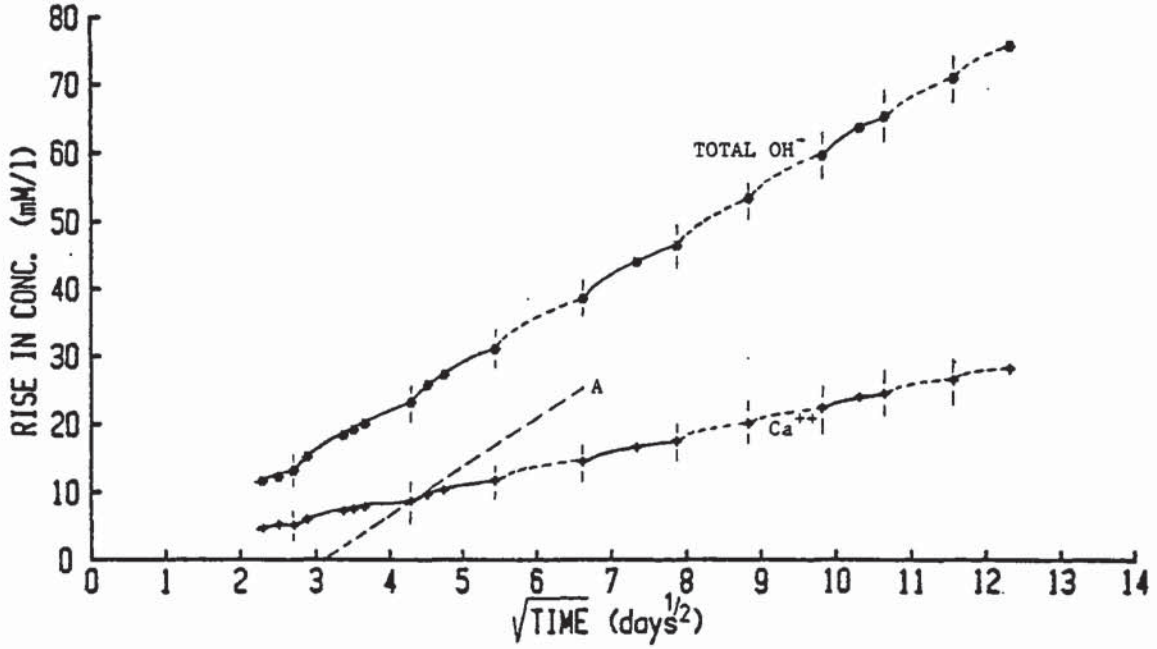

FIGURE 4.15 Rise in ionic concentration with $\sqrt{\text{time}}$ in the external solution due to leaching from OPC-B' paste.

t = Time of exposure (sec)

D = Effective diffusion coefficient ($cm^2 s^{-1}$)

Plots of Mt v's $\sqrt{t}$ should therefore produce straight lines whose gradients are related to the effective diffusion coefficients. The values of D for Na^+, K^+ and Cl^- ions thus calculated resulted in good correlation coefficients and are tabulated in table 4.8 (for an example of a full calculation see appendix 16). The effective diffusion coefficient for OH^- ions was calculated from the gradient of the plot shown in figure 4.13. This line was constructed after the OH^- ions accompanying the Ca^{++} (ie $Ca(OH)_2$) were subtracted from the total recorded OH^- concentrations.

The ionic concentrations at increasing depths into the cement pastes are shown in table 4.9 and are represented in graphical form by figures 4.16 and 4.17. The difference between the sum of ions ($\Sigma^+ - \Sigma^-$) represents mainly the sulphate ions so it can be seen (fig. 4.17) that this group too has produced a similar concentration profile as the other sets of ions.

In attempting to determine diffusivities for each set of ions as before (chapter 3 para. 3.4.1 and chapter 4 para. 4.4) it was revealed that none of the ionic species had diffused in the normal way as determined by Fick's 2nd law of diffusion. Plots of x v's y from the relationship,

TABLE 4.8 Effective diffusion coefficients determined from solution analysis.

ION	$Dx10^9 (cm^2 s^{-1})$	r
Na^+	17.2	0.999
K^+	26.4	0.999
OH^-	46.4	0.999
Cl^-	12.0	1.000
Ca^{2+}	$\sim$ 2.0	——

TABLE 4.9 Ionic concentrations with depth in OPC-B' (mM/l).

DEPTH x (cm)	OH^-	Cl^-	Na^+	K^+	Ca^{2+}	Σ^-	Σ^+	$\Sigma^+ - \Sigma^-$
0.175	75	14	58	18	7.2	89	90	1
0.350	136	32	122	35	3.8	168	165	3
0.700	246	67	248	73	2.7	313	326	13
1.050	326	102	356	104	2.4	428	465	37
1.400	351	119	394	120	1.9	470	518	48
1.750	409	157	469	140	2.1	566	613	47
2.100	444	168	496	164	2.0	612	637	25
2.450	463	192	551	177	2.0	655	732	77
2.800	480	191	556	188	1.8	671	748	77
3.150	514	215	599	201	1.9	729	804	75
3.500	516	210	592	211	1.9	726	807	136
3.850	527	215	589	203	1.9	742	796	54
4.200	535	228	629	226	1.9	763	859	96
4.550	531	232	626	221	1.8	763	851	88
4.900	539	230	636	232	1.7	769	871	102
5.250	534	241	648	229	1.8	775	881	106
5.600	543	231	643	241	1.8	774	888	119
5.950	542	247	659	238	1.5	789	900	111
*	619	220	710	263	1.5	839	976	137

* Ionic concentrations of parallel specimen.

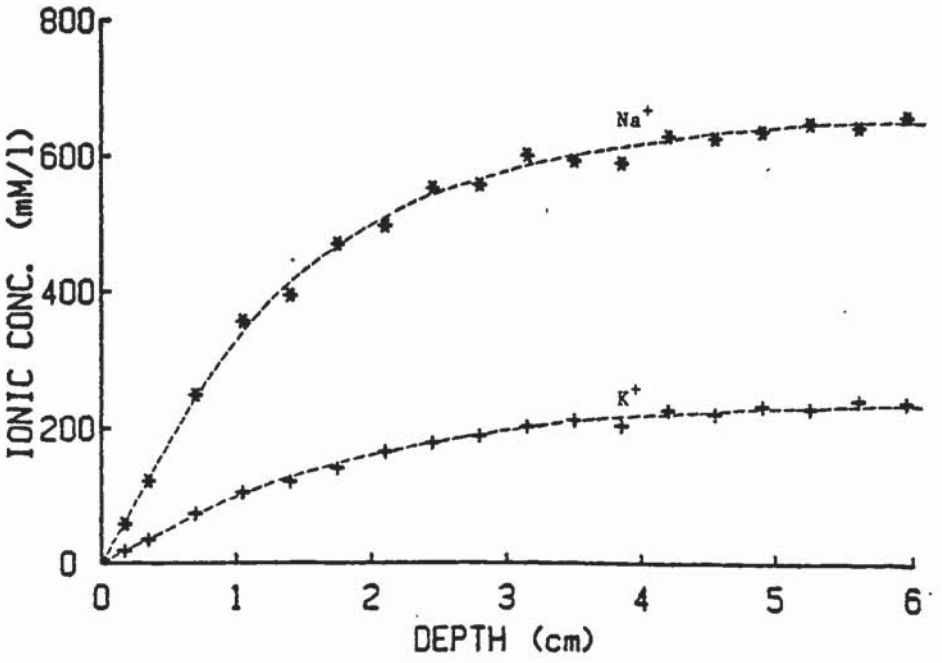

FIGURE 4.16 Concentration profiles of Na^+ and K^+ in OPC-B' exposed to water for 165 days.

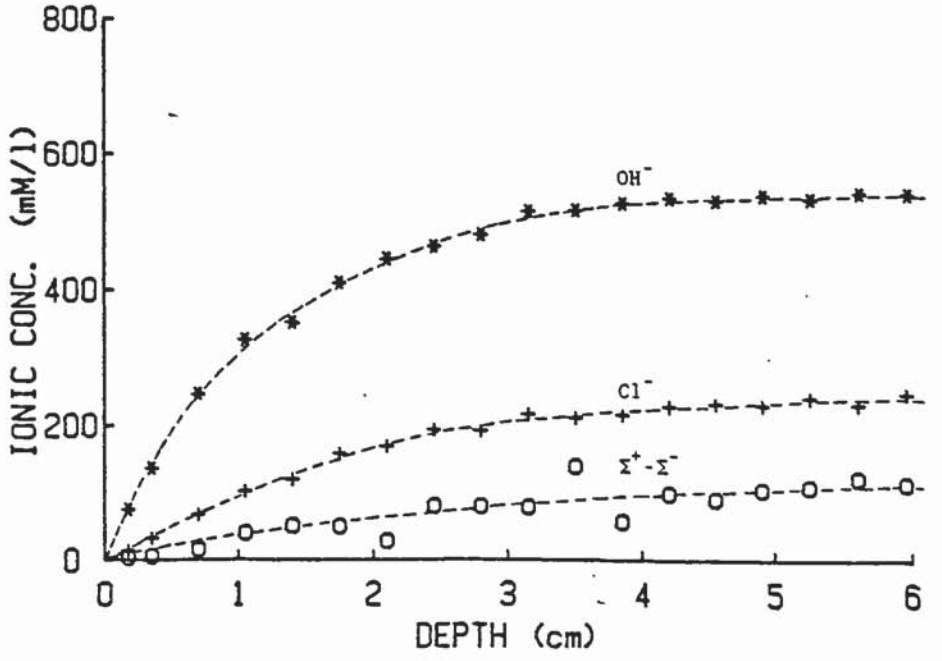

FIGURE 4.17 Concentration profiles of OH^-, Cl^- and $\Sigma^+\text{-}\Sigma^-$ in OPC-B' exposed to water for 165 days.

$$y = \frac{x}{2\sqrt{Dt}}$$

were not linear (as for example fig. 3.5) but had an increasing gradient with depth (fig. 4.18) suggesting a variation in the diffusion coefficients.

A solution enabling the accurate determination of the apparent variable diffusivities with depth, involves a complex mathematical treatment, similar to that reported by Crank [88], which is beyond the scope of this work.

A satisfactory way of representing the varying diffusion coefficients with depth was achieved involving principally the same method used in the preceding chapters. Starting from the surface, the curve was assumed linear up to a certain depth (shown on figure 4.18 by the vertical lines) and the appropriate coefficient calculated normally as shown in chapter 3 (para. 3.4.1 - see for example appendix 17). The resultant diffusivities are summarised in table 4.10. The degree of deviation from the normal is related to the correlation coefficient r and particularly to the negativeness of the intercept c. These values are shown in the same table for the depth up to 4.9 cm. Values were not considered beyond this depth because of the large errors involved owing to the nature of the relationship.

It can be seen from table 4.10 that in all cases, though to a varying degree, the diffusion coefficient decreases as the

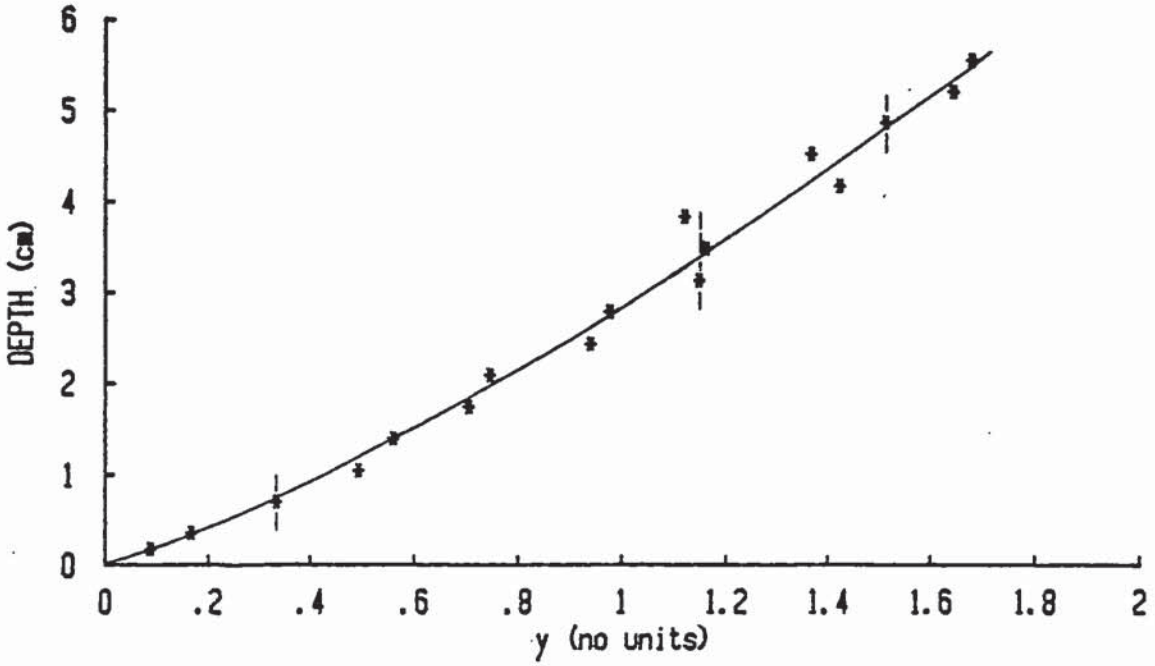

FIGURE 4.18 Plot of depth versus y for Σ^+ to enable the determination of the diffusion coefficient.

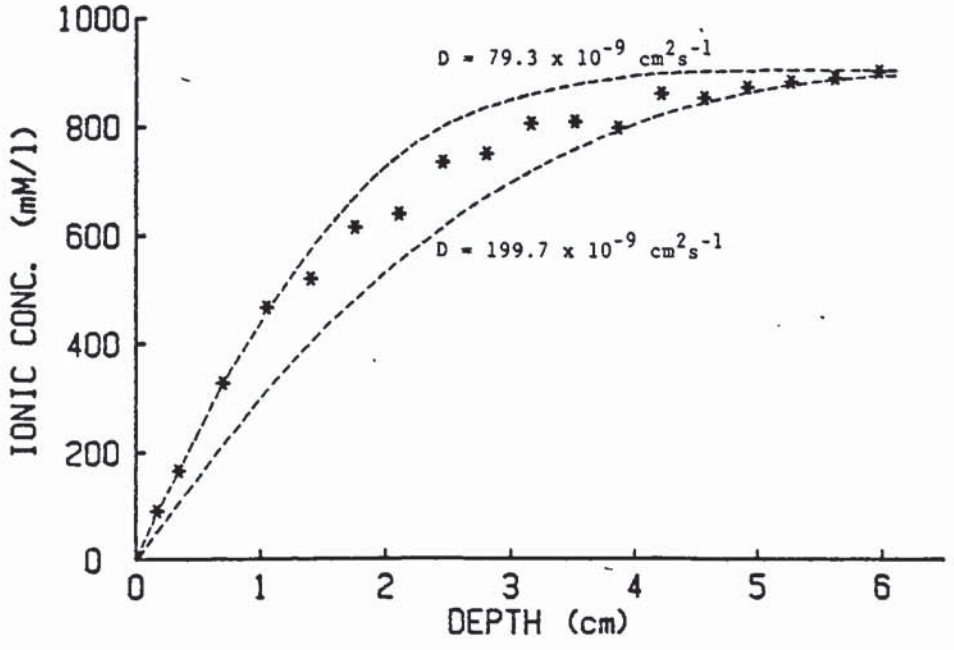

FIGURE 4.19 Concentration profile Σ^+ in OPC-B' at 165 days compared to theoretical concentration profiles for two diffusion coefficient values.

TABLE 4.10 Diffusion coefficients determined from concentration profiles showing increasing values with distance from the surface.

ION	$Dx10^9$ (cm^2s^{-1})			r	c(cm)
	0.7cm	2.8cm	4.9cm	FOR 4.9 cm	
Na^+	70.1	125.9	189.4	0.982	-0.442
K^+	112.8	182.9	210.3	0.990	-0.187
OH^-	54.2	121.3	143.6	0.992	-0.434
Cl^-	137.5	142.8	178.4	0.989	-0.138
Σ^+	79.3	147.2	199.7	0.987	-0.401

TABLE 4.11 Evaporable and non-evaporable water content with depth in OPC-B' paste.

DEPTH x (cm)	We%	Wn%	TOTAL WATER
0.175	39.69	18.62	58.31
0.350	38.36	18.70	57.06
0.700	36.38	20.03	56.41
1.050	34.88	19.20	54.08
1.400	35.67	20.21	55.88
1.750	35.59	19.19	54.78
2.100	35.20	20.17	55.37
2.450	34.31	18.82	53.13
2.800	35.80	20.17	55.97
3.150	35.32	19.93	55.25
3.500	35.04	19.81	54.85
3.850	34.77	19.24	54.01
4.200	35.65	20.80	54.97
4.550	35.29	19.32	54.61
4.900	35.08	19.77	54.85
5.250	35.81	19.03	54.84
5.600	35.52	20.59	56.11
5.950	35.66	19.95	55.61
*	31.89	18.98	50.87

* Water contents of parallel specimen.

surface is approached.

The theoretical concentration profiles for the diffusion coefficients determined for the Σ^+ ions at the depths of 0.7cm and 4.9cm respectively (ie 79.3 and 199.7 x $10^{-9}cm^2s^{-1}$) are represented by the broken lines in figure 4.19. If these are viewed in relation to the actual concentration profile, its deviation from normal becomes apparent.

If the cement paste is assumed to be uniform, then the variation of the diffusivity value must be caused by some kind of barrier at the surface restricting the movement of ions, as was the case with chloride diffusion in part I of this chapter (fig. 4.4). This will be discussed in more detail later.

Some physical change near the surface is evident from the evaporable and non-evaporable water contents (table 4.11) shown graphically in figure 4.20. There is a slight, though possibly insignificant, decrease in W_n but a definite increase in W_e as the surface is approached. This suggests a coarsening of the pore-structure allowing more water to penetrate from the outside.

The increased porosity can be seen clearly from the MIP results (fig. 4.21) where the total pore volume is increased dramatically near the surface. The leaching of $Ca(OH)_2$ is mainly responsible for the coarsening of the structure near the surface. The DTA (fig. 4.22) and X-ray diffraction (fig.

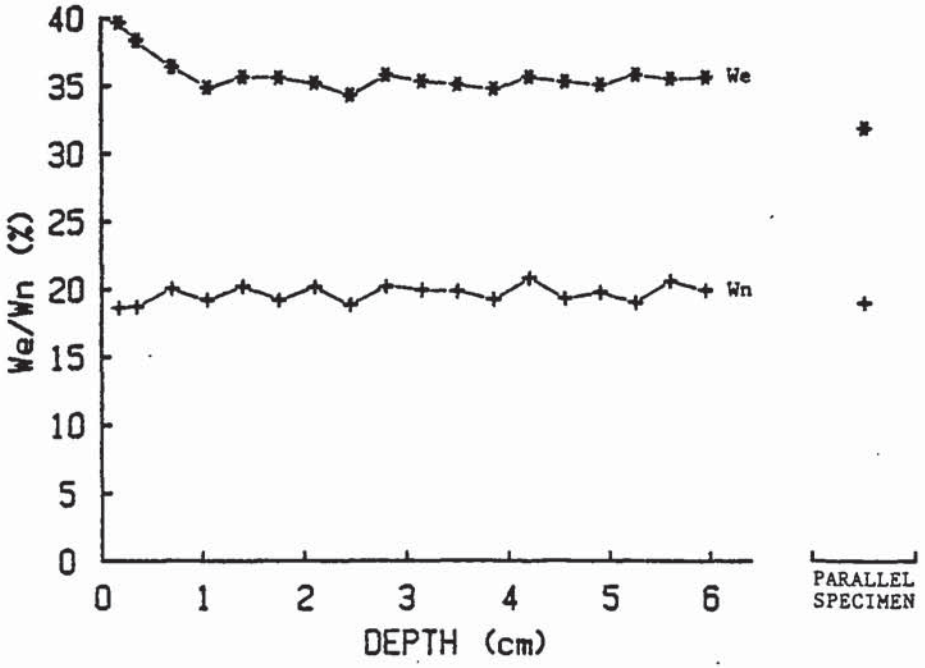

FIGURE 4.20 Variation of evaporable and non-evaporable water contents with depth in OPC-B' after 165 days.

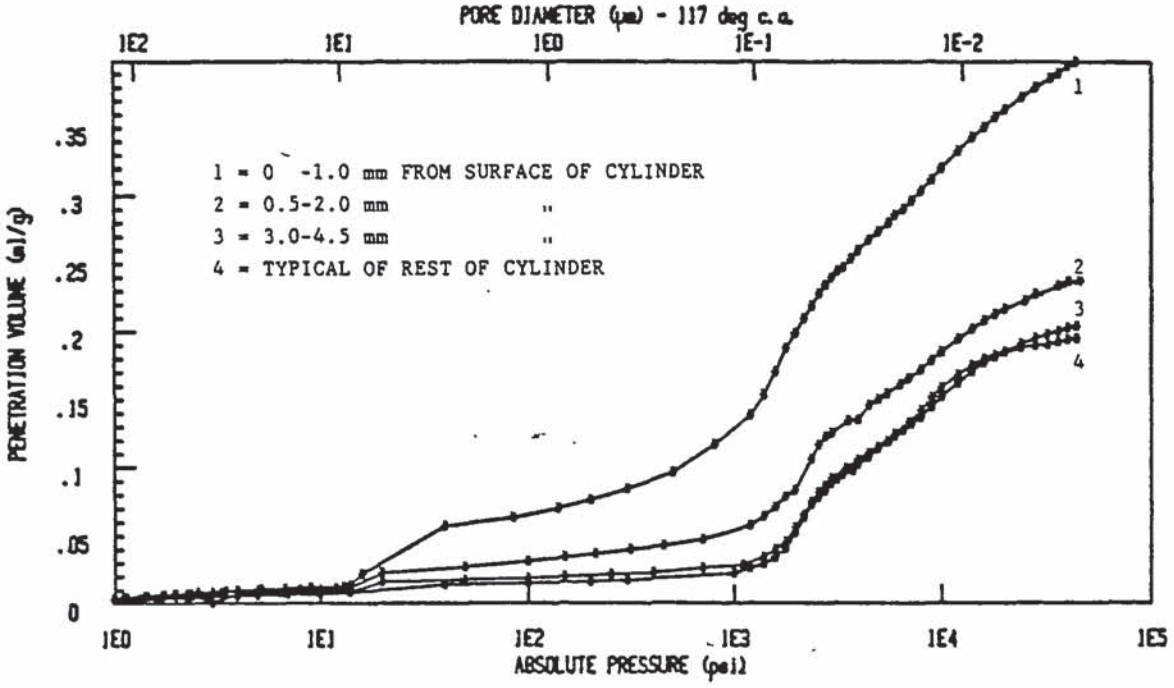

FIGURE 4.21 Variation of pore size distribution with depth in OPC-B' after 165 days.

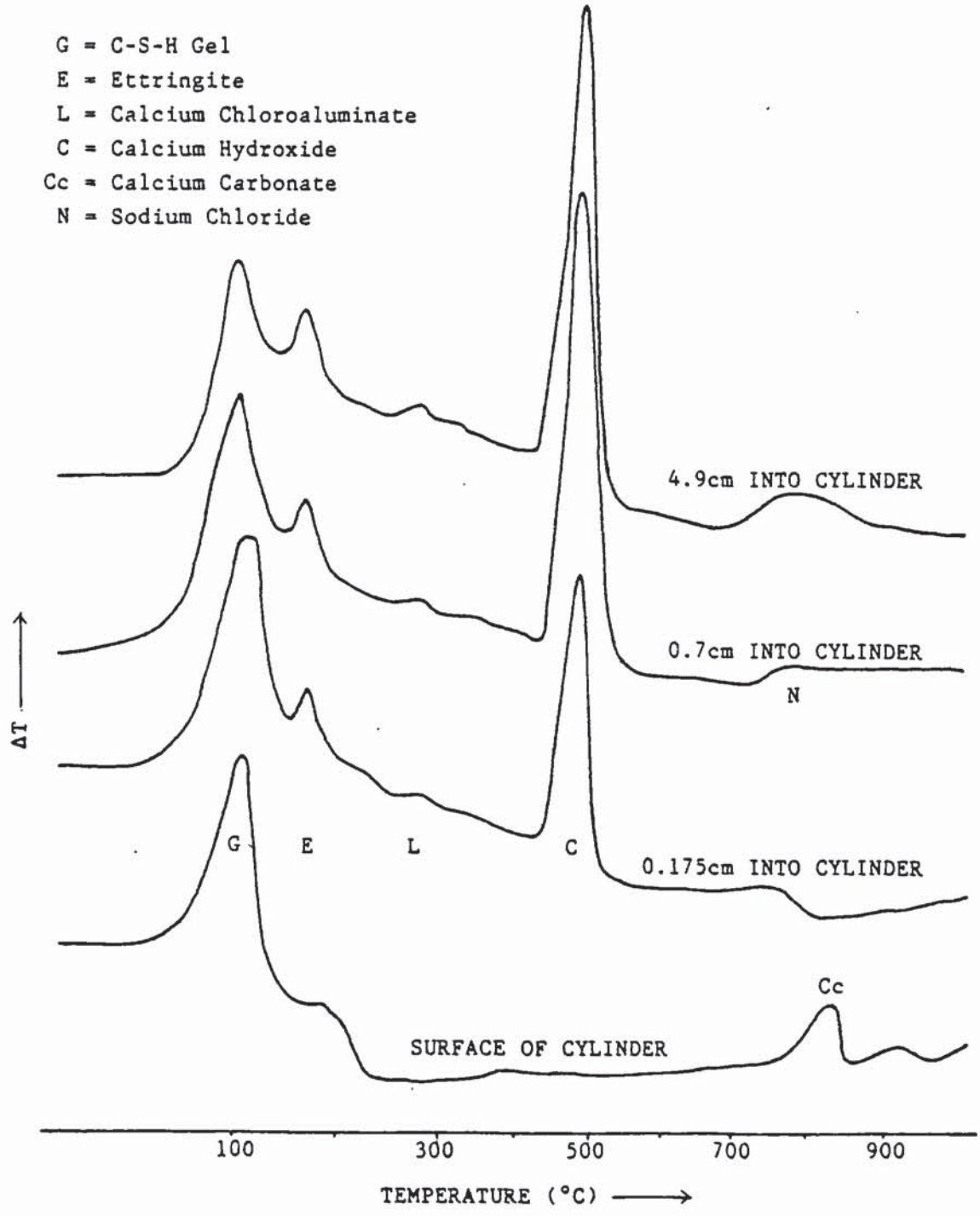

FIGURE 4.22 DTA thermographs of OPC-B' at increasing depths after exposure to deionised water for 165 days.

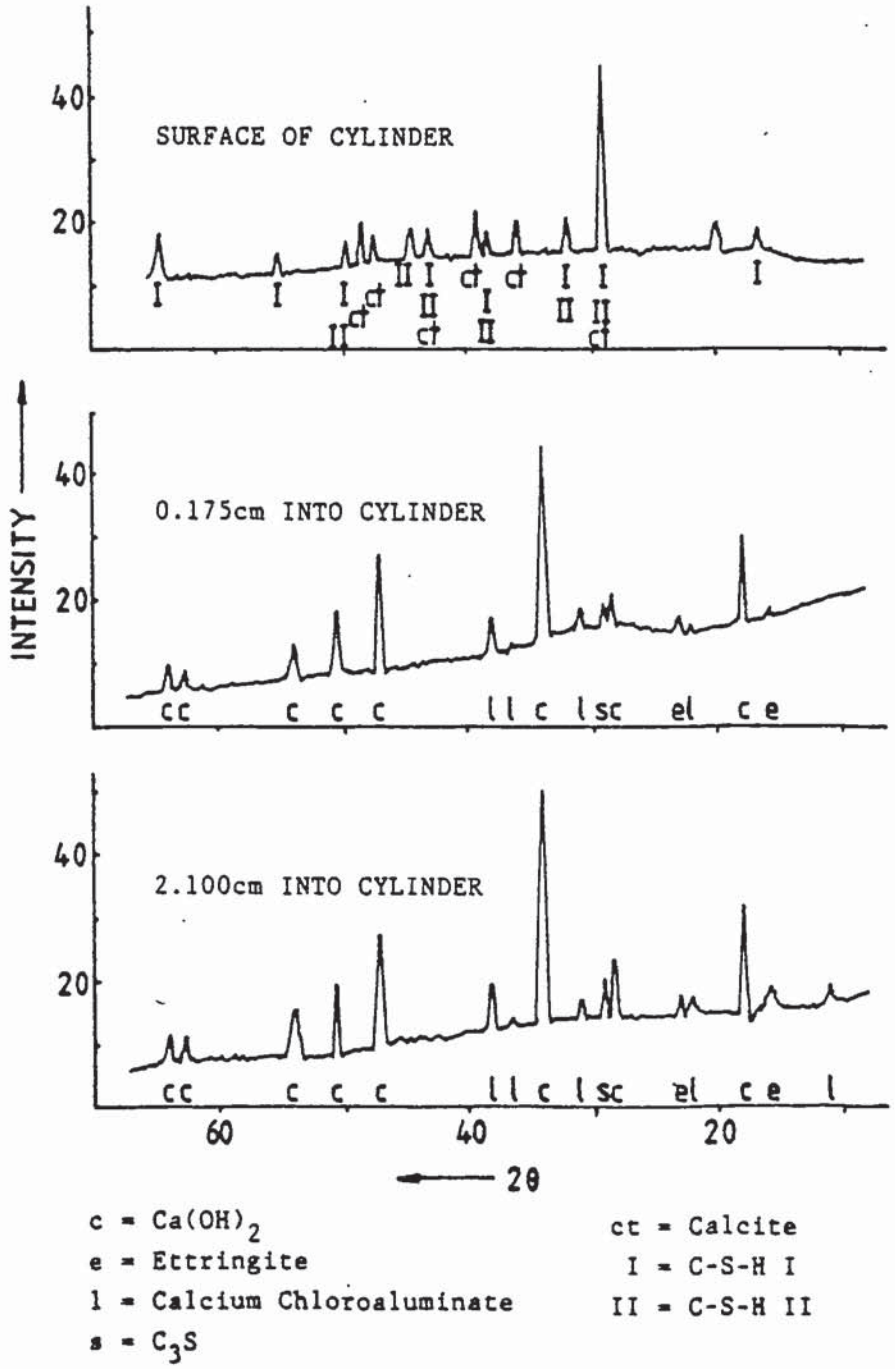

FIGURE 4.23 XRD traces of OPC-B' at increasing depths after exposure to deionised water for 165 days.

4.3) results suggest however, that it is not only the $Ca(OH)_2$ which is removed from the surface but also other phases such as ettringite and calcium chloroaluminate leaving behind mainly C-S-H gel and on the very surface, a small amount of calcite, (fig. 4.23).

The fact that chloroaluminate is leached out from the surface is also seen from the concentration profiles of chloride in its different forms as represented in figure 4.24 (see also table 4.12). It is evident therefore that phases such as the calcium sulpho- and chloro-aluminates are not stable in near neutral solutions. Exposure to such solutions causes their eventual breakdown and removal from the cement paste.

4.9 DISCUSSION OF RESULTS

If sulphate ions are also taken into account roughly represented in this case by $(\Sigma^+ - \Sigma^-)$ ions (see table 4.9), the observation of part I that there must be an ionic charge balance along the depth of the hardened cement paste, is confirmed. This fact further implies that the net cationic movement through any cross-sectional area of cement paste perpendicular to the direction of diffusion (ie the flux), must equal the net anionic movement in the same direction, as is clearly illustrated by the solution analysis results (table 4.7) representing the "flux" at the very surface of the specimens.

It is possible however that individual ionic species can mi-

TABLE 4.12 Free, Bound and Total amounts of chloride with depth in OPC-B' paste.

DEPTH x (cm)	FREE	BOUND	TOTAL
0.000	0.000	0.033	0.033
0.175	0.006	0.144	0.150
0.350	0.012	0.149	0.161
0.700	0.024	0.165	0.189
1.050	0.036	0.175	0.211
1.400	0.042	0.170	0.212
1.750	0.056	0.172	0.228
2.100	0.059	0.171	0.230
2.450	0.066	0.166	0.232
2.800	0.068	0.167	0.235
3.150	0.076	0.171	0.247
3.500	0.074	0.164	0.238
3.850	0.075	0.178	0.253
4.200	0.081	0.168	0.249
4.550	0.082	0.174	0.256
4.900	0.081	0.171	0.252
5.250	0.086	0.163	0.249
5.600	0.082	0.161	0.243
5.950	0.088	0.162	0.250
*	0.070	0.172	0.242

* Chloride contents of parallel specimen.

TABLE 4.13 Comparison of diffusivities determined by two different methods after "correction".

ION	$Dx10^9$ (cm^2s^{-1})			"CORRECTED" $Dx10^9$ (cm^2s^{-1}) (FROM SOLUTION ANALYSIS)
	4.9cm	2.8cm	0.7cm	
Na^+	189.4	125.9	70.1	40.0
K^+	210.3	182.9	112.8	61.4
OH^-	143.6	121.3	54.2	107.9
Cl^-	178.4	142.8	137.5	27.9

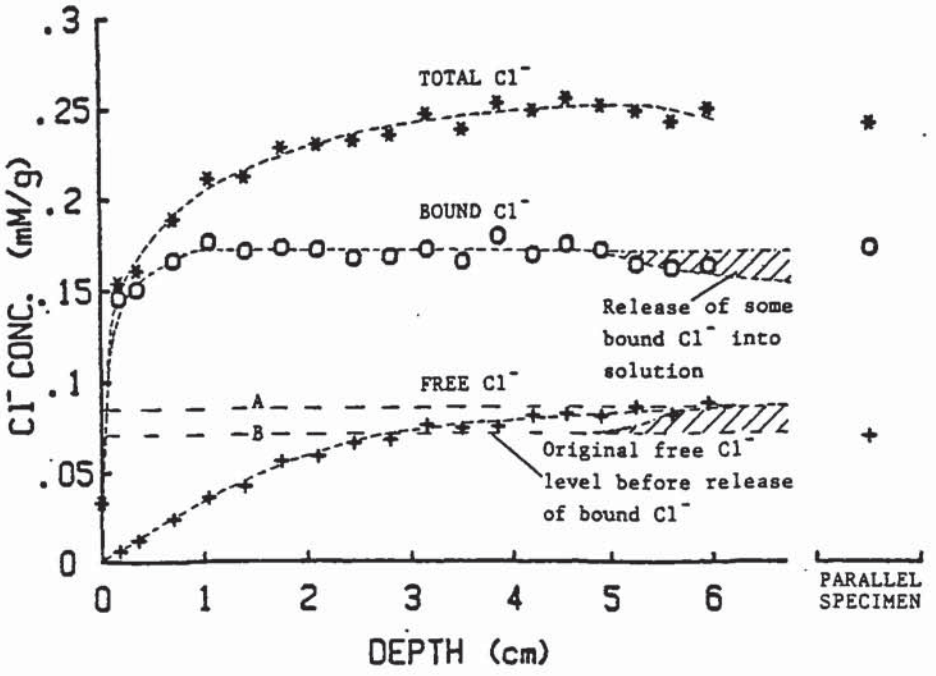

FIGURE 4.24 Total, Bound and free chloride concentration profiles in OPC-B' exposed to water for 165 days.

grate at various rates, as discussed previously, so that each may have a different apparent diffusion coefficient, but only if the charge balance condition is satisfied. This is shown to be true by the effective diffusivities of Na^+ and K^+ as determined from solution analysis (table 4.8). Potassium ions are more mobile, at least at the surface of the cement pastes, than the sodium ions.

As mentioned in chapter 3 part II, as these effective diffusivity values were calculated by a method which required the determination of the cement paste's cross-sectional area (see equation (1)), they were underestimated by a proportion roughly related to the ratio of "pore-solution" to "cement paste" cross sectional areas. This value is estimated to be 0.43 (see appendix 18) giving the "corrected" diffusivities shown in table 4.13.

By relating these to the diffusivities calculated at decreasing depths for the different ions (table 4.10) it can be seen that whilst for Na^+ and K^+ there is more or less a systematic decrease in the diffusion coefficient right to the surface of the cement pastes (table 4.13), this does not appear to be the case for the OH^- and Cl^- ions.Hydroxyl ions have entered the solution at a faster rate than their internal concentration profile had suggested, while the behaviour of the chloride ions was the opposite, even though there was also a small release of chlorides from the breakdown of the chloroaluminate phase near the surface (fig. 4.24).

This fact is substantiated by calculation (see appendix 19). Theoretically the amount of "substance" gained in the solution should equal the amount "lost" from the cement pastes. From table 4.14 the imbalance observed for OH^- and Cl^- ions is very evident. The imbalance of both ionic species may be explained as follows.

Table 4.15 represents the ionic concentrations in the cement pastes beyond the depth affected by diffusion and those of the parallel "normally" cured cement pastes. The latter values are also adjusted to allow direct comparison by taking into account the different evaporable water contents of the two conditions. It is evident from table 4.15 that whilst concentrations for Na^+ and K^+ remained the same within experimental error, the Cl^- concentration had shown an increase when the cement pastes were subjected to diffusion, countered to an extent by a decrease in the OH^- concentration.

A glance at the bound Cl^- concentration profile (fig. 4.24), reveals that some chloride release could have occurred, but only beyond the depth of about 5cm (see fig. 4.24). In calculating the amount of free chloride present in the cement paste before diffusion (see appendix 19) the level of chloride was assumed to be that represented by line A in figure 4.24, whereas in fact it could have been that shown by B. As a result, the amount of chloride assumed as "lost" from the cement paste would have been overestimated by a proportion equal to the difference between the two levels. If the

TABLE 4.14 Amount of substance "lost" from OPC-B' pastes against amount gained in solution.

ION	AMOUNT "LOST" (mM/l) CALCULATED-165 DAYS	AMOUNT GAINED (mM/l) FROM GRAPHS-165 DAYS
Na^+	16.3	15.81
K^+	7.4	7.31
OH^-	11.8	21.16
Cl^-	7.0	4.68

TABLE 4.15 Ionic concentrations of "normally" cured OPC-B' paste against paste used for the diffusion experiment.

TYPE OF SPECIMEN		IONIC CONC. (mM/l)				We(g/g)
		Na^+	K^+	OH^-	Cl^-	
NORMALLY CURED CEMENT PASTE	ACTUAL	710	263	619	220	0.32
	ADJUSTED*	649	240	566	201	
DIFFUSION SPECIMEN		655	240	545	240	0.35

* Adjustment from We values [ie $\frac{0.32}{0.35}$x710=649]

released chloride was countered by removal from solution of an equivalent amount of hydroxyl ions, the opposite error would have been encountered in calculating their level.

Finally, as the two sets of anions are more mobile than their cationic counter parts, they would have redistributed themselves, causing "smoothing" of their concentration profiles as seen in figures 4.17 and 4.24.

The main discrepancy in the results however, is the reduction of the apparent diffusivities as the surface is approached (table 4.13) suggesting, as mentioned earlier, that a barrier exists near the surface, restricting ionic movement. The restriction cannot be attributed to porosity as this increases from the leaching of $Ca(OH)_2$ and other phases (fig. 4.21).

One must therefore relate it to some other form of physical or chemical alteration of the cement paste at the surface which is exposed to the solution.

Lambert [95] working with pure cement minerals had suggested that diffusion of ions such as chlorides is emitted by passage through the C-S-H gel matrix. Variations in the composition of the gel at the surface may therefore influence diffusion characteristics. Slag and PFA based cements which, as shown earlier (see chapter 3 part II), reduce ionic diffusion rates considerably, are known for instance to have a gel structure of a low CaO/SiO_2 (C/S) ratio [93,94]. The earlier-assumed ionic "barrier" present at the surface of

the cement pastes, may therefore be caused by a reduced C/S ratio of the C-S-H gel.

As mentioned by Taylor [89] and supported by Kalousek [90] when C-S-H gel is placed in a lime solution, it gains or loses lime, depending on the concentration of the solution. This then alters the C/S ratio of the gel, as shown in figure 4.25 (reconstructed from references 91 and 92). Removal of $Ca(OH)_2$ from the surface of the cement pastes may therefore reduce the C/S ratio of the gel, transforming it probably to a type resembling that of slag and PFA based cement pastes.

A low C/S ratio gel may also explain the high positive zeta potentials of PFA based cement pastes, which were thought by Uchikawa et al [82] to cause the restriction of movement of cations (see chapter 3 part II). Such suggestions ofcourse require confirmation by further experimental work.

Single ionic species do not appear to be influenced directly by the leaching of $Ca(OH)_2$. Whilst the increase in concentration of Ca^{++} with time is in "steps" (figure 4.15) and directly related to the outer Ca^{++} concentration, the rest of the ionic accumulation is constant. As Ca^{++} ions are accompanied by an equivalent amount of OH^- ions diffusing at the same rate, there is presumably no need for any of the other ions to alter their "movement" as the net charge balance is still maintained. Because the changes in the outer solution were consistent

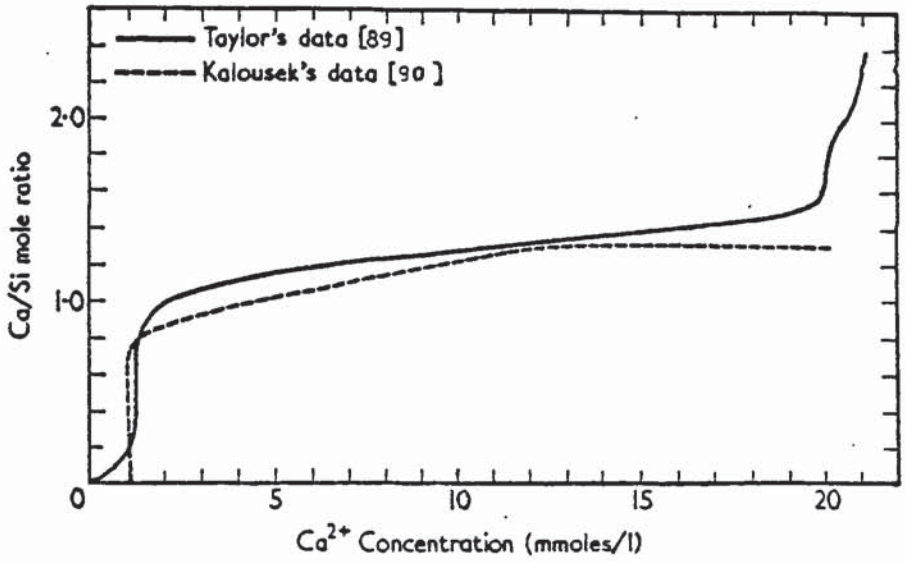

FIGURE 4.25 Metastable equilibrium curves showing the Ca/Si mole ratio of C-S-H(I) and the concentration of Ca^{2+} in solution at room temperature.

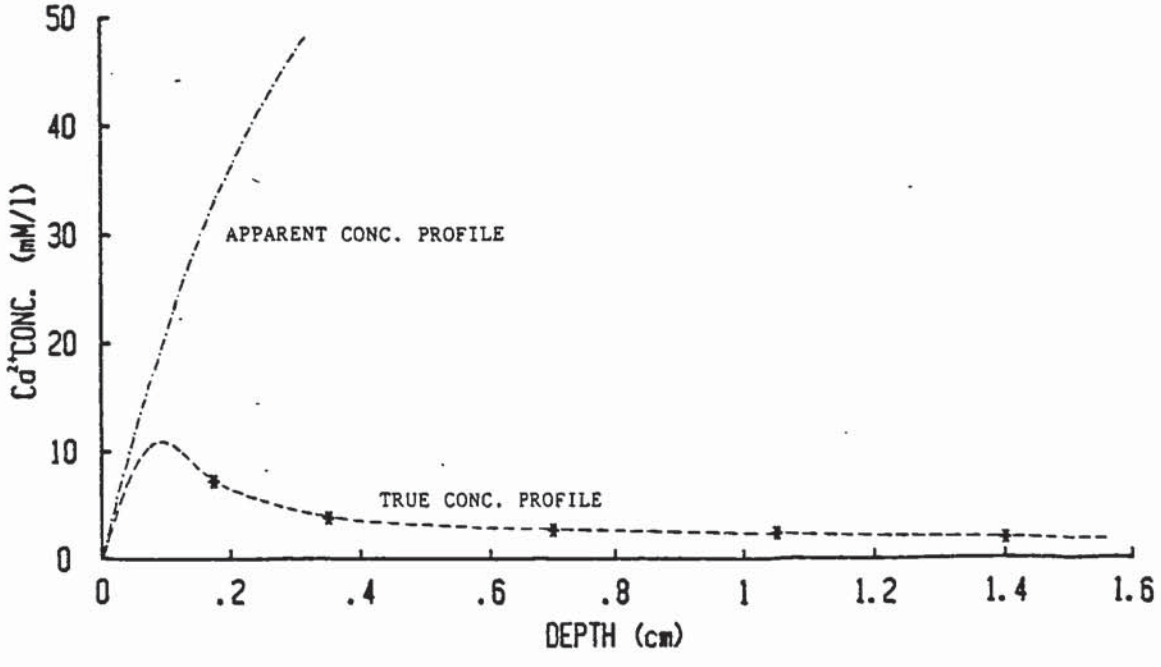

FIGURE 4.26 Ca^{2+} concentration profile in OPC-B' exposed to water for 165 days.

ie were made when the solution pH had risen to just below 12 (see para. 4.7) - the Ca^{++} concentration v's $\sqrt{time}$ plot can be assumed to be one single line and not a series of smaller curves (figure 4.15). The assumption is shown to be valid by the good correlation coefficient achieved for the relationship (r = 1.0).

As the parabolic relationship is satisfied, there should be an "internal" Ca^{++} concentration profile similar to those of the other ionic species (figure 4.16). The actual concentration profile as shown in figure 4.26 and determined by pore solution analysis (table 4.9) is evidently very different. The relationship points therefore to an "apparent" concentration profile a part of which is represented by the broken lines in figure 4.26.

The diffusion rate of Ca^{++} appears therefore to be controlled by two parameters,

(i) the outer solution's Ca^{++} concentration or pH (figure 4.15).

(ii) the inner "apparent" concentration profile.

The second parameter should be directly related to the amount of soluble $Ca(OH)_2$ available in the cement paste. For OPC-B' it is about 0.28 grammes per gramme of cement as shown in chapter 5 (see table 5.10).

If the Ca^{++} concentration of the outer solution is maintained at zero, thus eliminating parameter (i), the diffusion of Ca^{++} ions should be entirely dependent on their inner apparent concentration profile, so that the increase of the ionic species in solution would be linear and represented roughly by line A in figure4.15.

Based on such assumptions, equation (1) can then be used, as shown earlier, to estimate an effective diffusion coefficient for Ca^{++} (see appendix 16) giving a value of about 2×10^{-9} $cm^2 s^{-1}$, an order of magnitude lower than the other ionic species (table 4.8).

In lower $Ca(OH)_2$ content cements, the amount of Ca^{++} and the accompanying OH^- that can diffuse under the same conditions would thus be less, if as assumed, the amount of diffusing substance is directly proportional to the inner concentration (eq.(1)). It is possible therefore that two cements of different $Ca(OH)_2$ contents but of similar free chloride concentrations could offer variable protection to the embedded steel.

The ability of the cement paste to protect steel reinforcement may be roughly illustrated by assuming the outer solution in this experiment to be an oversimplified pit on the surface of the steel. The $[Cl^-]/[OH^-]$ ratio of the cement paste's pore solution, thought to be an important corrosion parameter, is a fairly high 0.44 before the onset of diffu-

sion. The relative amounts however, being released into the outer solution (ie the pit) give a considerably lower ratio of 0.06 mainly because of the extra hydroxyl diffusion from $Ca(OH)_2$. This important protection offered to steel by the $Ca(OH)_2$ or other OH^- bearing soluble phases present in cement paste will be discussed further in chapter 5 part II and chapter 6 part I.

Several important points have arisen from the results which can be summarised as follows;

(i) As was shown in part I, the most important "rule" with regards to ionic diffusion, is the zero net ionic charge throughout the pore solution network. From this it also follows that the flux of anions equals the flux of cations for any cross-section considered perpendicular to the direction of diffusion.

(ii) Diffusion rates of ions appear to be affected by physical or chemical changes in the structure of the cement paste. In this particular case it may involve a reduction in the CaO/SiO_2 ratio of the C-S-H gel, influencing the previously mentioned (chapter 3 part II) surface interaction between the cement particles and the diffusing ions.

(iii) It follows from (ii) that at least one of the reasons for the observed low diffusivities of

ions in "pozzolanic" cements (see chapter 3 part II), may be their ability to complex free $Ca(OH)_2$ and produce a low C/S ratio gel structure, thus increasing the surface interaction.

(iv) Ionic diffusion does not appear to be influenced directly by the leaching of $Ca(OH)_2$, which also appears to obey the diffusion laws enabling the estimation of its effective diffusion coefficient. In this particular case it is about $2 \times 10^{-9} cm^2 s^{-1}$.

(v) As chloride diffusion is independent of $Ca(OH)_2$ migration and visa-versa, the amount of "available" lime in the cement matrix appears to have a direct bearing on the local $[Cl^-]/[OH^-]$ ratio near a corrosion pit.

(vi) As a further development, the technique used to calculate diffusivities by the systematic analysis of the solution, ie by determining the flux at the surface, can be applied to other cement pastes, mortars or concretes where the steady-state diffusion technique involving thin slices of material is inapplicable. The advantage is that many ionic species co- or counter-diffusing can be studied concurrently and as the present results suggest, exposure periods can be short

as 4 or 5 readings may suffice. This technique can easily be applied when a facility for pore-solution analysis exists.

CHAPTER 5 THE NEUTRALIZATION OF CEMENT AND CONCRETE

5.1 INTRODUCTION

The second most important depassivation mechanism of steel reinforcement in concrete is that caused by the neutralization of the cement matrix. The normally highly alkaline and protective medium can lose its alkalinity either by severe leaching of hydroxyl ions into a more neutral solution like seawater, or by the action of atmospheric gases such as CO_2, a phenomenon termed carbonation. The former was discussed to some extent in chapters 3 and 4 where the leaching of ions present in cement into solution was studied. The more important way of neutralization is however carbonation.

Carbonation of concrete occurs when CO_2 from the atmosphere penetrates the pores and dissolves in the moisture present forming carbonic acid. Once this happens, all basic components of the concrete will react with the acid to form a salt i.e. $CaCO_3$ and water. Furthermore the neutralization of constituents such as $Ca(OH)_2$, which can offer a buffering capacity to the pore solution, destroys the very important property of easy OH^- replenishment of the steel surface as will be described later.

In order to enable a better understanding of the processes of acidic neutralization of the concrete, a two way programme was undertaken. These were the carbonating of cement pastes in various carbon dioxide atmospheres and the effect-

ing of neutralization with a deliberate addition of acid to fully hydrated cements.

As the second method was a controlled systematic neutralization process, it was possible also to observe the change in hydroxyl concentration as a function of added acid and therefore study the buffering property mentioned.

PART I - CARBONATION

5.2 INTRODUCTION AND LITERATURE REVIEW

Carbon dioxide can neutralize the surface layer of a concrete structure quite easily, but continuous pores must be penetrated in order for neutralization to occur deeper into the structure. Pores can be classified as closed, accessible, and continuous[96] as illustrated in figure 5.1. For ease of illustration the pores are assumed to be spherical connected by straight tubular capillaries having a distribution of pore sizes. Mass transport phenomena such as ion, moisture and gas movement are controlled especially by the continuous pores. If the cement matrix is completely dry, most, if not all, continuous pores would be open to easy air penetration but the CO_2 present in air would not be able to neutralize the solid alkaline matter in the absence of the aqueous phase, so carbonation would be minimal. On the other hand, if the pores are completely saturated with water, as might be the case of a fully submerged structure, CO_2 cannot enter the pores directly. It must first dissolve in the water near the surface and then penetrate the pores in the form of weak carbonic acid, leading to a negligible carbonation rate. It follows from this fact that a maximum carbonation rate would be achieved at some intermediate moisture content. The majority of the continuous pores would then be empty for easy CO_2 penetration, but enough moisture would be present to first dissolve the CO_2 and then neutralize the basic constituents of the structure[97].

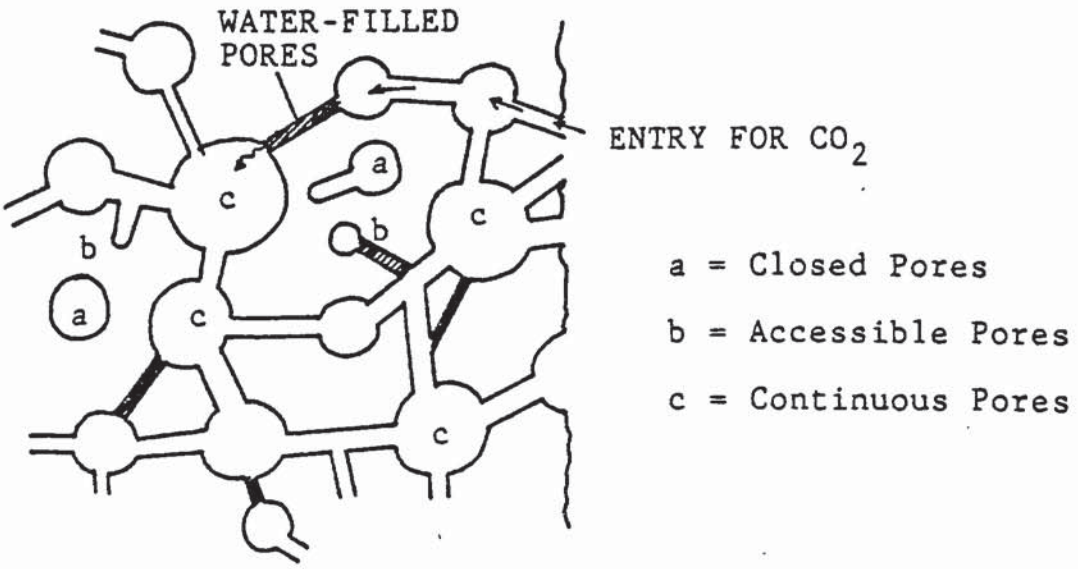

FIGURE 5.1 Simplified pore network of hardened cement paste.

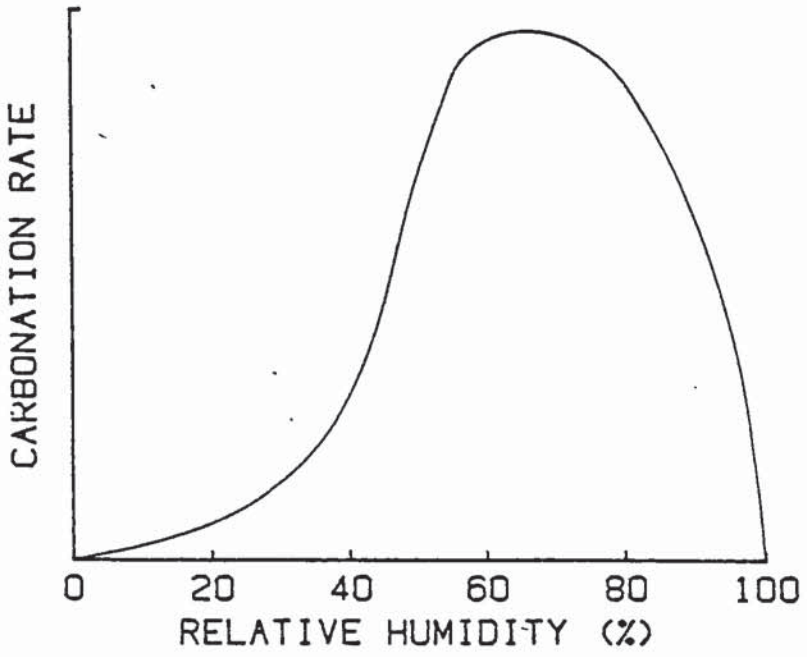

FIGURE 5.2 Rate of carbonation of hardened cement paste or concrete as a function of relative humidity. (After Tuutti).

Figure 5.2 shows the probable rate of carbonation as a function of relative humidity of the surrounding atmosphere. It is generally agreed by researchers that the fastest carbonation rate is achieved at relative humidities between 60% and 70% [98 - 100]. At higher R.H.'s more and more pores begin to fill up with moisture reducing the access of CO_2 as a higher proportion of water filled capillaries must be penetrated by the gas for the continuation of carbonation. According to Tuutti [57] even at a 99.9% RH there are still a substantial number of capillary pores which are not completely filled with water and small changes in the relative humidity at these high values entail considerable changes in the moisture content of the concrete, a fact which can be borne out of the shape of the curve in figure 5.2.

5.2.1 Rate of Carbonation

Carbonation depends mainly on the diffusion of CO_2 into the structure and partly on the counter-diffusion of $Ca(OH)_2$ and other soluble basic phases. It also depends to a lesser extent on the rate of drying or moisture movements outwards as the carbonation reactions cause the release of bound water. It is therefore primarily a diffusional phenomenon, where the carbonation front would be expected to move inwards at a rate proportional to the square root of time.

For the simple unidirectional diffusion of CO_2 into a "uniform" concrete, Page [101] suggested that the rate of advance of the carbonation front, if there is no variation of the diffusion

coefficient D, with time t, or depth, x, would be:

$$\frac{dx}{dt} = \frac{DC}{Ax}$$

(where A represents the quantity of alkaline substances reacting per unit volume of concrete) providing the temperature, relative humidity and CO_2 concentration, C, are constant.

On integration this yields a parabolic relationship,

$$x^2 = \frac{2DCt}{A}$$

$$\text{or} \quad x = K\sqrt{t}$$

Mayer [5] obtained such a relationship for the carbonation of mortars after an induction period where carbonation appeared to commence a certain time after exposure. As he had commented, for long carbonation times, such an induction period is negligible.

A similar relationship was obtained by Schubert and Efes[102] in their experiments with concrete cubes stored at 20° in a 65% RH environment either in air or in 10% CO_2. They had developed a formula for the rate of carbonation as follows:

$$d_k = k_o + V_k \sqrt{t}$$

where d_k is the depth of carbonation in mm

t is the time for carbonation in days

k_o is a constant for a particular condition

and V_k the carbonation rate in mm/day$^{\frac{1}{2}}$

Typical V_k values ranged from less than 1 for air cured specimens to up to 8 for CO_2 cured prisms. They had observed an

obvious dependence on W/C ratios for both curing conditions where higher amounts of water in the original mix resulted in higher carbonation rates.

Alekseev and Rozental [103] in similar experiments verified the square root relationship for short term studies but also observed deviations for longer periods of exposure. They speculated that the reason for the deviations were:

a) A continuing hydration of cement resulting in a higher density concrete and a reduction in CO_2 penetration.

b) A reduction of concrete diffusion permeability with an increasing carbonation layer.

c) A counter diffusion of $Ca(OH)_2$ so that when the flow of $Ca(OH)_2$ gets close in its magnitude to the CO_2 flow, displacement of the chemical reaction zone slows down or stops altogether.

They were able to support their theories to some extent with experimental results which showed that increasing amounts of accelerators such as $CaCl_2$, Na_2SO_4 and $Ca(NO_2)_2 + Ca(NO_3)_2$ slowed down the carbonation rates of their concretes. The retardation was caused, in their opinion by the increase of cement hydration rate and, as a consequence, by the decrease of concrete permeability to CO_2.

H.G. Smolczyk [104 - 107] reporting on long term studies undertaken in West Germany attempted to produce a formula which could predict carbonation rates of most concretes. He plotted carbonation depth after a ten year exposure v's $\frac{1}{\sqrt{B}}$

[104] where B is the compressive strength of the mortar or concrete after 28 days of water curing and found a linear relationship. From that he developed the equation below:

$$x \simeq a\left(\frac{1}{\sqrt{B}} - \frac{1}{\sqrt{B_G}}\right)\sqrt{t}$$

where a= rate constant

B_G= strength limit of carbonation (constant)

t= time of exposure

The two constants depend on the curing condition. His equation was based on 300 test values.

Following further statistical evaluations he later proposed a new formula [106,107] which took into account the W/C ratio of the mix.

$$x = a\left(\frac{W/C}{\sqrt{N_T}} - b\right)\sqrt{t}$$

where a and b are constants depending on carbonation conditions and N_T is the compressive strength of the concrete at T days, which he normally assumed to be 7 days. As there was a degree of deviation from the linear relationship with some concretes, which he attributed to the afterhardening of the structure, he assumed the value T to increase at the rate of about 1 day per year.

For a theoretical explanation of his relationship he turned to Verbeck and Helmuth [108] who had reported that a concrete's compressive strength is inversely proportional to its capillary porosity. Aided by the work of Mills [109] who showed an increase in capillary porosity with increasing

CaO/SiO_2 ratio at constant strength he arrived at the expression:

$$\text{strength} = \frac{f\,(CaO)}{f'(\text{Capillary porosity})}$$

For his relationship of,

$$\text{carbonation} \sim \frac{1}{\sqrt{\text{strength}}}$$

to be true, the following relationship should then exist,

$$\text{carbonation} \sim \sqrt{\frac{f'(\text{Capillary porosity}}{f(CaO)}}$$

which he believed to be true.

He also provided experimental evidence to support the relationship between strength and capillary porosity by determining both the porosities and compressive strengths of mortars cured for varying lengths of time. He assumed that capillary pores are pores with a diameter greater than 300Å. That reinforced the idea that higher W/C ratios result in faster carbonation rates as they also give rise to an increase in capillary porosity.

Treadaway et al [7] when using the Smolczyk formula for their preliminary investigations of carbonation in Bahrain, predicted lower carbonation rates than their measured values after a nine month exposure. It appears therefore that other parameters ommitted from the relationship may have a considerable effect on the rates. Ambient temperature ofcourse is one such important parameter and there is no doubt that temperatures in Bahrain would be higher than those in Germany, even

allowing for the fact that the Bahrain studies were conducted during the winter months. Since carbonation is primarily diffusional, the effect of temperature would be similar to that determined for hydroxyl diffusion in cement pastes in chapter 3, so that higher temperatures would lead to faster carbonation rates.

In short, although the formula developed by Smolczyk might predict carbonation rates in Germany to a high degree of accuracy, it cannot be used in countries of different climatic conditions so a more extensive study might be necessary to develop a more meaningful formula.

It was such unusually high carbonation rates that led to the extensive study in Bahrain where, apart from the differing carbonation rates, results were in general agreement with the other reported studies. Treadaway et al [7] had also found a dependence of carbonation rates of their concretes on pre-carbonated compressive strengths and W/C ratios. They also obtained a relationship between cement content and depth of carbonation after a nine month exposure. In general higher cement contents resulted in lower carbonation depths. This last observation points primarily to the fact that higher amounts of carbonatable material would delay the full neutralization of the concrete, as would be shown in part II of this chapter.

The results of Hamada [110] and Mayer [5] pointed to the same fact. Hamada had observed faster carbonation rates for BFS and Pozzolanic cement concretes but he attributed the

effect only to the reduced amount of $Ca(OH)_2$. Mayer had illustrated the effect of slag cements better by carbonating concretes of varying BFS contents. Higher BFS additions incured increases in the carbonation rates.

As was stated by Smolczyk,[13,14]

$$\text{carbonation} \sim \frac{1}{\sqrt{f(CaO)}}$$

so that an increasing CaO content reduces carbonation significantly. It seems likely therefore that concretes depleted in CaO by additives such as pozzolanas and slags would offer less resistance to neutralization, a phenomenon which is discussed in part II of this chapter.

5.2.2 Effect of Carbonation on Concrete Properties

Because of the intake of CO_2 by the carbonating phases of the cement matrix, carbonation may normally be associated with a mass increase and a reduction in porosity. One other not so obvious change which often occurs is shrinkage. Sauman[100] studied the phenomenon of shrinkage by carbonating mortars containing 27% cement and 6% CaO in various atmospheres and humidities. By measuring the change in length of his mortars with time he obtained a relationship between shrinkage and degree of carbonation. Higher CO_2 partial pressures resulted in higher shrinkage levels. He had also noticed that the maximum effect always occured at 75% relative humidities for any condition.

An explanation for this effect can be found in the theory de-

veloped by Powers [98]. He too observed that shrinkage only accompanied carbonation at intermediate R.H.'s. He explained this phenomenon as follows. The partial drying of the cement paste causes a compressive stress on the calcium hydroxide crystals. As the dissolved $Ca(OH)_2$ in the pore solution carbonates, more dissolves from the stressed crystals slowly releasing the compressive stresses. This gives rise to shrinkage which is proportional to the temporary increase of compressibility of the paste resulting from the removal of calcium hydroxide from regions under stress and deposition of $CaCO_3$ in stress free regions.

Even though there may be a net increase in mass, it would not necessarily prevent shrinkage as the newly formed $CaCO_3$ can neucleate and grow in pores. The other phases in the paste such as the gel, carbonate by topochemical reaction, as will be shown later, and therefore shrinkage would not occur.

The real effect would then be a decrease in porosity leading to a more compact structure. As was shown by Skalny and Bajza [111] higher compaction leads to higher strengths.

Manns and Weshe[112] did observe such a strength increase in some carbonated cement pastes but a decrease in others. In their experiments, pastes containing over 40% OPC by weight showed a definite increase in compressive strength but below that value, a decrease was observed and in general, the higher the OPC content, as opposed to BFS or trass, the higher the final strength achieved. An almost identical trend was observed for the change in weight of CO_2 with time and a good correla-

tion was found between strength and weight changes. For an explanation of these observations they looked at the different reactions of carbonation.

When $Ca(OH)_2$ is carbonated, there is a resultant increase in weight because in effect one mole of water is replaced by a heavier one mole of carbon dioxide.

$$Ca(OH)_2 + CO_2 + H_2O \longrightarrow CaCO_3 + 2H_2O$$

A similar weight increase would also occur for the carbonation of the C-S-H gel. At the other extreme however, ettringite would carbonate as follows:

$$C_3A.3CaSO_4.32H_2O + 3CO_2 + 3H_2O \longrightarrow$$
$$3CaCO_3 + 2Al(OH)_3 + 3CaSO_4.2H_2O + 30H_2O$$

In this case 27 moles of water are lost as opposed to a gain of 3 moles CO_2, resulting in a considerable weight loss. They argued that the cement pastes with the higher proportion of OPC would also produce more $Ca(OH)_2$. When carbonated, they would have a resultant weight increase as opposed to a net decrease in low $Ca(OH)_2$ cements where sulphoaluminates and other polyhydrate phases are most prominent. They were uncertain however as to the link between weight change and variation of strength, but it follows from the earlier argument that the amount of $Ca(OH)_2$ in the precarbonated paste determines the compaction and porosity of the carbonated paste and therefore the final strength. An overall decrease in weight would invariably cause a decrease in strength because of a less compact structure.

The results were reinforced by Mayer [5] who, as part of his extensive study on carbonated concrete, found a similar relationship between OPC content and strength increase in mortars exposed to an atmosphere of 80% RH and 10% CO_2. He observed a significant increase in compressive strength for carbonated OPC and low BFS mortars. A 50% BFS content induced only a small rise in strength whilst higher slag contents were largely ineffective. The strength of mortars made from supersulphated cement had decreased substantially.

There is a general agreement in published literature on the effect of carbonation on porosity [113 - 115] which, as assumed earlier, is reduced significantly. Rozental and Alekseev [113], with the aid of mercury intru sion porosimetry, had shown that pores in the range of 0.01-1μm diameter in carbonated mortars of 0.5 and 0.6 W/C ratios, had decreased by about half the volume. In general there was a displacement of the maxima of the pore volumes towards larger pores as well as the reduction mentioned. This effect may be caused to some extent by the dissolution of $Ca(OH)_2$ crystals present in larger pores followed by carbonation and nucleation of $CaCO_3$ in the higher moisture content smaller pores where dissolution of CO_2 might be easier. Certainly Rozental and Alekseev found that pores greater than 12μm in diameter had shown no evidence of carbonation when examined under the microscope. Pihlajavaara [116] in similar studies found that the most affected pores were in the range of 20 to 100nm diameter and that smaller or larger pores were mainly unaf-

fected. The smaller pores were likely to be gel pores, so it appears that no carbonation products were deposited there.

In determining the non-evaporable water contents of his OPC pastes, he established that carbonation had caused a considerable release of bound water as the hydrates had decomposed. As an example, for his 0.5 W/C ratio paste, the non-evaporable water content dropped from 17% to 7%. This was accompanied by an intake of CO_2 of 36%. All weights were by weight of the original unhydrated cement.

In a later publication, Pihlajavaara and Pihlman [117] studied the effect of W/C ratio and R.H. on the amount of CO_2 intake. They had found a definite dependence on these parameters, 0.45 W/C ratios resulting in higher "bound" CO_2 levels than 0.3 and similarly 70% RH causing an increase in CO_2 binding as opposed to 40%. A maximum CO_2 content of 32% was thus determined at the 0.45 W/C ratio level exposed at at 70% RH.

It is safe to assume that the greater part, if not all, of the CO_2 intake is by the CaO- bearing phases so that the 32% CO_2 level mentioned would represent about 40% carbonated CaO. If an OPC is assumed to contain 65% CaO by weight, then there still remains as much as 25% "unreacted" CaO in the carbonated paste. This figure is the same as that mentioned by Smolczyk [106] but he also stated that "the uncarbonatable CaO seems to be independent of the type of cement and the W/C ratio and has fairly consistent values between 25 and 30 wt-% of the cement".

In another paper [104] he showed this to be true for both OPC and BFS cements which were fully carbonated in air. It was not the case however for the same cements carbonated in 3% CO_2 atmospheres where the amount of CaO carbonating was consistently higher.

As mentioned earlier, T.C. Powers [98] had speculated that the less soluble phases in cement carbonated by topochemical reactions. His hypothetical account of the carbonation of the calcium silicate gel was as follows. If it is accepted that the calcium ions in the gel are between sheets of silica and at the exposed surfaces and that these particles are generally 2-3 sheets thick, then one half to two-thirds of the calcium is immediately available to solutes in the pores. As the surface calcium ions react with dissolved CO_2 the resultant calcium carbonate molecules remain attached to the underlying silica. A chemical reaction localized in the inner layer could still ensue, but since it would involve diffusion of atoms within the solid phase, the process might be a slow one.

If the same applies for all fairly insoluble CaO bearing phases in the structure then the observations that a substantial amount of CaO remains uncarbonated are not unrealistic. Furthermore, with higher CO_2 partial pressures, more of the core would carbonate owing to a higher concentration of the dissolved CO_2 in the pore solution enabling easier penetration to within the particles.

The "topochemical reaction" theory was supported experimentally by Sauman [99, 100] who had found that both C-S-H gel and 1·1Å- tobermorite when carbonated, did not change substantially in morphology even though the resulting structure was a mixture of SiO_2- gel, calcite and vaterite. A similar observation was reported by R.L. Berger [118] who studied uncarbonated and carbonated C_3S/C_2S pastes under the SEM.

All three modifications of $CaCO_3$, vaterite, calcite and aragonite, have been reported in the literature on carbonation but aragonite is the least common.

Sauman [99] had established that the C-S-H gel when carbonated formed first vaterite which then transformed either partly or fully to the more stable calcite. A relative humidity of 100% resulted in the rapid and complete transformation of the vaterite into calcite. Higher CO_2 levels of 30% also facilitated a more complete transformation. Aragonite was only formed to a very small extent. In another publication [119] he reported on the carbonation of the C_3AH_6 phase. His results pointed to the formation of a metastable complex carbonate as shown by the equation.

$$4(3CaO.Al_2O_3.6H_2O) + 3CO_2 + (1+X)H_2O \longrightarrow$$

$$3(3CaO.Al_2O_3.CaCO_3.XH_2O) + 2Al(OH)_3$$

This was then carbonated further to $CaCO_3$.

$$3CaO.Al_2O_3.CaCO_3.XH_2O + 3CO_2 + 3H_2O \longrightarrow$$

$$4CaCO_3 + 2Al(OH)_3 + XH_2O$$

The $CaCO_3$ was again in the form of vaterite with a later transformation to calcite.

11Å - tobermorite paste ($C_5S_6H_5$) showed a similar behaviour during carbonation [120] but an addition of 5% Al_2O_3 in the mix slowed down the carbonation rate and also resulted in the formation of less vaterite for the same conditions. A C_2SH paste carbonated even slower, showing that small variations in the gel structure could lead to different rates of carbonation.

R. Kondo et al [115] by carbonating mortar prisms through one surface only, were able to show a relative variation of the calcium carbonate modifications with increasing depth. At the deeper parts of the prisms where carbonation had been relatively fresh, the carbonate was of a more amorphous nature as compared to calcite found at intermediate depths. Nearer the surfaces, the amount of calcite decreased at the expense of the increasing vaterite. They claimed that calcite was formed more readily during early carbonation but vaterite was more likely at the later stages as the unhydrated C_3S starts to carbonate. As they had cited in the literature, hydrated C_3S tends to produce calcite but the unhydrated form produces vaterite.

Other studies [121-123] had shown that the formation of vate-

rite is favoured by high pH's, higher temperatures and lower humidities. A general argument might be that the finer crystalline vaterite would form more readily where the reactions are faster and where the nucleation of calcium crystals is easier as opposed to the slower but more stable large crystalline calcite. Where conditions permit, the vaterite could then slowly recrystalize to the coarser morphology. This is ofcourse only speculation as this is one area where conflicting results have been published.

In summarising, the affected properties after carbonation are:

(i) Mass, which can be either an increase or a decrease depending on the balance between water lost and CO_2 gained in the carbonation reactions.

(ii) Non-evaporable water, as the bound water is liberated.

(iii) Porosity, as pores are filled up by expansive $CaCO_3$ products or vacated by lost water.

(iv) Strength, according to final compactness, which is closely related to porosity.

(v) Shrinkage, depending on soluble carbonatable products such as $Ca(OH)_2$, and on relative humidity.

(vi) pH, with a reduction of hydroxyl ions in the pore solution leading to more neutral values.

The drop in pH is ofcourse the most obvious change that would

affect the steel reinforcement, as it destroys the normally passivating medium, and also the high pH buffering capacity offered to steel by soluble phases such as $Ca(OH)_2$. Another property not yet mentioned but which may have a significant effect on corrosion initiation, is the carbonation of the insoluble complex calcium chloroaluminate salt. In chapters 3 and 4 it was shown that a considerable amount of chloride could be removed from the pore solution by the complexation. As this phase is a CaO bearing phase, it would be expected to carbonate as follows:

$$3CaO.Al_2O_3CaCl_2.10\ H_2O + 3CO_2 + 3H_2O \longrightarrow$$
$$3CaCO_3 + 2Al(OH)_3 + CaCl_2 + 10H_2O$$

possibly topochemically, releasing a substantial amount of $CaCl_2$ back into the solution. The disadvantage of such a process is obvious when accompanied by the vast reduction in OH^- concentration whereby an original low $[Cl^-]/[OH^-]$ ratio is increased to far beyond acceptable values.

The effect need not be as straight forward as this. If one considers the case where the carbonation depth reaches a point where 10-15mm of uncarbonated material remains as cover for the steel, the bound chloride released into the solution in the carbonated zone would then start to diffuse inwards, towards the lower chloride levels surrounding the steel. The migration of chloride would be better facilitated by the counter diffusion of OH^- ions towards the neutral zone, leading to a higher chloride level than was previously anticipa-

ted (see figure 5.14).

It should be possible to minimize this unwelcome effect of chloride release and indeed of carbonation by choosing the right concrete structure. The rate of carbonation depends, as was discussed earlier, on the:

(i) Relative Humidity with a maximum between 60% and 70%.

(ii) CO_2 partial pressure in the atmosphere.

(iii) W/C ratio of the original mix.

(iv) Capillary porosity which also depends in part on W/C.

(v) Amount of carbonatable material, which in turn depends on the:

(a) Degree of hydration

(b) Amount of cement in the mix

(c) Type of cement

A high CaO content portland cement with a sufficiently low water to cement ratio and a high proportion of cement in the mix would thus give excellent anti-carbonation properties, especially if accompanied by a thick depth of cover for the protection of the reinforcement. The construction industry however needs firstly to be persuaded that such measures are economically viable. Furthermore, there may be cases where a thin depth of cover may be unavoidable, or where special cements need to be used for a particular property such as low

ionic diffusivity, which may be less resistant to carbonation.

For these reasons, carbonation of concrete would continue to be a problem for some time yet, and a continued study of the phenomenon is essential. It would be a great advantage if experiments could be accelerated as the process of "normal" carbonation can be so slow. The "speeding-up" method must be comparable to air-carbonation as much as possible.

In this part of chapter 5, an attempt was made to answer two important questions regarding carbonation.

(i) Whether accelerated carbonation in the form of high CO_2 content atmospheres would yield comparable results to the "normal" carbonation of an OPC, and,

(ii) Whether the bound chloride, present in the form of insoluble salts, is released back into the solution and to what extent.

5.3 EXPERIMENTAL PROCEDURE

To enable the comparison between natural and accelerated carbonation, it was necessary to study the following parameters, with cement pastes made from OPC and carbonated in different atmospheres.

a) Rate of carbonation,
b) Concentration of ions in the pore solution,
c) Proportion of free and bound chloride present in the pastes,
d) Water and CO_2 binding capacity and porosity,
e) Crystal structure of the resultant carbonation products,
f) Diffusion characteristics.

5.3.1 Preparation

The cement paste cylinders were made as normal from OPC-B' cement, with or without a 1%Cl^- addition, by weight of cement in the form of NaCl and were demoulded after an eight day curing period at 20°C. The cylinders were then sliced normally into 3mm discs (see chapter 2, paragraph 2.2) and placed in a "standing" position in groups of 36 chloride-free plus 36 chloride-rich discs on four specially made perspex racks. The racks were placed individually above a saturated $NaNO_2$ solution in air-tight containers at room temperature, thus maintaining the relative humidity to about 65% (fig 5.3), as recommended by the RILEM permanent committee [124]. A gas of a certain known composition was passed over the discs and

through a water trap for half an hour at 24 hour intervals. It was necessary to follow this procedure in order to avoid changes in humidities with the continued passage of the gas. The gases used were, N_2, 100% CO_2 and a mixture of 5% CO_2, 10% O_2 and 85%N_2. One container was simply exposed to the lab air for similar periods of time.

5.3.2. Rate of Carbonation

At regular intervals, discs were removed from the containers and broken by hand at right angles to the flat surfaces. A 1% phenolphthalein in alcohol solution was then applied to the freshly broken surfaces which were allowed to stand for about 10 minutes. The carbonation front was assumed to be the interface between the colourless and the red coloured parts of the surface, which was more often than not a clear straight boundary. A travelling microscope was used to measure the depth of carbonation on three different discs to the nearest 100μm, and the average value was recorded for each condition.

Thirty days after the complete carbonation of the chloride-free discs in the 5% CO_2 condition, all the discs from the three containers, excluding those exposed to air, were saturated with deionised water. This was achieved by first determining the evaporable water of representative discs in each condition and of "control" discs cured at a 100% RH environment, and then replacing the "lost water" by flooding the one surface of the discs with the appropriate amount of water, which was quickly absorbed by the cement. Any error was sub-

sequently corrected by allowing the discs to stand in a 100% RH environment, replacing the $NaNO_2$ solution by water in the same containers. After 7 days of such an exposure the new evaporable and non-evaporable water contents were determined (chapter 2, paragraph 2.5). The same procedure was repeated for the air-exposed discs 30 days after the complete carbonation of the non-chloride containing pastes. The "saturation" process was essential, because at 65% RH there is not sufficient water to be pressed for analysis. Any small changes incurred in the pore solution are unavoidable, but by following the same procedure for all conditions it was hoped that the results would be comparable.

5.3.3 Analysis of the Phase Composition

Samples from 4 different discs representing each condition, were ground to a powder and subjected to DTA and X-Ray Diffraction analysis (see chapter 2, paragraph 2.8). Powder from the same samples was also used for determining the total CO_2 content as described in chapter 2 paragraph 2.6. MIP investigations and total chloride determinations were carried out as normal (chapter 2, paragraphs 2.9 and 2.7).

5.3.4 Solution Analysis

Fourteen discs from each condition were then pressed with the use of the "pore-press" as described in chapter 2, paragraph 2.3, and the extracted solution analysed for the usual ions. In the case of low hydroxyl content solutions, a pH

electrode and a meter was used to determine the pH values (chapter 2, para. 2.4.2). Because only 2-3 ml of solution was available from each extraction, this was emptied in a tall and narrow plastic container only slightly larger in diameter to the electrode, so that more area of the electrode could be immersed in the solution. The pore solutions were then analysed for CO_3^{--} and HCO_3^- by titrating with 0.001 M HNO_3 while monitoring the pH (see results).

5.3.5 Diffusion Characteristics

Five non-chloride-bearing discs from each condition were also subjected to chloride diffusion at 25°C by the technique discribed for hydroxyl diffusion in chapter 3 part II. The solutions used in the compartments of the cells for the carbonated discs, were 1M NaCl in the one and deionised water in the other.

The "control" specimens which were exposed to either N_2 at 65% RH or to air at 100% RH had to be equilibrated in two litres of sat.$Ca(OH)_2$ for 60 days. The same solution was then used as the "base" solution in both compartments of the cell with an addition of 1 mole per litre NaCl in side 1. This technique ensured virtual equilibrium of the concentrations of ions in the pores and in the outer "base" solution so that any diffusion was caused only by the NaCl added in the one compartment and not influenced, for instance, by the leaching of potassium or similar ions from within the cement paste.

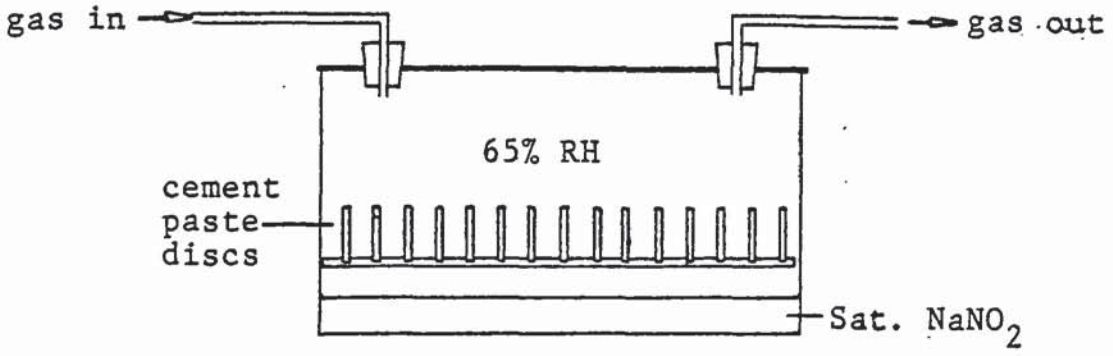

FIGURE 5.3 Equipment set-up used for the carbonation of OPC-B' cement pastes.

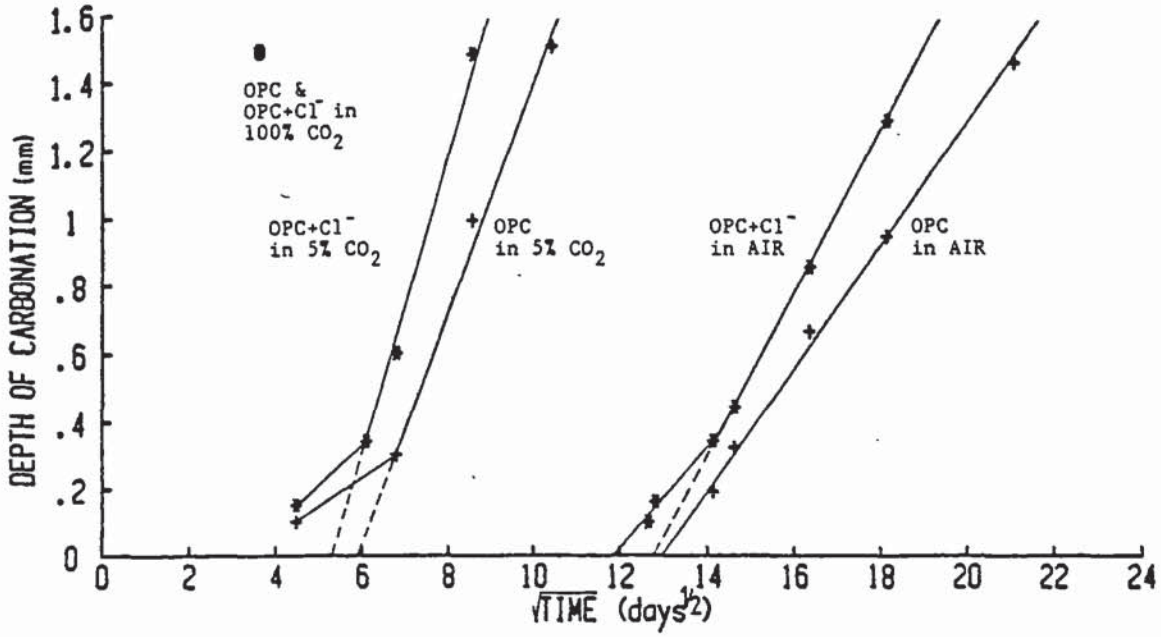

FIGURE 5.4 Plots showing the parabolic relationship between carbonation depth and time of exposure of OPC-B' pastes to different CO_2 atmospheres.

5.4 RESULTS

5.4.1 Rate of Carbonation

The increase in carbonation depth with the square root of time is represented graphically in figure 5.4 for four conditions, namely for discs with or without chloride exposed to air or to 5% CO_2. A full table can be found in appendix 20. It was not possible to determine such plots for discs exposed to 100% CO_2 as carbonation was very rapid and complete, even after 13 days when the first carbonation depths were determined.

After a certain induction period, the depth of carbonation increased linearly with the square root of time for all studied conditions. An equation similar to that used by Schubert and Efes [102] represented each condition adequately.

$$x = k\sqrt{t} - k_o$$

where x = depth of carbonation (mm)

t = time for carbonation (days)

k = the constant for the rate of carbonation ($mmday^{\frac{1}{2}}$)

k_o = constant relating to the induction period t_o by:

$$k_o = k\sqrt{t_o}$$

Values of k and t_o are tabulated in table 5.1. Higher values of k represent faster carbonation rates so a 5% CO_2 atmosphere

induces faster rates than air. There is also an effect caused by the added chloride which actually encourages faster carbonation. It is also evident from table 5.1 that a condition leading to a higher carbonation rate, also leads to a shorter induction period as will be discussed later.

5.4.2 Concentration of ions in the Pore Solution

Ionic concentrations and pH values of the extracted solution for each condition are represented in table 5.2. The amount of carbonates and bicarbonates shown are the maximum possible in the pore solution. When titrating a carbonate solution with acid, two inflections are established at around pH 9 and 4, where the first coincides with the point of conversion to bicarbonate and the second with the complete neutralization (125).

No such clear inflections were observed when monitoring the pH with the acid addition. The results shown are therefore those representing the amount of acid needed to neutralise an assumed total amount of carbonate or bicarbonate in the solution down to pH 4. This, although not perhaps totally representative, at least shows that very little sodium or potassium carbonate can exist in the extracted pore solution. (For the calculation of carbonates see appendix 21).

The same result is apparent from the amount of Na^+ and K^+ ions in the carbonated cements where values drop from 85 and 228 mM/litre respectively, to less than 25, indicating once

TABLE 5.1 Carbonation rate constants and induction periods for OPC-B' pastes carbonated in various atmospheres.

ATMOSPHERE	SPEC. NO.	$k(mm/day^{\frac{1}{2}})$	t_o(days)
AIR	B1	0.180	165.3
"	B2*	0.238	161.6
5% CO_2	C1	0.332	33.3
"	C2*	0.470	29.4

TABLE 5.2 Concentration of ions in the pore solution of OPC-B' pastes after exposure to various atmospheres (mM/l).

ATMOSPH.	NO.	pH	OH^-	Cl^-	Na^+	K^+	Ca^{++}	Σ^-	Σ^+	MAX. CO_3^{--}	POSS. HCO_3^-
N_2	A1	13.46	288	1	85	228	-	289	313	-	-
"	A2*	13.66	458	227	580	208	-	685	788	-	-
AIR	B1	11.45	2.8	8	22	4	31	11	88	15	1
"	B2*	10.48	0.3	651	369	23	221	651	834	7	4
5% CO_2	C1	9.22	$2x10^{-2}$	13	10	6		13	16	3	41
"	C2*	8.56	$4x10^{-3}$	545	300	20		545	320	-	25
100% CO_2	D1	7.42	$3x10^{-4}$	16	23	20		16	43	-	26
"	D2*	6.79	$6x10^{-5}$	533	330	31		533	361	-	10

TABLE 5.3 Ionic concentrations (mM/g) x 10^3.

NO.	OH^-	Cl^-	Na^+	K^+	Ca^{++}	Σ^-	Σ^+	CO_3^{--}	HCO_3^-
A1	80	0	24	64	-	80	88	-	-
A2*	158	79	201	72	-	237	273	-	-
B1	1	2	5	1	7	3	20	3	-
B2*	0	174	99	6	59	174	223	2	1
C1	0	2	2	1		2	3	1	8
C2*	0	137	75	5		137	80	-	6
D1	0	3	5	4		3	9	-	6
D2*	0	139	86	8		139	94	-	3

* OPC-B' pastes containing 1% Cl^- as NaCl.

more that the amount of sodium or potassium carbonate or bicarbonate in solution cannot be very high.

The drop in pH is also apparently dependent on the degree of carbonation. Higher CO_2 containing atmospheres induced lower pH values, but also the NaCl added in the original mix had caused a further reduction in pH.

Table 5.3 represents the amount of ions in each cement type in millimoles per gramme of unhydrated cement.

5.4.3 Total Free and Bound Chlorides

Total free and bound chlorides (see chapter 2, paragraph 2.7) and their different ratios, are shown in table 5.4.

It can be seen that, as suspected, a considerable amount of bound chloride is released back into the solution and, judging by the Ca^{++} content in carbonated cement B2, the released chloride is in the form of $CaCl_2$. As mentioned earlier the release would be caused by the carbonation of the calcium chloroaluminate phase. It appears that "normal" carbonation had encouraged more chloride release than accelerated carbonation, where for both the 5%CO_2 and the 100%CO_2 conditions the final free chloride had reached similar values.

5.4.4 Water and CO_2 Binding Capacity; Porosity

Tables 5.5 and 5.6 represent the evaporable and non-evaporable water contents before and after the addition of moisture.

TABLE 5.4 Total, free and bound chloride concentrations of OPC-B' pastes after exposure to various atmospheres (mM/g) x 10^3.

ATMOSPH.	NO.	TOTAL	FREE	BOUND	FREE / TOTAL	BOUND / TOTAL	BOUND / FREE
N_2	A2	239	79	160	0.331	0.669	2.025
AIR	B2	241	174	67	0.722	0.278	0.385
5% CO_2	C2	253	137	116	0.542	0.458	0.847
100% CO_2	D2	248	139	109	0.560	0.440	0.784

TABLE 5.5 Evaporable and non-evaporable water after exposure of the cements to various atmospheres and before moisture saturation (ie at 65% RH).

ATMOSPHERE	NO.	We(g/g)	Wn(g/g)	TOTAL(g/g)
N_2	A1	0.1523	0.1584	0.3107
"	A2*	0.1655	0.1641	0.3296
AIR	B1	0.0817	0.0221	0.1038
"	B2*	0.1085	0.0203	0.1288
5% CO_2	C1	0.0910	0.0388	0.1298
"	C2*	0.1095	0.0470	0.1565
100% CO_2	D1	0.1346	0.0555	0.1901
"	D2*	0.1582	0.0525	0.2107

TABLE 5.6 Evaporable and non-evaporable water and CO_2 contents after moisture saturation.

NO.	We(g/g)	TOTAL LOSS AT IGNITION	CO_2	Wn(g/g)	TOTAL WATER
A1	0.2790	0.1751	—	0.1751	0.4541
A2*	0.3459	0.1695	—	0.1695	0.5154
B1	0.2134	0.3525	0.3333	0.0192	0.2326
B2*	0.2673	0.4014	0.3844	0.0170	0.2843
C1	0.1921	0.4501	0.4098	0.0403	0.2324
C2*	0.2508	0.4793	0.4294	0.0499	0.3007
D1	0.2078	0.4956	0.4393	0.0563	0.2641
D2*	0.2604	0.5012	0.4484	0.0527	0.3131

* OPC-B' pastes containing 1% Cl^- as NaCl.

Total amount of CO_2 emitted at ignition to 1000°C is also shown in table 5.6 for each condition and once again the values are higher for the specimens in higher CO_2 atmosperes or with the chloride addition.

There are also differences in the water contents. The drop in the non-evaporable water represents the release of bound water owing to the carbonation reactions. The decrease in evaporable water points to a reduction in pore volume, a fact which is clearly seen from the MIP results, as shown in figures 5.5 and 5.6.

5.4.5 Crystal Structure of Carbonated Products

The Differential Thermal Analysis thermographs are represented in figure 5.7. The endothermal peaks associated with the $Ca(OH)_2$, calcium sulphoaluminate and calcium chloroaluminate phases are no longer evident in any of the carbonated conditions. Instead they are replaced by a shallow "hump" starting at about 500°C and often terminating at a peak at around 700°C and by a large peak at 900°C. If a NaCl addition was made in the cement originally, a peak is also observed just before 900°C. Often a peak appears at that position associated with NaCl [126].

A peak is still observed at just after 100°C but it is reduced substantially. This is often related to the dehydration of the C-S-H gel but its size for specimen D2, which showed maximum carbonation, may also suggest the release of

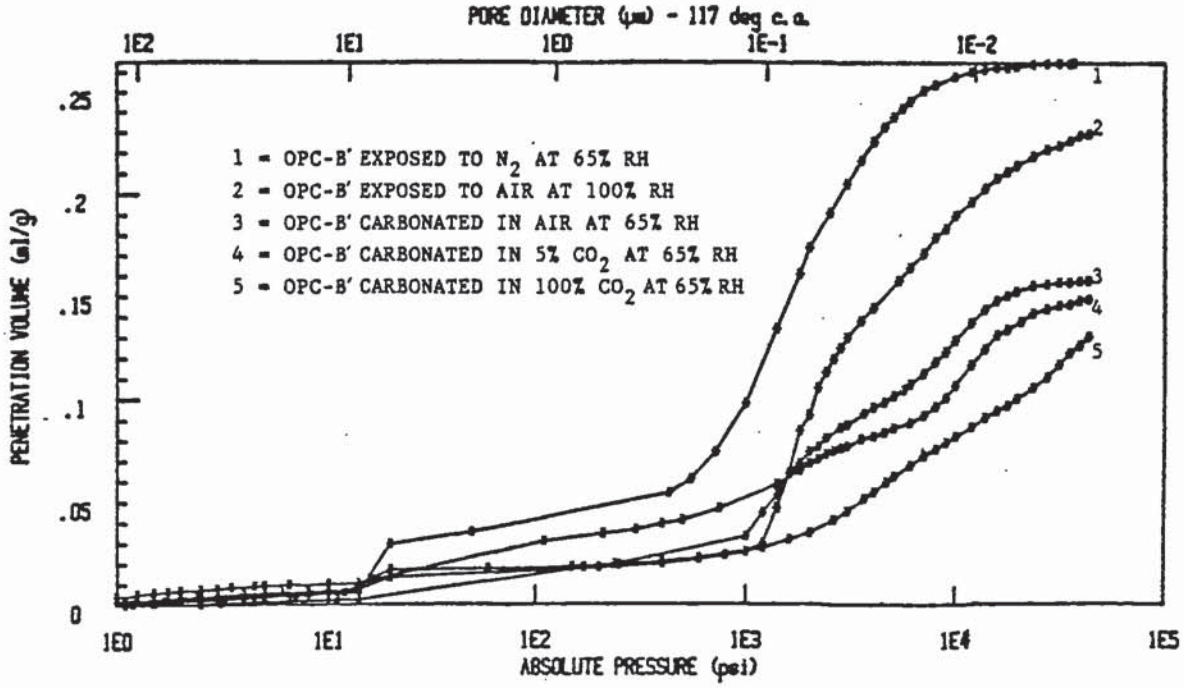

FIGURE 5.5 Pore size distribution curves of OPC-B' pastes after exposure to different atmospheres.

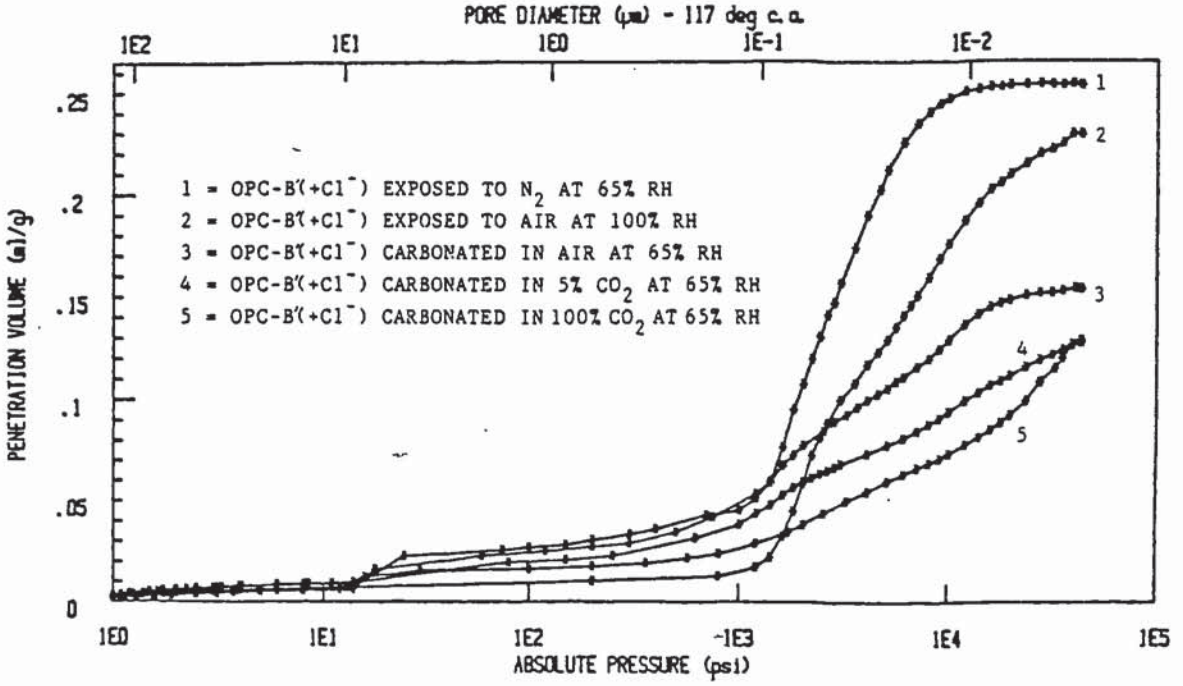

FIGURE 5.6 Pore size distribution curves of OPC-B' pastes containing 1% Cl^- (as NaCl) after exposure to different atmospheres.

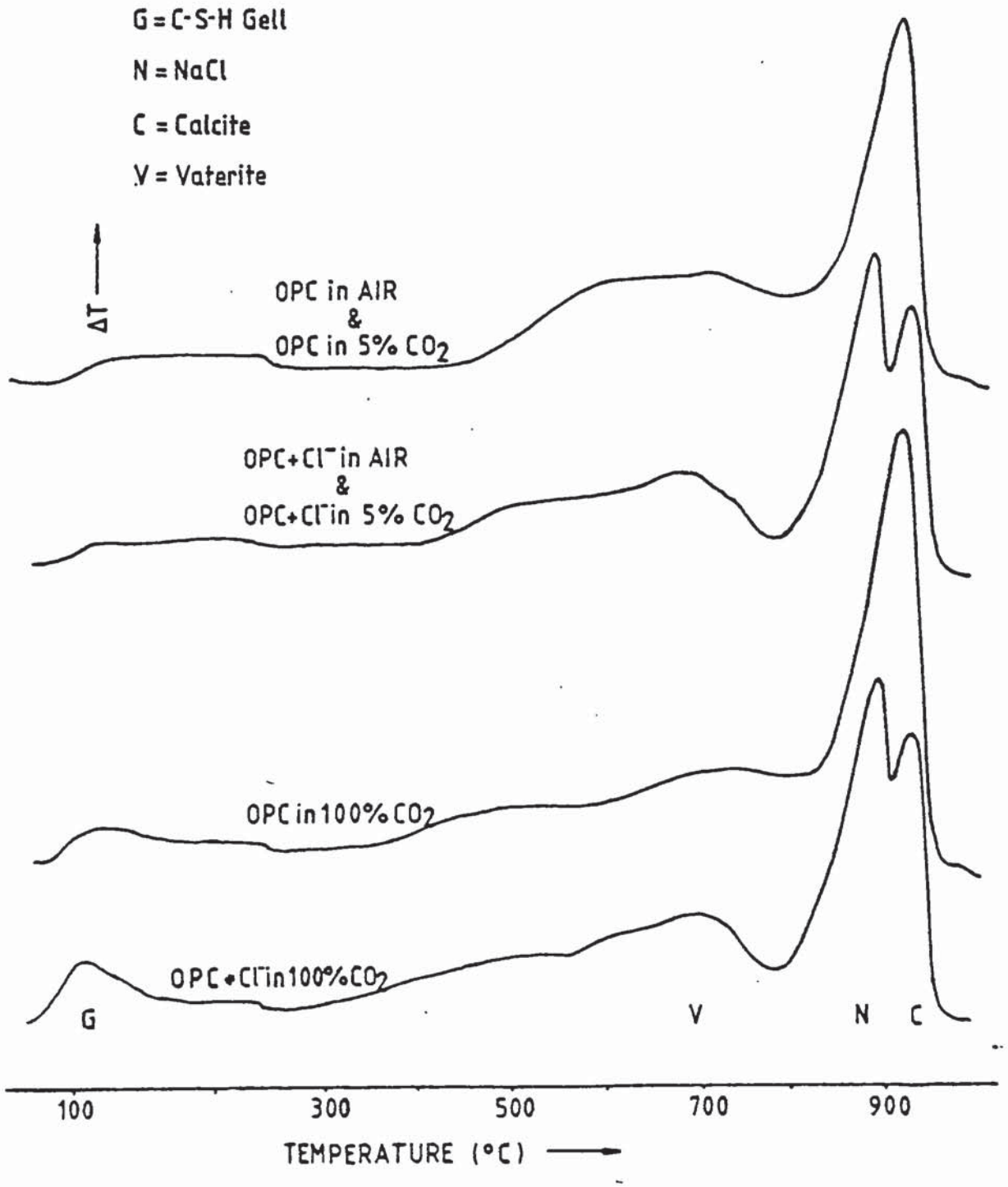

FIGURE 5.7 DTA thermographs of OPC-B' pastes with or without an addition of 1% Cl^- (as NaCl) carbonated in various atmospheres.

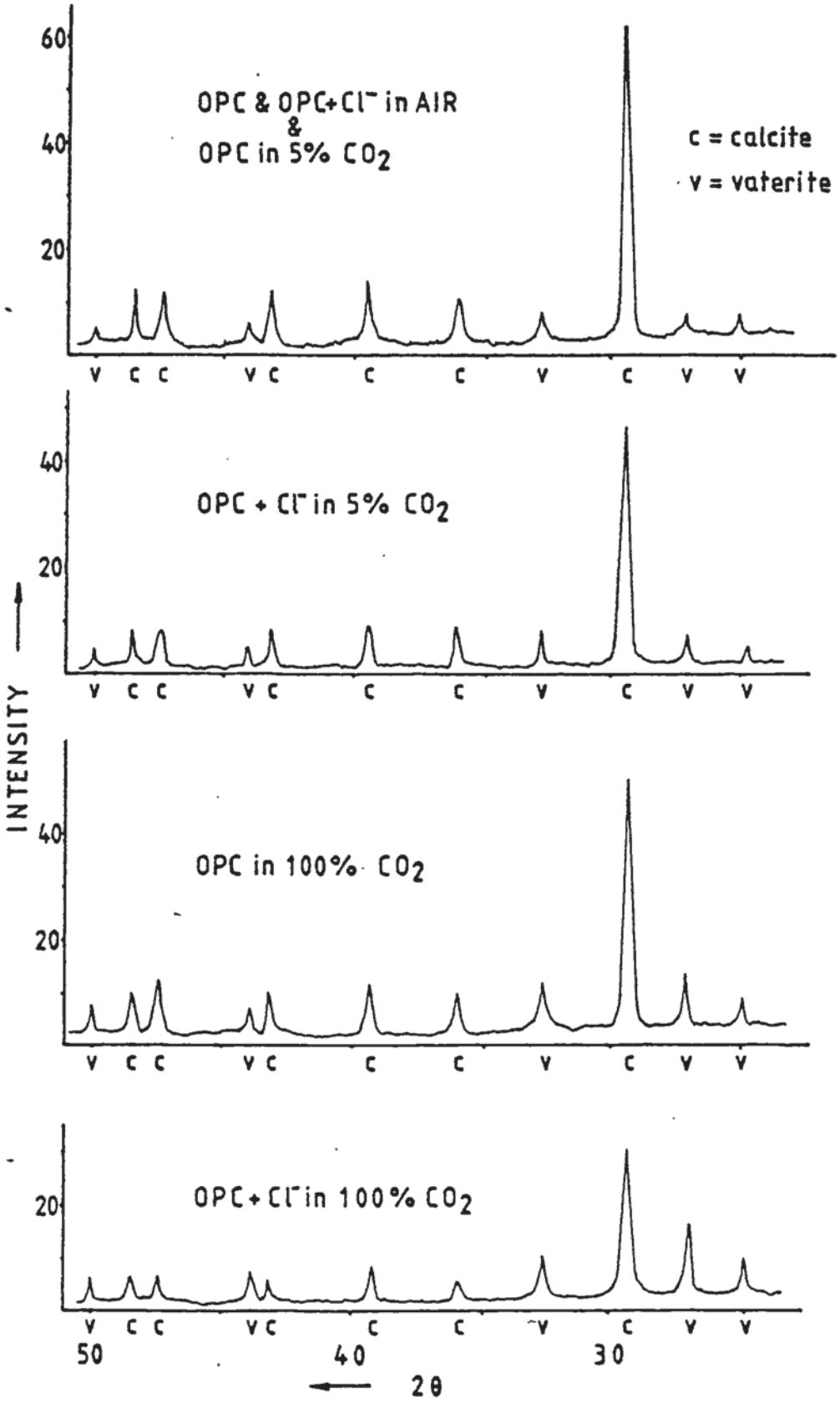

FIGURE 5.8 XRD traces of OPC-B' pastes with or without an addition of 1% Cl^- (as NaCl) carbonated in various atmospheres.

water which may have been "entrapped" within the fast-forming carbonation products owing to the excessive carbonation rate.

According to Lach and Sauman [127], calcite shows an endothermic reaction between 750°C to 900°C, but a less crystalline form of calcite decomposes at lower temperatures between 600°C - 750°C. Calcite II, as they had termed it, is formed during heating by the transformation of vaterite or aragonite to calcite at 505°C and 460°C respectively, and it exists in a very fine form having no time to crystallize properly into larger ordered crystals. The peaks obtained in the present work are thus associated with the highly crystalline calcite, formed during the carbonation process (peak at 900°C) and with the less crystalline form transformed from aragonite or vaterite (peak at 750°C).

X-Ray diffraction graphs (figure 5.8) show that only vaterite and calcite peaks are present for all the carbonated specimens. The ratio of vaterite to calcite appears to be the same for both air exposed specimens and for the non-chloride containing specimen exposed to 5%CO_2. It then increases with the rate of carbonation, so that the maximum amount of vaterite appears in the chloride containing specimen exposed to 100% CO_2.

5.4.6 Diffusion Characteristics

Diffusion coefficients for Na^+ and Cl^- ions are shown in table 5.7. By studying the diffusivities, it is clear that

TABLE 5.7 Effective Diffusion coefficients for Na^+ and Cl^- in OPC-B' before and after carbonation in various atmospheres.

ORIGINAL CURING CONDITION	EXPOSURE ATMOSPHERE	WHETHER CARBONATED	$D[Na^+]$ $(x10^9)$ cm^2s^{-1}	$D[Cl^-]$ $(x10^9)$ cm^2s^{-1}	$\frac{D[Na^+]}{D[Cl^-]}$
100% RH	AIR	NO	50.6	103.5	0.49
65% RH	N_2	NO	76.0	119.6	0.64
"	AIR	YES	228.2	230.2	0.99
"	5% CO_2	YES	120.3	113.2	1.06
"	100% CO_2	YES	294.4	281.9	1.04

Note: Full values of D can be found in appendix 12.

TABLE 5.8 Amount of $CaCO_3$, reacted and unreacted CaO in OPC-B' after carbonation (g/g)

NO	$CaCO_3$	REACTED CaO	UNREACTED CaO
B1	0.7574	0.4242	0.2098
B2*	0.8735	0.4849	0.1448
C1	0.9341	0.5216	0.1124
C2*	0.9759	0.5465	0.0875
D1	0.9984	0.5591	0.0749
D2*	1.0191	0.5707	0.0633

* OPC-B' pastes containing 1% Cl^- as NaCl.

carbonation in air and in the 100% CO_2 atmosphere has caused a considerable increase in the diffusion coefficients of both the Na^+ and Cl^- ions a fact reinforced by Traetteberg [61], who had found that carbonation had increased the penetration rate of chloride in cement pastes. Surprisingly carbonation in 5% CO_2 did not appear to influence the diffusivity of the chloride ions, a fact which will be discussed later. The increase in Na^+ ion diffusivity was also much less.

The increased porosity of the cement paste cured in a 65% RH environment had caused a slight increase in the diffusivity of both ions but in particular of Na^+ ions.

In agreement with results from chapters 3 and 4, sodium and chloride ions in carbonated cements diffused at the same rate, as no other ions were involved. But for the uncarbonated specimens in both cases, chloride diffused faster than sodium. This phenomenon will be discussed further in the discussion section.

5.5 Discussion

5.5.1 Rate of Carbonation

The carbonation front as determined by phenolphthalein, appears to be a sharp change from uncarbonated to carbonated material, but in reality this cannot be the case. Figures 5.9 a,b and c represent the systematic neutralization of the paste. As shown in figure 5.9a, the pH at the surface quickly drops to that of Sat.$Ca(OH)_2$ with the diffusing CO_2 neutralizing the sodium and potassium hydroxides. The pH remains at 12.5 for as long as there is sufficient $Ca(OH)_2$ near the surface to maintain a saturated solution. When this in no longer the case, the pH at the surface drops to a lower value, to a level where other basic constituents may buffer the solution, and so on.

Carbonation would only be apparent when the pH drops below 9. There may ofcourse be more plateaus depending on the type of cement, as will be shown in part II. As a consequence of this phenomenon, there would be an induction period, where no apparent carbonation would be evident, as ofcourse was shown by the results. Furthermore, the slower the carbonation, the longer the induction period would be. As was commented however by Mayer [5], for long carbonation times such an induction period is negligible.

For thin discs, as the carbonation front moves inwards systematically from both sides, successive plateaus start to be

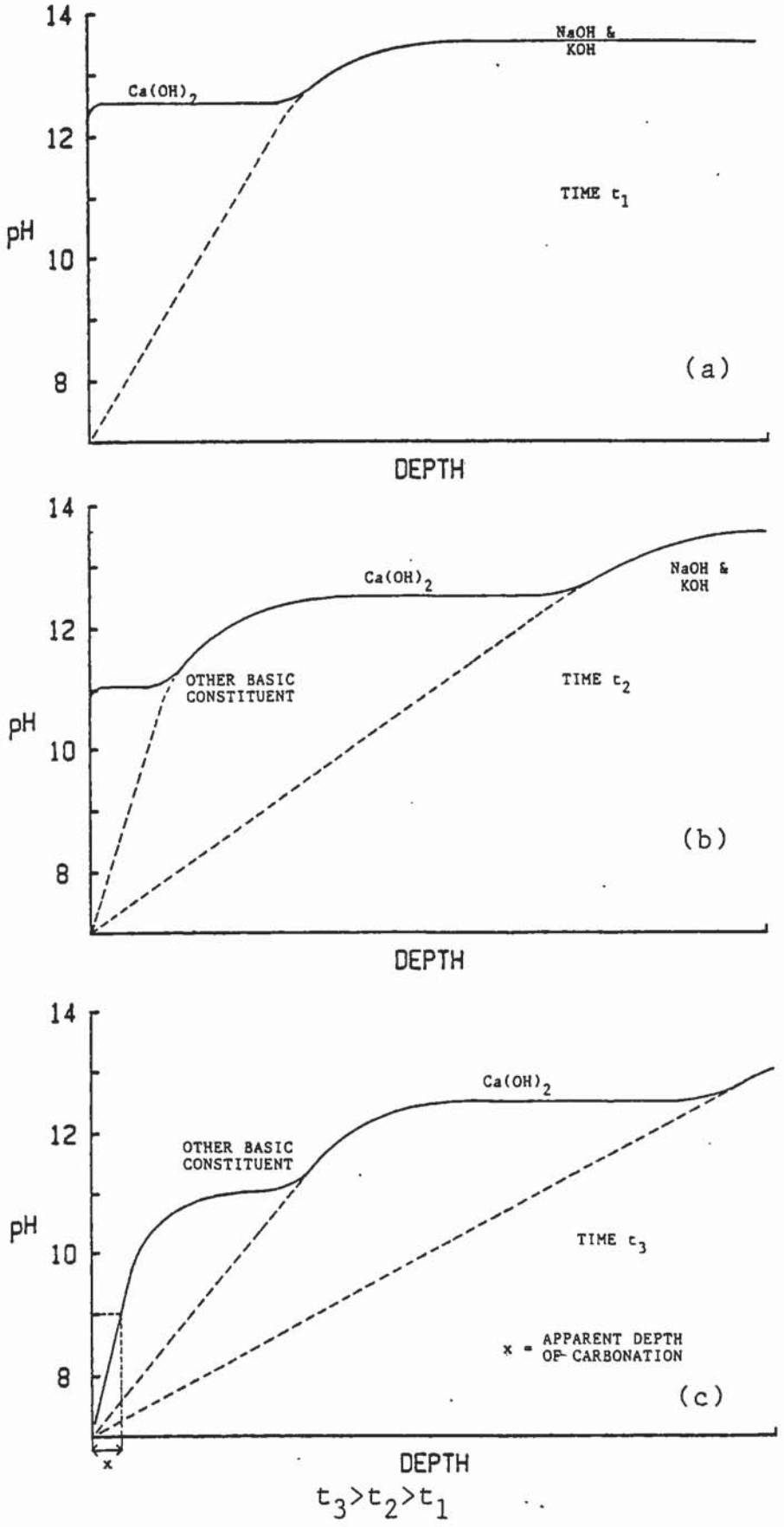

FIGURE 5.9 Schematic representation of the progressive neutralization of cement paste by the penetration of CO_2.

eliminated as the materials causing them are continuously neutralized. At an apparent complete carbonation, the pH profile would be as shown in figure 5.10.

This discs also represent a much more idealised situation as compared to larger structures as the internal moisture can reach equilibrium with the outside environment very quickly and any water released by the carbonation reactions can diffuse outwards rapidly. With such a condition, diffusion of $Ca(OH)_2$ towards the carbonation front would be minimal as there would be very few continuous water-filled channels, so the rate of carbonation would depend mainly on the diffusion of CO_2 into the structure. With no delaying processes, the formula derived earlier (see para. 5.2.1) holds, so that the depth of carbonation is proportional to the square root of time. This is apparent from the results with perhaps a slight deviation for the non-chloride containing pastes.

The same results indicate that even though higher CO_2 concentrations encourage carbonation they do not cause deviations from the parabolic relationship ($x \propto \sqrt{t}$), at least as far as the 5% CO_2 condition is concerned.

If we consider the derived equation on page 161

$$x^2 = \frac{2DCt}{A} \quad \text{and from}$$

$$x = k\sqrt{t}$$

then it can be seen that:

$k \propto \sqrt{C}$ for constant D & A values and where C is the CO_2 concentration in the atmosphere. For the atmospheres considered, if the concentration of CO_2 in air is 0.03% by volume, we should have:

$$\frac{k_1}{k_2} = \frac{\sqrt{5}}{\sqrt{0.03}} = 12.9$$

where k_1 is the calculated constant for 5% CO_2 and k_2 that for air. But,

$$\frac{k_1}{k_2} = \frac{0.332}{0.180} = 1.8$$

a value considerably lower than the theoretical value, so the diffusivity value D cannot be a constant. One property which may in fact effect D, is the porosity which has decreased more for the 5% CO_2 exposed specimens. It is the porosity, or perhaps more significantly the pore size distribution of the cement after the induction period, ie at the onset of the apparent carbonation, that is important in this respect. It must be remembered that substantial carbonation would have occurred already, as was demonstrated in figure 5.9.

The increase in the rate of carbonation by the addition of NaCl in the mix is to some extent surprising. One possibility may be related to the formation of the calcium chloroaluminate phase, which may be represented by the following equation.

$$3CaO.\ Al_2O_3 + 2NaCl + 10H_2O + Ca(OH)_2 \longrightarrow$$

$$3CaO.\ Al_2O_3.\ CaCl_2.\ 10H_2O + 2NaOH$$

This would have an effect of reducing the total carbonatable CaO content and increasing the NaOH. The sodium hydroxide being highly soluble would carbonate at a faster rate than the calcium hydroxide which it had replaced since the latter would have to first, dissolve when the pH is reduced sufficiently and then carbonate. There is not sufficient calcium chloroaluminate formed ,however ,in order for this to have a major effect so the NaCl actually acting as some form of catalyst may be closer to the answer.

5.5.2 Concentration of Ions in the Pore Solution

Perhaps the most striking result in the pore solution analysis, is the "removal" from solution of the alkali ions, Na^+ and K^+, on carbonation. One explanation may be the incorporation of the alkali ions in the C-S-H or the newly formed silica gel, in a similar way as happpens with slag and PFA cements [93]. As discussed by Roy and Idorn [93], lower CaO to SiO_2 ratios of the C-S-H gel caused by slag additions, increase the retention capacity of the gel for alkalis.

Butler et al [94], as cited by Roy and Idorn, [93] found with fly ash additions to portland cement, that the overall effect of the PFA/$Ca(OH)_2$ reaction was to reduce the C/S ratio of the reaction product as a whole and to cause the alkali metal ions to be trapped within this gelatinous material.

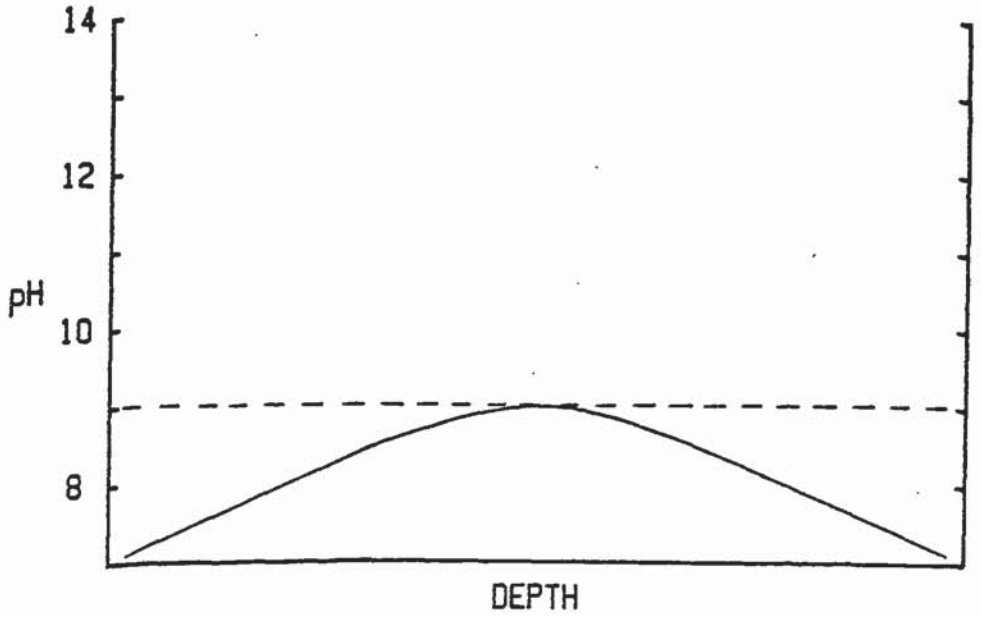

FIGURE 5.10 pH profile of an apparently fully carbonated cement paste disc, as indicated by the phenolphthalein test.

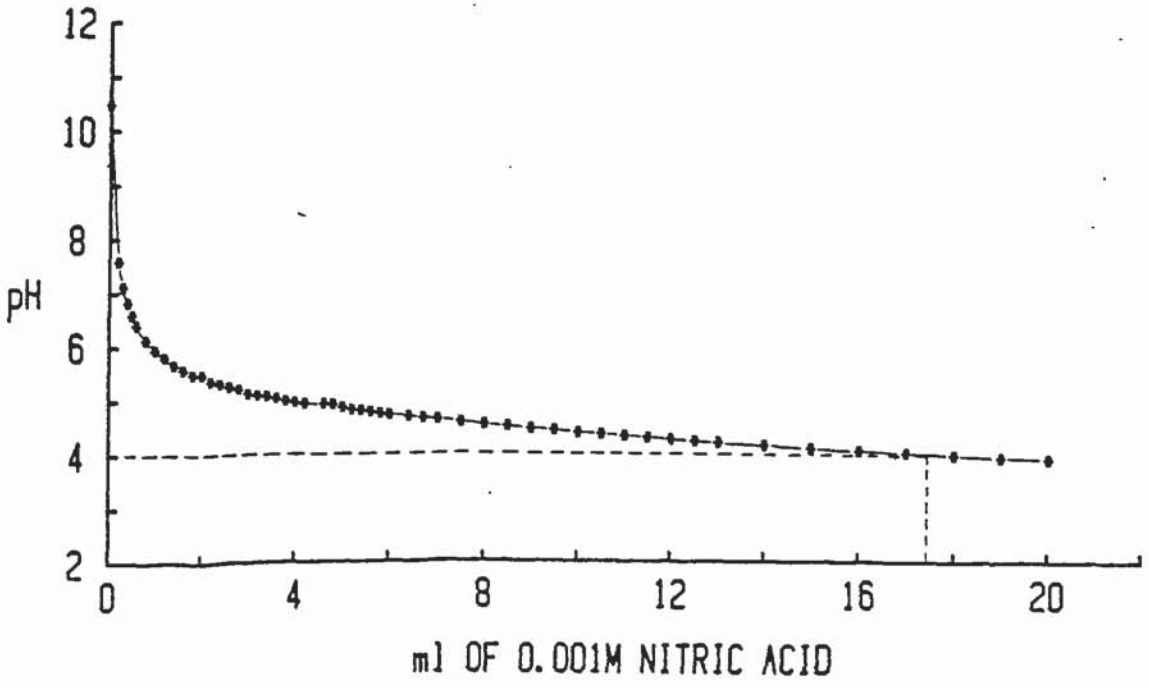

FIGURE 5.11 Neutralization of the pore solution, expressed from air carbonated cement pastes (specimen B2) for the determination of carbonates and bicarbonates.

Useful information is also provided by Page and Vennesland [128] who had studied the pore solution of portland cement with increasing amount of silica fume. An addition of 30% silica had the effect of reducing the pH to 11.9 and caused the near complete removal of Na^+ and K^+ ions from the pore solution. The explanation may be the same as that offered by Butler et al [94] as an abundance of SiO_2 exists in their hardened cement pastes.

A very low C/S ratio would exist in carbonated cement pastes, so the incorporation of the alkali metal ions in the gel is not therefore unrealistic.

Gonzales et al [42] monitored the reduction in pH of two Sat. $Ca(OH)_2$ solutions, one with an addition of 100mM NaOH plus 100mM KOH when bubbling CO_2 gas through them. They observed a plateau at pH 10.4 for the alkali containing solution which they attributed to a mixture of $NaHCO_3$ and Na_2CO_3. Such a mixture they claimed, buffers the pH at 10.4 presumably because the CO_3^{--} to HCO_3^- reaction is reversible.

It would not be too unrealistic to expect a similar behaviour for the pore solutions but as shown, this is not the case. Figure 5.11 represents the drop in pH with the addition of a weak nitric acid solution to 1.5ml of the pore solution from specimen B2 with an initial pH of 10.48. As it can be seen, the pH quickly drops to about 7 even with the addition of only 0.4ml of 0.001M HNO_3, suggesting a near absence of

carbonates from the solution.

Phenolphthalein is generally thought to change from colourless to pink beyond pH9. The fact that pH values of three cements (B1,B2&C1) were all above 9, led to the suspicion that these cements were not yet fully carbonated. Infact the specimens exposed to air did not change to a truly colourless condition but had small light pink "spots" within a colourless matrix (see figure 5.12a). After saturation, all of the area, except for a narrow band at the edges was covered by a light pink colour (figure 5.12b). Even the chloride depleted discs exposed to 5% CO_2 showed a small degree of pinkness after saturation.

This fact leads to the conclusion that the cores of certain particles, except near the edges, are not fully carbonated at the 65% RH environment, represented by the dots in figure 5.12a. Once the cements are saturated with water, hydroxyl ions from within the cores can be leached out into the pore solution raising once again the pH. It follows from this that complete carbonation for air exposed specimens does not happen until a certain time after the elimination of the dark pink colouration. There may infact be 3 bands of colouration as shown in figure 5.13. The beginning of the colourless band can be seen at the edges of specimen B1 on figure 5.12a.

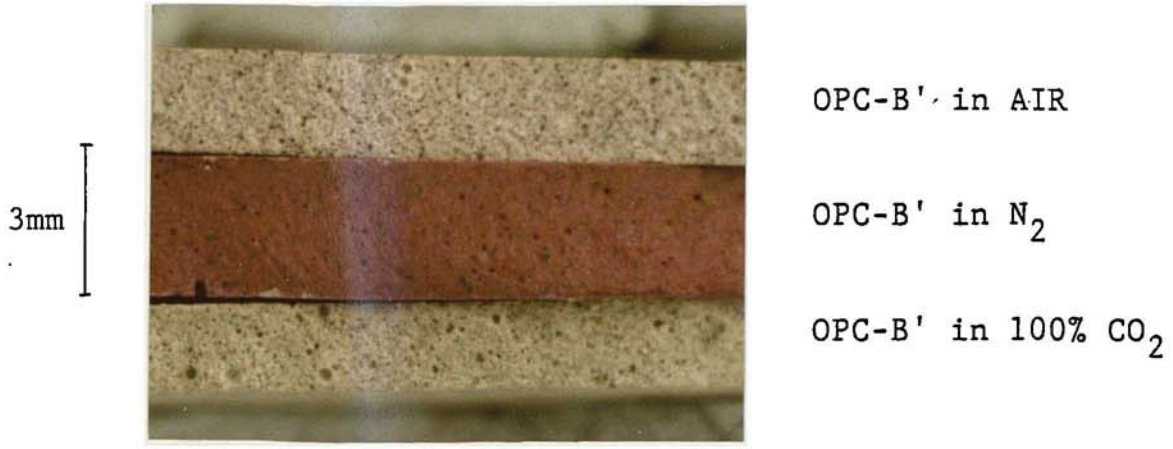

FIGURE 5.12a OBC-B' paste discs exposed to various atmospheres at 65% RH before saturation with moisture and after application of phenolphthalein indicator showing degree of carbonation.

FIGURE 5.12b OPC-B' paste discs exposed to various atmospheres at 65% RH after saturation with moisture and after application of phenolphthalein indicator showing degree of carbonation.

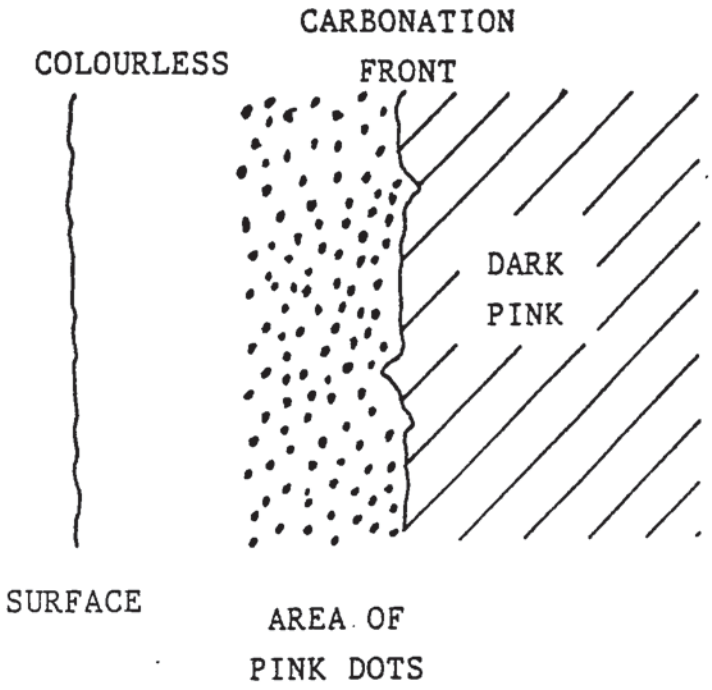

FIGURE 5.13 Progression of the carbonation front in hardened cement paste showing three possible bands after application of phenolphthalein.

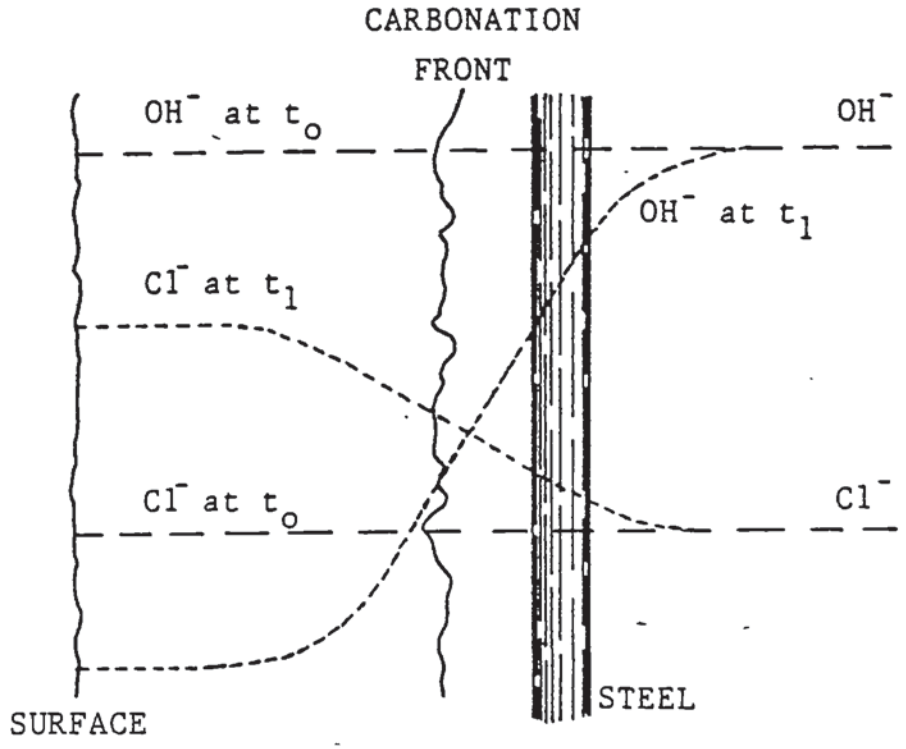

FIGURE 5.14 Diagram illustrating the increased risk of corrosion for the steel reinforcement from the release of chloride in the carbonated section of the concrete.

5.5.3 Free and Bound Chloride

In the absence of chloride, for corrosion initiation to occur, the carbonation front must reach, or go beyond, the steel reinforcement. As mentioned earlier, however, the release of any bound chloride present in cement can increase the risk of corrosion initiation even before the carbonation front has reached the steel. This detrimental effect can be seen clearly in figure 5.14.

The release of chloride and the reduction in pH in the carbonated section, set up concentration gradients for both Cl^- and OH^- ions forcing their movement in opposite directions. At a time t_1, the concentration profiles would be as shown in figure 5.14, so that near the surface of the steel the $[Cl^-]/[OH^-]$ ratio would be considerably higher than the original ratio which may have been below the threshold value.

The risk of corrosion can increase therefore even further when the concrete mix is contaminated with chlorides.

Chloride release is evidently higher for normal as opposed to accelerated carbonation conditions (see table 5.2). It is difficult to envisage the reason for such a difference. It may be caused by entrapment of the calcium chloroaluminate, or other chloride bearing phases, within rapidly forming carbonates, which may not have had sufficient time to redistribute themselves elsewhere, as might be the case for

the much slower carbonation in air.

5.5.4 Water and CO_2 binding capacity; porosity

The decrease in the evaporable water content (W_e), is fairly consistent for all cases with a reduction of at least 7% by weight of cement. The reduction in W_e is generally related to the decrease in capillary porosity and the results of the MIP studies (figures 5.5 & 5.6) confirm this point. Small differences do exist where in general more carbonation had caused a greater reduction in porosity.

Rozental and Alekseev [113] and Pihlajavaara [116] had found that only intermediately sized pores are affected by carbonation and that gel pores are largely unaffected (see earlier). Carbonation in the 100% CO_2 environment has however caused some difference in the porosity of the finer end of the distribution curves ie pores smaller than 0.02μm in diameter, (figures 5.5 & 5.6). Remembering that the specimens in the 100% CO_2 environment continued to be exposed to the atmosphere for more than 150 days after the apparent complete carbonation, the phenomenon may simply be caused by the systematic decrease of the pores with the continued topochemical carbonation of the cores of particles such as those of the C-S-H gel. In fact it appears that the whole curve has been displaced towards the smaller pore sizes as compared to the other two conditions which are fairly similar in shape.

Pihlajavaara's observation [116] that the non-evaporable water content dropped after carbonation, is confirmed by the results, (see table 5.6). It seems however that the slower the carbonation rates, the more the release of the non-evaporable water content. The result has a similar tendency to the degree of chloride release, so as mentioned earlier, it may be caused by the entrapment of either the water itself, or perhaps of the polyhydrate phases such as calcium chloroaluminate.

Pihlajavaara [116] had also found 0.36gms of CO_2 per gramme of unhydrated cement in his carbonated 0.5 W/C ratio cement paste, a value not too dissimilar to the 0.33gms calculated for the same type of cement carbonated under similar conditions (table 5.6). In addition, higher carbonation rates have resulted in higher amounts of bound CO_2 in the pastes. What is of more interest is the relatively small differences between CO_2 levels in the two accelerated conditions, particularly after the considerable"over-exposure" of the cements in the 100% CO_2 atmosphere. It seems therefore that once carbonation has been established by the phenolphthalein test, only slowly accessible CaO-bearing constituents remain uncarbonated, which can only carbonate by slow diffusion processes, as speculated by Powers [98], (see also part II of this chapter).

The total amount of CO_2 required to neutralize the cement paste completely can be calculated by considering all the

basic oxides in the cement (see appendix 22). For the particular cement used in this study, the total CO_2 required for the neutralization of 1gm of cement is 0.52gms. The majority of this (0.50g) is required to neutralize the CaO present, so an assumption that all the calculated CO_2 was used up by the CaO is not too unrealistic. With such an assumption made, the total reacted and unreacted CaO can be easily calculated. It can be seen from table 5.8 that for "normal" carbonation of the OPC-pastes, there still remains 0.21gms of uncarbonated CaO, a value only slightly lower than that mentioned by Smolczyk [106]. Even in the most aggressive condition there is still as much as 6% CaO left unreacted, implying once again that CaO present in the cores of particles is difficult to carbonate.

5.5.5 Crystal Structure

It is generally accepted that vaterite is the first modification of carbonate to be formed, but is later transformed into a more stable calcite[99,119]. In view of this, it would be expected that most of the carbonation products formed in the specimens exposed to 100% CO_2 would have had sufficient time to transform to the calcite phase. To the contrary, the faster the carbonation rate, the larger the amount of vaterite obtained.

This may infact be as a consequence of the increased speed of carbonation. The rapid formation of vaterite may force

its nucleation at unfavourable sites, where the product could be under compression hence unable to transform to the stable but more expansive form of calcite. It may be related more to the carbonation of calcium hydroxide, which is normally dissolved before nucleating at stress-free sites, but owing to the high speed of carbonation, part of it could carbonate topochemically, more like the other cement paste constituents and hence remain under compression.

This type of carbonation may also have a bearing on the observed pore-size distribution curve whereby, as mentioned earlier, pore sizes are reduced in a general form hence contributing to the overall displacement of the curve towards the finer end (see fig. 5.5)

5.5.6 Diffusion Characteristics

It is very interesting that for two of the carbonated cement conditions apparent chloride diffusivities were at least twice as high as for the equivalent uncarbonated condition. Na^+ ions as the only accompanying type of ion had the same diffusion coefficient in each case as that of Cl^-. The reason why this is not the case for the uncarbonated cements, as mentioned in chapter 3 part II is that there is an exchange of Cl^- and OH^- ions as they counterdiffuse. Table 5.9 provides some of the answers as to how the ion exchange can happen. If we consider specimens cured at a 100% RH, then it can be seen that at termination of the experiment (day 8),

TABLE 5.9 Ionic concentrations in the two compartments of the diffusion cell at different times during the diffusion of NaCl through OPC-B' discs originally cured at either 100% RH or 65% RH.

COMPARTMENT 1 (both 100% & 65% RH conditions-mM/l)

	OH^-
DAY 0	59
DAY 8	80
DIFFERENCE	+21

COMPARTMENT 2 (mM/l)

100% RH

	Cl^-	Na^+	OH^-	Σ^-	Σ^+	$\Sigma^- - \Sigma^+$	$Cl^- - Na^+$
DAY 0	0	2	43	43	2	41	-2
DAY 8	29	16	35	64	16	48	13
DIFFERENCE	+29	+14	-8	+21	+14	+7	+15

65% RH

DAY 0	0	2	43	43	2	41	-2
DAY 8	39	27	35	74	27	47	12
DIFFERENCE	+39	+25	-8	+31	+25	+6	+14

Note: The difference $\Sigma^- - \Sigma^+$ is not a true one as other ions have not been considered but serves only as a guide.

there is an excess of Cl^- ions as against the Na^+ ions. Taking into account the 2mM/l of Na^+ present originally, then the excess is 15mM/l. In the same compartment, there is only an 8mM/l reduction of OH^- ions, hence an excess of 7mM/l still remains. This can only be balanced by other cations, and one explanation might be an exchange of ions between $Ca(OH)_2$ and NaCl. Such a mechanism can produce $CaCl_2$ and release OH^- ions to counter-diffuse the incoming Cl^- ions. One can then expect an increase in the hydroxyl concetration in compartment 2 equivalent to the decrease in compartment 1 ie of 15mM/l. The actual increase is however 21 mM/l. The extra OH^- ions can only be accounted for by their release when part of the diffusing Cl^- is complexed by the C_3A phase in the cement paste.

What is even more interesting, is the fact that for both original curing conditions, even though the amount of diffusing ions is greater, the difference between the Cl^- and Na^+ ions is similar, as is the rise in OH^- concentration in compartment 1. This can only mean that the amount of complexed Cl^- was the same in both cases, and that the chloride complexing capacity of the cement is constant and independent of curing condition. (See also chapter 7). The fact that the faster diffusion of Cl^- ions through the paste does not influence its complexing capacity, is specifically due to the fact that a concentration gradient is set up along the disc, so that the chloride concentration in the pore solution remains

constant irrespective of the speed of diffusion.

As the higher diffusivity of the Cl^- ions compared to Na^+, is caused by the counter-diffusion of OH^- ions, in the absence of such a condition, the chlorides would depend on the co-diffusing Na^+ ions, and hence have a similar lower diffusivity. Consequently, the ionic diffusivity for discs in the 5% CO_2 atmosphere can be considered as generally higher than for the uncarbonated condition. In other words, ions in the carbonated pastes are more mobile.

The extra mobility may be associated with the change of structure, from the normal cement paste, to a mass of mainly calcium carbonate. The surface interaction mentioned in chapter 3 which was thought to be responsible for slowing down the diffusion of ions in cement pastes may no longer be as important, so mobility can increase.

The reduction in porosity from carbonation on the other hand, would have the opposite effect, so that the cement carbonated in air, may have sufficiently larger pores to allow faster diffusion. With regards to cements exposed to 100% CO_2, it could be the type of pores that may be important and not the size and total volume, as the shape of the curve differs substantially from the other two, (figures 5.5 and 5.6). Alternatively, the accelerated carbonation may have reduced the effect of the surface interaction even further.

Whatever the reasons, the result is that carbonation causes an increase in the mobility of the chloride ions in cement pastes and presumably in concretes. The consequence would be a faster pit propagation which, aided by the reduction in pH, could lead to quite considerable corrosion rates for the steel reinforcement. The concept of ion replenishment of pits will be discussed further in part II of this chapter and in chapter 6.

The purpose of this work was primarily to establish whether accelerated carbonation can replace "normal" carbonation for research purposes. All methods of carbonation had yielded similar pore solution ionic concentrations, similar reductions in porosity, evaporable and non-evaporable waters, caused the release of bound chloride and increased ionic mobilities. In most cases, the degree of change varied with carbonation condition, but whether these small differences are significant would depend only on the type of research needed and on the accuracy required.

It was important also to establish what happens to the bound chloride in cement after carbonation. The results clearly showed a definite release of a substantial amount of chloride back into the solution.

It is evident that risk for corrosion initiation of steel reinforcement is increased in the following ways:

(i) Reduction in pH

(ii) Chloride release if present in the cement.

(iii) Combined diffusion of chloride towards the steel from an adjacent carbonated area and of OH^- ions towards the neutralized area.

(iv) Increased diffusivity of chloride ions leading to easier penetration from an outside source.

Further work on carbonation is reported in chapter 6 part II, where the effect of moisture content of the carbonated concrete on corrosion propagation will be looked at in order to establish the degree of risk of the steel in uncontaminated carbonated concrete.

PART II - SYSTEMATIC CEMENT PASTE NEUTRALIZATION - THE CONCEPT OF BUFFERING IN CEMENTS

5.6 INTRODUCTION

Cement pastes are made up of a number of basic constituents all of which are at least partly neutralized during the process of carbonation[106,119,129]. The work described in part I did not offer any information on the individual phases but only on the cement paste as a whole. As neutralization could only be detected when the pH fell below 9, useful information on the neutralization process down to that pH value was unobtainable.

As was assumed earlier (para. 5.5) the pH of the pore solution remains at around 12.5 for as long as soluble $Ca(OH)_2$ is available, offering the cement a kind of buffering capacity. No information however exists to date, confirming the expected buffering caused by the $Ca(OH)_2$ or on the pH variation and possible further buffering caused by the other basic constituents present in the cement.

Such information is not only important for the fuller understanding of cement neutralization but also in order to elucidate the principle of hydroxyl replenishment of the steel corrosion pit as mentioned in chapter 4 part II.

A simple but effective technique was therefore developed to study in detail the above mentioned pH variation during the

neutralization of a selection of cements down to pH 9. This was achieved by the systematic addition of nitric acid to a pre-weigh ed powdered sample of fully hydrated cement paste whilst monitoring the hydroxyl concentration of the solution (see para. 5.7 for full details of the process). The results of this work are reported in this part of chapter 5.

5.7 EXPERIMENTAL PROCEDURE

Triplicate cement paste cylinders made from OPC-B', SRPC, OPC-B' + 30% PFA andOPC-B' + 65% BFS were produced as described in chapter 2 (para. 2.2). After a prolonged curing period of 12 months in their sealed moulds at 22±2°C to achieve virtually full hydration, the specimens were crushed and ground to a powder using a pestle and mortar, sieved through a 150μm wire mesh and stored in sealed polythene bags which were placed inside airtight containers until required.

Five grammes of each type of cement were placed undividually inside a large syringe (fig. 5.15) to which 10ml of deionised water were added. The mixture was thoroughly shaken to achieve "wetting" of all the cement powder. The purpose of using a syringe as a container was so that it could be possible to exclude any air irrespective of the volume. A rubber bung tightly fitted inside the slightly enlarged hole at the top of the syringe provided adequate airtightness (fig. 5.15).

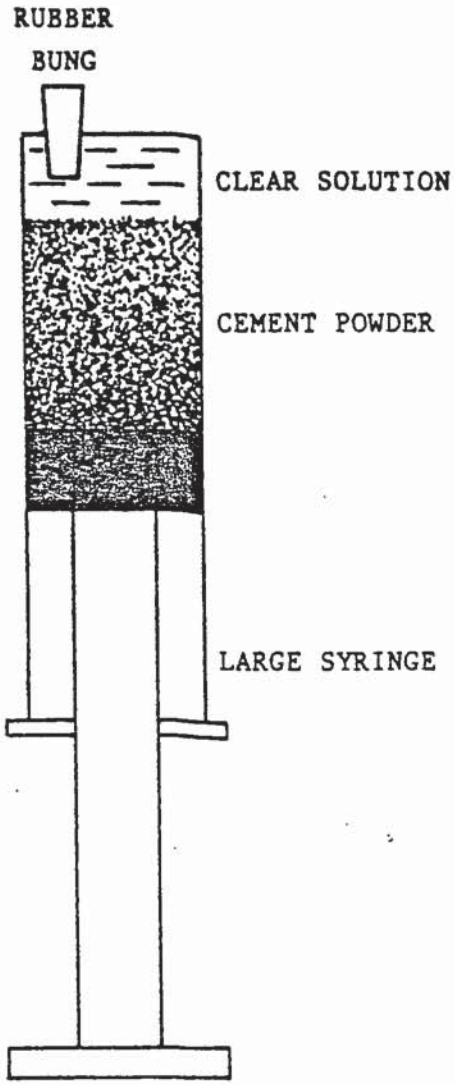

FIGURE 5.15 Syringe adapted for use in the systematic neutralization of powdered fully hydrated cement pastes.

Four such specimens were made for each type of cement which were allowed to stand upright so that a few millilitres of solution could separate at the top. The specimens were reshaken thoroughly daily up to a period of two weeks after which three 100µl aliquots of the clear solution were withdrawn from each container and analysed for OH^- concentration as described in chapter 2 (para. 2.4.1). An addition of 300µl of 1M HNO_3 was then made to each syringe and the process of shaking, resting in an upright position, withdrawing clear solution for analysis and replacing it by an equal volume of acid was repeated, allowing a week for the cement constituents and solution to reach equilibrium.

The nitric acid additions were gradually increased to 0.4, 1,2 and finally 3ml, each time withdrawing the equivalent volume of solution from the containers prior to the additions and analysing for OH^- concentration. The increased additions although reducing the "resolution" were necessary owing to time considerations. At the lower pH values titrations were carried out on 1ml aliquots with the use of 0.001M HNO_3.

A further 1 gramme of each individual cement powder was placed in a conical flask and titrated with 1M nitric acid by the same method as was used for the titration of solutions (chapt. 2 para. 2.4.1) using phenolphthalein as the indicator. When the end point was reached, ie when the solution became colourless, the flask was stoppered with a rubber

bung and allowed to stand for several days until the pink colouration had returned. A further addition of acid was then made until the pinkness was eliminated and again the flask was stoppered and allowed to stand. This process was repeated until no more pinkness was observed in the solution, indicating the complete neutralization of the cement as indicated by the phenolphthalein indicator. Duplicate titrations were carried out with good reproducibility.

In order to correct the mass of each cement powdered sample to that of the original added dry cement, evaporable and non-evaporable water contents were determined by the method described in chapter 2 (para. 2.5). Phase identification of each pre-neutralized cement type was made by the use of the DTA (chapter 2, para. 2.8.1).

5.8 RESULTS

The reduction in pH of the solutions with nitric acid addition are represented graphically in figures 5.16, 5.17, 5.18 and 5.19. The actual OH^- concentrations are also shown on the same figures. (The full results are represented in appendix 23). All PFA specimens had gellified at pH-11 so no further information could be obtained.

It is clear from the results that the drop in pH is not constant but occurs in stages producing several plateaux at which the hydroxyl concentration remains effectively constant. Each plateau represents a different soluble phase in

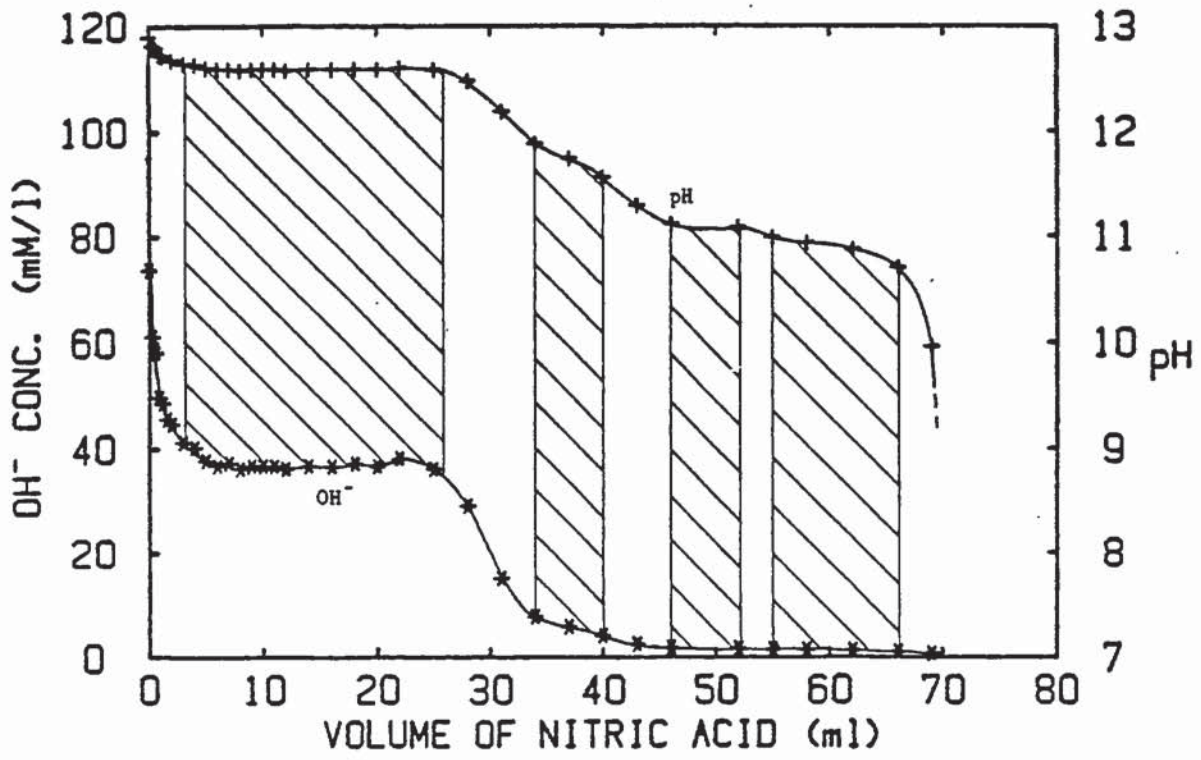

FIGURE 5.16 Reduction in pH of 5gms of fully hydrated powdered OPC-B' with the addition of nitric acid.

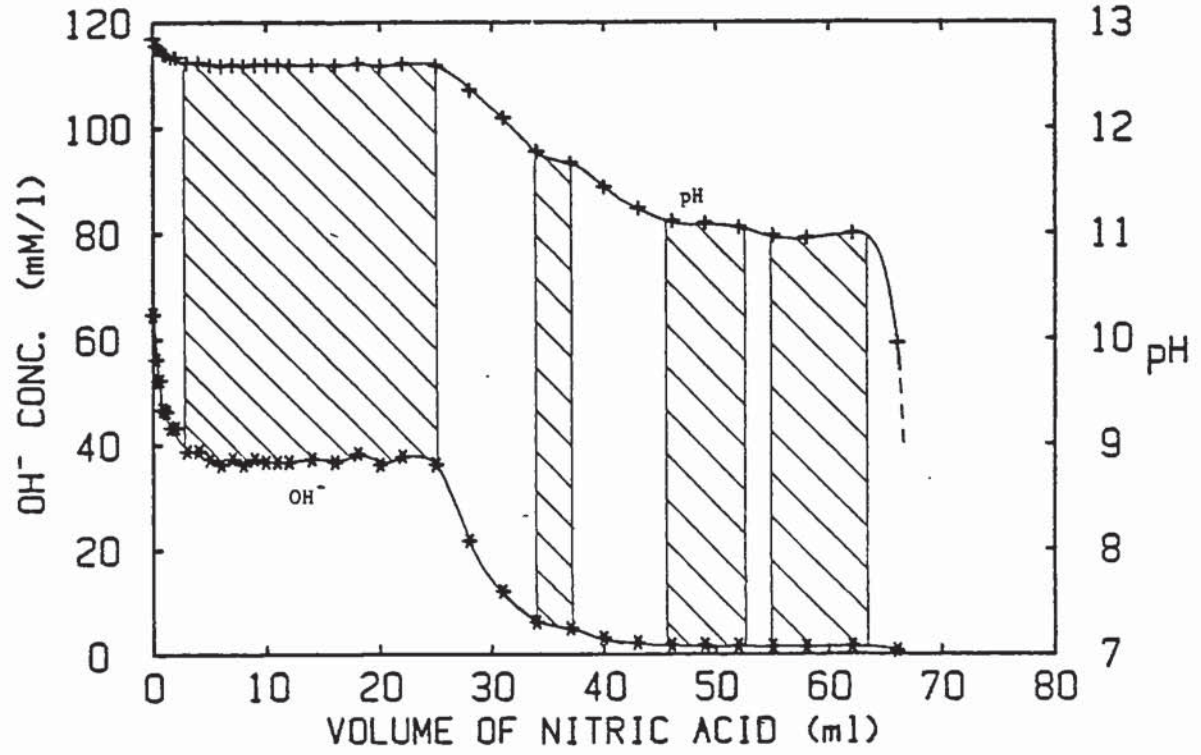

FIGURE 5.17 Reduction in pH of 5gms of fully hydrated powdered SRPC with the addition of nitric acid.

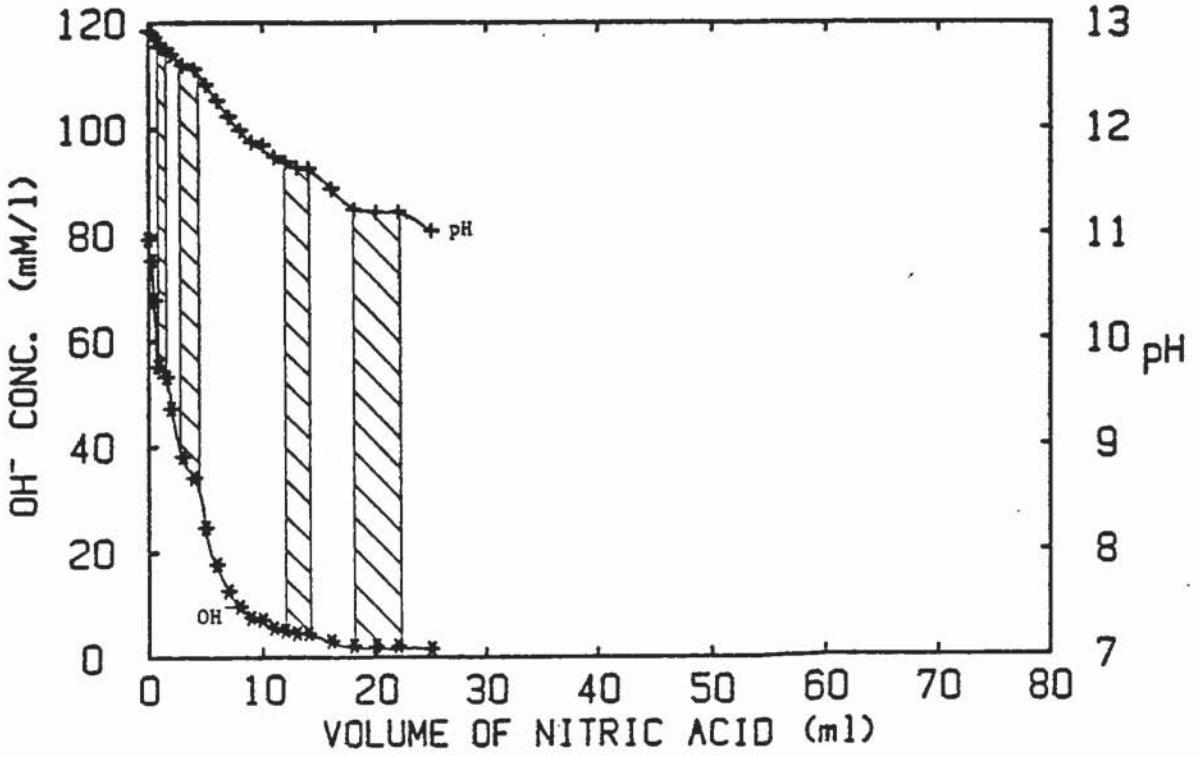

FIGURE 5.18 Reduction in pH of 5gms of fully hydrated powdered OPC-B'/30% PFA with the addition of nitric acid.

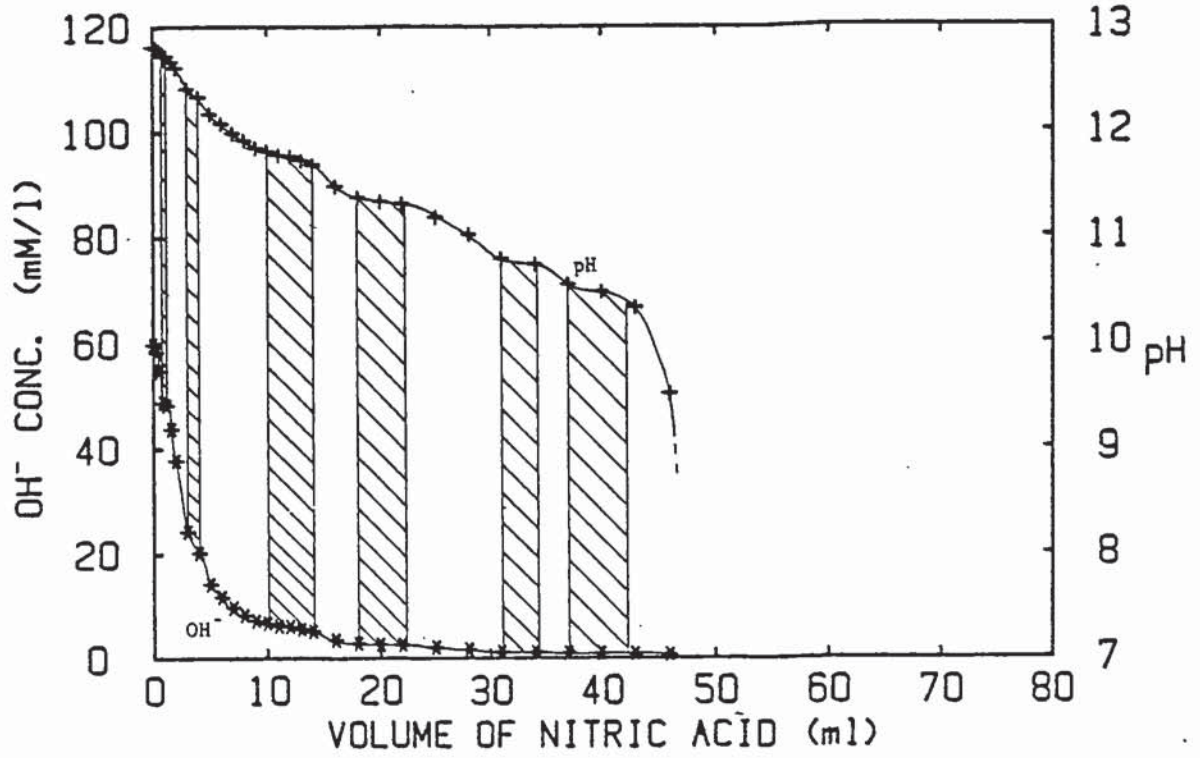

FIGURE 5.19 Reduction in pH of 5gms of fully hydrated powdered OPC-B'/65% BFS with the addition of nitric acid.

the cement paste.

The clearest and probably most important plateau is that obtained at pH 12.56 for both the OPC-B' and SRPC cements. It is reasonable to assume that this plateau is caused by soluble $Ca(OH)_2$. Furthermore the "length" of the plateau could give an indication of the amount of free $Ca(OH)_2$ present in each type of cement. The calculated contents are shown in table 5.10 against the theoretical amounts. (For a full calculation see appendix 24). The results are in the form of grammes of $Ca(OH)_2$ per gramme of unhydrated cement. Correction of the mass was necessary from the evaporable and non-evaporable water contents represented in table 5.11. The discrepancy between the two sets of values is probably due to errors encountered in the Bogue calculations which assume accurate oxide compositions. In the case of the BFS cement, as no "arrest" was observed at pH 12.56 it was assumed that all the $Ca(OH)_2$ was in dissoved form in the solution so the amount shown in table 5.10 is the maximum possible in solution. These results will be discussed further in the next paragraph.

The total amount of 1M HNO_3 required to neutralize 1gm of unhydrated cement is represented in table 5.12. The first column represents the amount of acid required for the controlled systematic neutralization, the second column the amount needed to neutralize the "parallel" 1-gm samples of powdered cements and the last column the theoretical amount

TABLE 5.10 Amount of $Ca(OH)_2$ in cement paste (g/g).

TYPE OF CEMENT	$Ca(OH)_2$	
	CALCULATED	THEORETICAL
OPC-B'	0.284	0.249
SRPC	0.286	0.328
OPC-B'/30% PFA	0.026	—
OPC-B'/65% BFS	0.007	—

TABLE 5.11 Evaporable and non-evaporable water contents.

CEMENT	g/g OF CEMENT	
	We	Wn
OPC-B'	0.2446	0.1972
SRPC	0.2579	0.1664
OPC-B'/30% PFA	0.2955	0.1416
OPC-B'/65% BFS	0.2834	0.1397

TABLE 5.12 Amount of 1M nitric acid required to neutralize 1gm of cement (ml).

CEMENT	SLOW NEUTRAL. OF CEMENT	FAST NEUTRAL. OF CEMENT	THEORETICAL AMOUNT
OPC-B'	19.9	19.8	23.4
SRPC	18.8	19.1	23.7
OPC-B'/30% PFA	—	13.1	17.5
OPC-B'/65% BFS	13.1	13.0	21.0

of acid to neutralize all the basic constituents as calculated in appendix 22.

The lower experimental values compared to the theoretically calculated amounts show that even when the exposed cement particle surface area is increased by the grinding of the paste to a powder neutralization is still not complete. This observation signifies that cores of cement particles are virtually inacessible by the acid as was the case with the apparently completely carbonated OPC specimens exposed to 100% CO_2 (chapter 5, part I).

The DTA thermographs (fig. 5.20) show variations between the cements verifying particularly the differences in amounts of $Ca(OH)_2$. It can be seen that there is still a small amount of $Ca(OH)_2$ present in the BFS cement paste as presumed earlier even though no plateau is evident in figure 5.19 at the equivalent pH value.

5.9 DISCUSSION OF RESULTS

The most interesting observation of the results is the actual number of different plateaux (as many as six for BFS) produced during the neutralization process of the cements. These are summarised in diagramatic form in figure 5.21. The plateaux suggest a form of buffering being offered by several individual phases.

It is clear also that PFA and particularly BFS cements have produced distinctly different pH arrests to those observed

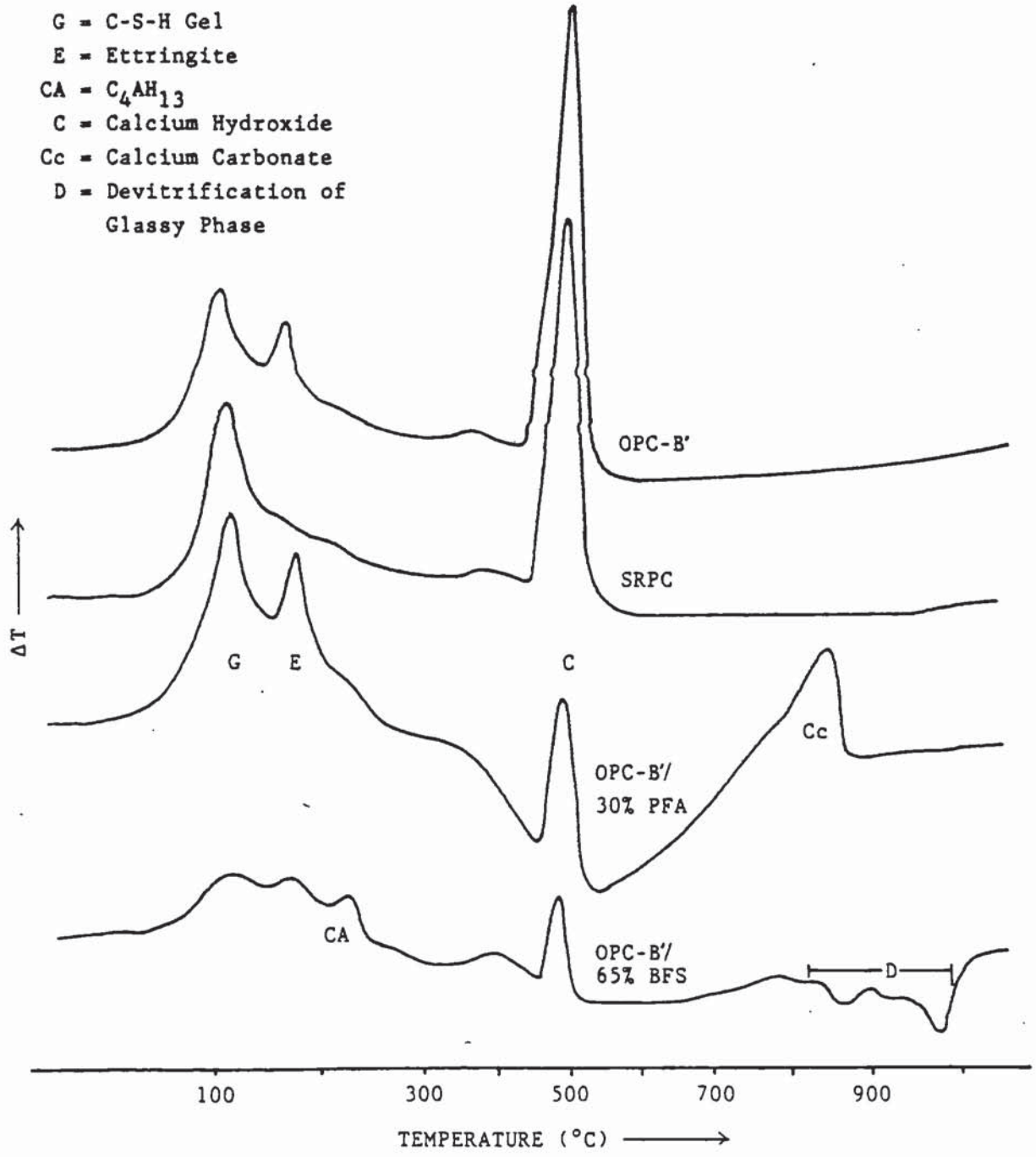

FIGURE 5.20 DTA thermographs of hardened cement pastes cured for 12 months in their sealed moulds.

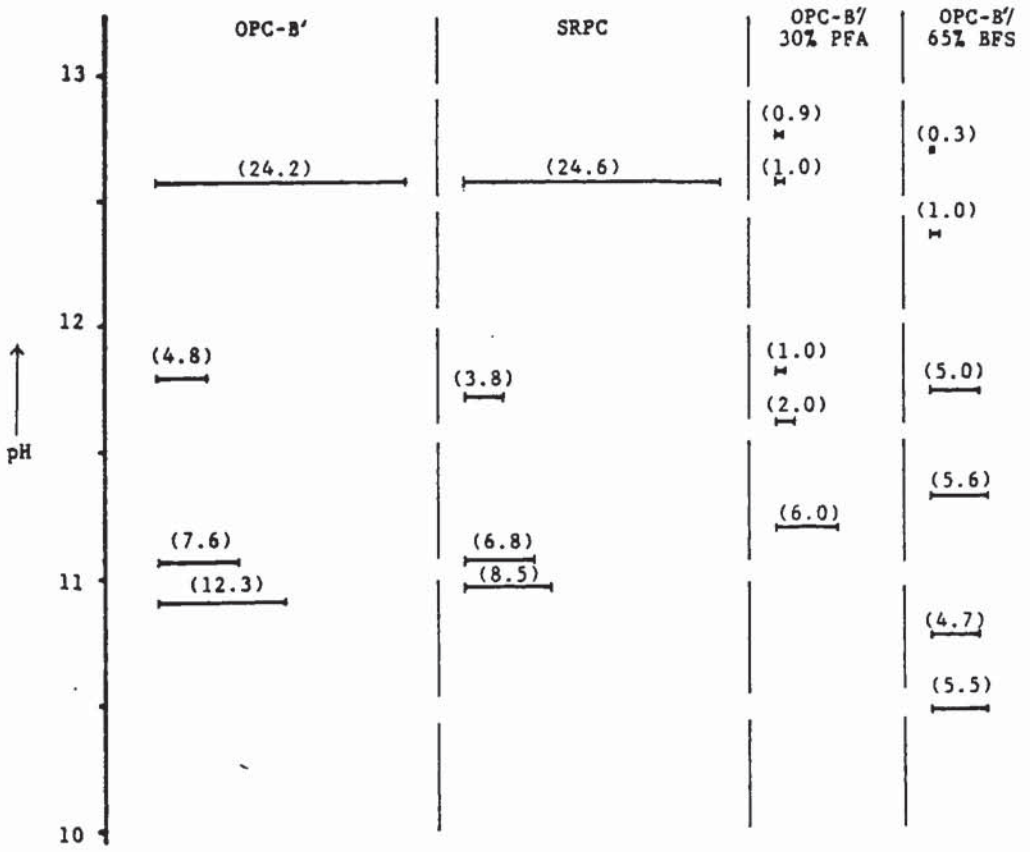

FIGURE 5.21 Diagramatic representation of the observed plateaus during the neutralization of powdered fully hydrated cement pastes. (Figure in brackets indicates the amount of 1M HNO_3 in ml for every 5gms of cement).

for OPC-B' and SRPC. If each plateau, as assumed, represents a separate phase, it is obvious that PFA and BFS cements consist of different hydration products from portland cements. What these phases are is very difficult to determine without the use of a very accurate qualitative analytical technique, involving analysis of cements before and after attainment of the relevant pH. Infrared spectroscopy [131] is one possibility but the technique may not be sensitive enough to detect the small quantities involved.

The DTA results (fig. 5.20) have highlighted only a few differences in the phase compositions. BFS for instance contains C_4AH_{13} [132] (~200°C on fig. 5.20d) a phase not present in the other cements, but C-S-H gel and $Ca(OH)_2$ are present in all cements to a varying degree and ettringite (150°C) is detectable in all but the SRPC. The fact that SRPC and OPC-B' have virtually identical "pH-profiles" suggests that ettringite, absent in SRPC, does not produce a pH arrest and hence does not offer a buffering capacity to the cement.

BFS cements are high in MgO so it is not unrealistic to expect some free $Mg(OH)_2$ in the hydrated cement paste causing a pH arrest at around pH 10.5 as indeed can be seen on figure 5.21.

As to the other plateaux one can only speculate at this

stage with regards to the phases that can cause them. Apart from $Ca(OH)_2$ (pH 12.56) the other plateaux are however in most cases small suggesting only small amounts of the respective phase. The C-S-H gel, making up the bulk of the hydration product cannot therefore be represented by any of the arrests but as a substantial amount of added acid cannot be accounted for by individual plateaux (see unshaded areas under graphs in figures 5.16 to 5.19) neutralization of the gel must be systematic and continuous. It may involve the removal of CaO from within the gel "framework" as the pH is reduced (see chapter 4, para. 4.9) followed by the subsequent neutralization. As the solubility of the C-S-H is low, CaO in the cores of the gel particles would be virtually inaccessible and their neutralization would involve veryslow diffusion processes as mentioned in part I of this chapter (para. 5.5.2).

Although carbonation may not be a strictly identical neutralization process as it involves a gaseous state, nevertheless, the present technique indicates the amount of material that requires neutralization before full carbonation can be detected. The phenolphthalein indicator does indicate a true carbonation depth because as it can be seen by all the "pH-profiles" the pH remains at 10.5 or higher before a sharp drop is encountered signifying complete neutralization. What it does not detect however is the progressive drop in pH.

Figure 5.9c (partI) may be best represented by the shape of figures 5.16 to 5.19 for each cement type respectively - the low pH side representing the surface of the cement paste - indicating, as mentioned earlier, (para. 5.5.1) that a depth beyond the virtual carbonation band exists where partial neutralization would have occured with pH values equal or lower than 12.56 depending on the type of cement.

Problems would then occur with corrosion of steel reinforcement lying in an apparently uncarbonated section of cement matrix when chloride is also present as mentioned earlier (para. 5.5.3 - see also fig. 5.14).

Assuming that CO_2, being a gas, does not suffer from the same surface interactions encountered by ions during the process of diffusion, the migration of the gas into any of the four types of cement should not be very dissimilar as it would depend primarily on the porosity or pore structure of the cements (fig. 3.14). Carbonation rates would then depend mainly on the amount of carbonatable material present in each cement type. On such a parameter therefore it appears that PFA and BFS cements could suffer from somewhat faster carbonation rate as compared to portland cements, a fact supported by many researchers [5,110,130]. Others have argued however [45-47] that in practice PFA, slag and silica fume based cement pastes do not carbonate much faster than portland cement pastes owing to a more compact pore

structure.

It was assumed in chapter 4 part II (para. 4.9) that the amount of $Ca(OH)_2$ in chloride-rich cements determines almost entirely the relative concentrations of OH^- to Cl^- ions sustained inside a pit as the two anionic species are consumed during the corrosion process. If this is true then clearly PFA and BFS cement pastes owing to their reduced amount of $Ca(OH)_2$ would not on the face of it, offer as low a $[Cl^-]/[OH^-]$ ratio as the portland cements, hence increasing the likelihood of pit formation and propagation. Other "buffers" present in the cements are of low quantity (fig 5.21) so their effect would be considerably less. The low mobility of the ions in "pozzolanic" cements may however, counter the above-mentioned detrimental effect. The whole concept of pit formation and growth will be discussed in more detail in chapter 6 part I.

The technique used in this work may be developed further and provided it can be speeded up it could be used, with the aid of an accurate pH-meter, as an analytical technique to identify types of cement matrices of concrete structures if other known techniques are inapplicable. With further study so that phases causing pH arrests are identified it could possibly develop into a quantitative analytical technique, using simple and inexpensive equipment.

One can finally summarise the findings of this work as fol-

lows:

(i) Many soluble cement constituents act as buffers, "holding" the pH of the pore solution at constant values until each individual phase is neutralized.

(ii) The most important of these buffers with regards to the protection of steel reinforcement against corrosion, is the $Ca(OH)_2$ both because of its high pH value and because of the high amount that exists in portland cements.

(iii) Substitution of portland cement by PFA, and particularly BFS, reduces the amount of free $Ca(OH)_2$ owing to their pozzolanic action. The effect is a reduction in the high pH buffering capacity of the cement paste. When chloride induced pitting corrosion occurs, such cements may be unable to maintain a high OH^- concentration inside the pit.

(iv) The same substitutions cause a reduction in the total amount of basic material present in cement. Consequently the cements' ability to resist neutralization is lowered.

(v) The technique developed here for the systematic neutralization of cements, is a simple and inexpensive method of identifying the type of cement matrix, as each cement should possess a unique "pH-profile". Furthermore it can be deve-

loped into a quantitative chemicoanalytical technique enabling the determination of many cement constituents.

CHAPTER 6 ELECTROCHEMICAL STUDY OF CORROSION OF STEEL IN CEMENT & CONCRETE

6.1 INTRODUCTION

In the preceding chapters, various properties of the four investigated types of cement, such as diffusion characteristics (chapter 3), resistance to carbonation and buffering capacity (chapter 5) were studied. It is necessary to relate such properties to the actual corrosion mechanism in order to understand their effects. This was attempted by selecting a range of electrochemical techniques used extensively for corrosion studies in metal/electrolyte systems [135,136] and now adopted for steel embedded in cement pastes or concrete [50,137,138].

As previously mentioned, cement paste normally offers steel a highly protective environment owing to the high alkalinity of its pore solution. For a very simplified system where only this electrolyte is considered, the protective nature of the solution can be indicated by potential-pH diagrams (see figures 6.1 & 6.2). The mechanism of protection is by the formation at the surface of a thin continuous ferric oxide film reducing the dissolution rates of the metal to an insignificant value. The steel is then said to be in a passive state (figure 6.1).

The first depassivating mechanism mentioned in chapter 3, resulting from the introduction to the solution of aggres-

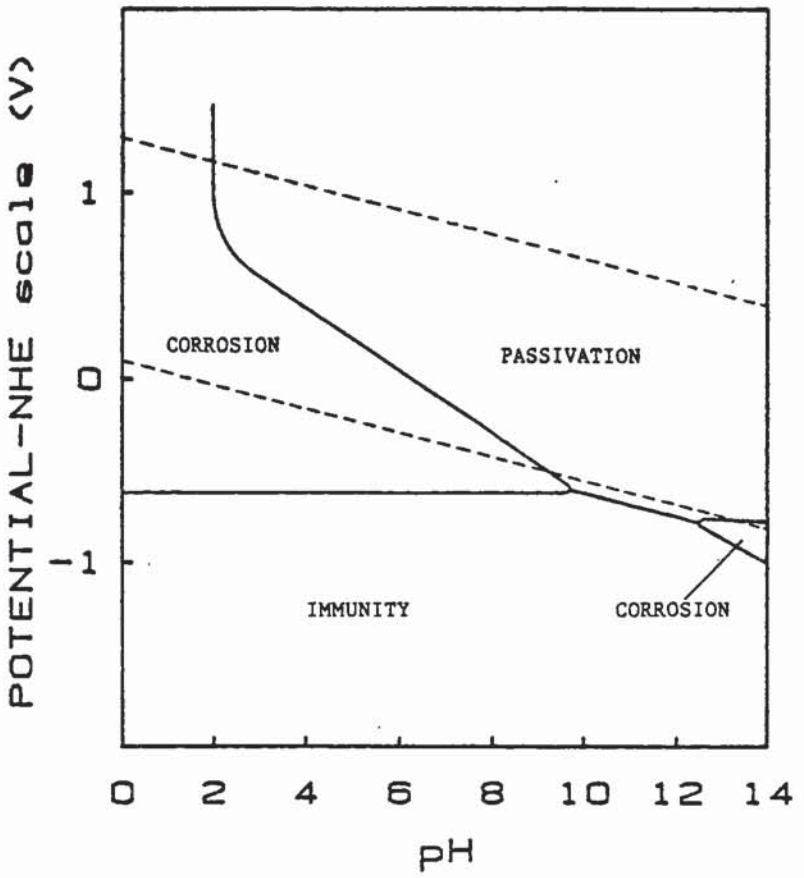

FIGURE 6.1 A simplified form of the Pourbaix diagram for iron.

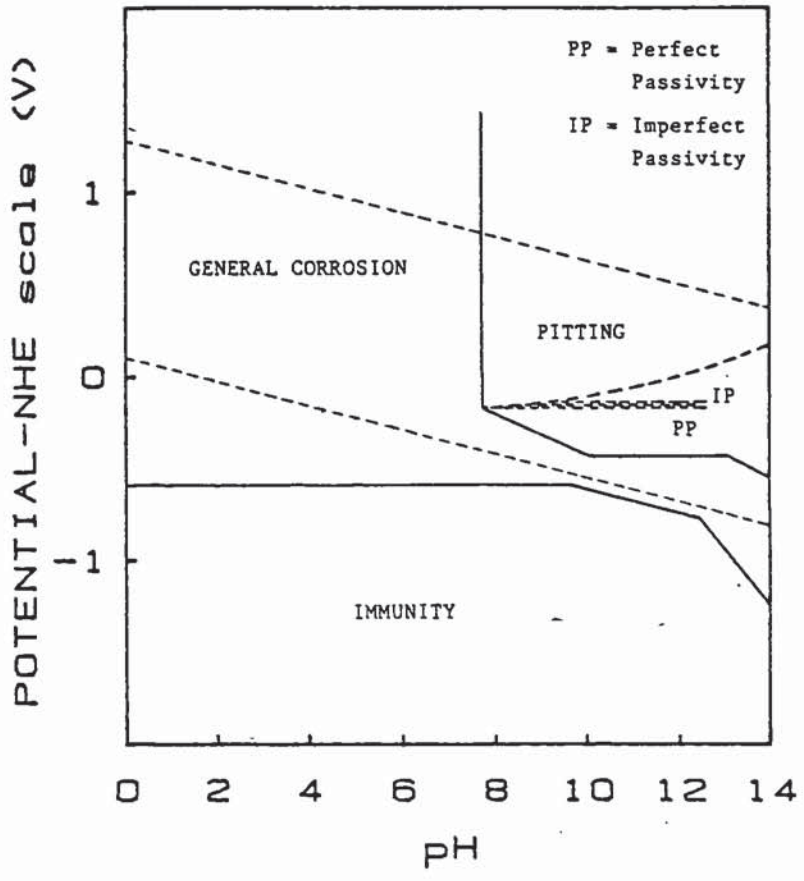

FIGURE 6.2 Plot of potential against pH for iron in a rapidly stirred 1 molar chloride solution.

sive anions such as chlorides (figure 6.2) causes the localized breakdown of the passive oxide layer inducing the development of pits (see para. 6.2).

Chloride contamination of the cement matrix electrolyte as shown earlier, can occur from an outside source by the process of diffusion (see chapter 3 part I). As was also shown (chapter 3 part II) by varying the cement type it is possible to decrease the diffusion rates of chloride and other ions thus reducing the likelihood of chloride build-up around the steel.

Once chloride contamination does occur however particularly by alternative means such as from penetration through cracks in the structure or from their introduction at the mixing stage, the cement's ability to tolerate chlorides and thus prevent corrosion then becomes important. This property may be related to a variety of factors such as, the degree of "buffering" offered by the cement, as discussed in chapter 5 part II, or to structural and physical characteristics of the cement, such as the physical barrier produced by the portlandite layer at the cement-matrix steel interface [26].

As pitting is the most common type of corrosion associated with chloride contamination, pitting characteristics of iron were investigated by potentiostatic polarization methods. The iron wires were embedded in a selection of cement pastes whose pore electrolyte was specifically and care-

fully controlled to offer direct comparison. This work is reported in part I.

The second depassivating mechanism described in chapter 5 is caused by the neutralization of the cement paste during carbonation. This has the effect of reducing the pH of the electrolyte to neutral values causing the general corrosion of the steel (figure 6.1).

As mentioned in chapter 5, carbonation is more likely to be rapid at intermediate relative humidities but in such conditions there is a reduced risk of corrosion owing to the reduction of the pore solution electrolyte, so maximum corrosion can only occur at very high R.H's [41].

An attempt to establish corrosion rates of steel embedded in naturally carbonated concrete was made, by monitoring the corrosion intensities and potentials during wet-dry cycles applied to partly carbonated specimens obtained from 30-year old structures. It was also attempted to adopt alternative electrochemical techniques for monitoring corrosion rates and identifying the existence of carbonated cement matrix around the steel. This work is reported in part II.

PART I PITTING OF IRON IN CEMENT PASTES

6.2 INTRODUCTION AND LITERATURE REVIEW

Pitting, as already mentioned, is a type of localized corrosion appearing on the surface of metals which normally show low dissolution rates. In the case of steel reinforcement surrounded by a cement matrix, pitting is the most common type of failure when the structure is exposed to the aggressive chloride anions. The pitting process in such a complex system would inveriably be more complicated than in normal aqueous environments. In order to understand this process however, it is necessary first to establish the actual mechanism of pitting in alkaline or pore-solution substitute solutions.

6.2.1 Pitting of metals in aggressive solutions

It has been established that for a given metal in a specific aggressive electrolyte there exists a particular pitting potential[139-143]. This pitting potential, Ep, is defined as "the potential below which the metal remains passive and above which pitting nucleates on the surface" [140]. Ep can be determined by a variety of electrochemical techniques, the most common being the potentiostatic polarization method where the potential is increased at equal time intervals and the resulting current density recorded.

Figure 6.3 shows a typical E-i diagram for iron in an alka-

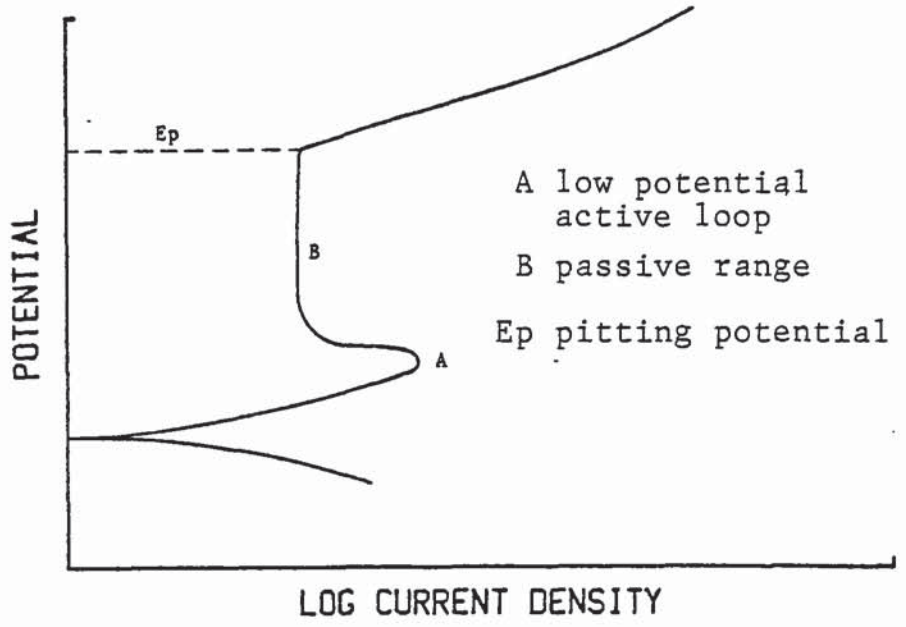

FIGURE 6.3 Typical potentiostatic scan for iron in an alkaline solution containing NaCl.

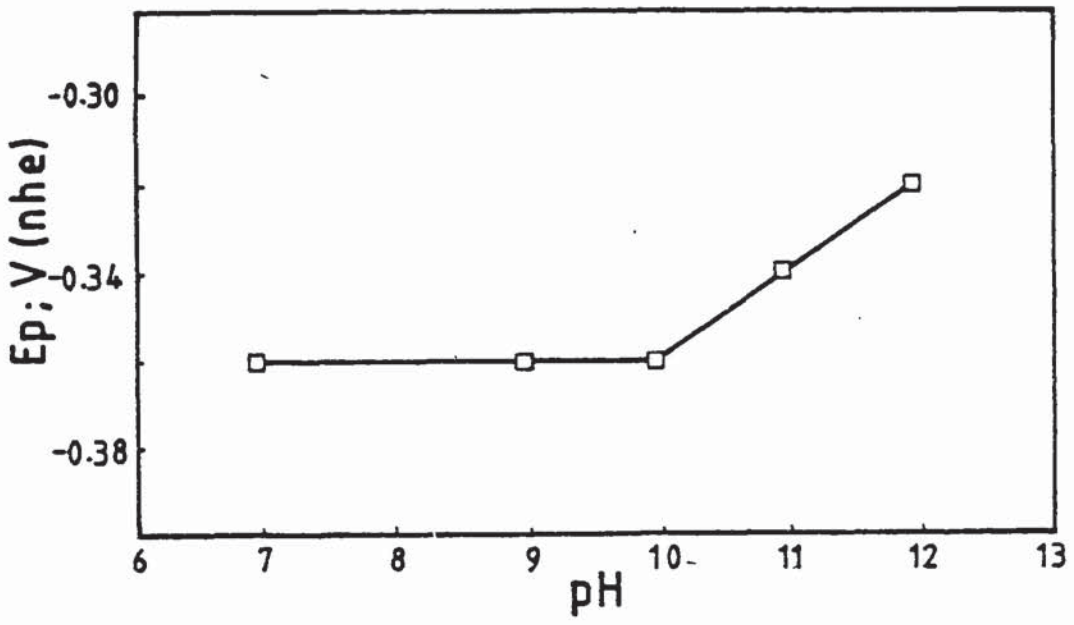

FIGURE 6.4 Effect of the pitting potential of iron in deaerated 1M NaCl solution of 25°C (After Galvele).

line solution containing NaCl. This is typified by a low potential active loop (A) where general dissolution of the metal occurs followed by a passive range (B) where a passive oxide film is established on the surface leading to small current densities. Finally at Ep a pit develops on the surface of the iron where concentrated dissolution occurs resulting in higher current densities.

Venu et al [135] had used this electrochemical technique to study the behaviour of iron in NaOH solutions. They concluded that increasing amounts of chloride shifted the value of Ep in a negative direction.

The same was observed by Leckie and Uhlig [141] in their studies of 18-8 stainless steel in NaOH solutions. They were able to obtain a relationship in the form of,

$$Ep = A - B \log [Cl^-]$$

A similar relationship was established by Galvele [142] for a number of metals including iron, in alkaline solutions.

The concentration of hydroxyl ions in the electrolyte was found by Galvele [140] to have the opposite effect on Ep at pH values over 10 but in more neutral or acidic solutions the pitting potential remained constant (see figure 6.4).

Galvele in a series of publications [142 - 144] attempted

to show why the pitting potential was pH dependent and also succeeded in developing a pit model for any metal in aggressive alkaline or neutral solutions. His work followed that of Pickering and Frankenthal[145] who had shown that ionic conentrations were different inside the pit compared to the bulk electrolyte after developing a small pit model.

Galvele had considered the same unidirectional pit model (figure 6.5) as such a consideration simplifies matters considerably and allows an easier development of the theory. He had worked on the following main assumptions [143]:

(i) The metal dissolves at the bottom of the pit by the following reaction:

$$Me = Me^{n+} + ne \quad ....(1)$$

(ii) Reaction (1) occurs in a sodium salt of an aggressive but non-complexing anion. The pH of the solution could have any value and is given as a boundary condition.

(iii) Reaction (1) is followed by rapid hydrolysis reactions simply by the loss of successive protons.

$$Me^{n+} + H_2O \rightarrow Me(OH)^{(n-1)+} + H^+ \quad .....(2)$$

$$Me(OH)^{(n-1)+} + H_2O \rightarrow Me(OH)_2^{(n-2)+} + H^+$$

$$Me(OH)^{2+}_{n-2} + H_2O \rightarrow Me(OH)^{+}_{n-1} + H^+$$

$$Me(OH)^{+}_{n-2} + H_2O \rightarrow Me(OH)_n + H^+$$

As the reactions are very fast he also assumed that, at

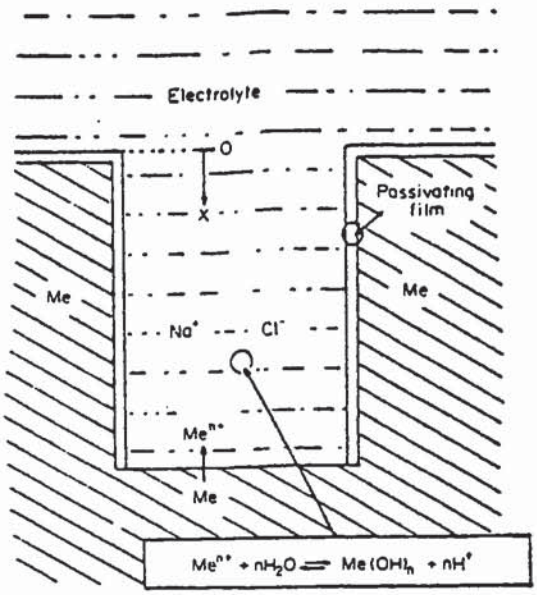

FIGURE 6.5 Unidirectional pit model (After Galvele).

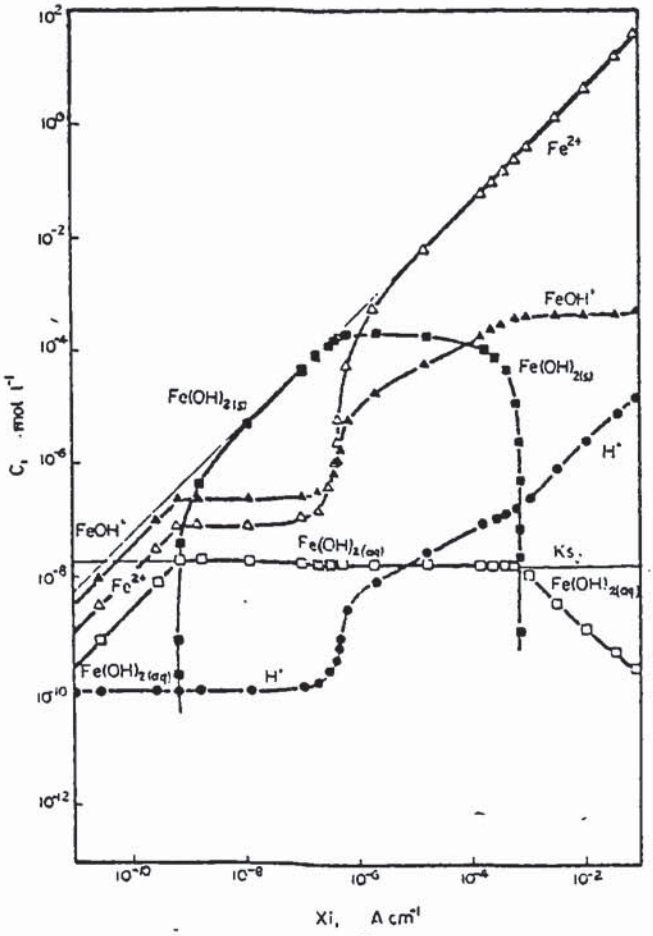

FIGURE 6.6 Concentrations of Fe^{2+}, $FeOH^{+}$, $Fe(OH)_{2(aq)}$, $Fe(OH)_{2(s)}$ and H^{+} as a function of the product of the depth x and the current density i in a unidirectional pit for iron in a pH-10 solution (After Galvele).

least at the pit initiation stage, steady-state conditions exist.

For iron the following general reaction is true, taking also into account precipitated $Fe(OH)_{2(s)}$

$$3Fe^{2+} + 3H_2O + 2OH^- \rightarrow Fe(OH)^+ + 3H^+ + Fe(OH)_{2(aq)} + Fe(OH)_{2(s)} \quad . \; . \; . (3)$$

s1 s2 s3 s4 s5 s6 s7

If D1 to D7 are the diffusivities of species S1 to S7, their concentrations C1 to C7 inside the pit can then be calculated by considering such equations as,

$$D1\frac{dC1}{dx} + D4\frac{dC4}{dx} + D7\frac{dC7}{dx} = \frac{i}{2F} \quad . \; . \; . \; . \; (4)$$

for the flow of Fe atoms*, and

$$D2\frac{dC2}{dx} + D3\frac{dC3}{dx} + D4\frac{dC4}{dx} + 2D7\frac{dC7}{dx} = o \quad . \; . \; . \; (5)$$

for the flow of O atoms, etc. and from considerations of hydrolysis and limiting concentration equilibrium constants (143).

The diffusivities D for each species were assumed by Galvele to be $10^{-5} cm^2 s^{-1}$ except for OH^- where $D=5.3 \times 10^{-5} cm^2 s^{-1}$ and for H^+ where $D=9.3 \times 10^{-5} cm^2 s^{-1}$. He represented his results in the form of plots of concentration versus the product xi where x is the depth of the-pit in cm and i the current density flowing through it (figure 6.6).

For a pH 10 solution the relative concentrations are as

---

* Gälvele has shown the term for s6 to be equal to zero as the concentration C6, when precipitation takes place, is constant.

shown in figure 6.6. At xi values up to about 5 x $10^{-7}Acm^{-1}$ the pH inside the pit is the same as that of the bulk solution. As xi increases, the pH is reduced sharply accompanied by a change in the relative concentration of corrosion products. This last fact can be seen more clearly in a plot of Fe(II) versus xi (figure 6.7). A particular xi value evidently exists above which the amount of solid $Fe(OH)_2$ decreases sharply as it is replaced by Fe^{++}.

Galvele had assumed that up to this xi value, the solid product of $Fe(OH)_2$ causes repassivation but if it is exceeded, then dissolution can occur reinforced by the local acidification of the solution. He termed this, the critical xi value and was able to calculate such values theoretically for a range of pH's (table 6.1). Figure 6.8 represents Galvele's results graphically in terms of concentrations of solid or aqueous $Fe(OH)_2$ for each pH and the arrows indicate the critical xi values. Below pH 10 there is either not sufficient precipitated $Fe(OH)_2$ or none at all to cause repassivation of the pit walls, which supports his earlier experimental findings (figure 6.4), but above pH 10, a relationship exists of the form,

$$Ep = A + BpH$$

where A and B are constants.

De Wexler and Galvele [146] had studied the pitting of Al in NaCl solutions whilst mechanically straining the metal. They showed that below the determined pitting potential

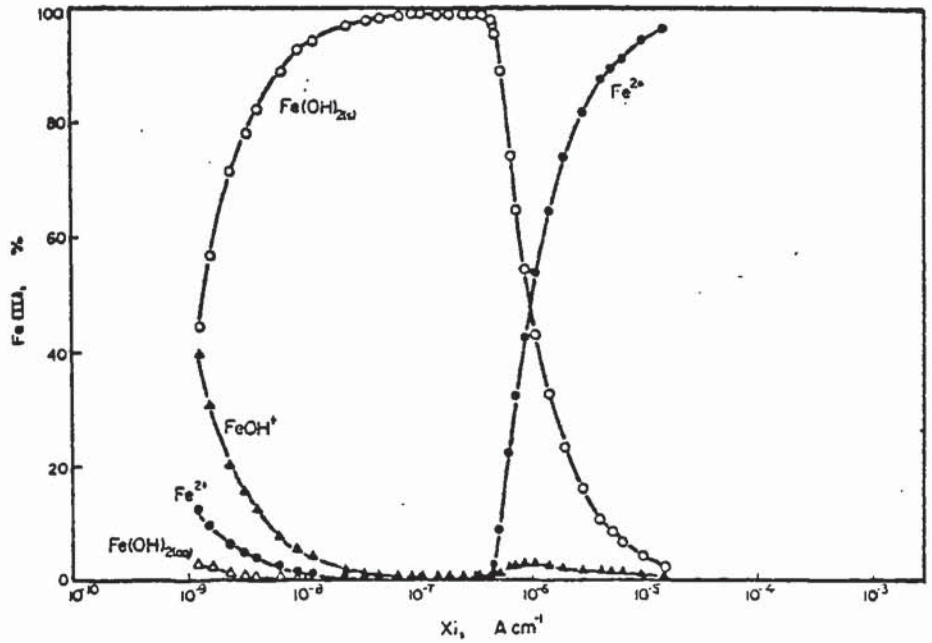

FIGURE 6.7 Distribution of iron corrosion species as a function of xi (depth x current density) in a unidirectional iron pit at pH10 (After Galvele).

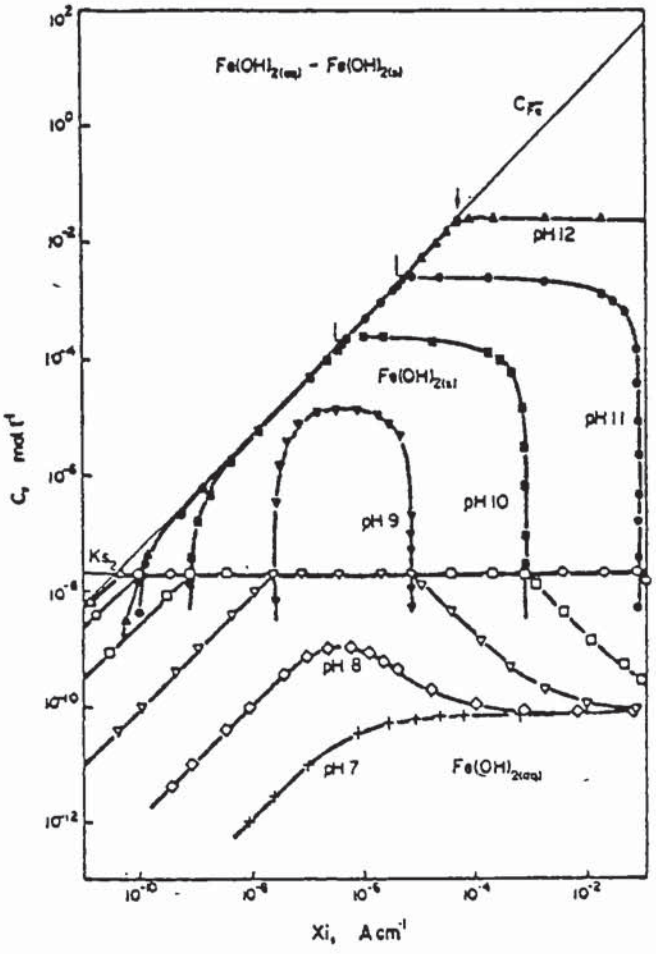

After Galvele

FIGURE 6.8 Effect of external pH on the concentration of $Fe(OH)_{2(aq)}$ and $Fe(OH)_{2(s)}$ as a function of the product xi (depth x current density) in a unidirectional iron pit.

TABLE 6.1 Variation of $xi_{crit.}$ with pH of solution.

pH	CRITICAL xi (Acm^{-1})
10	5×10^{-7}
11	5×10^{-6}
12	5×10^{-5}

(After Galvele)

even though bare metal was exposed by continuous oxide film rupture, there was always repassivation, but above Ep there was pitting.

In relating these results to his model, Galvele [143] suggested that if pits initiate at breaks in the oxide film, then the depth of the pit x at initiation is equal to the thickness of the film so for a constant film the higher critical xi values of the more alkaline solutions require higher current densities (hence higher potentials).

Galvele had also demonstrated that the pitting potential is the sum of three components [142,143,147].

$$Ep = E_c + \eta + \Delta\phi$$

where

E_c = the corrosion potential in the pit-like solution

η = the positive polarization necessary to draw enough current density through the pit to reach the critical xi value for pitting.

and $\Delta\phi$ = the electrical potential inside the pit when ion migration has to be taken into account.

A measurable electrical potential appears only for very high xi values and very low chloride concentrations [142]. Furthermore, for more neutral solutions the value of η is negligible so the pitting potential Ep has a similar value to the corrosion potential Ec in the pit-like solution

[148,149]. As the pH is increased however the higher xi value required is represented by the increasing positive polarization η.

In a later publication Gravano and Galvele[144] introduced the concept of buffers in the pitting model and found that increasing amounts of borate buffers in the bulk solution increased the critical xi values, considerably, so apart from an increased η there was also a contribution to the pitting potential by the electrical potential drop $\Delta\phi$ inside the pit resulting in a much higher pitting potential.

6.2.2. Application of the pitting theory to steel embedded in cement.

Recently potentiodynamic or potentiostatic polarization techniques have been applied to steel in cement paste or concrete[137,150], but difficulties have been encountered related mainly to the high electrical resistance of the concrete and the long experimental times involved (8). The latter is mostly related to the slow migration and diffusion rates of ions and corrosion products in the cement matrix.

Such slow diffusion rates can complicate the pitting mechanism. Pitting would start at positions where the steel reinforcement is in direct contact with the pore electrolyte. For simplicity this can be assumed to be a roughly hemispherical pore (figure 6.9). When the pitting potential of

the steel for the particular electrolyte contained in the pore is reached, a pit can develop, but with the consumption of OH^- and Cl^- ions their concentrations in the solution of the pore would decrease, as their diffusivities within the cement paste would be in the order of $10^{-9}cm^2s^{-1}$ (see chapter 3) as compared to $10^{-5}cm^2s^{-1}$ inside the pore and pit. For a portland cement possessing $Ca(OH)_2$ crystals however, a form of buffering would be achieved. The mechanism would be rather different to that involving borate buffers (see earlier) but the result would be the same.

The local buffering offered by free $Ca(OH)_2$ would maintain the pH of the pore solution at a pH of 12.6. Consequently the ratio of $[Cl^-]/[OH^-]$ would tend to decrease and hence the required pitting potential would rise enabling the repassivation of the pit walls. The ionic concentration of the pore would then tend to recover to their original values which would again depassivate the pit and the whole cycle would be repeated. Serious pitting can therefore only occur at a potential where even a low chloride concentration can maintain a pit in its active form.

Dehghanian and Locke [150] obtained potentiostatic and potentiodynamic polarization data for steel embedded in concrete produced from type I (11% C_3A) and type V (3% C_3A) portland cements and exposed to various NaCl containing solutions for periods up to 170 days. In their potentiostatic polarization experiments, they increased the potential at

increments of 50mV every 3 minutes (~17mV/min) and for potentiodynamic scans they used a scan rate of about 17mV/min. In both cases they obtained increasing current densities with overall higher c.d.s for the high C_3A content concrete. There was however no mention of pitting potentials even though some E-i plots had shown sudden increases at certain potentials.

Preece et al [137] were also interested only in the leakage currents during potentiostatic scans. They had used this method to study the electrochemical behaviour of steel embedded in mortars made from OPC, SRPC, BFS, PFA or DSP (dense microsilica cement). Typical current densities at the passive range after slow scans of a few tens of millivolts per day were in the order of $10^{-4}A/m^2$. BFS based mortars however had produced current densities approximately 50 times greater than the other mortars, either as they suggested, due to lower OH^- availability or to a less protective passive film.

Some specimens were also immersed in 1MNaCl solutions for a length of time whilst holding the potential at +100mV to accelerate corrosion before subjecting them to the same anodic potentiostatic polarization scans. They had encountered however considerable scatter, particularly for OPC based mortars, as some had corroded prior to the scans and others had not. Steel specimens in SRPC based mortars had all corroded and resulted in current densities in the order

of 0.1 to $1A/m^2$. There was no evidence of corrosion for the other three types of mortars hence producing potential-current scans not too dissimilar to the non-chloride containing specimens. These results are in accord with the diffusion results obtained inchapter 3 part II. Blended cements, having the lowest chloride diffusivities, had not allowed sufficient chloride to penetrate the mortars and initiate corrosion, whilst SRPC, with very little complexing capacity, had allowed more chloride to penetrate and cause corrosion.

The last two reviewed papers did not appear to utilise their results to the full and may have been able to obtain more meaningful results, by using considerably less time consuming techniques, such as linear polarization (47). They did however serve as a guide to the difficulties encountered when applying potentiostatic polarization techniques to steel embedded in cements or concretes. First there is the problem of knowing the pore solution composition of the electrolyte in contact with the steel. If chloride is to be diffused from an outside source it has to be remembered that different cements offer varied diffusion characteristics, as Preece et al (137) had found out.

Secondly the scan rate should be low enough to allow as near as possible equilibrium conditions. Comparing the two publications, Dehghanian and Locke (150) with relatively

fast scan rates (~17mV/min) had recorded passive current densities 2 to 3 orders of magnitude higher than Preece et al [137], who had used very slow scan rates. For such slow scan rates to be achieved however, it required all the specimens to be connected in parallel and with so many variable pore electrolyte compositions, resistivities of cements, pore structures etc it cannot be possible to guarantee the same exact potential for each individual specimen.

Such problems, as well as the fact that no available published work existed on pitting potentials of steel in cements made the task of developing a technique for the determination of pitting potentials very difficult. The purpose of the work was to establish pitting characteristics of steel embedded in a selection of cement pastes when the variable of pore solution was eliminated. This was to be achieved by equilibrating the cement paste electrolytes to a specific outer solution. The inner pore solution was then to be monitored with the use of the pore solution expression device (chapter 2 para. 2.3). Any variations in pitting characteristics between the types of cements should then be caused by differences in the physical or chemical structure of the solid cement paste. The findings of the experiment are reported in this part of the chapter.

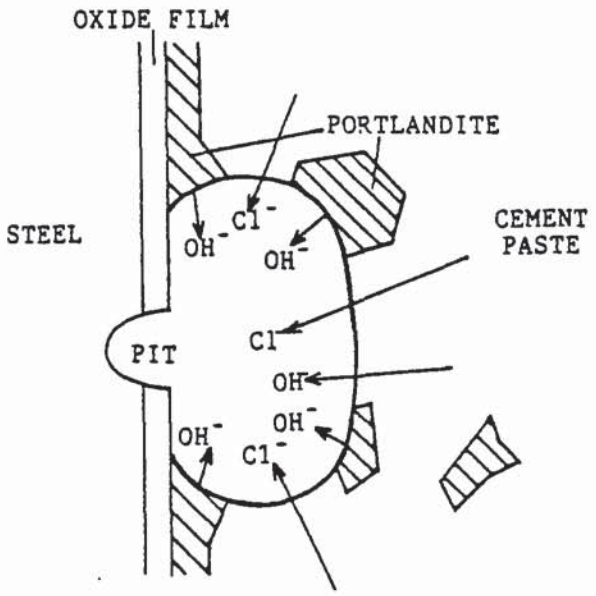

FIGURE 6.9 Pit model of steel in hardened cement paste.

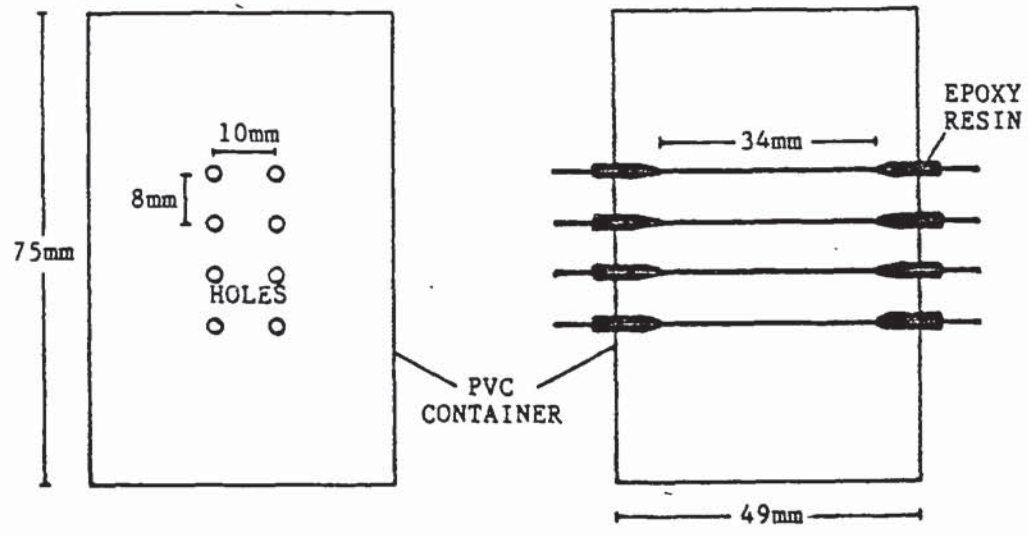

FIGURE 6.10 Drawings of PVC containers used as moulds for the preperation of hardened cement pastes showing the position of the inserted wire specimens.

6.3 EXPERIMENTAL PROCEDURE

The four varieties of cement pastes used previously for the diffusion experiments (chapter 3 part II) and the buffering experiments (chapter 5 part II) namely OPC-B', SRPC, OPC-B' /30% PFA and OPC-B'/65% BFS, were also used for this investigation in an attempt to relate those properties to pitting of the embedded iron.

The iron used was in the form of a 0.5mm diameter drawn wire of 99.9% purity, as supplied by Goodfellow Metals. This wire was sliced into approximately 70mm strips. Each individual strip was rubbed lightly with 600 grade carbide paper, washed thoroughly in teepol and degreased in acetone. Both ends of each specimen were then masked-off with "sealocrete" epoxy resin based paste, so that a central length of 34mm remained exposed. The specimens were once more degreased in acetone and stored in a desiccator for 24 hours.

The embedding of the wires into cement pastes was achieved by the following procedure. Two parallel rows of holes 10mm apart were drilled at 8mm intervals along both sides of PVC containers perpendicular to their axis (figure 6.10). A total of 8 wire specimens were then threaded through the holes, so that each container had two rows of 4, as shown schematically in figure 6.10. Any remaining gaps were filled with paraffin wax applied by brush from the outside. The PVC containers were then ready to be used as normal

(chapter 2 para. 2.2) for the production of cement pastes. A total of 5 such pastes were thus prepared for each type of cement.

After a curing period of 3 days, the cement pastes were demoulded and sliced into 4 discs, as described in chapter 2 (para. 2.2), so that each disc contained two parallel iron wires centrally positioned as shown in figure 6.11(A). The discs were ground down to a thickness of 6mm on 600 grade carbide paper. The protruding wires were trimmed to within 0.5mm of the surface on the one side and connected to 30cm long wires on the other. Any exposed metal was finally masked-off by lacquer and paraffin wax. The finished specimens were then stored in a solution of sat.$Ca(OH)_2$ at 20±2°C for further curing, until required.

Four parallel non-electrode-containing cement pastes were also produced in the normal way (chapter 2 para. 2.2). After a 3 day curing period they were demoulded and sliced into discs. Twelve 6mm and four 3mm discs of each type of cement were immersed in four separate sealed containers filled with 1 litre of sat.$Ca(OH)_2$ solution and maintained at 20±2°C. The hydroxyl concentration of each separate solution was monitored regularly by titrating 1ml aliquots (see chapter 2 para. 2.4.1). Each solution was replaced when the pH approached 12.9. These discs were to be used as control specimens.

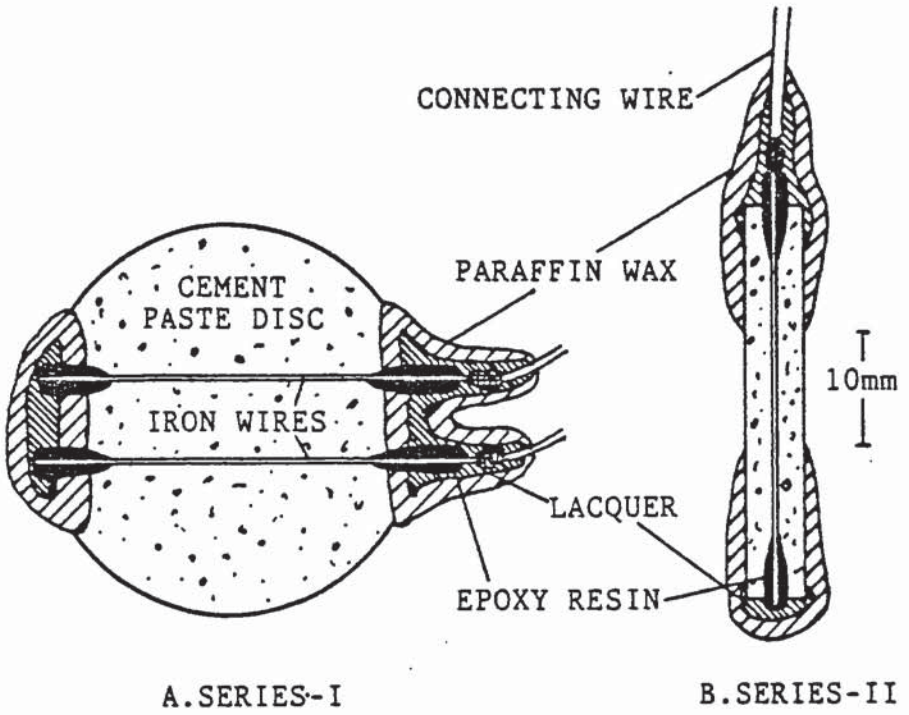

FIGURE 6.11 Specimens used for potentiostatic polarization studies.

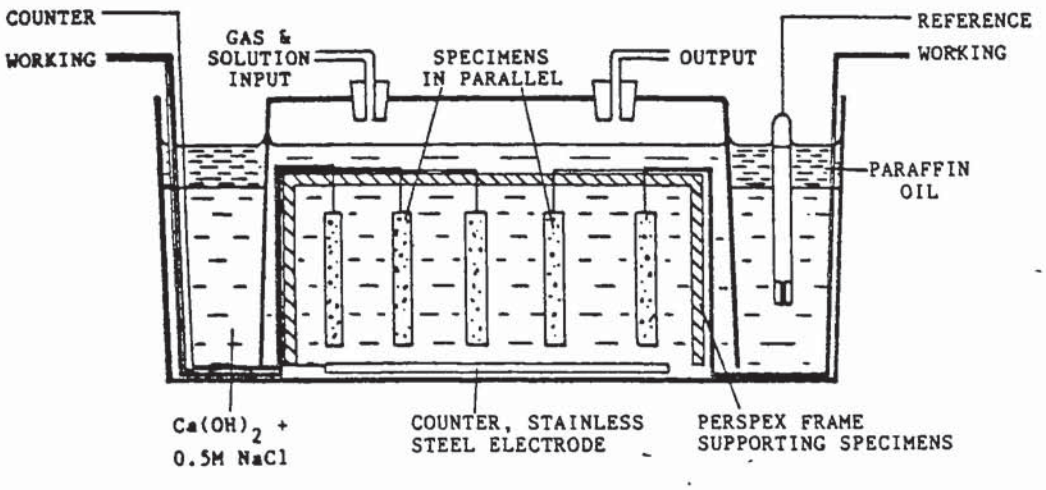

FIGURE 6.12 Apparatus set-up for the Series-I experiments.

Five electrode-containing discs (ie 10 electrodes) of each cement type were removed from the solution after 28 days and positioned vertically on a perspex arrangement placed inside a container. Another slightly smaller container, fitted with an inlet and outlet, was inverted over the specimens so the final arrangement was as shown schematically in figure 6.12. The "container" was then filled with 3 litres of deaerated sat.$Ca(OH)_2$ solution.

Deaeration was achieved by employing a "nilox scrubber" arrangement as described by Gilroy and Mayne[151] and depicted in figure 6.13. It was shown by them, that by passing white spot N_2 through the apparatus for a minimum of 1 hour it is possible to reduce the amount of residual oxygen to 0.003±0.001p.p.m.[151].

The exposed "outer" solution of the container was covered with a thick layer of parraffin oil, to reduce the likelihood of oxygen contamination. Once a week the solution was syphoned out to a level where paraffin oil could not enter the inner part of the container and replaced with freshly deaerated solution, always kept at 20±2°C. N_2 was constantly passing over the "inner" solution to maintain an equilibrium.

The potential of each separate specimen was monitored on a digital voltmeter versus a saturated calomel electrode inverted in the solution (figure 6.12). When the potential of the specimens had fallen to about-600mV or lower, sig-

nifying high polarization of the oxygen reduction reaction owing to the reduced amount of oxygen inside the cement pastes (see figure 6.22), the solution was replaced by one containing 0.5M NaCl and saturated with $Ca(OH)_2$.

At the same time an equal amount of NaCl was introduced to the solutions of each of the four sets of control specimens. Each of the five solutions were replaced once a week and analysed for OH^- and Cl^- by the techniques described in chapter 2 (para. 2.4). The potentials of all the wire specimens were also continuously monitored.

After 144 days when the change in concentration of the outer solutions was negligible, five 6mm cement paste discs from each cement type were surface dried and pressed in the pore solution expression device to extract the pore solution of each group of discs (chapter 2 para. 2.3). These were analysed for OH^-, Cl^-, Na^+ and K^+ as described in chapter 2 (para. 2.4). The same procedure was repeated after 314 days.

In addition, at 314 days the 3mm discs were used to determine evaporable and non-evaporable water contents (chapter 2 para. 2.5) and total amount of chloride (chapter 2 para. 2.7), as well as to obtain DTA data (chapter 2 para. 2.8.1).

After 350 days of exposure to the NaCl solution, once the inner pore solution of the discs was in approximate equilibrium with the outer solution, pitting runs were started.

These were in the form of potentiostatic polarization scans, where the potential of the specimen was increased by 60mV increments at constant time intervals of either 10, 15 or 20 minutes whilst monitoring the current density.

For this purpose the "AMEL model 551" potentiostat was employed, enabling the required potential to be "dialed" on. The current was read-off a digital voltmeter via the potentiostat variable resistor. As a counter-electrode a long plate of stainless steel was positioned underneath the specimens (figure 6.12).

The run was terminated when the current density had reached a value of at least $1A/m^2$, or the potential was 540mV. Potential-current density plots were then produced for each specimen.

Originally for iron specimens embedded in OPC or SRPC pastes, the scans were started at -720mV (v's SCE) without any prior reduction of the surface film of the iron. For later runs however, wires embedded in PFA and BFS based cement pastes, as well as those in series-II (see later), were held at -960mV for a period of up to 8 days, in an attempt to reduce the surface film. The results obtained by the above procedure are henceforth refered to as "series-I" results.

Suspicions that crevice corrosion may have been influencing corrosion of these earlier runs-as two specimens embedded

in BFS cement pastes had shown signs of a small degree of crevice attack-and that the apparatus was not completely "air-tight" led to a further development of the set-up, and the results are termed "series-II".

Discs with embedded iron wires were prepared as described previously and cured in a sat.$Ca(OH)_2$ solution at 20±2°C for 28 days, before being ground down on carbide paper to a 3mm thickness, ie half the original size. This allowed a shorter period of exposure to the NaCl solution before equilibration of the pore solution could be achieved. As diffusion of ions in cements is proportional to the square root of time, then for a disc half the thickness, equilibration should be achieved at a quarter of the time. It was therefore thought sufficient to expose the cement pastes to a constant sat.$Ca(OH)_2$ + 0.5M NaCl solution for 70 days for the portland cements and 115 days for the others.

In order to minimise the likelihood of crevice corrosion, each disc was masked-off with paraffin wax on both sides, exposing only 10mm of cement paste in the centre so that the chloride concentration could be at its highest in the middle section of the wire (figure 6.11.B). The connecting wires of the specimens, were threaded through 7mm diameter glass tubes, 25cm long, four at a time, so that 2 discs were allocated to each tube. The tubes were filled with paraffin wax to provide airtightness and fitted in a purpose-built "pyrex" cell, which could accomodate three glass

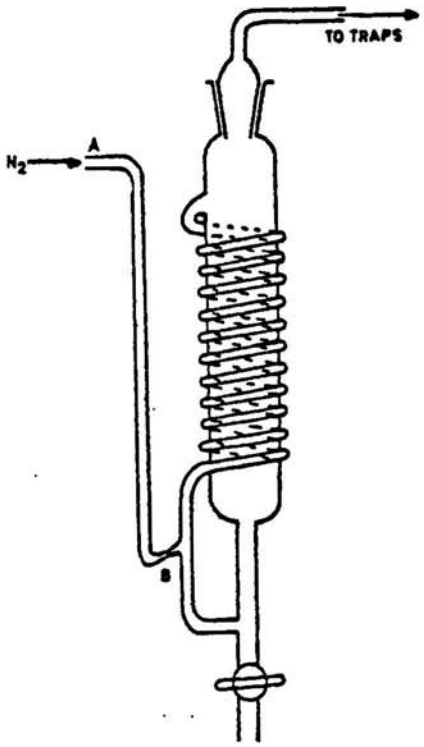

FIGURE 6.13 Glass de-aeration apparatus (After Hersch)

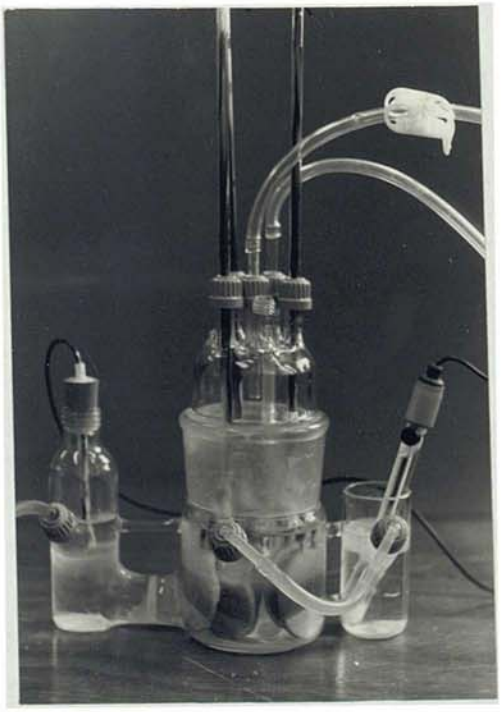

FIGURE 6.14 Purpose-built cell for potentiostatic polarization studies.

tubes (ie 12 specimens).

Two such cells (figure 6.14) were employed, one containing OPC and SRPC paste discs and the other BFS and PFA based discs. Each cell incorporated the following features:

(i) Separate cell fitted with gas output to a water trap and connected to the central cell by a porous partition and housing a platinum wire counter electrode.

(ii) Separate "open" cell connected to the main cell via an "agar" salt bridge and housing the calomel reference electrode.

(iii) Inlet for solution direct from the "nilox" scrubber.

(iv) Outlet for solution.

(v) Inlet for N_2 gas.

(vi) Outlet for gas to water trap.

(vii) Provision for insertion of 3 glass tubes containing the specimens.

All connections were made airtight by the use of rubber seals.

The potentials and corrosion intensities of all the specimens, using the manual linear polarization technique (chapter 2 para. 2.10.1), were recorded periodically, until potentiostatic polarization scans could be performed on each

specimen as described earlier.

Finally, iron wires prepared and masked, as reported earlier, but not embedded in cement paste, were exposed to sat.$Ca(OH)_2$ solution for 28 days to produce a similar surface film as those embedded in cement and were then introduced into the cell. The solution was again deaerated and the potential of the wires and corrosion intensities monitored.

When the potential of each had fallen to about -500mV, 0.5M NaCl was introduced to the solution and left for a further 14 days. Each one was then subjected to potentiostatic polarization scans at 60mV increments every 10 minutes starting from -720mV or -960mV. Two of the specimens had previously been held at -960mV for 5 days in order to reduce the surface film.

6.4 RESULTS

6.4.1 Pore Solution Analysis and Phase Determination

The results of the pore solution analysis are summarised in table 6.2. It is evident that whilst the pore solution of OPC and SRPC pastes have virtually equilibrated with the outer solution, PFA and particularly BFS based cements had not done so completely, even after a 314 day exposure.

It was because of this that it was decided to expose the PFA and BFS based electrode specimens for a further period

TABLE 6.2 Solution analysis of the pore liquid of cement paste discs after immersion in sat.$Ca(OH)_2$+0.5M NaCl.

Expressed solution after 144 days (mM/l)

TYPE OF CEMENT	Cl^-	OH^-	Na^+	K^+	Σ^-	Σ^+
OPC-B'	483	58	508	1	541	509
SRPC	474	56	503	2	530	505
OPC-B'/30% PFA	400	55	400	24	455	424
OPC-B'/65% BFS	372	57	388	23	429	403

External solution after 144 days(mM/l)

TYPE OF CEMENT	Cl^-	OH^-	Na^+	K^+	Σ^-	Σ^+
OPC-B'	470	57	515	1	527	516
SRPC	467	55	516	3	522	519
OPC-B'/30% PFA	464	56	514	8	520	522
OPC-B'/65% BFS	465	57	514	5	522	519

Expressed solution after 314 days (mM/l)

TYPE OF CEMENT	Cl^-	OH^-	Na^+	K^+	Σ^-	Σ^+
OPC-B'	-	-	-	-	-	-
SRPC	479	58	515	3	537	518
OPC-B'/30% PFA	446	61	495	19	507	514
OPC-B'/65% BFS	416	56	450	20	472	470

External solution after 314 days (mM/l)

TYPE OF CEMENT	Cl^-	OH^-	Na^+	K^+	Σ^-	Σ^+
OPC-B'	461	57	515	1	518	516
SRPC	470	58	515	2	528	517
OPC-B'/30% PFA	473	56	515	7	529	522
OPC-B'/65% BFS	465	57	512	2	522	514

TABLE 6.3 Free, Total and Bound amounts of Chloride for cement pastes exposed to sat. $Ca(OH)_2$+0.5M NaCl for 314 days (mM/g).

TYPE OF CEMENT	FREE Cl^-	TOTAL Cl^-	BOUND Cl^-	$\frac{\text{FREE}}{\text{TOTAL}}$
OPC-B'	0.171	0.590	0.419	0.290
SRPC	0.172	0.425	0.253	0.405
OPC-B'/30% PFA	0.188	0.558	0.370	0.337
OPC-B'/65% BFS	0.162	0.696	0.534	0.233

TABLE 6.4 Evaporable and non-evaporable water contents for cement pastes exposed to sat.$Ca(OH)_2$ + 0.5M NaCl for 314 days (mM/g).

TYPE OF CEMENT	We(%)	Wn(%)	TOTAL(%)
OPC-B'	35.45	19.45	54.90
SRPC	35.98	16.46	52.44
OPC-B'/30% PFA	42.11	13.94	56.05
OPC-B'/65% BFS	38.88	13.42	52.30

of time; a total of 400 days for PFA and 450 days for BFS. Although it was appreciated that complete equilibration of these cements would not have been possible, even allowing for the extra exposure period, the pore solutions of all cements were believed to be sufficiently similar and gave a $[Cl^-]/[OH^-]$ ratio of 8±0.5 or better, a parameter which, as discussed earlier, is thought to be important for pitting corrosion.

The total amount of chloride contained in each of the cements was also determined, as a matter of interest and the results are tabulated in table 6.3. Free and bound amounts of chloride are also shown in the same table, as well as the free-to-total chloride ratio of each cement type. These values were calculated by use of the evaporable and non-evaporable water content data (table 6.4), as discussed in chapter 2 (para. 2.5).

DTA thermographs had confirmed the complexing of part of the chloride to calcium chloroaluminate (figure 6.15), with a peak at around 280°C, but only a small peak was detectable for SRPC (figure 6.15b). It is surprising therefore that as much as 0.253mM/g of chloride is present in the bound form in SRPC (table 6.3). It suggests therefore that chloride may also be taken out of solution by other means, but this will be discussed in more detail in chapter 7.

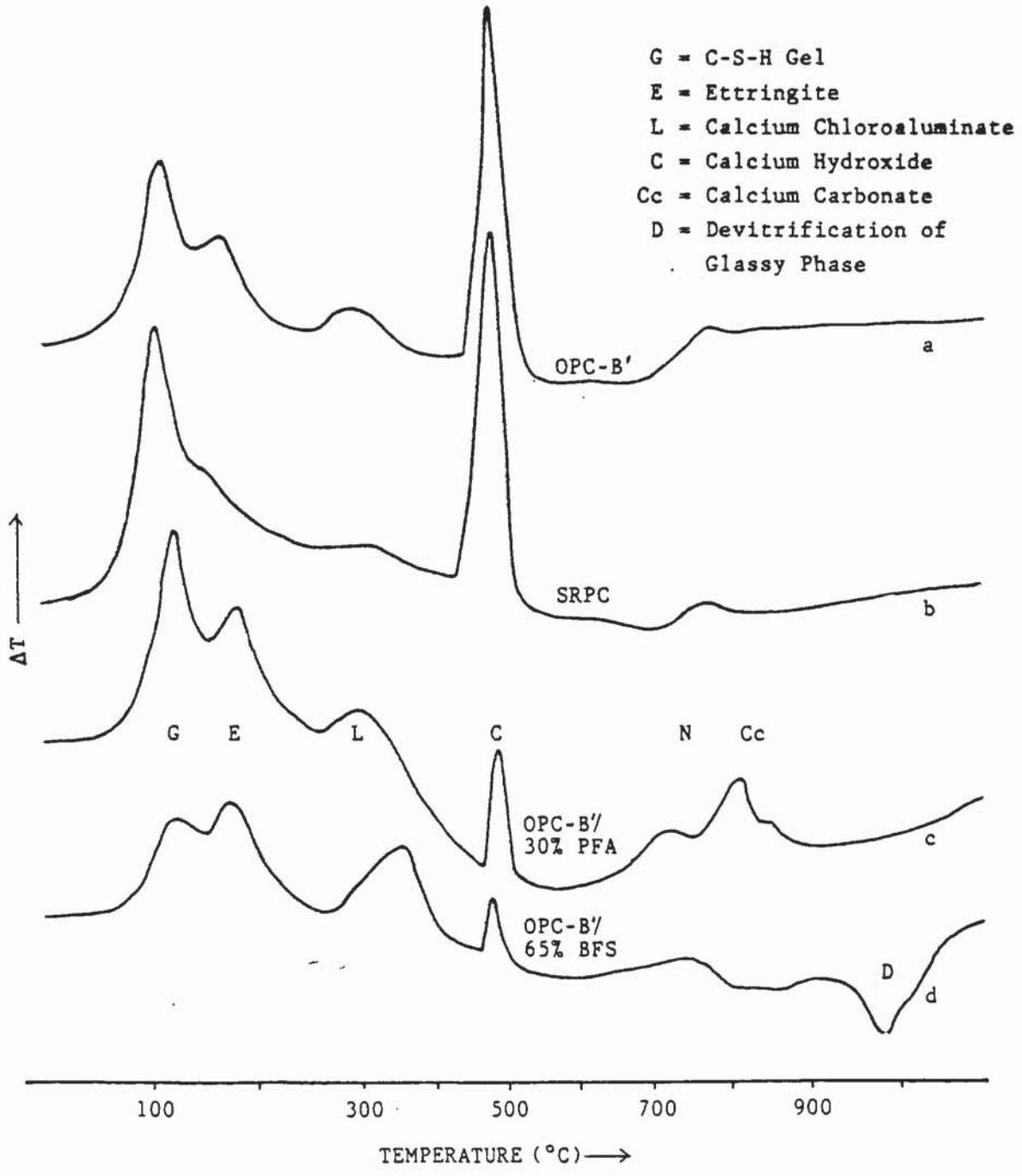

FIGURE 6.15 DTA thermographs of hardened cement pastes exposed to 0.5M NaCl + sat. $Ca(OH)_2$ for 314 days.

6.4.2 Pitting of Iron in Solution

Figure 6.16 represents two typical potential-current diagrams of polarization scans of iron wires immersed in a solution of sat.$Ca(OH)_2$ + 0.5MNaCl. The difference between the two is only that the one, represented by b in figure 6.16, had had its protective oxide film reduced prior to the polarization scan by holding its potential at -960mV for 5 days. Failure to do so had allowed the previously formed thicker oxide film to remain almost unchanged during the scan and hence require a higher current i to reach the critical xi value necessary for pit initiation, as was discussed earlier.

The average values of pitting potential for each type of "pretreatment" are shown in table 6.5. When the oxide film had been previously reduced, the value of Ep was very consistent in both runs and had a value of -420mV, a very much lower value than the "non-reduced" specimens. The original average potentials and corrosion intensities of these "pre-reduced" specimens are also shown in table 6.5.

6.4.3 Pitting of Iron in Cement Pastes

Figure 6.17 represents a typical E-i plot of a potentiostatic polarization scan, obtained for specimens embedded in OPC or SRPC pastes from series-I. As was the case with similar "non-reduced" specimens in solution, the double active loop, observed in the "reduced" specimens (figure

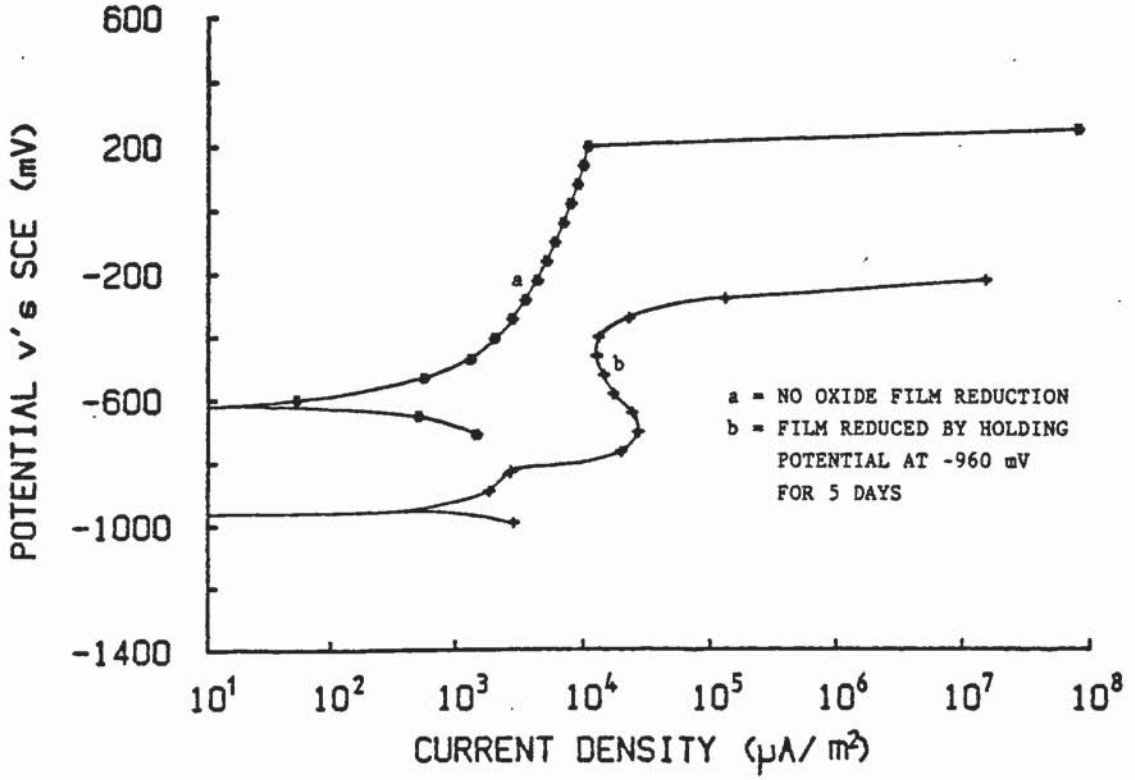

FIGURE 6.16 Anodic potentiostatic scans of iron wires in a 0.5M NaCl + sat. $Ca(OH)_2$ solution with or without an initial oxide film reduction.

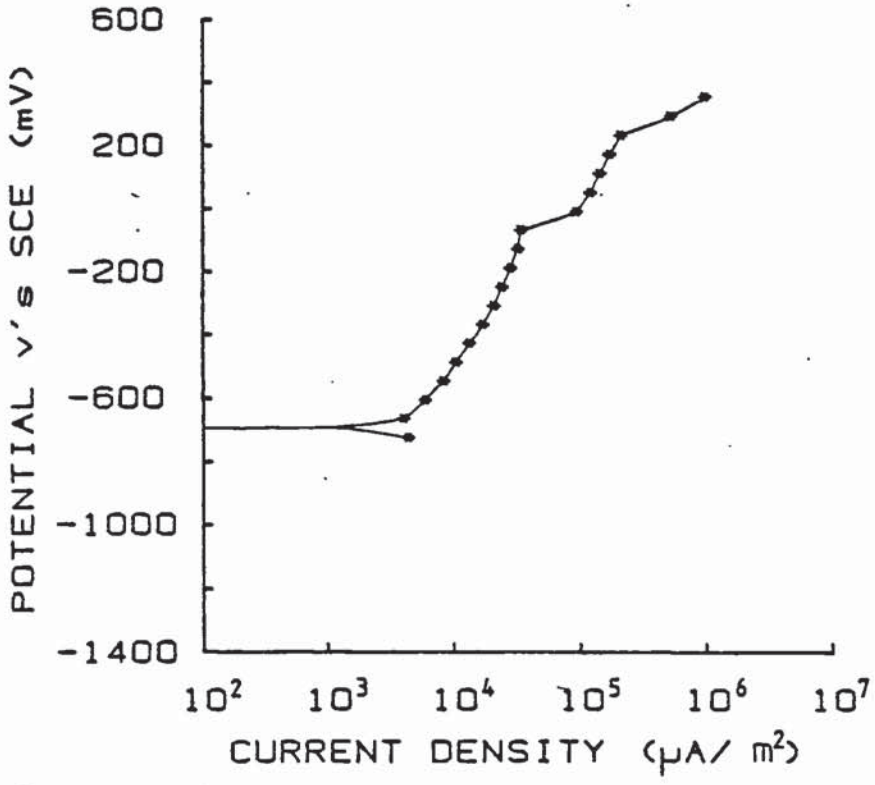

FIGURE 6.17 Typical anodic potentiostatic scan of iron wire embedded in OPC-B' or SRPC paste without an initial oxide film reduction and immersed in 0.5M NaCl + sat. $Ca(OH)_2$.

TABLE 6.5 Pitting potentials, rest potentials and corrosion intensities of Fe wires immersed in solution of sat.$Ca(OH)_2$ + 0.5M NaCl.

CONDITION OF SURFACE OXIDE FILM	PITTING POT.(Ep) (mV)	BEFORE ADDITION OF Cl^-			
		BEFORE DEAERATION		AFTER DEAERATION	
		Ecorr (mV)	Icorr ($\mu A/m^2$)	Ecorr (mV)	Icorr ($\mu A/m^2$)
"UNREDUCED"	90				
"PREREDUCED"	-420	-120	6.3×10^2	-525	1.3×10^3

TABLE 6.6 Rest potentials and corrosion intensities of iron wires embedded in different cement pastes at different stages of their immersion into sat.$Ca(OH)_2$ before and after deaeration of the solution and introduction of 0.5M NaCl.

TYPE OF CEMENT	BEFORE DEAERATION		15 DAYS AFTER DEAERATION (BEFORE Cl^-)		70 DAYS AFTER INTRO.OF Cl^-	
	Ecorr (mV)	Icorr ($\mu A/m^2$)	Ecorr (mV)	Icorr ($\mu A/m^2$)	Ecorr (mV)	Icorr ($\mu A/m^2$)
OPC-B'	-172	8.6×10^2	-642	1.8×10^3	-576	5.0×10^3
SRPC	-174	8.8×10^2	-629	1.5×10^3	-627	4.1×10^3
	BEFORE DEAER. 1 DAY AFTER EXPOS. TO SOL.		4 DAYS AFTER DEAERATION		115 DAYS AFTER INTRO.OF Cl^-	
OPC-B'/30% PFA	-431	1.9×10^3	-546	2.8×10^3	-590	8.3×10^3
OPC-B'/65% BFS	-646	—	-699	5.4×10^3	-650	5.7×10^3

6.16), is absent. There is also no clear "passive" current density, but only a steady increase with increasing potential. Furthermore, there is no single pitting potential, but between 0 and 3 sudden "surges" of current with a type of "repassivation" inbetween (see figure 6.17).

The results are best summarised graphically by figure 6.18. Each individual "current-surge" of all the potentiostatic polarization scans are shown on the graph, in terms of degree of "severity" of current increase, on a scale of 1 to 4, versus the potential at which it had occurred. (the scale is explained in figure 6.18).

As it was established that oxygen evolution occurred at around 600mV, specimens which had not shown any sudden current increases up to that potential, were represented on the graph on the potential axis at 600mV.

The lowest potentials at which the current increases had occurred for each degree of severity were joined up by a line representing each type of cement, thus producing a kind of a "profile". By taking these profiles to represent the "reluctance" of the embedded wires to pit, it appears that specimens contained in SRPC pastes, are offered slightly less protection than those embedded in OPC. There is however such a high degree of scatter, that it is not possible to suggest whether there is any significant difference between the pitting potentials of the wires contained in cement pastes and those of the wires immersed in

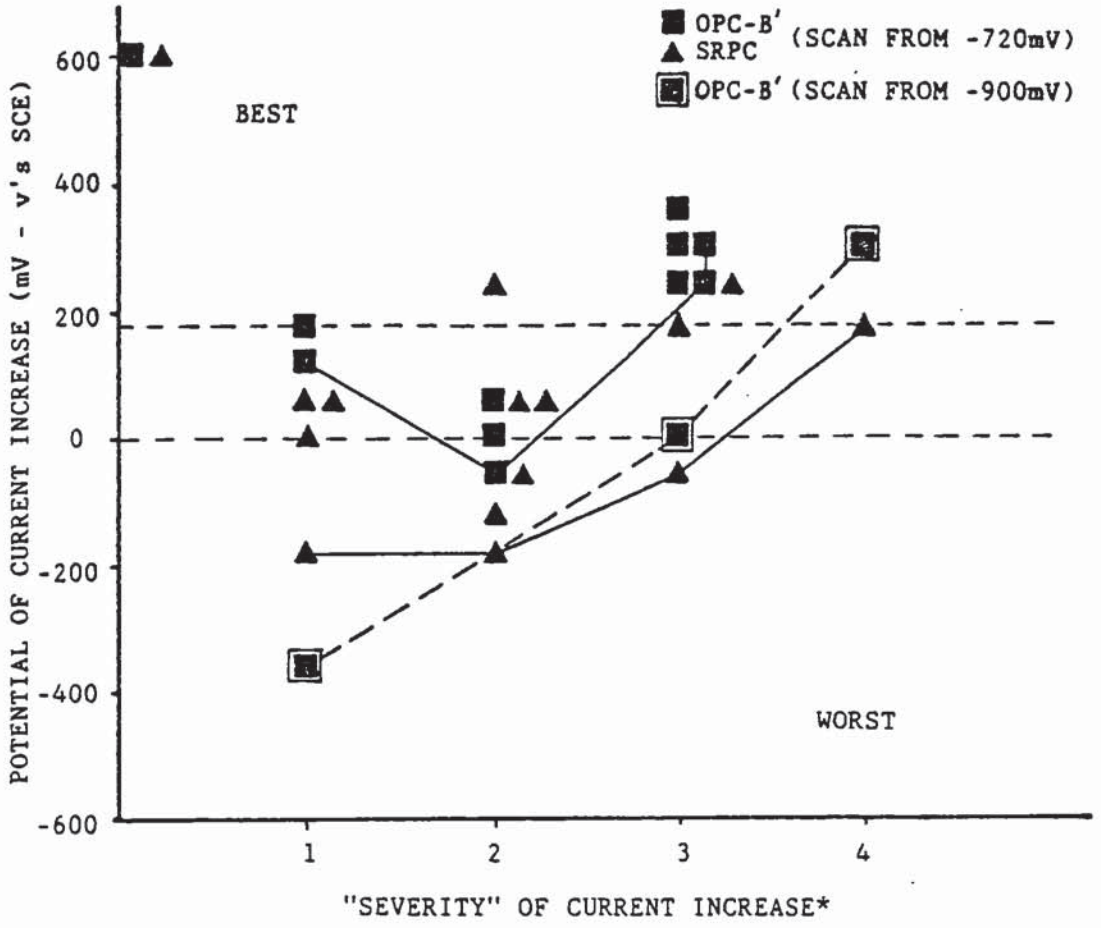

* Increase in current density as follows:

1	up to	x2
2	"	x3
3	"	x10
4	over	x10

FIGURE 6.18 Sudden current increases during the potentiostatic scans of iron wires embedded in OPC-B' and SRPC pastes, represented in terms of "severity" of increase.

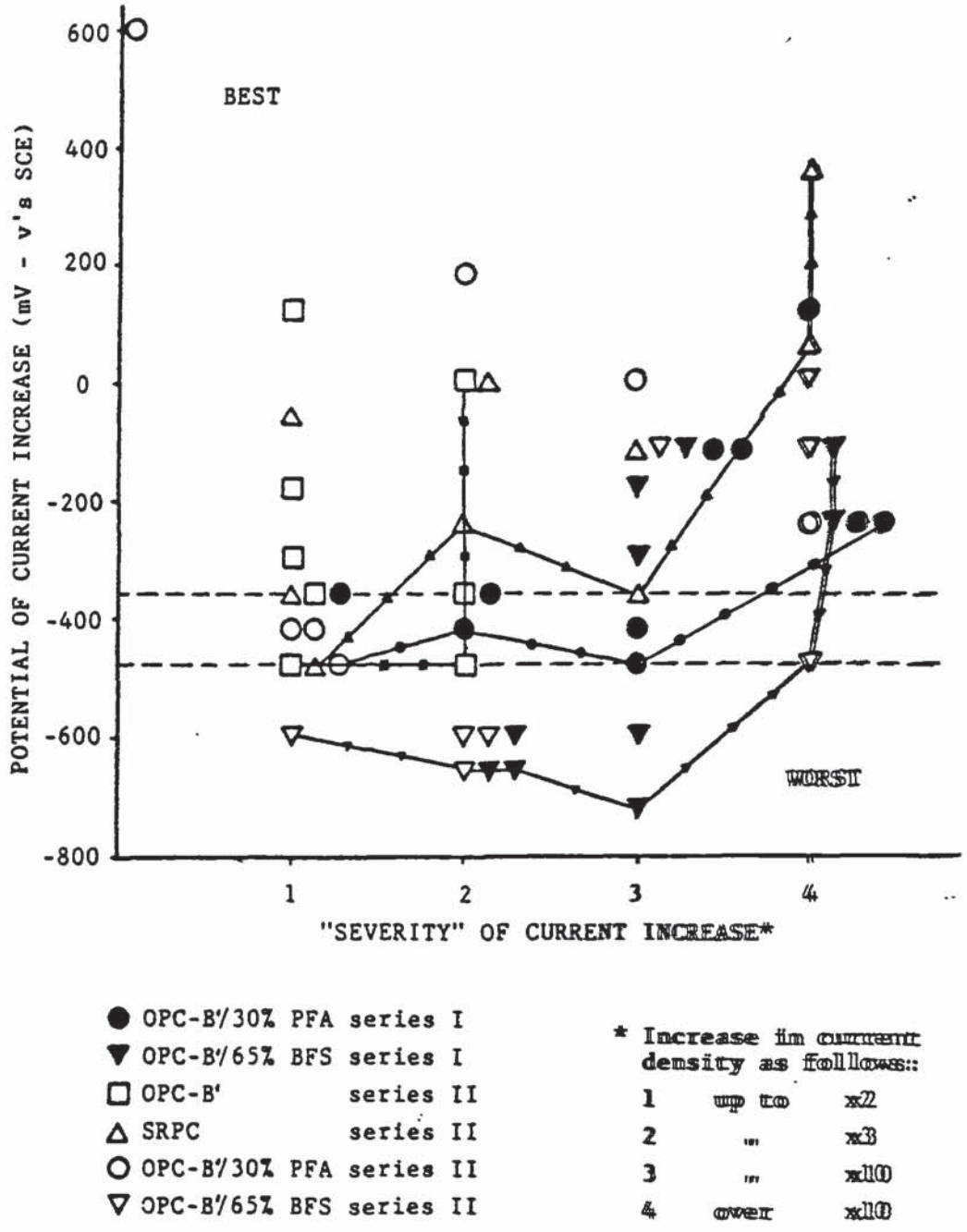

FIGURE 6.19 Sudden current increases during the potentiostatic scans of iron wires embedded in a selection of cement pastes, represented in terms of "severity" of increase.

solution. The latter are shown in figure 6.18 by the horizontal broken lines, each line representing one specimen.

One specimen embedded in OPC which had been held at -900mV for 20 minutes, enabling some reduction of the oxide film to take place, had produced a considerably worse "profile" (figure 6.18). Indeed the initial current-surge, although small, had occurred at a potential of -360mV, which is very close to the pitting potential of iron in solution as shown earlier.

A similar trend was shown by all the specimens which had been held at -960mV for several days. These include the wires embedded in PFA and BFS based cements of series-I and all those of series-II. The results of both series are represented collectively by figure 6.19. The "profiles" for each cement type were constructed as before and suggest a ranking order for cements, in terms of the protection each offers to iron wire, of OPC, SRPC, PFA and BFS. A considerable overlap occurs with the first three cements but BFS appears to be very much the worst. The reason for this phenomenon will be discussed later.

There was a wide variation of E-i plots obtained for all cements types and some typical ones are shown in figure 6.20a-f. The active loop, typical of solution work, was not always present and more often than not it was rather "weak" (figure 6.20d). There was normally however, a constant pas-

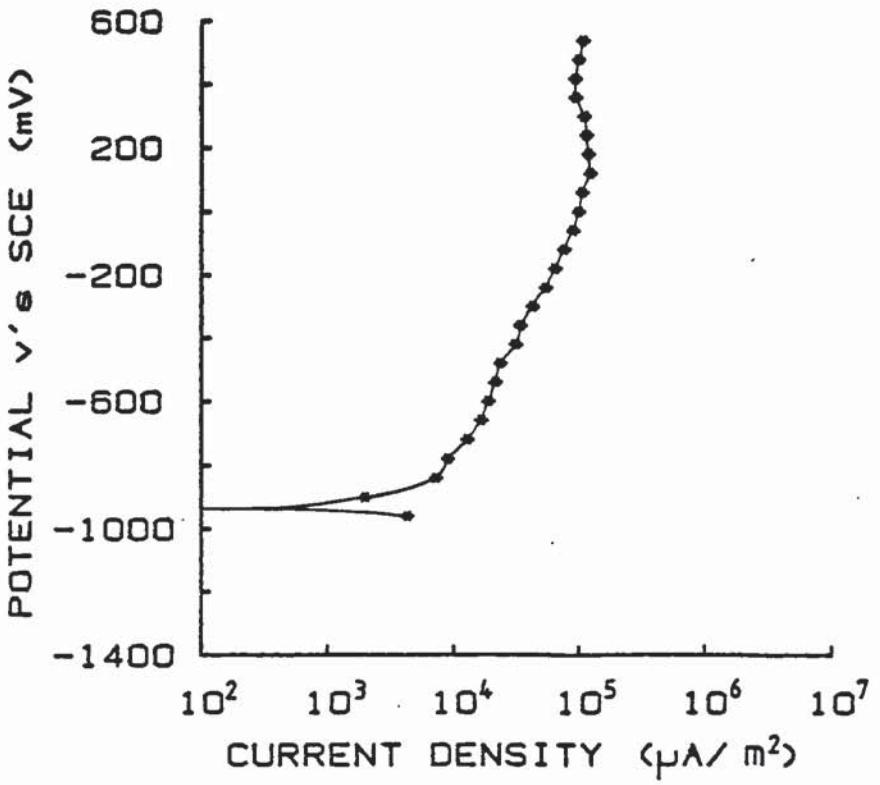

FIGURE 6.20a Anodic potentiostatic scan of iron wire embedded in OPC-B' paste and immersed in 0.5M NaCl + sat. $Ca(OH)_2$.

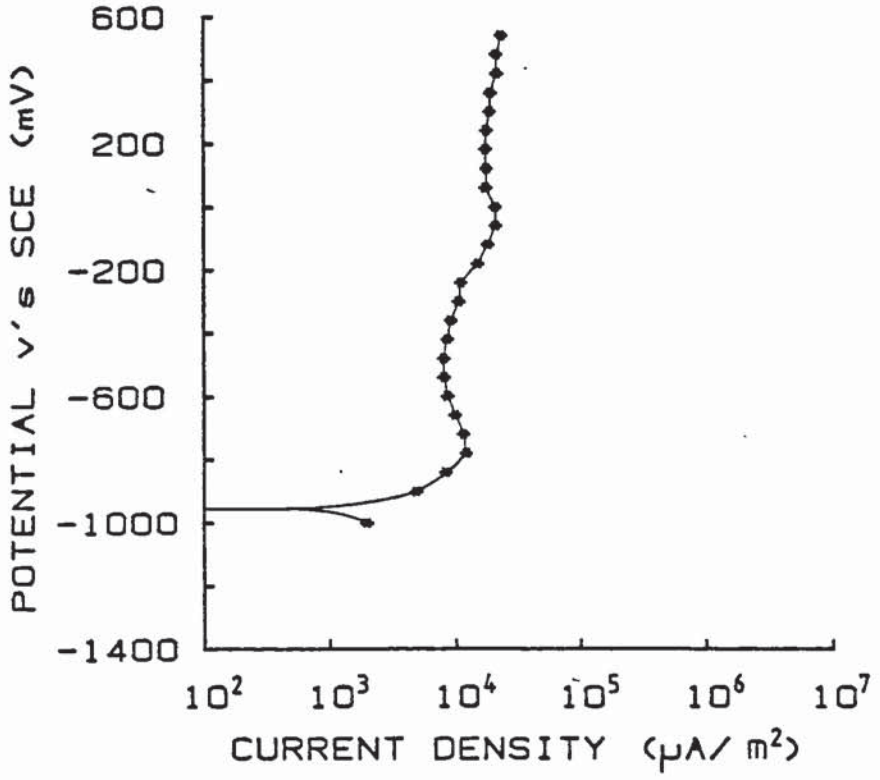

FIGURE 6.20b Anodic potentiostatic scan of iron wire embedded in OPC-B' paste and immersed in 0.5M NaCl + sat.$Ca(OH)_2$.

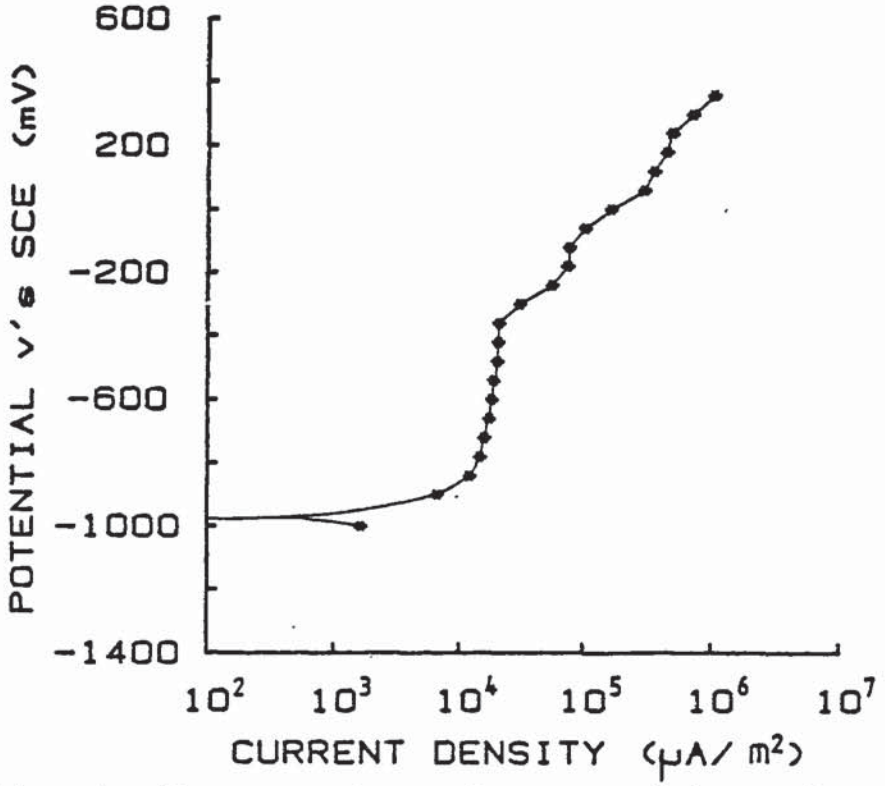

FIGURE 6.20c Anodic potentiostatic scan of iron wire embedded in SRPC paste and immersed in 0.5M NaCl + sat.$Ca(OH)_2$.

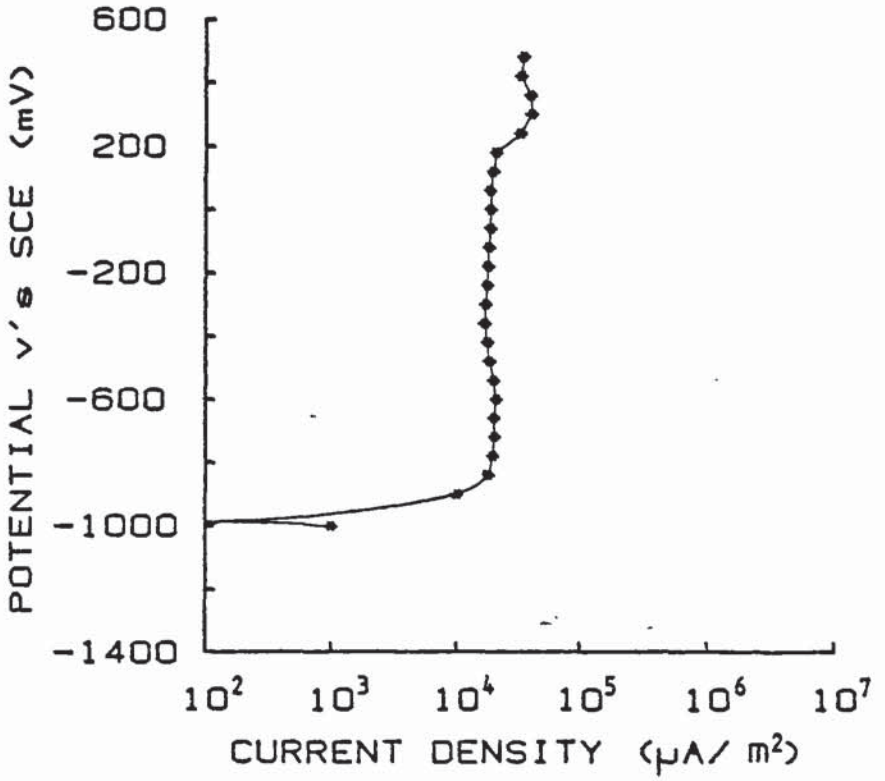

FIGURE 6.20d Anodic potentiostatic scan of iron wire embedded in OPC-B'/30% PFA paste and immersed in 0.5M NaCl + sat. $Ca(OH)_2$.

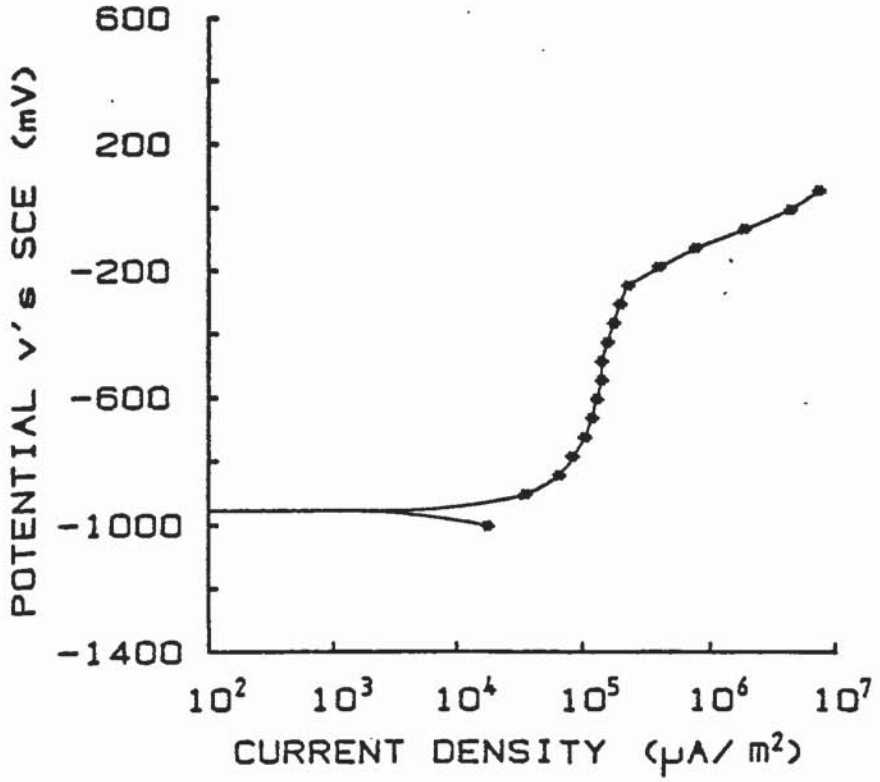

FIGURE 6.20e Anodic potentiostatic scan of iron wire embedded in OPC-B'/30% PFA paste and immersed in 0.5M NaCl + sat. $Ca(OH)_2$.

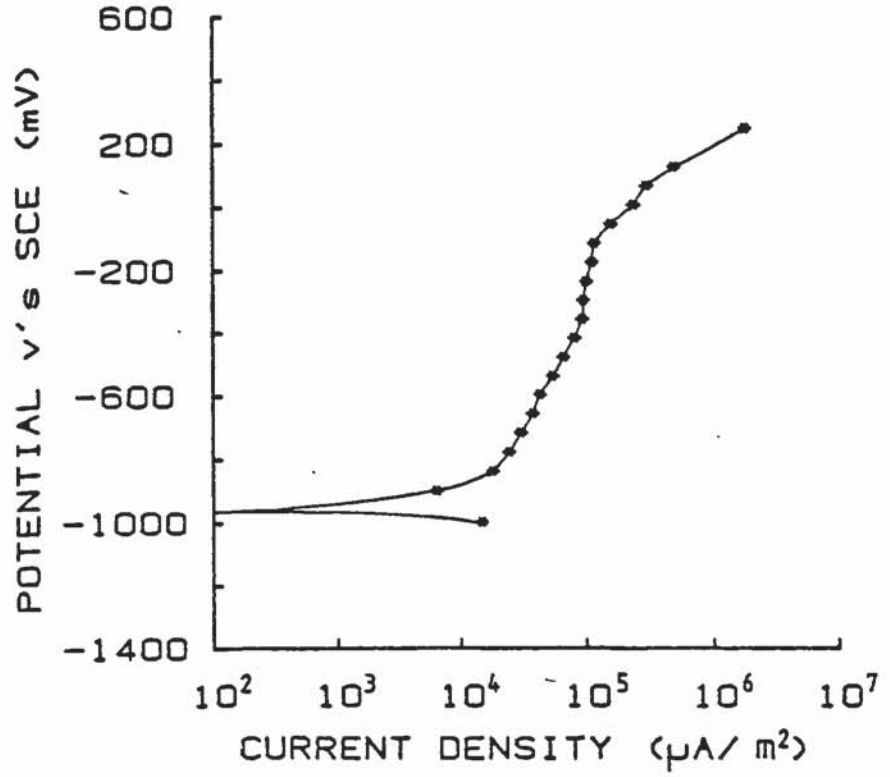

FIGURE 6.20f Anodic potentiostatic scan of iron embedded in OPC-B'/65% BFS paste and immersed in 0.5M NaCl + sat. $Ca(OH)_2$.

sive leakage current for each and as before, there was not a single pitting potential for each specimen, but several, with "repassivation" inbetween. Leakage current densities were normally two orders of magnitude higher than those reported by Preece et al [137] but of the same order as those recorded by Dehghanian and Locke [150]. The reason for the variation, as discussed earlier, was the scan rates where normally slower scan rates result in lower leakage currents.

6.4.3 Potential and Corrosion Intensity Monitoring-Visual Examination (Series-II Specimens).

Table 6.6 represents the mean rest potentials and corrosion intensities of specimens embedded in the different cement types at various stages. Corrosion intensities had generally increased, accompanied by the potential drop after deaeration of the electrolyte, even before the introduction of NaCl. The addition of chloride had caused a further increase in the corrosion intensities presumably owing to the penetration of a sufficient number of chloride ions within the oxide film increasing its conductivity.

Individual Icorr values recorded just before the potentiostatic polarization scans, together with "passive" leakage currents (ie B in figure 6.3), are shown in table 6.7.

At termination of the experiments, each specimen was broken open for visual examination. The condition of each is summarised in table 6.7. One or two specimens of each cement

TABLE 6.7 Passive leakage current densities (Ipass) during potentiostatic polarization scans, corrosion intensities (Icorr) before polarization and visual examination after polarization.

TYPE OF CEMENT OPC-B'	Ipass ($\mu A/m^2$)	Icorr ($\mu A/m^2$)	SURFACE CONDITION
1	2.5×10^4	4.1×10^3	One large pit in middle
2	8.0×10^3	1.3×10^3	Many small pits
3	1.0×10^5	7.7×10^3	Few small pits
4	5.0×10^4	5.1×10^3	"
5	1.0×10^5	6.8×10^3	One large pit in middle
MEAN	6.0×10^4	5.0×10^3	
UNPOLARIZED		2.6×10^3	No pits
SRPC			
1	2.5×10^4	3.8×10^3	Few small pits
2	2.5×10^4	2.9×10^3	Two medium-sized pits
3	6.0×10^4	8.1×10^3	Many medium-sized pits
4	2.0×10^4	1.6×10^3	"
MEAN	3.0×10^4	4.1×10^3	
UNPOLARIZED		1.2×10^4	No pits
"		2.6×10^3	"
OPC-B'/30% PFA			
1	2.0×10^4	4.4×10^3	Many small pits
2	1.5×10^5	9.6×10^3	Many medium sized pits
3	9.0×10^4	1.2×10^4	"
4	3.0×10^4	1.8×10^3	Few small pits
5	1.5×10^5	1.4×10^4	"
MEAN	9.0×10^4	8.3×10^3	
UNPOLARIZED		4.3×10^4	No pits
OPC-B'/65% BFS			
1	4.0×10^4	8.3×10^3	heavily pitted
2	3.0×10^4	3.3×10^3	"
3	5.0×10^4	7.6×10^3	"
4	3.5×10^4	3.7×10^3	"
MEAN	4.0×10^4	5.7×10^3	
UNPOLARIZED		7.4×10^3	Signs of corrosion
"		5.8×10^3	"

type were not subjected to any polarization, in order to have "control" specimens for comparison. All such specimens embedded in OPC, SRPC cements, were clean and bright. On the two wires embedded in the BFS based cement pastes there were some signs of corrosion. There was however no crevice corrosion at all, owing to the enforced reduced chloride level at the "danger" points, achieved by the design of specimens (see figure 6.11).

6.5 DISCUSSION OF RESULTS

It is evident that by reducing the protective oxide film of the iron specimen prior to potentiostatic polarization, the potential at which pitting can occur is lowered. This was observed in both the solution work (table 6.5) and in the case of specimens embedded in cement pastes (figures 6.17 & 6.20), but pitting did not always occur at the same potential.

If only the first "current-surge" of the results summarised in figure 6.19 are plotted (figure 6.21), then it can be seen that the majority of the wires embedded in OPC, SRPC and PFA cement pastes, had their first "current-surge" within 60mV of the pitting potential of iron in solution (shown by the band in figure 6.21) as determined earlier.

In most cases this first current increase was very small and was followed by "repassivation", which is best represented by figure 6.20b. As shown earlier (figure 6.9), a pit

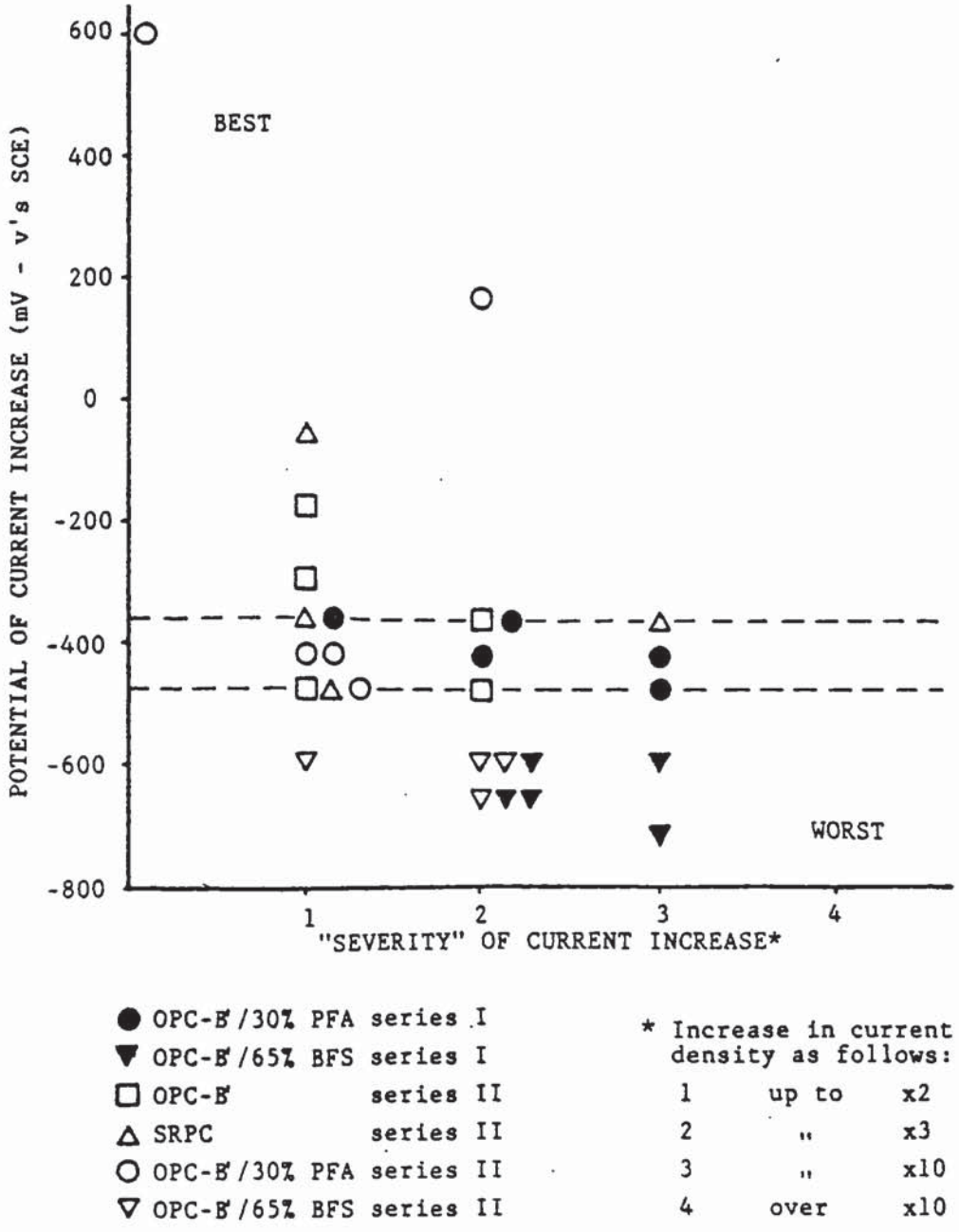

FIGURE 6.21 The first sudden current increase encountered during the potentiostatic scans of iron wires embedded in a selection of cement pastes, represented in terms of "severity" of increase.

can develop at a point where the iron wire is exposed to solution, ie inside a pore. Once this happens, the consumption of chloride and hydroxyl ions reduces their concentration inside the pore, but buffering mainly by the $Ca(OH)_2$ phase, forces the relative concentration of $[Cl^-]$ to $[OH^-]$ to fall, as was described in paragraph 6.2.2, which causes some repassivation, until either the ionic concentrations of the local pore-solution recovers, or the potential is high enough to cause pitting with a lower $[Cl^-]/[OH^-]$ threshold.

A second possible way which can cause an apparent repassivation is the actual physical restriction as the pore is filled-up with corrosion product,but in such a case the current density might be expected to be more erratic than it has been.

If it is assumed that the first "repassivation" method is more important, then as the BFS based cements have no apparent solid phase of $Ca(OH)_2$ (see chapter 5 part II), they cannot offer the same hydroxyl replenishment capacity as the portland cements. This alone however cannot explain the considerably lower potential (less than -600mV) at which the first "current-increase" occurs, as it is lower than the actual pitting potential for iron in solution (table 6.5).

The fact that there were signs of corrosion on the unpola-

rised wires contained in BFS cements even though their potential was never higher than -600mV, suggests that pit initiation at least, can occur at such potentials for this type of cement. As there was no apparent increase of corrosion intensity up to 115 days (table 6.6), corrosion of these wires must have happened after this period, suggesting a slow initiation stage.

The answer for these lower apparent "pitting" potentials, may in fact be found in the suggestion made by Page et al [26], that a portlandite layer formed on the surface of the steel when exposed to portland cement, forms both a physical and a chemical barrier against corrosion. In the case of BFS, as there is only a small amount of $Ca(OH)_2$, neither the physical nor the chemical protection mechanisms can apply on the whole steel surface. There would therefore be many areas where the steel would be exposed to cement particles possessing little hydroxyl replenishment capacity. If no portlandite is available in the near vicinity, then these "interfaces" could encourage a form of crevice corrosion.

As was shown by Galvele [140], crevices have the effect of increasing the distance x, hence requiring a lower current density i to reach the critical xi value (see earlier) which can initiate a pit. This can be achieved with a lower potential.

As some buffering is still offered by BFS at lower pH values (see figure 5.21), a similar repassivation mechanism would apply, but very quickly this would be exhausted allowing the eventual complete breakdown seen on all specimens.

The PFA based cement on the other hand, may still possess enough free $Ca(OH)_2$ to form the abovementioned protective portlandite layer around the iron wire (see figure 5.21).

By such a parameter, the ranking order of, portland cement, PFA, BFS suggested by the "profiles" in figure 6.19, appears reasonable. SRPC however, with a similar buffering capacity to OPC, seems to be somewhat less protective in both series-I and II specimens, a fact which may be related to the diffusion coefficient of chlorides. It was shown in chapter 3 part II that chloride diffuses twice as fast in this particular SRPC as in OPC. This would then lead to an easier chloride replenishment of the pit, maintaining a high $[Cl^-]/[OH^-]$ ratio for longer periods.

On the other hand, the slow diffusion of ions through BFS does not appear to improve the protective ability of the cement, once a critical $[Cl^-]/[OH^-]$ ratio had been reached, simply because both chloride and hydroxyl ions need to diffuse mainly from the "bulk", so their relative concentration would remain constant and high.

It would appear therefore, from the above argument, that

the corrosiveness of the pore solution in this experiment is mainly related to the relative $[Cl^-]/[OH^-]$ ratio that can be maintained near the pit.

Page et al [152] had used such a ratio to explain the variable corrosion rates of steel embedded in the same four types of cements in which a set amount of NaCl additions were made. Their corrosiveness rank order matches that in table 6.3 where the free to total chloride ratio of the cement is considered. The chloride complexing capacity of the cement is, in their case, the most important and "overiding" parameter, hence BFS with the biggest chloride complexing capacity removes more of the chloride from solution, which results in a lower $[Cl^-]/[OH^-]$ ratio.

In similar experiments, Andrade and Page [153] had shown that up to a 1% Cl addition (as NaCl) could be tolerated equally by both OPC and BFS based cements, producing fairly similar and low corrosion rates of the embedded steel bars. Their $[Cl^-]/[OH^-]$ ratios were 0.69 and 0.31 for OPC and BFS respectively, much lower than the value of 8±0.5 used for this experiment.

In reality therefore, owing to the ability of BFS to complex much of the chloride, a fairly high chloride addition could be tolerated before the critical $[Cl^-]/[OH^-]$ ratio could be reached, which would initiate corrosion of the steel reinforcement. These chlorides need either to be introduced at

the mixing stage which, owing to control restrictions (10) are unlikely in this country, or migrate through cracks in the structure, as diffusion through the cement matrix would be extremely slow.

At the other extreme, the very high chloride diffusivity and low chloride complexing capacity properties offered by SRPC pastes, allows the easy build-up of chloride around the steel when the structure is exposed to chlorides, enabling a high $[Cl^-]/[OH^-]$ ratio to be reached very quickly and hence initiate corrosion.

The main conclusion to be drawn therefore from this pitting experiment, is that the buffering property offered by cement pastes becomes important once a certain critical $[Cl^-]/[OH^-]$ ratio is reached. The absence of free lime, as seems to be the case in the BFS based cement studied here, introduces problems in the presence of chlorides, possibly reducing the $[Cl^-]/[OH^-]$ ratio required for corrosion initiation. Furthermore a type of crevice corrosion could occur at the steel-cement interface, owing to the "lenghthening" of the "pit-depth", leading to a lower local current density requirement for the promotion of pitting.

The main conclusions may thus be summarised as follows.

(i) The potentiostatic polarization technique, although problematic, can be applied to steel embedded in cement pastes to determine its cor-

rosion behaviour. Unlike work in solutions, a typical pitting potential may not be accurately determined for iron in cement pastes, owing to the complexity of the system. Results are further complicated by apparent repassivation after pit initiation, owing to the reduction in the $[Cl^-]/[OH^-]$ ratio in solution.

(ii) By specifically modifying the pore solution of cements by equilibration, to enable direct comparison, it was shown that only small differences exist in the degree of protection offered to steel by the OPC, SRPC and PFA cements. There was however a significant difference, both in the pitting potential and in the actual amount of corrosion observed for iron wires embedded in the BFS based cement pastes. The lowered protection offered by BFS was thought to be mainly due to its considerably lower buffering capacity.

(iii) The near non-existent buffering of the BFS, is also thought to introduce further problems in the form of "crevice" corrosion, requiring lower local current densities for initiation of corrosion. It seems likely however that the problems considered in (ii) and (iii), for BFS may be insignificant unless a certain critical

$[Cl^-]/[OH^-]$ ratio, which may be lower than for other cements, is reached.

(iv) It was determined that the pore solution expressed by the expression device, was an accurate representation of the true solution within the pores. Results for the truly equilibrated conditions were always correct within ±3%, indicating that the technique is currently the best available.

Footnote:

Since the completion of this work, research carried out by Sykes and Balkwill[172] has reinforced the results obtained in this chapter. Their investigation has shown that pitting of steel can occur more easily if it is in contact with a chloride-rich solid alkaline gel, as compared to an equivalent chloride solution. Such a gel can be assumed to represent the BFS-based cement paste used in the present investigation which produced similar results. Furthermore, as was the case with the lime-rich portland cements, the introduction of $Ca(OH)_2$ to their gel had delayed the onset of pitting.

PART II CORROSION OF STEEL IN CARBONATED CONCRETE

6.6 INTRODUCTION

It was determined in chapter 5 part I that carbonation of the cement matrix can reduce the pH of the pore electrolyte solution of a concrete structure considerably, causing depasivation of the steel reinforcement (see figure 6.1). The corrosion rate would however, depend on the moisture content of the structure.

While it is generally accepted that a certain minimum amount of moisture is required in order to guarantee the presence of an electrolyte in the pore-network, it is by no means certain that the same minimum level would cause a high enough corrosion rate for it to be considered detrimental. On the other extreme, a moisture saturated structure, may be dense enough to restrict the oxygen availability and reduce the corrosion rate to an insignificant value (see figure 6.22).

Gonzalez et al [41] in an attempt to determine the effect of moisture content of the structure on corrosion rates, had carried out corrosion tests on steel embedded in carbonated mortars with or without a 2% $CaCl_2$ addition. They had achieved carbonation by curing their specimens in a 100% CO_2 atmosphere at a constant 50% R.H. The exposure conditions were a succession of 15 day periods in environments of 50% R.H., 100% R.H., partial immersion in distilled water

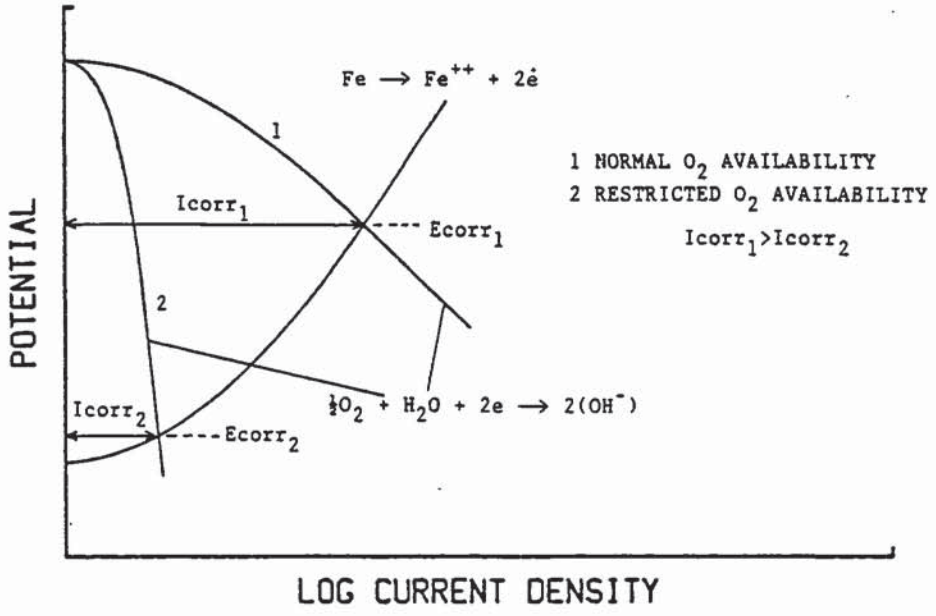

FIGURE 6.22 Potential/current diagram for iron showing the effect of oxygen restriction.

and again 50% R.H.

They were able to show that during the exposure of the mortars to the 50% R.H. environment, provided there were no chloride additions, corrosion intensities of the steel bars were much lower than a certain minimum value they had assumed as critical. Exposure of the mortars to a 100% R.H. environment and particularly their partial immersion in water, had caused sharp increases in the corrosion rates to levels considered unacceptable. The addition of chloride did however keep Icorr values always above the critical level.

It appears from these results that, in the absence of depassivating agents, such as chlorides, a minimum relative humidity (higher than 50% in this case), is necessary to cause critical corrosion. It may be possible therefore, by exposing a structure to a constantly low R.H. environment, to limit the danger from carbonation induced corrosion of the reinforcement.

Work was therefore initiated along similar lines to Gonzalez et al, with the final objective of determining such critical R.H. values for concretes.

In view of the fact that "natural" carbonation may offer slightly different properties to accelerated carbonation (see chapter 5 part I), it was thought advisable to produce specimens from carbonated concrete structures exposed to

the atmosphere. As a first requirement of the programme therefore, a method of producing electrodes from structures, which could be used in the laboratory for corrosion measurements at a variety of R.H.'s, was developed.

As a suitable electrochemical technique for evaluating the corrosion behaviour of the reinforcing bars, the now established linear polarization method [47] (see chapter 2 para. 2.10.1) was chosen. The technique of A.C. impedance (chapter 2 para 2.10.2) was also employed for a small comparative study, mainly to evaluate its usefulness in the field of corrosion of steel in concrete. It is this preliminary work which is reported in part II of this chapter.

6.7 EXPERIMENTAL PROCEDURE

The specimens used for this investigation were sectioned from 30 year old concrete beams made from portland cement. They were taken from either the kitchen or the bathroom of a three-storey-flat, so they were exposed only to an internal atmosphere for their entire life-span. The original oxide composition of the cement was not known, but once complete carbonation had occurred the cement matrix would almost certainly have been a fairly consistent mass of $CaCO_3$.

The rectangular beam, provided by the B.R.E. contained two steel bars on the one side and three roughly equidistant bars on the other in a triangular configuration (see figure

6.23). All rods had a diameter of about 8mm and were approximately 25mm apart. The depth of cover was between 20 and 40mm. This beam was sectioned perpendicular to the steel reinforcements at roughly 80mm intervals with the use of a diamond wheel using deionised water as a lubricant. The sections were finally cut to a manageable size, as shown in figure 6.23, giving final approximate dimensions of 60x40x80mm and each containing two or three equidistant steel bars.

Phenolphthalein was then applied to the two surfaces perpendicular to the steel in order to determine the depth of carbonation. An average carbonation depth of about 25-30mm meant that the steel bars could be separated into 3 groups.

(i) All those contained in fully carbonated concrete,

(ii) All those exposed to both carbonated and uncarbonated concrete,

(iii) All those contained in uncarbonated concrete. In this group only bars surrounded by at least 5mm of uncarbonated material were included.

Five steel electrodes were thus chosen for each of the first two groups but only three could be found for group iii.

Small holes a few millimetres in depth were drilled centrally on the one side of the steel bars which were tapped

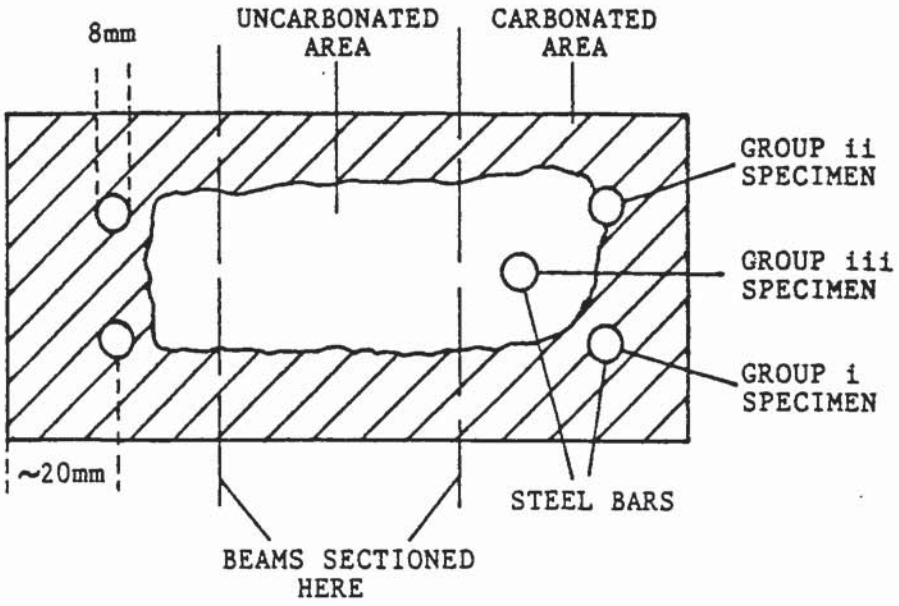

FIGURE 6.23 Cross section of a partly carbonated concrete beam showing the depth of carbonation and the position of the embedded steel bars.

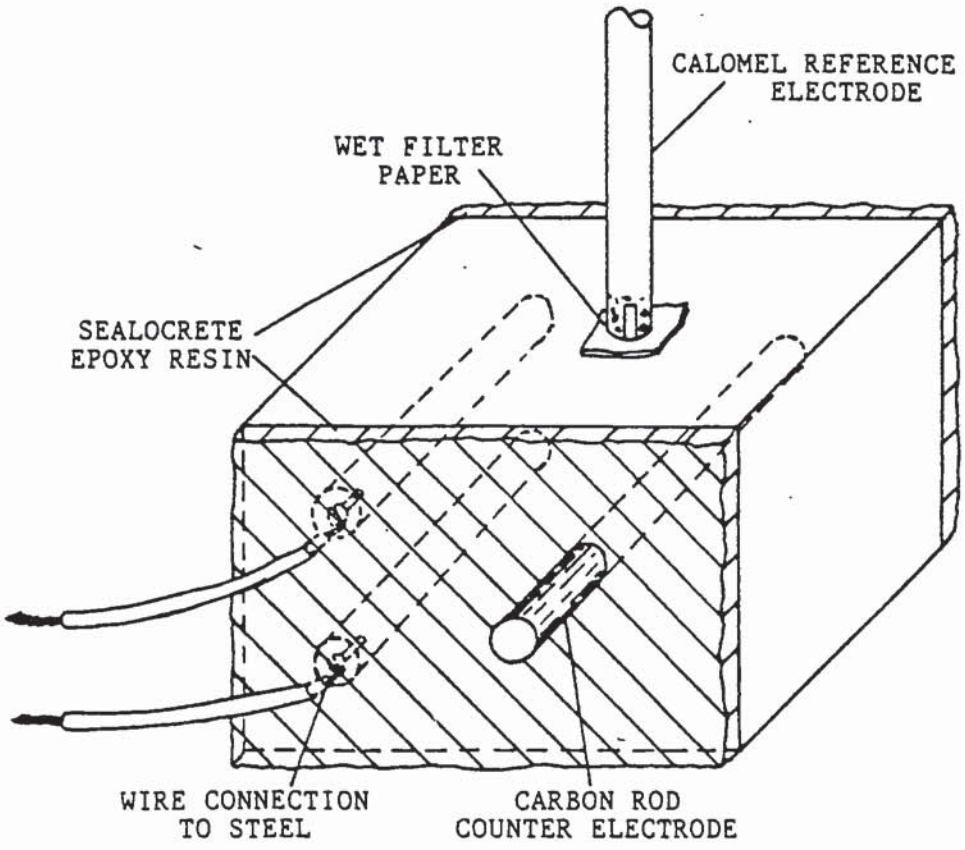

FIGURE 6.24 Final specimen arrangement for corrosion measurements.

in order to accept small steel screws. This enabled the fixing of a small length of wire on each specimen, in order to facilitate their connection to any electrical equipment.

As a counter electrode, graphite bars of a similar size to the steel electrodes were used. These were inserted, one for each concrete specimen, in holes drilled parallel to the steel specimens. The carbon rods were cemented to the walls of the holes with a thin layer of portland cement slurry. All exposed metal was finally carefully covered with "sealocrete" epoxy resin. The final specimen arrangement was as shown in figure 6.24. The surface area of each electrode was estimated by measuring the length and diameter of each steel specimen.

All the specimens were allowed to stand in the lab atmosphere for three weeks to allow equilibration before being subjected to the same wet-dry cycles as follows:

(i) Full immersion in deionised water for 1 day,

(ii) 100% R.H. for 6 days,

(iii) Lab environment for 7 days,

(iv) Air tight box containing dry crystals of $MgCl_2$ for 6 days,

(v) 100% R.H. for 7 days.

The cycle was repeated this time allowing a longer period for drying.

At regular intervals, normally of 2 days, the corrosion intensity, (Icorr), rest potential (Ecorr), and weight of each specimen were recorded. The electrochemical studies were carried out using the "E.G.&G./P.A.R. model 350" microprocessor fitted with an I.R. compensation module for compensation of the Ohmic drop between the reference and working electrodes (see chapter 2 para. 2.10.1).

Good electrical contact between the calomel reference electrode and the concrete specimen was achieved by inserting a small piece of a wet filter paper at their contact point (figure 6.24).

The four "best" "fully-carbonated" and the three "fully-uncarbonated" specimens were then allowed to dry naturally in the lab air before being used for the small comparative study between the A.C. impedance and linear polarization techniques.

This simply involved the recording of Icorr and Ecorr values for each specimen in their dry form by linear polarization using the manual method (chapter 2 para. 2.10.1) and then subjecting them to the A.C. impedance technique, as described in detail in chapter 2 (para. 2.10.2) either with or without I.R. compensation. The manual linear polarization technique was employed so that the I.R. compensation value, determined by each technique, could be comparable, as the positive-feedback facility on the AMEL-551 potentio-

stat was used in each case for this purpose.

The specimens were finally fully immersed in deionised water and once more subjected to both electrochemical techniques after a two day exposure period.

6.8 RESULTS

6.8.1 Variation in Corrosion Rates with Moisture Content

The variation of the corrosion intensities against time are best represented by figure 6.25, each value being the average for one of the three groups of specimens. It is clear from the graph that whilst Icorr remained fairly consistent at less than $10^3 \mu A/m^2$ for the specimens contained in uncarbonated concrete (group iii), specimens embedded in carbonated material (group i), showed considerable variation with time. As was observed by Gonzalez et al [41], high moisture contents had always produced high corrosion rates, but exposure of the specimens to the air had caused a sharp drop in the corrosion rates almost immediately. A similar but less "dramatic" variation was observed for the steel electrodes contained in the "partly-carbonated" concrete (group ii).

The opposite pattern was determined when considering the change in the rest potential for each group of specimens with time. This is represented by figure 6.26. High corrosion intensities were always accompanied by more negative

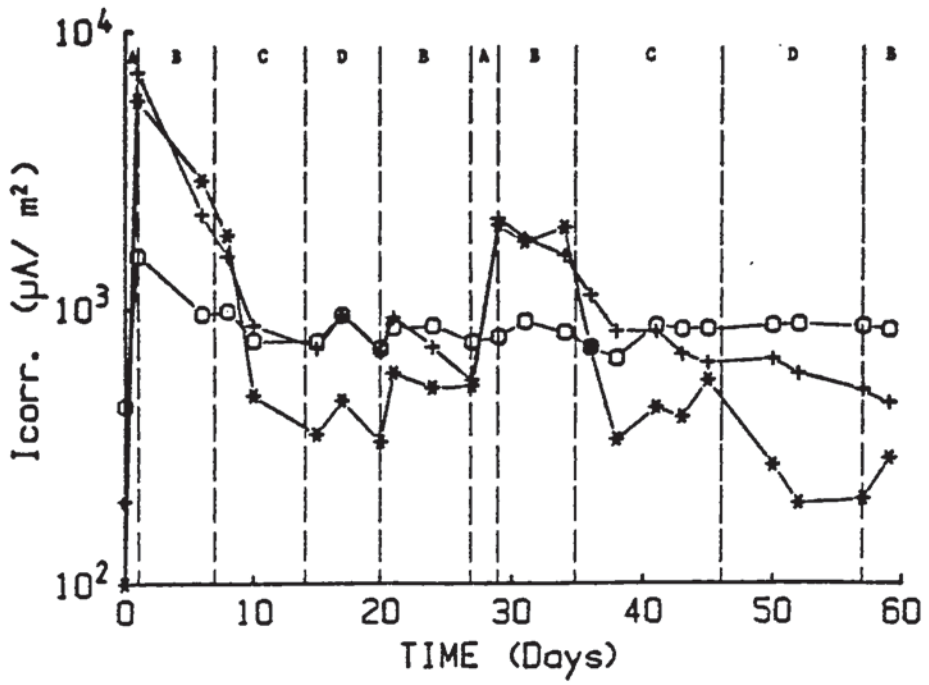

FIGURE 6.25 Variation of Icorr with time of exposure and environment.

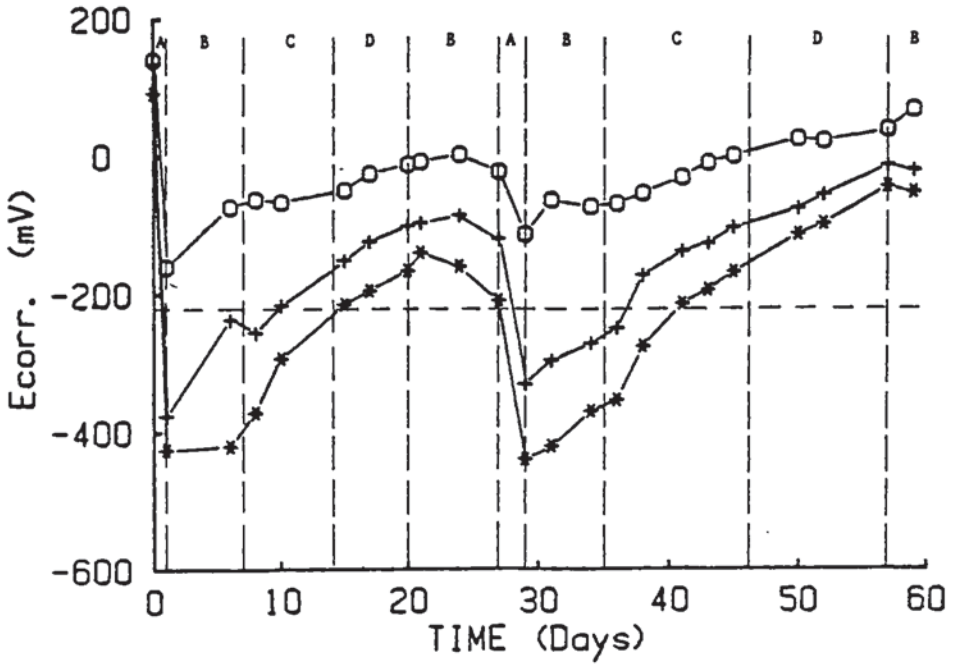

FIGURE 6.26 Variation of Ecorr with time of exposure and environment.

o steel embedded in uncarbonated concrete

\+ steel embedded in partly carbonated concrete

* steel embedded in fully carbonated concrete

Note: For key to environments (A to D) see fig. 6.27

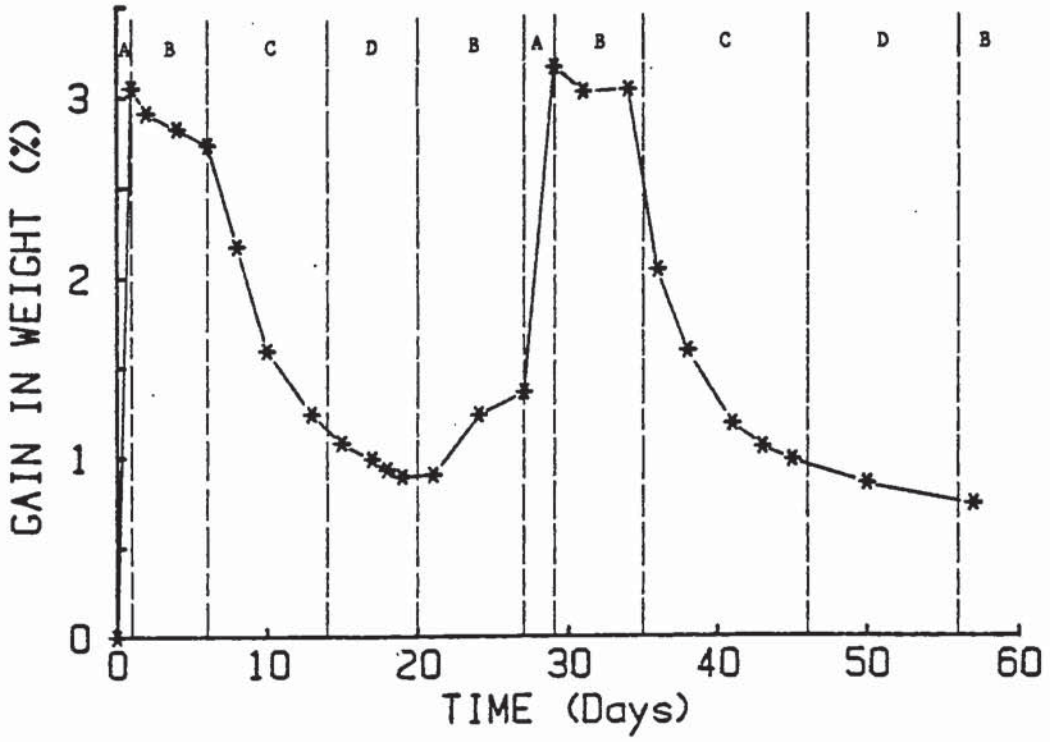

FIGURE 6.27 Variation of weight of concrete specimens with time of exposure and environment.

Key to environments:

A Fully immersed in deionised water
B Exposed to 100% RH
C Exposed to lab air
D Placed in airtight box containing $MgCl_2$ crystals.

potentials.

The influence of the outer environment on the inner moisture content of the concrete specimens is clearly seen in figure 6.27, which represents the average excess in weight as a percentage of the original mean dry weight.

6.8.2 Comparative Study of Electrochemical Techniques

Figures 6.28a to d represent typical complex impedance diagrams (Nyquist Plots) as determined by the A.C. impedance technique, for one of the specimens (C2) contained in carbonated concrete in its "dry" (figure 6.28a) and "wet" (figure 6.28c) condition.

Comparing figure 6.28a to figure 2.9 (see chapter 2 para. 2.10.2) which represents an "ideal" steel-concrete system, then the similarities are obvious. The semicircle although a little "compressed" and not always complete, is present. A slight extrapolation of the plot was therefore sufficient to give both the values of Rt (equivalent to Rp in linear polarization) and RΩ (equivalent to the I.R. drop) as shown in figure 6.28.a. This enabled the calculation of Icorr values for all "carbonated" specimens in either their wet or dry condition, with the use of the equation,

$$Icorr = \frac{B}{Rp} \qquad (Rp=Rt)$$

where B=26mV (see chapter 2 para. 2.10.1) and these are tabulated in table 6.8.

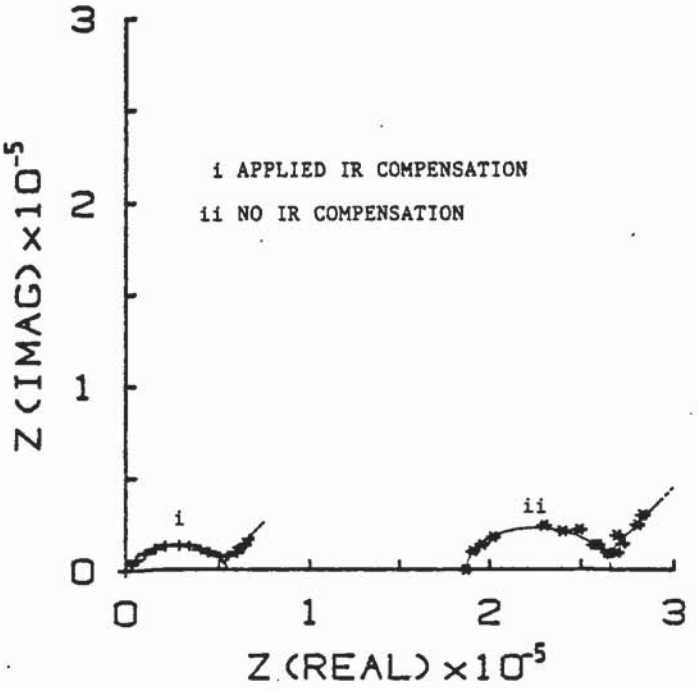

FIGURE 6.28a Nyquist plot of steel in dry carbonated concrete with or without IR compensation (spec.C2)

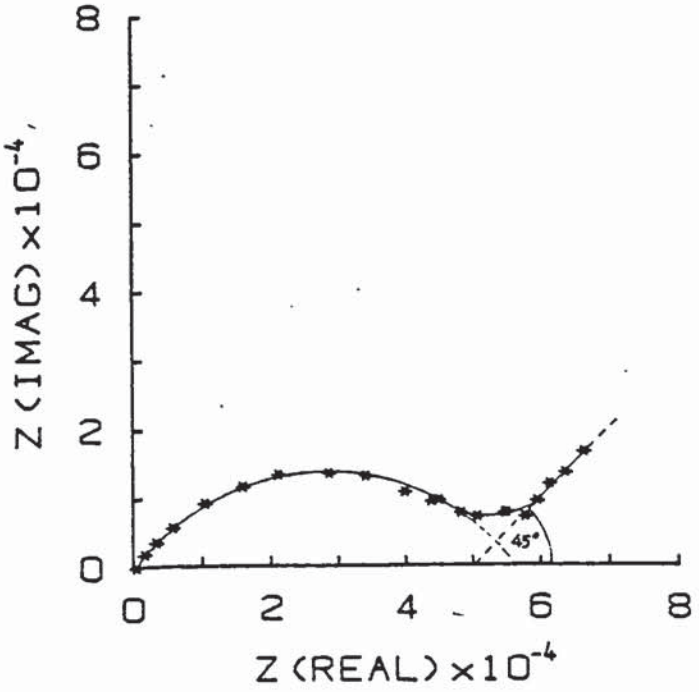

FIGURE 6.28b Nyquist plot of steel in dry carbonated concrete, with IR compensation (spec.C2).

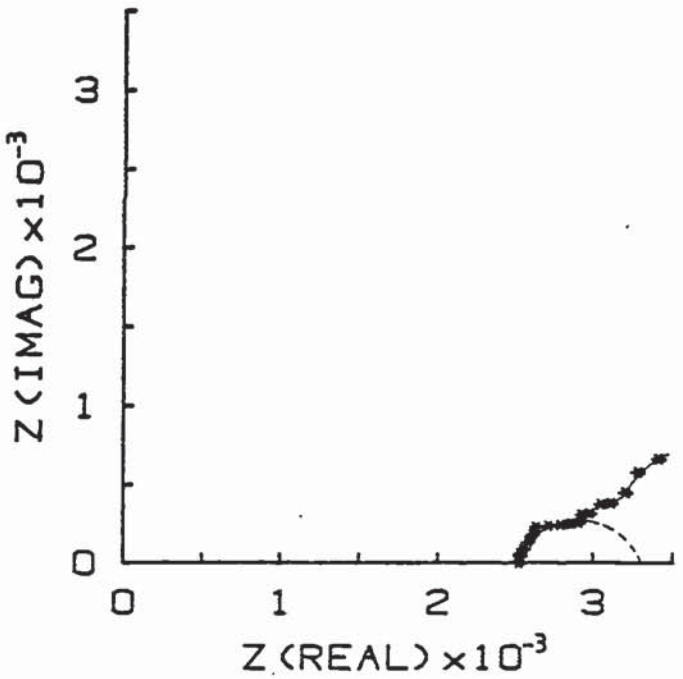

FIGURE 6.28c Nyquist plot of steel in wet carbonated concrete, without IR compensation (spec.C2)

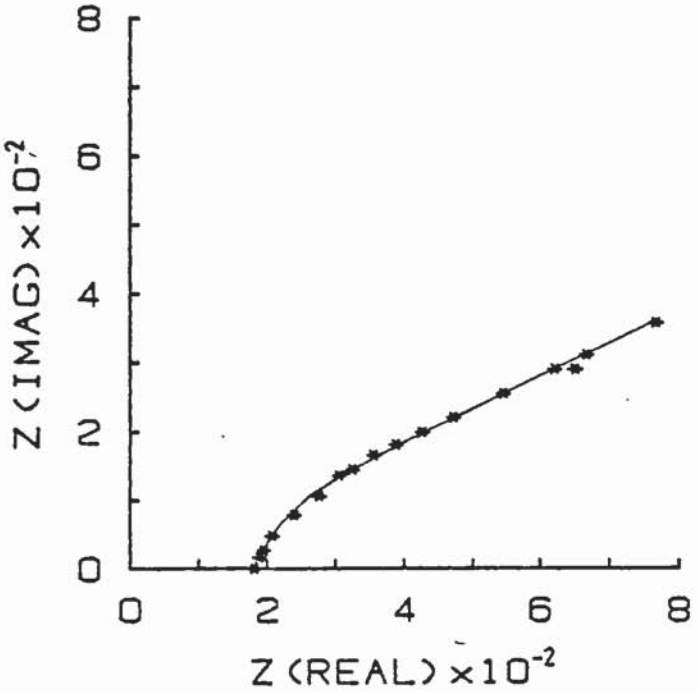

FIGURE 6.28d Nyquist plot of steel in wet carbonated concrete, with IR compensation (spec.C2).

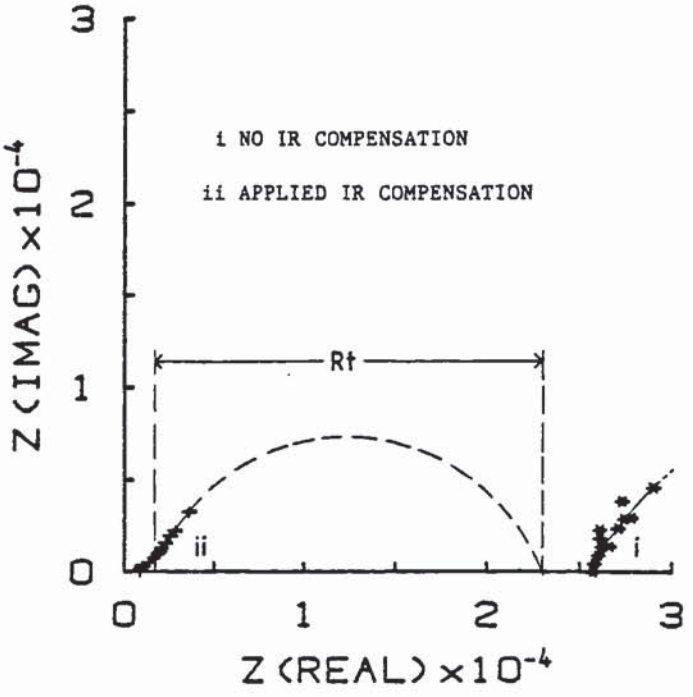

FIGURE 6.29a Nyquist plot of steel in dry uncarbonated concrete, with or without IR compensation (spec.U3)

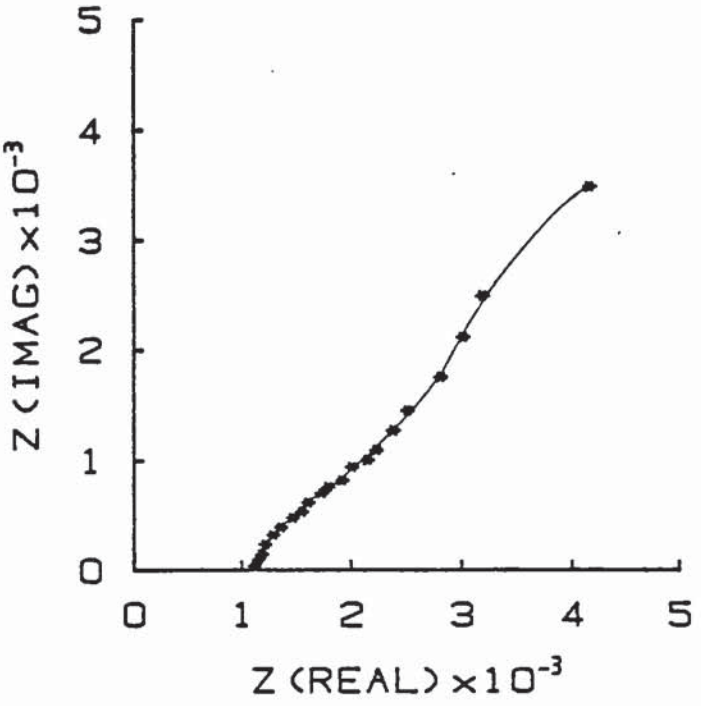

FIGURE 6.29b Nyquist plot of steel in dry uncarbonated concrete, with IR compensation (spec.U3)

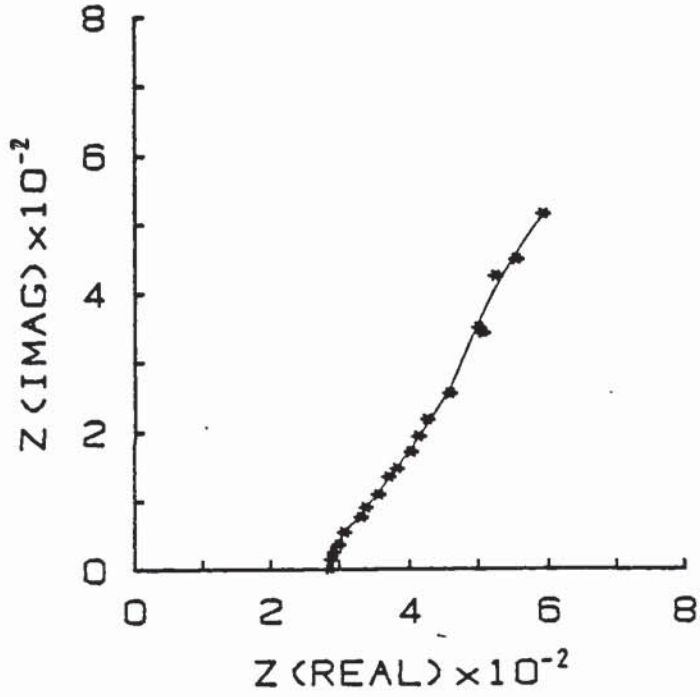

FIGURE 6.29c Nyquist plot of steel in wet uncarbonated concrete, without IR compensation (spec.U3).

The straight line at an angle of 45° (see for example figure 6.28b) always found for the "dry" specimens represents the Warburg impedance [51], but this concept will be discussed in the next section.

The high RΩ values (table 6.8) were compensated by the positive feed-back of the "AMEL-551" potentiostat in further runs. As a result, RΩ was, at least partly, eliminated, displacing the Nyquist plot to the left of the graph (figure 6.28 a(i)). More importantly the compensation resulted in a better resolution (compare for example figure 6.28a&b) without significantly altering the values of Icorr (see table 6.8) which were similarly determined as above.

Nyquist plots of the specimens embedded in both "dry" and "wet" uncarbonated concrete either with or without I.R compensation were however very dissimilar (figures 6.29a to c). These are typical of non-corroding systems encountered elsewhere [53] making it almost impossible to evaluate the value of Rt, as the semi-circle of the Nyquist plot is very incomplete (figure 6.29). An attempt was however made by careful extrapolation using compasses(an example can be seen in figure 6.29aii) and the resultant Icorr values, calculated as before, are shown in table 6.9.

The equivalent Icorr values and I.R. drops determined for all the specimens and conditions by the linear polarization technique (chapter 2 para.2.10.1) are also included in

TABLE 6.8 Rest potentials, corrosion intensities and IR drops for steel in carbonated concrete as determined by two methods.

		LINEAR POLARIZATION			A.C. IMPEDANCE						
					WITHOUT IRcomp			WITH IRcomp			
	SPEC.	IRdrop R_Ω Ω	Ecorr (mV)	Icorr ($\mu A/m^2$)	IRdrop R_Ω Ω	Ecorr (mV)	Icorr ($\mu A/m^2$)	Comp.IR Ω	IRdrop R_Ω Ω	Ecorr (mV)	Icorr ($\mu A/m^2$)
DRY CONDITION	C1	2.2×10^5	+118	3.7×10^1	2.1×10^5	+114	7.2×10^1	2.1×10^5	6.7×10^3	+99	6.8×10^1
	C2	1.8×10^5	+142	6.9×10^1	1.9×10^5	+159	1.5×10^2	2.0×10^5	5.4×10^2	+152	2.0×10^2
	C3	1.2×10^5	+152	1.1×10^2	1.2×10^5	+140	7.3×10^2	1.4×10^5	2.2×10^3	+140	4.9×10^2
	C4	1.5×10^5	+168	9.0×10^1	1.6×10^5	+173	3.2×10^2	1.1×10^5	1.5×10^3	+158	1.3×10^3
	MEAN	1.7×10^5	+145	7.7×10^1	1.7×10^5	+147	3.2×10^2			+137	5.1×10^2
WET CONDITION	C1	2.6×10^3	-565	8.0×10^3	2.7×10^3	-573	1.8×10^4				
	C2	2.5×10^3	-430	3.5×10^3	2.5×10^3	-439	1.7×10^4				
	C3	1.6×10^3	-565	8.5×10^3	1.6×10^3	-573	2.4×10^4				
	C4	1.8×10^3	-519	7.1×10^3	1.9×10^3	-528	2.8×10^4				
	MEAN	2.1×10^3	-520	6.8×10^3	2.2×10^3	-528	2.2×10^4				

TABLE 6.9 Rest potentials, corrosion intensities and IR drops for steel in uncarbonated concrete as determined by two methods.

		LINEAR POLARIZATION			A.C. IMPEDANCE						
					WITHOUT IRcomp			WITH IRcomp			
	SPEC.	IRdrop R_{Ω} Ω	Ecorr (mV)	Icorr (μA/m²)	IRdrop R_{Ω} Ω	Ecorr (mV)	Icorr (μA/m²)	Comp.IR Ω	IRdrop R_{Ω} Ω	Ecorr (mV)	Icorr (μA/m²)
DRY CONDITION	U1	2.2×10^{4}	+199	3.2×10^{2}	2.6×10^{4}	+187	7.1×10^{2}	2.3×10^{4}	1.1×10^{3}	+191	1.4×10^{3}
	U2	1.2×10^{4}	+159	4.0×10^{2}	1.7×10^{4}	+149	5.0×10^{2}	1.4×10^{4}	2.5×10^{3}	+147	1.0×10^{3}
	U3	2.0×10^{4}	+198	2.6×10^{2}	1.5×10^{4}	+195	8.7×10^{2}	2.0×10^{4}	8.6×10^{2}	+188	5.0×10^{2}
	MEAN	1.8×10^{4}	+185	3.3×10^{2}	1.9×10^{4}	+177	6.9×10^{2}			+175	9.7×10^{2}
WET CONDITION	U1	2.8×10^{2}	-299	1.4×10^{3}	2.9×10^{2}	-312	5.6×10^{3}				
	U2	2.8×10^{2}	-247	7.1×10^{2}	2.8×10^{2}	-261	5.8×10^{3}				
	U3	2.0×10^{2}	-178	7.3×10^{2}	2.0×10^{2}	-193	4.5×10^{3}				
	MEAN	2.5×10^{2}	-241	9.5×10^{2}	2.6×10^{2}	-255	5.3×10^{3}				

tables 6.8 (carbonated) and 6.9 (uncarbonated) together with their rest potentials (Ecorr).

6.9 DISCUSSION OF RESULTS

As was assumed earlier, the results represented by figure 6.25 suggest the existence of a critical moisture content of the carbonated concrete below which corrosion could be considered negligible. Further work must be carried out however, in which the moisture content of the structure is specifically and accurately controlled, in order that this critical level is estimated.

It needs to be remembered also, that a certain corrosion current density that may be considered acceptable for steel in uncarbonated concrete may not necessarily be acceptable if the steel was embedded in carbonated material. There may, for instance, be a decrease of the surface area of the exposed steel caused by the reduction in porosity of the structure from carbonation (see figure 5.5). As the Icorr values are represented as corrosion currents per unit area of the whole steel specimen and not of the part exposed to the pore electrolyte, this effect may need to be considered. On the other hand the different properties of carbonated concrete may restrict the flow of current, and reduce corrosion (indeed there is a tenfold increase in the I.R. compensation required for carbonated concrete as shown in tables 6.8 & 6.9). Such results should therefore be sub-

stantiated by gravimetric weight loss methods [40].

In this case, where oxygen availability is not restricted, the corrosion behaviour of the specimens could also be assessed by studying their rest potentials (figure 6.26). As an example, an arbitrary critical Ecorr value can be considered, ie at -220mV, represented by the horizontal broken line in figure 6.26. By such criteria, the steel specimens embedded in carbonated concrete remain in the critical zone for a somewhat longer period after their exposure to air (ie at 7 and 36 days in figures 6.25 and 6.26), than if Icorr values alone were to be considered (figure 6.25), supporting the above mentioned differences in the two types of concrete.

The corrosion intensities calculated by linear polarization in the comparative study, had shown a similar trend of results. By wetting the concrete, the corrosion intensities of the specimens contained in fully carbonated concrete had increased by two orders of magnitude (table 6.8), whereas Icorr values for those embedded in uncarbonated material had remained below $10^3 \mu A/m^2$ (table 6.9).

Corrosion intensities determined by the A.C. impedance technique were always higher, often by as much as an order of magnitude (tables 6.8 & 6.9). They were in any case more of an estimate than a calculation as far as the specimens contained in uncarbonated concrete were concerned.

Bode plots, ie log modulus of impedance versus log frequency diagrams (figure 6.30), have recently been used to determine the corrosion behaviour of similar systems [48,154] and to calculate Rt values and hence Icorr [53]. A typical Bode plot of the Randles circuit (figure 2.6), is as shown in figure 6.30. Rt in this case is the "distance" between the two horizontal parts of the curve.

The equivalent Bode plots of figures 6.28b and 6.29b are represented by figures 6.31 and 6.32 respectively. It can be seen that in neither case was the typical plot of figure 6.30 obtained, so corrosion intensities were unobtainable by this method. What these two diagrams show however, as do the equivalent Nyquist plots, is that the two types of specimens show a different corrosion behaviour, when the concrete is dry.

The straight line at an angle of 45° seen in figure 6.28b representing the Warburg impedance, normally accounts for mass transfer limitations due to diffusion processes adjacent to the electrode [51]. Why it should happen in carbonated concrete is uncertain but the situation normally exists when the electrode surface is covered with reaction products or some other coating, or with absorbed solution components. This may to some extent explain the reduced corrosion rates of steel in carbonated concrete at low moisture levels, as the phenomenon is not present in wet carbonated concrete (figure 6.28d).

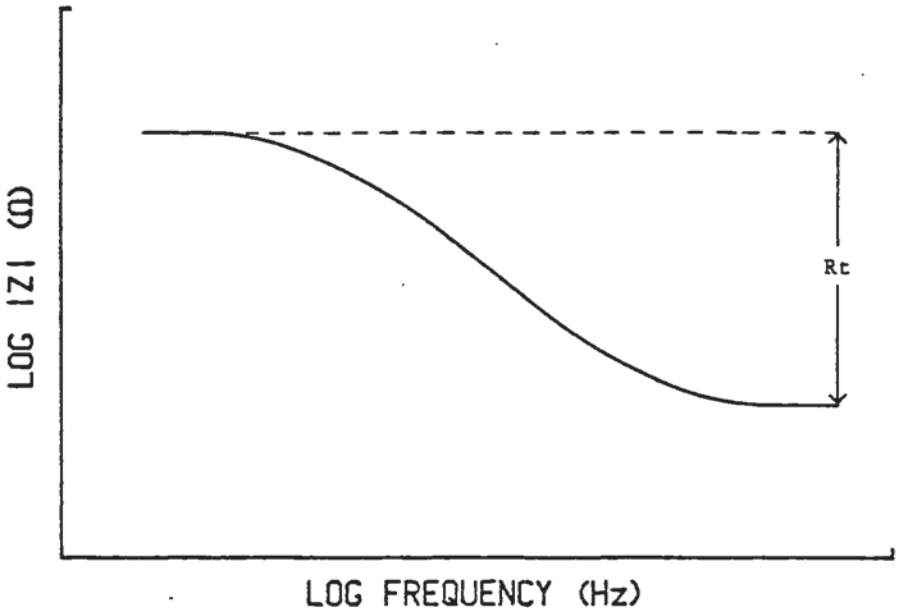

FIGURE 6.30 Typical Bode plot of the Randles electrochemical circuit.

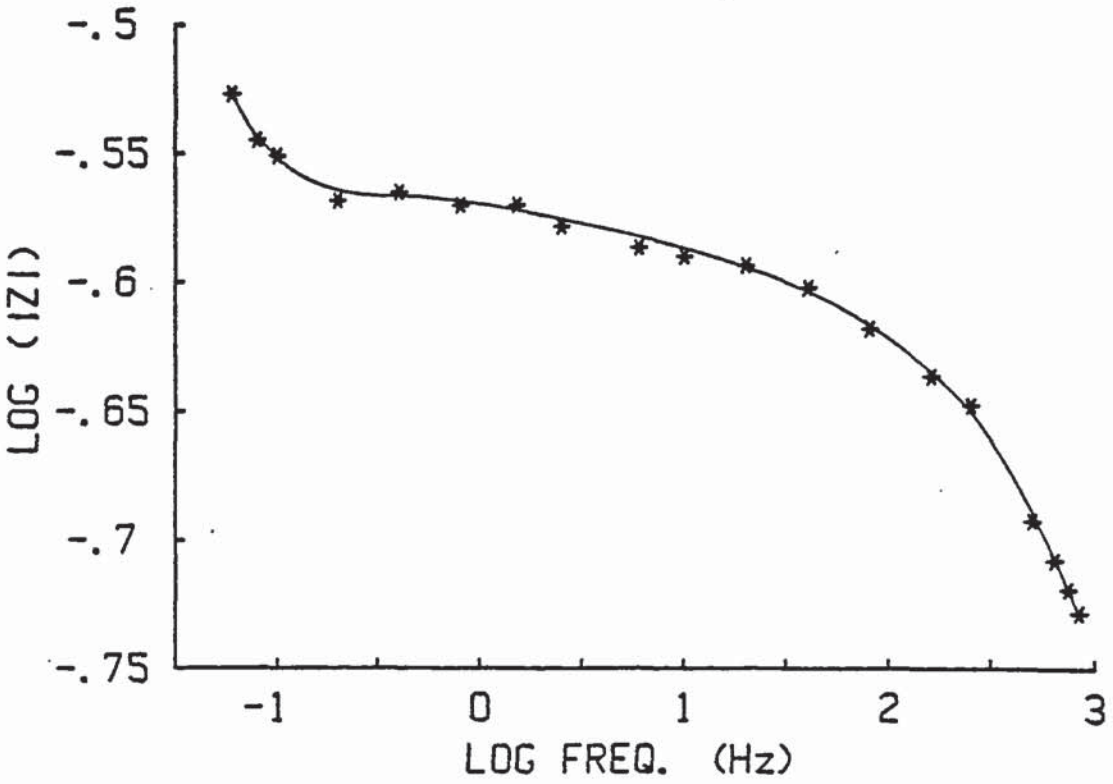

FIGURE 6.31 Bode plot of steel in dry carbonated concrete, with IR compensation (spec.C2).

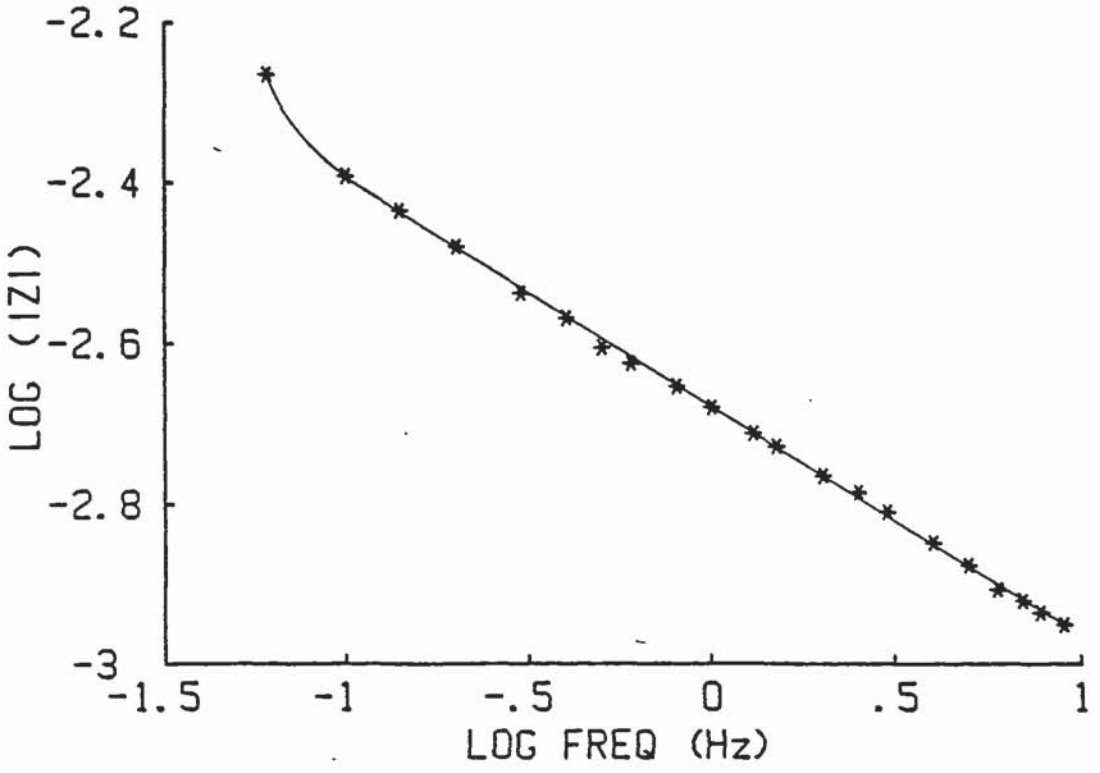

FIGURE 6.32 Bode plot of steel in dry uncarbonated concrete with IR compensation (spec.U3).

There must ofcourse be more concentrated research on the topic to substantiate the results, but an interesting line to follow would be that of identifying carbonated concrete simply by the application of the A.C. impedance technique on the steel embedded in it.

Further identification may in fact be made by determining the I.R. drop between the embedded steel and the reference electrode. As was discussed earlier, this value was always an order of magnitude higher for carbonated than for uncarbonated concrete (tables 6.8 & 6.9).

In summarising, the main conclussions are,

(i) Corrosion of steel in carbonated concrete does not appear to be a problem at low moisture levels but corrosion intensities increase sharply with the wetting of the concrete. Results point to a certain critical moisture content below which corrosion of the reinforcement could be tolerated, but further work is required to enable the determination of such a value.

(ii) The A.C. impedance technique at its present state offers no advantages in determining corrosion rates of steel in concrete over the linear polarization method. It shows however promise as a tool for studying corrosion mecha-

nisms in such systems and in particular, in identifying carbonated concrete, although a lot more research is needed in the area.

CHAPTER 7 GENERAL DISCUSSION AND CONCLUSIONS

As previously mentioned, corrosion of steel reinforcement in a concrete structure normally occurs by one of two mechanisms, viz, chloride induced pitting and carbonation induced general corrosion. The properties of a selection of cement pastes relating to the two corrosion mechanisms, were therefore investigated in order to improve the understanding of the processes involved and aid selection of cement materials for various applications.

7.1 CHLORIDE INDUCED CORROSION

In a relatively crack-free concrete structure, pitting would normally occur only when a sufficient concentration of chloride accumulates around the steel reinforcement from an outside source. This chloride level is known to be related to the hydroxyl concentration of the solution so that a certain critical $[Cl^-]/[OH^-]$ ratio exists below which corrosion is prevented [56-58].

It was demonstrated however that for steel embedded in concrete or hardened cement paste the threshold $[Cl^-]/[OH^-]$ ratio of the pore solution was normally higher than for steel in the equivalent solution [59-60].

Page [26] explained the better protection of the steel from the cement matrix by the effect of the portlandite layer around the steel reinforcement acting both as a ready

OH^- replenisher and as a physical barrier against Cl^- penetration.

Work described in chapter 6 part I generally supported this view, showing that although pit initiation often occurred at potentials predicted by results from the equivalent solution, pit propagation was slower and appeared to depend mainly on the buffering property offered by the cement paste.

Substitution of the portland cement by PFA and BFS reduced the buffering capacity of the cement (chapter 5 part II), which subsequently resulted in a somewhat diminished protection of the steel reinforcement particularly in the case of BFS substitution.

If the portlandite layer is as important as it appears, then any treatment of either the concrete or the steel aimed at improving corrosion properties, may reduce the effect of the portlandite layer and prove more detrimental in the long run, once chloride contamination takes place. If the steel is coated, for instance, a pinhole that may appear on the surface of the coating, will in effect lengthen the "pit-depth" x, which will result in a higher xi value (see chapter 6 part I). This may allow pit initiation to occur at lower chloride levels, provided the cathodic reaction can also take place.

7.1.1. The Role of Diffusion of Ions in Cements

In practice the reduced buffering capacity of the BFS based cement paste would normally be countered by its high chloride complexing capacity (see table 6.3) and in particular, by its low ionic diffusion coefficient. The critical $[Cl^-]/[OH^-]$ ratio although possibly lower than for portland cements, would rarely be reached.

As was shown in chapter 3 part II, the diffusion coefficient of both Cl^- and OH^- ions in well-cured OPC- 65% BFS cement pastes was at least an order of magnitude lower than in similarly cured portland cement pastes. PFA substitution had a similar effect which raises the question of whether it is the pozzolanic action of such cements that may influence the mobility of ions. It is known for instance, that the removal of $Ca(OH)_2$ from the cement paste by the pozzolanic reaction causes a reduction in the CaO/SiO_2 ratio of the C-S-H gel [93,94]. If the diffusion of ions is mainly restricted by the gel [95], one possibility, as mentioned in chapter 4, is that the reduced C/S ratio of the gel increases the surface interaction between the gel walls and the diffusing ions, causing a reduction in their mobility.

A gel possibly depleted in CaO at the surface of a portland cement paste, was shown in chapter 4 part II to cause some reduction in ionic diffusivity similar to that observed

for pozzolanas. Whether the same reduction in diffusivity is observed when the influenced surface layer is rich in other cations such as Na^+ and K^+, as might be the case when the structure is exposed to seawater, is not known so further work is necessary in this respect.

Generally the diffusion rates of anions, such as chlorides, in cement pastes were shown in chapter 5 part I to be faster than the accompanying sodium cations, supporting the work of others [77,83]. It was also shown, however, that this could occur only if an ionic charge balance could be maintained, in this case by the counter-diffusion of hydroxyl ions. In the absence of counter-diffusion, as was the case for diffusion in carbonated portland cements (chapter 5 part I) and for diffusion of NaOH (chapter 3 part II), the diffusivities of both the co-diffusing species were the same.

The condition of ionic charge balance was shown in chapter 4 to be the main requirement to be satisfied in the mechanism of ionic diffusion. Thus migration of a single ionic species can only be viewed as a part of a more complex system of ions and not as a separate entity.

When an ionic species is partly removed from the pore-solution network, ie by its complexation into a solid phase, the intricate ionic system is disturbed, enforcing the release or removal of other ionic species, followed by their

redistribution so that the basic requirement of ionic charge balance is maintained.

Such a redistribution mechanism was observed when part of the free chloride was complexed by cement constituents, causing the release of an equivalent amount of hydroxyl ions which was followed by their redistribution, as this anionic species appears to be the most mobile in cement pastes.

7.1.2 The Effect of Chloride Complexation

Research carried out by Verbeck [74] (see also chapter 3 para. 3.5) had demonstrated that corrosion of the steel reinforcement embedded in concrete exposed to a chloride solution can be reduced by increasing the C_3A content of the cement because of the complexation of part of the chloride. A similar result was obtained in chapter 3 part I where it was shown that the diffusion rate of free chloride was reduced somewhat by complexation giving a ratio of apparent diffusivities for free and total chlorides of 0.65.

The reduction in the apparent diffusion coefficient by the complexation is however small compared to the reduction achieved by blending the same portland cement with PFA or BFS (chapter 3 part II). Furthermore, as argued by Hjorth [76], published values for chloride diffusivities of OPC and SRPC pastes or mortars as calculated by the "thin-disc" technique, overlap over a wide range of values and are always significantly higher than for blended cements.

As was seen in chapter 6 part I, even a low C_3A content SRPC paste was capable of complexing a substantial amount of chloride resulting in a free to total chloride ratio of 0.405. Theoretically (see appendix 25) the maximum amount of chloride that could be bound by the C_3A phase is 0.141 mM/g, a value somewhat lower than the actual value of 0.253 mM/g(table 6.3). Further complexation must have occurred therefore by phases other than the C_3A.

Ramachandran [155, 156] had claimed that a high proportion of the chloride ions in solution are rapidly removed forming an interlayer chemisorbed complex within the C-S-H gel. Later [157] he suggested that in mature C_3S pastes in the presence of $CaCl_2$, a significant proportion of Cl^- ions becomes bound to hydration products.

Such findings were however disputed by other workers[158,159] Lambert et al [159] had demonstrated, for instance, that "the hydration products of substituted tricalcium silicate showed no detectable capacity to bind chloride ions".

Reactions involving the ferrite phase, C_4AF, leading to the formation of calcium chloroaluminate and chloroferrite hydrates have been shown to occur [72] but their importance in binding free chloride is believed to be small [24].

The apparent discrepancies in the literature on the ability of cement hydration products to complex chloride ions may arise partly by possible different complexing mechanisms of

the various types of chloride [160].

Results taken from the various chapters and summarised in table 7.1 disclose a further discrepancy. Whilst the resultant amount of bound chloride in 0.5 w/c OPC-B paste, containing an addition of NaCl, remained fairly constant at about 0.17mM/g, irrespective of curing condition and total chloride, the bound chloride was more than double when chloride free hardened cement pastes were exposed to a NaCl solution (table 7.1). This appears to be contrary to published results [161] where it was suggested that chloride present on mixing is complexed to a greater extent than Cl^- penetrating the structure from an external environment. The apparent increase in complexing capacity may however be related specifically to the cement paste's exposure to a Sat.$Ca(OH)_2$ solution. In any case (ie A or B in table 7.1) there appears to be a maximum complexing capacity above which any excess in total chloride remains as free in solution.

7.2 CARBONATION INDUCED CORROSION

The carbonation related neutralization of cement pastes, mortars or concretes, is well documented,[106,162] as is the increased risk of corrosion of the steel reinforcement[5,110]. Gaps still exist however in areas such as the pore solution chemistry of the carbonated material, the fate of bound chlorides during carbonation and the effect of R.H. on the cor-

TABLE 7.1 Fate of chlorides introduced to OPC-B pastes either at the mixing stage or in the external curing solution.

A. Chloride introduced in the mix.

CURING CONDITION	CHAPT.	AMOUNT OF Cl^- ADDED	AMOUNT OF Cl^- (mM/g) TOTAL	FREE	BOUND
1) 520 days in enclosed container	4(II)	1% as NaCl	0.242	0.070	0.172
2) 360 days enclosed, 150 days in water.	4(II)	1% as NaCl	0.250	0.080	0.170
3) 90 days enclosed, 225 days in contact with OPC-B (enclosed)	4(I)	2% as NaCl	0.500	0.330	0.170
4) 8days enclosed, 152 days at 65% RH, saturated with water, 8 days at 100% RH.	5(I)	1% as NaCl	0.239	0.079	0.160

B. Chloride introduced in the external solution.

CURING CONDITION	CHAPT.	AMOUNT OF Cl^- ADDED	AMOUNT OF Cl^- (mM/g) TOTAL	FREE	BOUND
1) 90 days enclosed * 100 days in solution.	3(I)	1M NaCl in sat.$Ca(OH)_2$	0.725	0.330	0.395
2) 3days enclosed, 314 days in solution as 6mm discs.	6(I)	0.5M NaCl in sat.$Ca(OH)_2$	0.590	0.171	0.419

* Calculated from extrapolation of the curves in fig. 3.6 to the surface of the specimen exposed to solution.

rosion rate of the steel reinforcement once carbonation of the concrete occurs. Work described in this thesis had attempted to fill some of these gaps.

7.2.1 Effect of Carbonation on the Pore Solution Chemistry

As was shown in chapter 5 part I, apart from the obvious reduction in the concentration of OH^- ions during carbonation, the concentration of the accompanying cations such as Na^+ and K^+ ions was also reduced. On the other hand the breakdown of the chloride containing phases had the effect of increasing the free chloride content in solution. Such a release in chloride, aided by the reduction in pH, will increase the risk of corrosion of the reinforcement dramatically, owing to the rapid rise in the $[Cl^-]/[OH^-]$ ratio. As was discussed in chapter 5, even at a depth beyond the carbonation front, the risk of corrosion may still be higher because of the increased ratio of the two anionic species (see figure 5.14).

7.2.2 Effect of Carbonation on Ionic Diffusivities

Carbonation of the cement matrix appears to reduce the effect of the previously mentioned surface interaction between the gel particles and the diffusing ions resulting in an apparent increase in ionic diffusivities (see chapter 5 part I). The protection of steel reinforcement embedded in carbonated concrete would consequently diminish further if chlorides are introduced to the structure. The combined

effect of a faster chloride penetration and the reduction in pH would quickly raise the $[Cl^-]/[OH^-]$ ratio to well beyond safe limits.

If the same increase in diffusivity on carbonation is encountered for carbonated BFS and PFA based concretes, a structure originally designed for low chloride permeability may lose its "chloride-resistant" property and increase the risk for corrosion of the reinforcement. This concept will be discussed further in the next section.

7.2.3 Corrosion Rates of Steel in a Carbonated Structure

In the absence of aggressive ions, such as chlorides it was shown in chapter 6 part II that corrosion of steel in carbonated concrete only becomes critical above a certain moisture content, supporting the findings of Gonzalez et al [41]. The preliminary nature of the investigation did not, however, permit the determination of the actual value of the critical moisture level of the concrete. The accurate evaluation of such a value requires a more controlled and systematic study.

The A.C. Impedance technique applied for corrosion studies of steel embedded in concrete, although not entirely successful in its use for corrosion monitoring, has shown promise as a tool for studying the corrosion mechanisms of such corrosion cells. Corrosion of steel in dry carbonated concrete was shown, for instance, to produce a unique

Nyquist-plot, suggesting a form of diffusion control of the corrosion process, an effect not found in the equivalent uncarbonated concrete.

7.3 EVALUATION OF THE EFFECT OF DIFFERENT CEMENTS ON THE CORROSION OF STEEL

Corrosion-related properties of the different cement pastes studied were shown by this investigation to vary considerably. Consequently the degree of protection offered to the steel reinforcement would vary accordingly.

Earlier work on the same cements [152] containing a fixed total chloride content, permitted a ranking order for the parameters of:

(i) the relative concentrations of chloride to hydroxyl ions in the pore electrolyte and,

(ii) the diffusivities of chloride ions.

As the w/c ratio of the cements used for the present investigation was the same as for the earlier work, the results obtained permit a similar comparative ranking on other parameters viz,

(i) diffusivities of the OH^- ions.

(ii) relative diffusivities of OH^- and Cl^-

ions ($D[OH^-]/D[Cl^-]$).

(iii) chloride complexing capacity of the cements

(iv) buffering capacity of the cements

(v) resistance of the cements to neutralization.

(vi) resistance of the embedded steel to pitting corrosion.

Page et al [152] had argued that for stable pit growth to be sustained, the local Cl^- concentration must rise with respect to the concentration of the OH^- ions, so the parameters of relative $[Cl^-]$ to $[OH^-]$ concentrations and chloride diffusivities (I and II respectively in table 7.2) should predict to a reasonable accuracy the resistance of the embedded steel to chloride induced corrosion. The validity of the predicted rank orders was confirmed to a large extent by corrosion measurements of embedded steel electrodes (see column III, table 7.2).

Furthermore, they suggested that pit propagation may depend primarily on the ability of a cement matrix effectively to restrain the diffusional supply of Cl^- ions whilst maintaining a local buffered alkaline environment around the pit.

This would mainly apply when the ionic consumption at the pit is high or when the electrolyte pH is nearer 12.6 at which, as was seen in chapter 5 part II, buffering can occur

TABLE 7.2 Different rank orders for the selection of cements studied.

	(a) CHLORIDE COMPLEXING CAPACITY	I $[Cl^-]/[OH^-]$	II $D[Cl^-]$	III Icorr	(b) $D[OH^-]/[Cl^-]$
BEST	OPC-B/65% BFS	OPC-B/65% BFS	OPC-B/65% BFS	OPC-B/30% PFA	OPC-B
	OPC-B	OPC-B	OPC-B/30% PFA	OPC-B/65% BFS	OPC-B/30% PFA
	OPC-B/30% PFA	OPC-B/30% PFA	OPC-A	OPC-A	OPC-B/65% BFS
	OPC-A*	OPC-A	OPC-B		OPC-A
POOREST	SRPC	SRPC	SRPC	SRPC	SRPC

* From ref. 152. I, II, III, from ref. 152.

	(c) $D[CL^-]$	(d) $D[OH^-]$	(e) BUFFERING CAPACITY	(f) RESISTANCE TO PITTING	(g) RESISTANCE TO NEUTRALIZATION
BEST	OPC-B/65% BFS	OPC-B	OPC-B	OPC-B	OPC-B
	OPC-B/30% PFA	SRPC	SRPC	SRPC	SRPC
	OPC-A	OPC-B/30% PFA	OPC-B/30% PFA	OPC-B/30% PFA	
	OPC-B	OPC-A			OPC-B/30% PFA
POOREST	SRPC	OPC-B/65% BFS	OPC-B/65% BFS	OPC-B/65% BFS	OPC-B/65% BFS

because the solubility of $Ca(OH)_2$ becomes significant. Only when this or a lower pH value is reached at the pit will diffusion of $Ca(OH)_2$ be significant (see chapter 4 part II). If on the other hand the ionic consumption at the pit is not high, ie when passivity is maintained owing to a less than critical $[Cl^-]/[OH^-]$ ratio, most of the OH^- replenishment will occur from the sodium and potassium hydroxides present in the pore electrolyte.

In a specifically controlled pore solution of a fixed chloride and hydroxyl concentration where the pH is that of Sat. $Ca(OH)_2$, as was the case for the pitting experiments (chapter 6 part I), hydroxyl replenishment of the pit will depend almost entirely on the availability of the $Ca(OH)_2$. Consequently, the resistance of the steel to pitting will be related to the degree of buffering (see table 7.2 columns e and f).

As discussed in chapter 6, under more normal conditions, buffering of the pore solution could have the effect of increasing the critical $[Cl^-]/[OH^-]$ratio required for significant corrosion to occur. This critical ratio will need therefore to be evaluated as it is an important parameter concerning the corrosion of reinforcing steel and may depend on the type of cement or more specifically on its buffering capacity.

Column g (table 7.2) represents the ability of a cement to

resist neutralization, as obtained by the experiment involving the systematic addition of acid to fully hydrated cement powders (see chapter 5 part II). It was argued earlier (chapter 5) that as diffusion of CO_2 through the cement matrix is unlikely to be governed by the same rate-limiting factors encountered in ionic diffusion, carbonation rates may depend primarily on the amount of carbonatable material, so the rank order in column g may also apply for the cement's ability to resist carbonation.

Whilst a number of studies support such a ranking[5,110,130] there is evidence that porosity is more important as a parameter for carbonation and that in reality there is little difference in carbonation rates of the various types of cements [27,133,134].

This is clearly an important area where more concentrated research is necessary. For example, BFS-based cements may be chosen for the protection of steel reinforcement against corrosion because of their low ionic diffusivities and high chloride complexing capacity. If there is a risk of a high carbonation rate, on-carbonation of the structure, these two properties may be destroyed causing the release of any bound chlorides and may allow faster chloride penetration to the steel surface increasing the risk for corrosion substantially. These possible carbonation effects on BFS cements are ofcourse only speculation so this is another important area where research is required.

The results in this investigation generally demonstrate that none of the investigated cements can be considered ideal for preventing both chloride and carbonation induced corrosion. For example, PFA and particularly BFS based cement pastes, although excellent for minimizing the penetration of chloride, may be suspect with regards to carbonation and do not offer a good high-pH buffering capacity. On the other hand, a portland cement would offer better buffering but would have limitations with regards to chloride penetration. A high C_3A content in the cement although able to reduce chloride penetration rates to an extent, may not do so sufficiently to counter the risk of other possible detrimental effects such as sulphate attack.

It should be possible nonetheless to select a certain cement type for a particular application. Rank orders can be very useful for such a selection process, provided they are used sensibly and their limitations are appreciated. It must be remembered that these reported results are based purely on well-characterised and optimally produced cement pastes.

It should also be remembered that certain assumptions were necessary in order to facilitate the calculation of constants such as diffusion coefficients and carbonation rates which in practice may not be strictly correct.

Various ways of determining such constants may also result in different values. For example, calculated diffusion coef-

ficients by the two methods requiring the determination of the flux at a given cross section and the cross-sectional area (chapter 3 part II and chapter 4 part II) were constantly lower than the values evaluated by the other technique, which required analysis of the ionic concentration profile, by a factor roughly equivalent to the porosity of the structure.

Furthermore there is no guarantee that cement pastes or concretes cured at not so ideal conditions will retain their good corrosion related properties, so a great deal of research is still needed in order to confirm the previously discussed findings. Exposure tests of the sort being done by the Building Research Establishment and the Bahrain Ministry of Works Power and Water on carbonation of concrete (7) are an essential step in research (see also section 7.5).

7.4 GENERAL CONCLUSIONS

The conclusions of the present investigation may be summarised as follows:

(i) Ionic diffusion in "fault-free" cement pastes normally occurs according to Fick's 2nd law of diffusion enabling the determination of effective diffusion coefficients for a number of ionic species.

(ii) A basic requirement for ionic diffusion is that

an ionic charge balance is maintained throughout the pore solution network, so that the "movement" of a given ionic species both influences and is influenced by the "movement" of all the other ionic species. Complexation of this species requires the release into solusion of other sets of ions.

(iii) Diffusion of ions in cement pastes appears to be restricted by a form of surface interaction between the ions, particularly the cations, and the gel particles. Calculated activation energies for anions (41-45kj/mole) support the surface interaction concept and suggest that anionic movement is influenced by the accompanying cationic species.

(iv) The blending of portland cements by PFA and BFS appears to increase the effect of the surface interaction causing a reduction in ionic diffusivities. Carbonation of portland cements on the other hand, appears to minimise the effect of the surface interaction so the resulting ionic diffusivities are higher, even though porosity decreases.

(v) A maximum chloride complexing capacity appears to exist for portland cement pastes but this is reduced substantially on carbonation, cau-

sing the release of previously bound chlorides into the pore solution.

(vi) The rate of carbonation of portland cements depends on the CO_2 concentration in the atmosphere and, is proportional to the square root of time. An induction period exists, before the onset of apparent carbonation, related to the time required to neutralize all the basic constituents near the surface of the specimen.

(vii) Carbonation causes the modification of some cement paste properties, ie porosity is decreased, ionic diffusivities are increased and Na^+ and K^+ ions are removed from the pore solution. The extent of the modifications appear to be influenced partly by the amount of CO_2 in the atmosphere.

(viii) The pozzolanic action of PFA and BFS based cements causes the reduction of the $Ca(OH)_2$ phase normally present in hydrated cement pastes. Such a reduction in free lime diminishes the high-pH buffering capacity of the cement paste necessary for good steel reinforcement protection. The total amount of carbonatable material present in cement pastes is also reduced by the blending of portland cements.

(ix) The mechanism of pitting of steel in cement

pastes appears to be more complex than in the equivalent solutions. Buffering of the cement paste pore solution by the $Ca(OH)_2$ appears to play an important role under specific laboratory conditions where the pore liquid is virtually Sat.$Ca(OH)_2$. The removal of this phase by the addition of BFS increases the risk for pitting of the steel.

(x) The corrosion rate of steel in carbonated concrete, increases with the increase in moisture content of the structure. A critical moisture level appears to exist above which corrosion is significant.

(xi) The A.C. Impedance technique, offers no advantages over the D.C. linear polarization technique in determining corrosion rates, but shows promise as a tool for studying the corrosion mechanisms of steel in concrete.

7.5 SUGGESTIONS FOR FUTURE WORK

As curing condition has some effect on the hydration and hence on certain physical or chemical properties of the cement matrix,[163] it is not unrealistic to expect somewhat altered corrosion-related properties too. The degree of change with curing condition may vary with different cements and may be more pronounced for cements more susceptible to

temperature or moisture variations, as some blended cements tend to be [27,164-166]. A detailed study on the effect of such variations on corrosion-related properties is therefore important.

Furthermore, any results obtained under laboratory conditions, as are the findings reported in this work, must be checked and confirmed by long-term field exposure tests. This is particularly true with regards to carbonation experiments, where the present results relate only to thin discs of cement paste, exposed to CO_2 at a constant R.H., conditions which in practice do not exist.

Returning to more fundamental aspects, many questions have arisen which require precise answers. As briefly mentioned earlier, a knowledge of OH^- and Cl^- concentration profiles in carbonated cement pastes within and beyond the apparent carbonation depth is of high importance in relation to the corrosion-related parameter of $[Cl^-]/[OH^-]$ ratio.

The near absence of the $Ca(OH)_2$ solid phase in BFS based cements was believed in chapter 6 to be the main reason for the apparent reduced ability of the cement to resist pitting of the embedded steel under specific conditions. PFA on the other hand, with just a small amount of $Ca(OH)_2$, was not much worse than the high lime-containing portland cements, suggesting that the lime-rich layer around the steel reported by Page [26,167] may still be present. Some SEM

work on the steel-BFS cement paste interfacial zone supporting such suggestions would be of high value.

Various degrees of blending may alter the buffering offered by the cements. It could be that a certain critical percentage substitution of BFS or PFA exists above which no $Ca(OH)_2$ solid phase is possible, so the buffering capacity of a range of blended cements should be looked at using the method described in chapter 5 part II. This technique should be developed further to enable the quantitative as well as the qualitative analysis of all the detectable phases.

A suggestion was put forward in chapter 4 part II, linking the lowered ionic diffusivities of the portland cement paste to a reduced CaO/SiO_2 ratio of the gel. Such an effect could be investigated by determining ionic diffusivities of cements with variable C/S ratio gels and obtaining a relationship. Furthermore, as mentioned earlier, diffusivities of ions in carbonated blended cements should be determined as well as the fate of any originally bound chloride.

The present investigation has attempted to widen the knowledge on the mechanisms of corrosion and protection of steel reinforcement in concrete as a function of the cement matrix by covering a wide range of cement properties. Many of the conclusions were made tentatively and require confirmation from further studies, particularly from exposure tests. It is hoped that this work has at least asked the right ques-

tions which can generate further research in the important field of steel reinforcement corrosion.

APPENDIX 1 Chloride Calibration Curve.

Absorption values (ABS) as read-off the spectrophotometer were translated into Cl^- concentrations from the following calibration curve constructed from chloride standards.

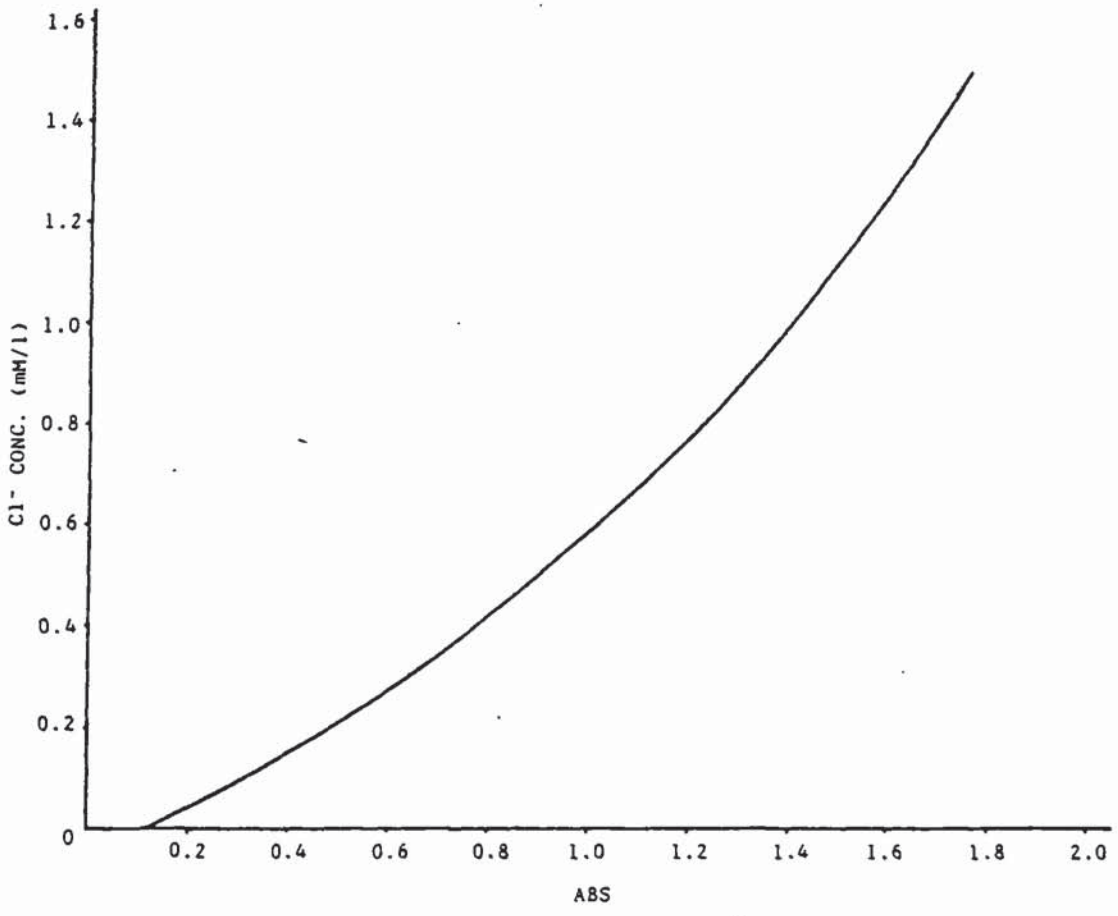

APPENDIX 2 Derivation of equations used for the determination of evaporable and non-evaporable water contents in cement pastes (After Lambert - ref. 34)

The mass of the cement paste before and after heating to 105 and 950° C may be defined as follows:

$$Wo = Wc + We + Wn + Wa \quad (1)$$

$$W_{105} = Wc + Wn + Wa \quad (2)$$

$$W_{950} = Wc \frac{(100-i)}{100} + Wa \quad (3)$$

where,

Wo = original mass of cement (g)

W_{105} = mass of cement at 105° C (g)

W_{950} = mass of cement at 950° C (g)

Wc = mass of unhydrated cement (g)

We = mass of evaporable water (g)

Wn = mass of non-evaporable water (g)

Wa = mass of admixtures (g)

and i = loss-on-ignition (% g / g of unhydrated cem.)

From these equations expressions for evaporable and non-evaporable water contents may be developed.

(1) - (2)

$$We = Wo - W_{105} \quad (4)$$

if $$Wa = \frac{Wc \times a}{100} \quad (5)$$

where, a = admixture content (% g/g of unhydrated cem.)

From (3),

$$W_{950} = \frac{Wc(100-i) + (Wc \times a)}{100} = \frac{Wc(100-i+a)}{100} \quad (6)$$

$$Wc = \frac{100 \times W_{950}}{(100-i+a)} \quad (7)$$

EVAPORABLE WATER (% g/g unhydr.cem.) $= \frac{We}{Wc} \times 100\%$

Sub. Wc from (4)

$$E.W.(\%) = \frac{Wo - W_{105}}{Wc} \times 100$$

sub. Wc from (7)

$$E.W.(\%) = \frac{Wo - W_{105}(100-i+a)}{100 \times W_{950}} \times 100$$

$$E.W.(\%) = \frac{Wo - W_{105}}{W_{950}} \times (100-i+a)$$

NON-EVAPOR. WATER (%g/g unhydr.cem.) $= \frac{Wn}{Wc} \times 100\%$

From (2),

$$Wn = W_{105} - Wc - Wa$$

Sub. Wa from (5)

$$Wn = W_{105} - Wc - \frac{Wc \times a}{100}$$

$$Wn = W_{105} - Wc \left(1 + \frac{a}{100}\right)$$

sub. Wc from (7)

$$Wn = W_{105} - \frac{100 \times W_{950}}{(100-i+a)} \left(1 + \frac{a}{100}\right)$$

$$Wn = \frac{W_{105}(100-i+a) - (100+a) W_{950}}{(100-i+a)}$$

Divide by Wc from (7) and multiply by 100 to give the non-evaporable water (%).

$$N.E.W.(\%) = \frac{[W_{105}(100-i+a) - (100+a)W_{950}][100-i+a]}{(100-i+a) \times 100 \times W_{950}} \times 100$$

$$N.E.W.(\%) = [W_{105}(100-i+a) - W_{950}(100+a)] \frac{1}{W_{950}}$$

Worked Example.

To calculate evaporable and non-evaporable water contents for OPC-B' paste. Example from table 4.11 at 1.4 cm depth (chapter 4)

Wt of crusible	26.4916 g
Wt of crusible + sample	28.6889 g
Wt of crusible + sample at 105° C	28.1914 g
Wt of crusible + sample at 950° C	27.8969 g
Wt of sample (Wo)	2.1973 g
Wt at 105° C (W_{105})	1.6998 g
Wt at 950° C (W_{950})	1.4053 g
Loss-on-ignition (i)	0.9 g/g
Addition of NaCl (a)	1.65g/g

$$E.W.(\%) = \frac{Wo - W_{105}}{W_{950}}(100-i+a)$$

$$= \frac{2.1973 - 1.6998}{1.4053}(100-0.9+1.65)$$

$$= 35.67\%$$

$$N.E.W.(\%) = [W_{105}(100-i+a) - W_{950}(100+a)] \frac{1}{W_{950}}$$

$$= \frac{1.6998(100-0.9+1.65) - 1.4053(100+1.65)}{1.4053}$$

$$= 20.21\%$$

$$\text{TOTAL WATER} = 35.67 + 20.21 = 55.88\%$$

APPENDIX 3 Total Free and Bound Chloride Determination.

Worked example of calculation for sample 1.4cm into OPC-B' paste cylinder (chapter 4 part II - table 4.12)

Wt of sample at 105° C = 0.9335 g

Need to correct to Wt at 950° C

From appendix 2,

W_{105} = 1.6998g gives W_{950} = 1.4053 g

$\therefore$ W_{105} = 0.9335g gives W_{950} = 0.7718 g

$$\text{Total Chloride (mM/g)} = \frac{\text{Conc. of solut.(mM/1) x Dilution}}{W_{950} \times 1000}$$

$$= \frac{12.60 \times 13}{0.7718 \times 1000}$$

$$\text{TOTAL } Cl^- = 0.212 \text{ mM/1}$$

$$\text{Free Chloride (mM/L)} = \frac{\text{Conc. of sol.(mM/1) x We(g/g)}}{1000}$$

$$= \frac{119 \times 0.3567}{1000}$$

$$\text{FREE } Cl^- = 0.042 \text{ mM/1}$$

$$\text{Bound Chloride (mM/1)} = \text{TOTAL } Cl^- - \text{FREE } Cl^-$$

$$= 0.212 - 0.042$$

$$\text{BOUND } Cl^- = 0.170 \text{ mM/1}$$

APPENDIX 4 DTA Identification Peaks.

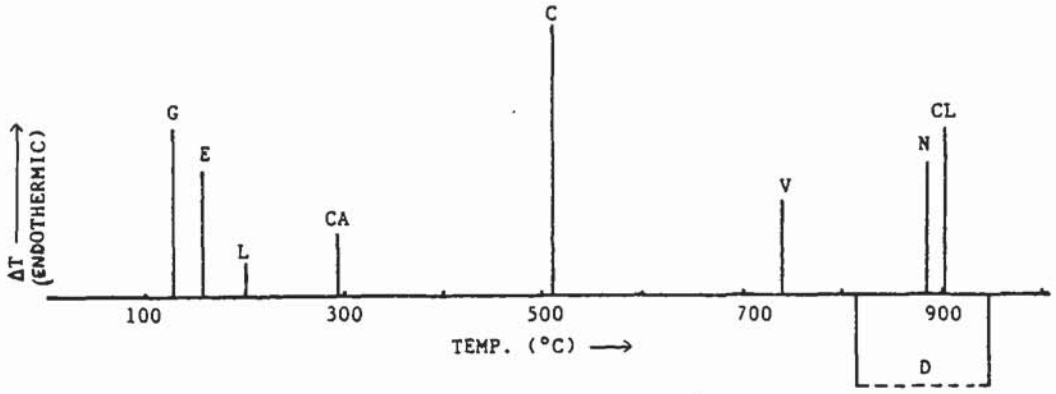

	From ref.		From ref.
G = C-S-H Gel	126	V = Vaterite	127
E = Ettringite	"	N = Sodium Chloride	126
L = Calcium Chloroaluminate	"	CL = Calcite	127
CA = C_4AH_{13}	"	D = Devitrification of Glassy Phase	126
C = Calcium Hydroxide	"		

APPENDIX 5 Example of identification of XRD trace.

From figure 4.23, surface of cylinder (chapter 4) the following values for 2θ, d-spacing (based on CuK_α = 1.542 Å) and relative intensity I were determined:

			STANDARD DATA (ref. 37)		
2θ	d(Å)	I	C-S-H (I)	C-S-H (II)	CALCITE
16.6	5.34	19	5.3 (vvw)		
19.9	4.46	19			
29.3	3.05	45	3.07 (vs)	3.07(vvs)	3.035(vvs)
32.0	2.80	21	2.80 (s)	2.80 (vs)	
35.9	2.50	20			2.495 (m)
[38.2 [38.3	2.36] 2.35]	18	2.4 (w/d)	2.4 (m)	
39.4	2.29	22			2.285 (s)
43.1	2.10	19	2.1 (w/d)	2.1 (vvw)	2.095 (s)
44.6	2.03	19		2.0 (ms)	
47.6	1.91	18			1.913 (ms)
48.5	1.88	20			1.875 (ms)
49.8	1.83	17	1.83 (s)	1.83 (vs)	
55.2	1.66	15	1.67 (mw)		
64.8	1.44	18	1.40 (w)	1.40 (mw)	
77.7	1.23	12	1.23 (vw)	1.225 (w)	

The values of d and I were compared to standard data as shown in the table, to identify the phases. In this case three possible phases were identified. Concidering that C-S-H gel is much less crystalline than calcite, C-S-H must be the most predominant phase althouth it is difficult to say whether it is type-I or type-II.

Key to table: scale of decreasing relative intensities:
vvs, vs, s, ms, m, mw, w, vw, vvw; (d = diffuse)

APPENDIX 6 Pore-size distribution calculation example.

From fig. 3.14 sample no. 2 (chapter 3),
Wt of sample dried at 105° C (Ws) = 5.3175 g
Cell factor = 0.000751 cc/count

A = Applied pressure
B = Penetration Counter
C = Corrected Counter indication (B-Result of blank run)
D = Pore Diameter (117° Contact angle) (124.9 ÷ A) -μm
E = Volume of Pores of Indicated Diameter and larger
C x (Cell factor ÷ Ws) -ml/g

The above values are determined for increasing applied pressures and tabulated as follows:

A	B	C	D	E
1	11	11	124.9	0.00155
3	27	27	41.6	0.00381
6	33	33	20.8	0.00470
9	36	36	13.9	0.00508
14	39	39	8.92	0.00551
50	58	58	2.50	0.00819
150	65	65	0.833	0.00918
300	74	74	0.416	0.01045
450	85	85	0.278	0.0120
600	100	100	0.208	0.0141
1000	102	102	0.125	0.0144
1200	168	168	0.104	0.0237
1400	271	271	0.0892	0.0383
1600	559	559	0.0780	0.0789
1800	743	743	0.0694	0.105
2000	860	858	0.0625	0.121
2200	930	928	0.0568	0.131
2600	1032	1029	0.0480	0.145
2800	1084	1081	0.0446	0.153
3200	1145	1142	0.0390	0.161

cont. over

A	B	C	D	E
3500	1187	1183	0.0357	0.167
4000	1248	1243	0.0312	0.176
4500	1300	1295	0.0278	0.176
5000	1351	1345	0.0250	0.190
6000	1436	1427	0.0208	0.201
7000	1491	1481	0.0178	0.209
8000	1553	1542	0.0156	0.218
9000	1602	1590	0.0139	0.225
10000	1646	1633	0.0125	0.231
12000	1710	1695	0.0104	0.239
14000	1763	1749	0.00892	0.247
16000	1802	1781	0.00781	0.251
18000	1835	1812	0.00694	0.256
20000	1860	1835	0.00625	0.259
24000	1900	1872	0.00520	0.264
28000	1931	1896	0.00446	0.268
32000	1958	1918	0.00390	0.271
36000	1984	1937	0.00347	0.274
40000	2010	1957	0.00312	0.276
44000	2026	1962	0.00284	0.277

A plot of E v's A and/or D then produces a pore-size distribution curve as shown in fig.3.14.

APPENDIX 7 Calculation of Icorr using the "manual" method.

For specimen U1 in the dry condition, table 6.9 (chapter 6)

$$Ecorr = 199mV$$

Potential first moved 10mV above Ecorr (+209mV) using potentiostat. After 30 secs,

$$I = +235nA$$

Potential then moved back to Ecorr and left for 30 secs. Potential then moved 10mV below Ecorr (+189mV). After 30 secs,

$$I = -201nA$$

Then,

$$\text{mean } I = \text{Modulus of mean currents}$$

$$= \frac{235 + 201}{2} = 218nA$$

$$\text{Polarisation Resistance} = Rp = \frac{\Delta E}{\Delta I} = \frac{10mV}{218nA}$$

$$Icorr = \frac{B}{Rp} \qquad \text{where } B = 26mV$$

$$= \frac{26 \times 218}{10} = 566.8nA$$

$$\text{Area of exposed steel} = 17.85cm^2$$

$$Icorr\ (C.D.) = \frac{566.8}{17.85} = 31.8nA\ cm^{-2}$$

$$= 3.2 \times 10^2\ \mu A\ m^{-2}$$

APPENDIX 8 Example of A.C. impedance data collection and representation.

For specimen U3 (fig.6.29b) -Chapter 6.

Area of specimen = 17.85 cm^2

Current range setting on potentiostat acting as amplifier of output = 1 μA

IR compensation (using +ve feedback) = 2.3×10^4 Ω

Ecorr (setting on potentiostat) = 191 mV

To work out amplification of output ,

From, $R = \frac{V}{I}$ (where V=1 volt fsd of output)

Internal variable resistance = $\frac{1(V)}{1(\mu A)} = \frac{1}{10^{-6}(A)} = 10^6$ Ω

Recorded values of modulus of impedance should be multiplied by $x10^6$

FREQ. (Hz)	|Z|	ANGLE θ	CORRECTED |Z|	Z' (Ω)	Z'' (Ω)
0.06	$5.43x10^{-3}$	-40	$5.43x10^3$	$4.16x10^3$	$3.49x10^3$
0.10	4.05 "	-38	4.05 "	3.19 "	2.49 "
0.14	3.67 "	-35	3.67 "	3.01 "	2.11 "
0.20	3.31 "	-32	3.31 "	2.81 "	1.75 "
0.30	2.90 "	-30	2.90 "	2.51 "	1.45 "
0.40	2.70 "	-28	2.70 "	2.38 "	1.27 "
0.50	2.48 "	-26	2.48 "	2.23 "	1.09 "
0.60	2.37 "	-25	2.37 "	2.15 "	1.00 "
0.80	2.22 "	-25	2.22 "	2.01 "	$9.38x10^2$
1.00	2.09 "	-23	2.09 "	1.92 "	8.17 "
1.30	1.94 "	-23	1.94 "	1.79 "	7.58 "
1.50	1.87 "	-22	1.87 "	1.73 "	7.01 "
2.00	1.72 "	-21	1.72 "	1.61 "	6.16 "
2.50	1.64 "	-19	1.64 "	1.55 "	5.34 "
3.00	1.55 "	-18	1.55 "	1.47 "	4.79 "
4.00	1.42 "	-16	1.42 "	1.36 "	3.91 "
5.00	1.33 "	-14	1.33 "	1.29 "	3.22 "
6.00	1.24 "	-11	1.24 "	1.22 "	2.37 "
7.00	1.20 "	-7	1.20 "	1.19 "	1.46 "
7.40	1.18 "	-6	1.18 "	1.17 "	1.23 "
7.80	1.16 "	-5	1.16 "	1.16 "	1.01 "
8.20	1.15 "	-3	1.15 "	1.15 "	$6.02x10^1$
8.80	1.12 "	-2	1.12 "	1.12 "	3.91 "
9.00	1.12 "	0	1.12 "	1.12 "	0

Note: $Z' = |Z| \times \cos \theta$
$Z'' = |Z| \times \sin \theta$

where, |Z| = modulus of impedance
Z' = real impedance
Z'' = imaginary impedance

APPENDIX 9 Solutions to Fick's 2nd law of diffusion.

Need to solve Fick's 2nd law:

$$\frac{dC}{dt} = D\frac{d^2C}{dx^2}$$

Given that $C = C_{(x,t)}$ when $t>0$

$C = f(x)$ " $t=0$

From Barrer [ref.70] general solution is:

$$C = \frac{1}{2\sqrt{(\pi Dt)}} \int_{-\infty}^{+\infty} f(x') \exp\left[-\frac{(x-x')^2}{4Dt}\right] dx'$$

CASE 1 Two solids joined together, one with concentration C_o & the other 0.

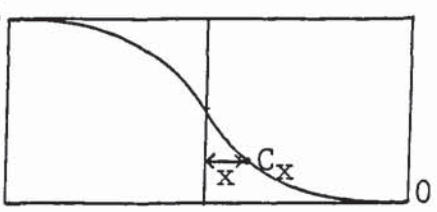

At $t=0$ $C_x = C_o$ for $x<0$

$C_x = 0$ for $x>0$

For all +ve values of x the concentration at t and point x becomes:

$$C_x = \frac{C_o}{2\sqrt{(\pi Dt)}} \int_{o}^{\infty} \exp\left[-\frac{(x-x')^2}{4Dt}\right] dx'$$

$$C_x = \frac{C_o}{\sqrt{\pi}} \int_{x/2\sqrt{Dt}}^{\infty} e^{-y^2} dy \qquad \text{if } y^2 = \frac{(x-x')^2}{4Dt}$$

$$C_x = \frac{C_o}{2}\left[1 - \frac{2}{\sqrt{\pi}} \int_{0}^{x/2\sqrt{Dt}} e^{-y^2} dy\right]$$

The 2nd term is the Gaussian error function (erf (y))

$$\therefore\ C_x = \frac{C_o}{2}[1-\text{erf}(y)] \qquad \text{where } y = \frac{x}{2\sqrt{Dt}}$$

$$C_x = \frac{C_o}{2}[1+\text{erf}(y)] \qquad \text{for } x<0$$

CASE 2 One side constant C_o the other C=0 at t=0.

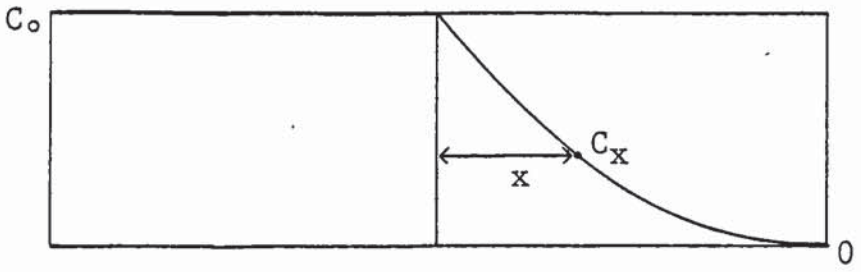

When the supply at the plane x=0 is constant the boundary conditions are:

$$C_x = C_o \text{ at } x = 0 \text{ for all } t$$
$$C_x = 0 \text{ at } x > 0 \;\&\; t = 0$$
$$C_x = C_{(x,t)} \text{ at } x > 0 \;\&\; t > 0$$

and the solution giving concentration C at point x and time t is:

$$C_{(x,t)} = \frac{C_o}{\sqrt{(\pi Dt)}} \int_o^\infty \exp\left[-\frac{(x-x')}{4Dt}\right] dx'$$

$$C_x = C_o \left[1 - \frac{2}{\sqrt{\pi}} \int_o^{x/2\sqrt{Dt}} e^{-y^2} dy\right]$$

$$\therefore C_x = C_o \left[1 - \text{erf}(y)\right]$$

APPENDIX 10 Example calculation of the effective diffusion coefficient D, from a solution to Fick's 2nd law.

From table 3.1 (chapter 3)
Extrapolation of curve to t=0 gives C_o = 1.085 M/l ie conc. at the surface of the specimen.

First calculate erf(y) from, $C_x = C_o [1-erf(y)]$ (append.9)
Then look at values of y in tables [ref.71]

C_x (M/l)	DEPTH x (cm)	erf(y)	y
0.991	0.175	0.087	0.08
0.838	0.35	0.228	0.20
0.670	0.70	0.382	0.35
0.572	1.05	0.473	0.44
0.366	1.40	0.663	0.68
0.292	1.75	0.731	0.78
0.135	2.10	0.876	1.10
0.059	2.45	0.946	1.37
0.039	2.80	0.964	1.48
0.024	3.15	0.978	1.62
0.014	3.50	0.987	1.76
0.015	3.85	0.986	1.75
0.007	4.20	0.994	1.96

Regression analysis [ref. 168] of plot x v's y (see fig. 3.5) gives:

slope b = 2.2026cm
intercept c = 0.000
correl. coeff. r = 0.991

and from $b = 2\sqrt{Dt}$
(where t = 100 x 24 x 3600 secs.)

Effect. Diff. $D = 118.8 \times 10^{-9}\ cm^2 s^{-1}$

For the 95% confidence intervals (see appendix 13 for example of calculation)

$b = 2.026 \pm 0.179$cm

Range for $D = 98.7 — 140.7 \times 10^{-9}\ cm^2 s^{-1}$

APPENDIX 11

A. Solution to Fick's 1st law of Diffusion.

For one-dimentional, steady-state diffusion the simple linear law known as Fick's 1st law is applicable.

$$J = -D \frac{dC}{dx} \qquad (1)$$

where,

J = Flux or diffusion current density - the amount of material diffusing in a unit time per unit area perpendicular to the x-axis.

D = Diffusion coefficient

C = Volume concentration

x = Distance along direction of diffusion

Under steady-state conditions, the above equation can be integrated to:

$$J = -D \frac{C2-C1}{\Delta x} \qquad (2)$$

where C1 & C2 are concentrations at the ends of the diffusional length Δx.

For a thin disc of thickness 1 we have:

$$J = \frac{D}{1} (C1-C2) \qquad (3)$$

For a diffusion cell as in fig. 3.11 the flux of ions entering the "low" compartment is given by:

$$J = \frac{V}{A} \frac{dC2}{dt} \qquad (4)$$

From (3) & (4) we have:

$$\frac{D}{1} (C1-C2) = \frac{V}{A} \frac{dC2}{dt}$$

Assume C1 is constant

$$\int_{C2=k}^{C2=C2} -d\frac{(C1-C2)}{(C1-C2)} = \frac{DA}{V1} \int_{t=t_o}^{t=t} dt$$

$$\left[-\log_e (C1-C2) \right]_k^{C2} = \frac{DA}{V1} (t-t_o)$$

$$\log_e \left(\frac{C1-k}{C1-C2} \right) = \frac{DA}{V1} (t-t_o)$$

$$\log_e \left(1 + \frac{C2-k}{C1-C2} \right) = \frac{DA}{V1} (t-t_o)$$

For $t > t_o$, $\quad C2-k \ll C1-C2$

ie, $\quad C2 \ll \frac{C1+k}{2}$

and:

$$\frac{C2-k}{C1-C2} = \frac{DA}{V1} (t-t_o)$$

if, $\quad S = \frac{C2-k}{t-t_o}$

then: $\quad D = \frac{SV1}{A(C1-C2)}$

B. Example calculation of effective diffusion coefficient D.

Fig. 3.12 shows the graph of disc 3 for SRPC paste in NaOH. Its slope is:

$$S = \frac{2.62 \times 10^{-5}}{6.91 \times 10^{5}} = 3.79 \times 10^{-11} \text{ moles cm}^{-3}\text{s}^{-1}$$

V(volume of solution in comp. 2) = 78 ml
l(thickness of disc) = 0.27 cm
A(cross sectional area of disc) = 9.19 cm^2
C1(conc. of solution in comp. 1) = 1.0×10^{-3} moles cm^{-3}
C2(conc. of solution in comp. 2) = 3.2×10^{-5} moles cm^{-3}

from $\quad D = \frac{SV1}{A(C1-C2)}$

$$D_3 = \frac{3.79 \times 78 \times 0.27 \times 10^{-11}}{9.19 \times 9.68 \times 10^{-4}} = 89.7 \times 10^{-9} \quad (cm^2 s^{-1})$$

APPENDIX 12 Effective Diffusion coefficients for the various cement pastes as determined by the "thin-disc" method (chapter 3 part II)

All values are $x10^{-9}$ cm^2s^{-1}

A. $D[OH^-]$ for OPC-B at various temperatures (table 3.8)

No.	9°C	15°C	25°C	35°C	45°C
1	30.0	77.4	104.2	185.4	343.8
2	35.3	94.4	107.7	199.2	361.7
3	53.8	111.1	121.8	160.6	363.0
4	46.5	62.2	118.4	173.6	312.2
5	35.6	42.4	111.4	188.3	326.4
6	—	76.1	111.5	200.1	297.2
MEAN	40.2	77.3	112.5	184.5	334.0

B. $D[OH^-]$ for various cements at 25°C (table 3.10)

No.	OPC-A	SRPC	OPC-B/ 30% PFA	OPC-B/ 65% BFS
1	72.4	71.6	47.2	6.9
2	24.8	86.9	36.5	4.2
3	33.2	89.7	48.3	7.8
4	30.2	93.5	24.3	5.7
5	39.7	77.5	35.3	3.9
6	—	80.0	32.0	—
MEAN	34.1	83.2	37.3	5.7

C. Effective ionic diffusivities for OPC-B at 25°C cured originally in two different solutions (table 3.9)

	CURING SOLUTION		
	KOH	SAT.$Ca(OH)_2$	
No.	$D[OH^-]$	$D[Na^+]$	$D[OH^-]$
1	113.6	72.0	72.3
2	139.3	85.7	92.2
3	94.2	98.3	94.7
4	123.3	90.1	105.7
5	128.4	75.5	85.5
6	165.8	—	—
MEAN	127.4	84.3	90.1

D. NaCl Diffusion in OPC-B' at 25°C cured originally in two different relative humidities (table 5.7)

	100% RH		65% RH	
No.	$D[Na^+]$	$D[Cl^-]$	$D[Na^+]$	$D[Cl^-]$
1	53.5	115.2	56.0	107.0
2	69.2	113.1	78.5	118.3
3	53.0	105.2	76.8	117.0
4	30.9	84.4	212.5*	237.1*
5	46.5	99.8	92.5	136.0
MEAN	50.6	103.5	76.0	119.6

* Disc showed cracking therefore the reading was ignored.

E. NaCl diffusion at 25°C in carbonated OPC-B' exposed to various atmospheres. (table 5.7)

	AIR		5% CO_2		100% CO_2	
No.	$D[Na^+]$	$D[Cl^-]$	$D[Na^+]$	$D[Cl^-]$	$D[Na^+]$	$D[Cl^-]$
1	193.1	196.7	128.3	107.5	304.7	284.7
2	227.3	230.8	107.3	92.1	340.3	322.2
3	279.0	261.2	108.6	105.0	221.6	198.4
4	129.8	148.4	121.1	124.4	230.9	309.9
5	311.8	314.0	136.3	137.2	274.3	294.5
MEAN	228.2	230.2	120.3	113.2	294.4	281.9

APPENDIX 13 Calculation of the activation energy for OH^- diffusion in OPC-B (fig. 3.13)

Using the values of appendix 12 A and, taking, x as $\frac{1}{T}$ in °K (ie for 9°C = 282°K & $\frac{1}{T} = 3.546 \times 10^{-3}$) and, y as $\log_{10}D$ (ie for $D = 30.0 \times 10^{-9}$ & $\log_{10}D = -7.523$) values of Σx, Σy, Σx^2, Σxy, Σy^2 and n can be calculated. For this example these are as follows:

$\Sigma x = 9.7046 \times 10^{-2}$ $\quad\quad$ $\Sigma xy = -0.6732$

$\Sigma y = -200.7855$ $\quad\quad$ $\Sigma y^2 = 1393.1651$

$\Sigma x^2 = 32.5357 \times 10^{-5}$ $\quad\quad$ $n = 29$

Need to determine values a & b of the best fit equation [ref. 168]

$$y = a + bx$$

where,

$$b = \frac{n\Sigma xy - \Sigma x \Sigma y}{n\Sigma x^2 - (\Sigma x)^2} = 2158.99$$

and

$$a = \frac{\Sigma y - b\Sigma x}{n} = 0.3013$$

$\therefore$ best fit equation is,

$$y = 0.3013 - 2158.99x$$

Activation Energy

$$D = D_o e^{\left(\frac{U}{RT}\right)}$$

$$\log_e D = \log_e D_o - \frac{U}{RT}$$

$$\log_{10} D = \log_{10} D_o - \frac{U}{2.303RT}$$

$\therefore$ slope of line (figure 3.13) is,

$$-\frac{U}{2.303R}$$

$$-U = 2.303 \times 8.314 \times (-2158.99)$$

$$U = 41339 \text{ J/mole}$$

$$U = 41.3 \text{ kJ/mole}$$

Correlation coefficient

$$r = \frac{n\Sigma xy - \Sigma x \Sigma y}{\sqrt{[\{n\Sigma x^2 - (\Sigma x)^2\}\{n\Sigma y^2 - (\Sigma y)^2\}]}}$$

$$r = -0.96$$

95% confidence intervals

$$S^2_{y/x} = \frac{\Sigma y^2 - a\Sigma y - b\Sigma xy}{n - 2}$$

$$S_{y/x} = 0.0883$$

$$b \pm t_{\frac{1}{2}\alpha, n-2} \times \frac{S_{y/x}}{\sqrt{[\Sigma x^2 - \frac{(\Sigma x)^2}{n}]}} \quad \text{where } \alpha = 0.025$$

$$b \pm 2.052 \times 114.18$$

$$\therefore U = 41.3 \pm 4.5 \text{ kJ/mole}$$

APPENDIX 14 Statistical comparison between the effective diffusion coefficients of hydroxyl ions as NaOH v's KOH in OPC-B.

Test Null hypothesis, [ref. 169]

$$H_o: \mu_1 = \mu_2$$

$$H_1: \mu_1 > \mu_2$$

where $\mu_1 = \bar{x}_1$ & $\mu_2 = \bar{x}_2$

$D[OH^-]$ for KOH		$D[OH^-]$ for NaOH	
x_1	x_1^2	x_2	x_2^2
11.36	129.05	10.42	108.58
13.93	194.04	10.77	115.99
9.42	88.74	12.18	148.35
12.33	152.03	11.84	140.19
12.84	164.87	11.14	124.10
16.58	274.90	11.15	124.32
$\Sigma x_1 = 76.46$	$\Sigma x_1^2 = 1003.62$	$\Sigma x_2 = 67.50$	$\Sigma x_2^2 = 761.53$
$\bar{x}_1 = 12.74$		$\bar{x}_2 = 11.25$	

Note: All values of x_1 & x_2 are multiplied by 10^8

$$\text{Sum of squares for 1} = \Sigma x_1^2 - \frac{(\Sigma x_1)^2}{n_1} = 29.267$$

$$\text{Sum of squares for 2} = \Sigma x_2^2 - \frac{(\Sigma x_2)^2}{n_2} = 2.154$$

$$Sp^2 = \frac{\text{Sum of squares 1} + \text{Sum of squares 2}}{(n_1 + n_2) - 2}$$

$$= \frac{29.267 + 2.154}{10} = 3.142$$

$$t = \frac{(\bar{x}_1 - \bar{x}_2) - \Delta_o}{\sqrt{Sp^2 \left(\frac{1}{n_1} + \frac{1}{n_2}\right)}} = \frac{(12.74 - 11.25) - 0}{\sqrt{(3.142 \times \frac{1}{3})}} = 1.456$$

For a 1 tail test: $t_{0.05,10} = 1.812$ from tables [ref. 170]

$\therefore H_o$ true at the 5% level of significance.

APPENDIX 15 Ionic concentrations of the pore solution of OPC-B paste at various depths (ch.4 part I)

TABLE A. Ionic Concentrations at 100 days (M/litre)

x(cm)	Na^+	Cl^-	OH^-	x(cm)	Na^+	Cl^-	OH^-
0.35	0.513	0.180	0.533	-0.35	1.005	0.446	0.598
1.05	0.225	0.023	0.466	-1.05	1.298	0.775	0.599
1.75	0.112	0.002	0.409	-1.75	1.402	0.838	0.588
2.45	0.096	0.001	0.386	-2.45	1.405	0.938	0.540
3.15	0.114	0.001	0.386	-3.15	1.435	0.965	0.503
3.85	0.091	0.001	0.386	-3.85	1.402	0.984	0.505
4.55	0.114	0.002	0.378	-4.55	1.432	0.970	0.515

TABLE B. Ionic Concentrations at 225 days (M/litre)

x(cm)	Na^+	K^+	Cl^-	OH^-	x(cm)	Na^+	K^+	Cl^-	OH^-
0.35	0.570	0.319	0.185	0.595	-0.35	0.906	0.300	0.562	0.629
0.70	0.433	0.346	0.115	0.574	0.70	1.140	0.289	0.688	0.685
1.05	0.328	0.331	0.037	0.527	-1.05	1.250	0.300	0.777	0.691
1.40	0.270	0.370	0.022	0.481	-1.40	1.343	0.301	0.855	0.702
1.75	0.205	0.350	0.004	0.475	-1.75	1.345	0.306	0.900	0.701
2.10	0.171	0.348	0.001	0.459	-2.10	1.375	0.309	0.920	0.691
2.45	0.143	0.338	0.001	0.444	-2.45	1.438	0.319	0.954	0.680
2.80	0.135	0.354	0.001	0.428	-2.80	1.435	0.323	0.992	0.680
3.15	0.105	0.331	0.001	0.439	-3.15	1.375	0.299	0.980	0.672
3.50	0.120	0.323	0.001	0.389	-3.50	1.435	0.330	0.998	0.672
3.85	0.105	0.325	0.002	0.418	-3.85	1.375	0.306	0.991	0.664
4.20	0.120	0.323	0.001	0.397	-4.20	1.405	0.315	0.986	0.661
4.55	0.114	0.341	0.003	0.406	-4.55	1.475	0.319	1.010	0.661
4.90	0.120	0.344	0.001	0.398	-4.90	1.435	0.323	1.001	0.658
5.25	0.114	0.333	0.003	0.378	-5.25	1.410	0.290	1.002	0.653
5.60	0.120	0.323	0.001	0.387	-5.60	1.405	0.315	1.005	0.646
5.95	0.111	0.319	0.002	0.392	-5.95	1.438	0.313	-	-

TABLE C. Concentrations at 225 days (M/litre)

x(cm)	Σ^+	Σ^-	$\Sigma^+-\Sigma^-$	x(cm)	Σ^+	Σ^-	$\Sigma^+-\Sigma^-$
0.35	0.889	0.780	0.109	-0.35	1.206	1.191	0.015
0.70	0.779	0.689	0.090	-0.70	1.429	1.373	0.056
1.05	0.659	0.564	0.095	-1.05	1.550	1.468	0.082
1.40	0.640	0.503	0.137	-1.40	1.644	1.557	0.087
1.75	0.555	0.479	0.076	-1.75	1.651	1.601	0.050
2.10	0.519	0.460	0.059	-2.10	1.684	1.611	0.073
2.45	0.481	0.445	0.036	-2.45	1.757	1.634	0.123
2.80	0.489	0.449	0.040	-2.80	1.758	1.672	0.086
3.15	0.436	0.440	-0.004	-3.15	1.674	1.652	0.022
3.50	0.443	0.390	0.053	-3.50	1.765	1.660	0.105
3.85	0.430	0.420	0.010	-3.85	1.681	1.655	0.026
4.20	0.443	0.398	0.045	-4.20	1.720	1.647	0.073
4.55	0.455	0.409	0.046	-4.55	1.794	1.671	0.123
4.90	0.464	0.399	0.065	-4.90	1.758	1.659	0.099
5.25	0.447	0.381	0.066	-5.25	1.700	1.655	0.045
5.60	0.443	0.388	0.055	-5.60	1.720	1.651	0.069
5.95	0.430	0.394	0.036	-5.95	1.751		

APPENDIX 16 Example Calculation of the Effective Diffusion Coefficient by Monitoring the Rise in Ionic Concentration of the External Solution.

By monitoring the amount of "substance" diffusing out of a unit area of cement paste it is possible to calculate the effective diffusion coefficient of that "substance" in the cement by using a solution to Fick's 2nd law of diffusion [ref. 87],

$$Mt = 2C_o\sqrt{\frac{Dt}{\pi}} \quad \text{or,}$$

$$\sqrt{D} = \frac{Mt}{\sqrt{t}}\frac{\sqrt{\pi}}{2C_o}$$

where, C_o = original concentration of "substance" in the cement paste (mM cm^{-3})

t = time (sec.)

D = effective diffusion coefficient ($cm^2 s^{-1}$)

For graphs 3.13 to 3.15 (chapter 4), slope S' is in units of mM $litre^{-1}$ $day^{-\frac{1}{2}}$.

For the calculation we require a value of S, $(\frac{Mt}{\sqrt{t}})$ in units of mM cm^{-2} $s^{-\frac{1}{2}}$

ie $$S = \frac{S' \times \text{Volume of solution}}{\text{Total exposed cement paste area} \times 293.94^*}$$

(* to change $days^{\frac{1}{2}}$ to $s^{\frac{1}{2}}$)

Since, 12 specimens were exposed to 5 litres of solution,

Volume of sol. = 5 litres

Total area of cem= $(\frac{4.8}{2})^2 \times \pi \times 12 = 217.15\ cm^2$

$$S = S' \times 7.833 \times 10^{-5}$$

and, $$\sqrt{D} = S' \times \frac{\sqrt{\pi}}{2C_o} \times 7.833 \times 10^{-5}$$

Example Calculation of D for Na^+

Slope S' of figure 4.13 can be calculated as in appendix 13 ie best fit equation is,

$$y = -0.050 + 1.235x$$

(Correlation Coefficient r = 1.000)

$$S' = 1.235 \text{ mM litre}^{-1} \text{ day}^{-\frac{1}{2}}$$

From, $$\sqrt{D} = S' \times \frac{\sqrt{\pi}}{2C_o} \times 7.833 \times 10^{-5} \qquad (A)$$

where, $$C_o = 566 \text{ mM litre}^{-1} = 0.566 \text{ mM cm}^{-3}$$

$$D = 17.2 \times 10^{-9} \text{ cm}^2\text{s}^{-1}$$

Estimation of D for Ca^{++}

Molar weight of $Ca(OH)_2$ = 74.1

74.1 g $Ca(OH)_2$ = 1000 mM Ca^{++}

From table 5.10,

1g OPC-B' contains 0.284g $Ca(OH)_2$

ie contains 3.833 mM Ca^{++}

Assume Evaporable Water of cement = $0.35 \text{cm}^3/\text{g}$ (table 4.11) and assume all $Ca(OH)_2$ is available for diffusion,

$$\therefore \text{ "Free" } Ca^{++} = \frac{\text{Amount of } Ca^{++} \text{ in mM cm}^{-3}}{We}$$

$$= 10.95 \text{ mM cm}^{-3}$$

From fig. 4.15 slope S' of line A = 7.0 mM $\text{litre}^{-1}\text{day}^{-\frac{1}{2}}$

From (A),

$$D \sim 2.0 \times 10^{-9} \text{ cm}^2\text{s}^{-1}$$

APPENDIX 17 Calculation of "variable" D for Σ^+ ions at various depths into OPC-B' paste exposed to water for 165 days.

The conc. profile of fig. 4.19 is assumed as half of that in fig. 4.1 as shown below (ie LP), P being the surface of the specimen.

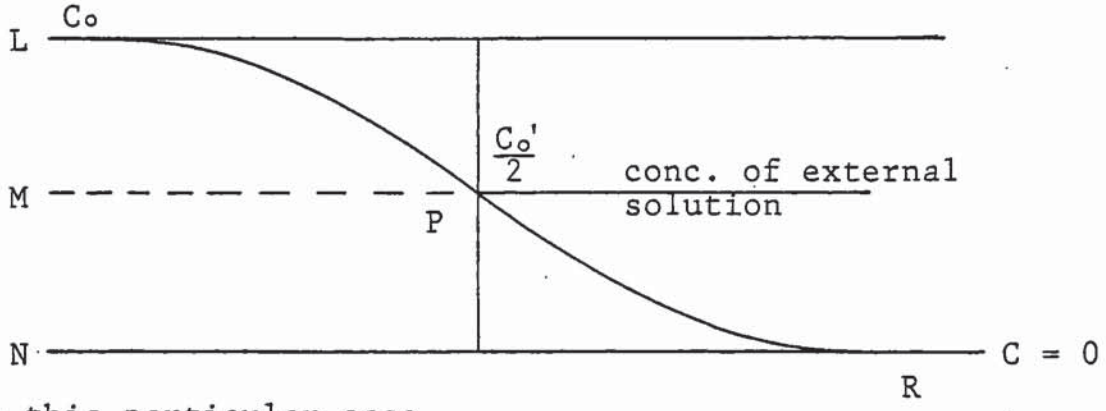

In this particular case,

$$C_o' = 900 \text{ mM/l}$$

and, $\frac{C_o'}{2} = 0$ (ie conc. of external solution)

Values should therefore be adjusted so that C = 0 is at R and not at P.

as, $\bar{MN} = LM = 900$ mM/l

the adjustment is,

$$C_o = C_o' + 900$$
$$C_x = C_x' + 900$$
$$\frac{C_o}{2} = \frac{C_o'}{2} + 900 = 900 \text{ mM/l}$$

Calculations of D can then be carried out as in appendix 10 using the following equation:

$$C_x = \frac{C_o}{2}[1+\text{erf}(y)]$$ see appendix 9 case 1.

For Σ^+ ions

C_x' mM/l	C_x mM/l	erf(y)	y	x cm	r	c cm	b cm	D cm^2/s
90	990	0.100	0.088	0.175				($x10^{-9}$)
165	1065	0.183	0.166	0.35		-0.022	2.244	88.3
326	1226	0.362	0.334	0.70		-0.008	2.126	79.3
465	1365	0.517	0.493	1.05	0.999	-0.021	2.149	81.0
518	1418	0.576	0.560	1.40	0.990	-0.067	2.442	104.6
613	1513	0.681	0.704	1.75	0.993	-0.092	2.550	114.0
637	1537	0.708	0.745	2.10	0.987	-0.151	2.778	135.3
732	1632	0.813	0.940	2.45	0.992	-0.149	2.771	134.6
748	1648	0.831	0.977	2.80	0.991	-0.192	2.897	147.2
804	1704	0.893	1.147	3.15	0.994	-0.196	2.906	148.1
807	1707	0.897	1.160	3.50	0.992	-0.243	3.022	160.1
796	1696	0.884	1.119	3.85	0.982	-0.316	3.209	180.6
859	1759	0.954	1.420	4.20	0.986	-0.309	3.196	179.1
851	1751	0.946	1.364	4.55	0.985	-0.367	3.313	192.5
871	1771	0.968	1.510	4.90	0.987	-0.401	3.374	199.7

Considering values up to x = 0.35cm, the slope of the plot x v's y (see fig. 4.18) can be calculated and,

$$b_{0.35} = 2.244\text{cm}$$

$$D_{0.35} = 88.3 \times 10^{-9}\ \text{cm}^2\text{s}^{-1}$$

Similarly by concidering values up to x = 0.7cm,

$$b_{0.7} = 2.126\text{cm}$$

$$D_{0.7} = 79.3 \times 10^{-9}\ \text{cm}^2\text{s}^{-1}$$

intercept $c_{0.7} = -0.008\text{cm}$

etc. up to the depth of 4.9cm (see table above).

Note:

An assumption was made in the above calculations that the line of the slope b was linear, which is not strictly true but an alternative method of calculating the effective diffusion coefficient D, (similar to ref. 88) would involve complex mathematical treatments which are beyond the scope of this work. Values of D should be seen only as good estimates.

APPENDIX 18 Estimation of the "correction" factor for the effective diffusion coefficients determined by methods requiring the cross-sectional-area of the cement paste.

Require to work out the cross-sectional fraction of pore area as compared to the total cross-sectional area of the cement paste.

From We, Wn determinations of table 4.2 (see for example appendix 2) work out comparative weights of cement paste at the three stages:

Fully hydrated	Dried at 105°C	Ignited at 950°C
1g	0.78g	0.64g
	1g	0.82g

From Mercury Intrusion work (fig.4.21 no 4)

Total pore volume = 0.2 cm^3/g of cement dried at 105°C
= 0.24 cm^3/g of ignited cement

For a cylindrical specimen 4.8 cm dia x 7.5 cm high

160g of unhydrated cement give a volume of 136cm^3
1g " " " " 0.85cm^3

ie 0.85cm^3 of hydrated cement give 0.24 cm^3 of pores
1 cm^3 " " " 0.28 cm^3 of pores

Assuming a uniform pore distribution,

Pore cross-sectional area fraction = $\sqrt[3]{0.28}$ = 0.43 cm^2

To 'correct" effective diffusion coefficients calculated by the "thin-disc" method, ie for OH^- in OPC-B pre-cured in sat.$Ca(OH)_2$ (table 3.9),

$$D = 90.1 \times 10^{-9} \ cm^2 s^{-1}$$

$$\text{"CORRECTED" } D = \frac{90.1}{0.43} \times 10^{-9} = 209.5 \times 10^{-9} \ cm^2 s^{-1}$$

APPENDIX 19 Estimation of amount of diffused substance from within OPC-B' pastes into the outer solution.

Example calculation for Na^+ ions (chapter 4 part II)

Length of cylindrical cement paste = 7.5 cm
Mass of hydrated cement paste $\sim$240 g
Mass of original dry cement $\sim$160 g (0.5 W/C)

Consider the exposed cylinder up to a depth of 6.125 cm
This is divided into 17, 0.35cm discs.

Note: The first 0.175cm near the surface is ignored as the conc. can be considered negligible after diffusion had taken place.

For a length 6.125 cm mass = 130.6 g
for a length 0.35 cm mass = 7.5 g

Consider Na^+:

Assume original conc. (table 4.9) = 655 mM/l
assume average We (table 4.11) = 0.35 g/g

$$\text{Free amount of } Na^+ = \frac{655 \times 0.35}{1000} = 0.229 \text{ mM/g}$$

For a length of 6.125 cm,

$$\text{Total } Na^+ = 0.229 \times 130.6 = 29.9 \text{ mM}$$

After diffusion had taken place:

Add-up individual concentrations (table 4.9)

$$\text{ie } 122 + 243 + \cdots + 659 = 8813 \text{ mM/l}$$

$$\text{Total } Na^+ = \frac{8813 \times 0.35}{1000} \times 7.5 = 23.1 \text{ mM}$$

Amount of "lost" Na^+ = 29.9 - 23.1 = 6.8 mM

There are 12 cylinders exposed to 5 litres of solution

$$\text{Final conc. of sol.} = \frac{6.8 \times 12}{5} = 16.3 \text{ mM/l}$$

APPENDIX 20 Increase in carbonation depths with time, of OPC-B' pastes with or without a 1% Cl^- addition exposed to various atmospheres.

t (day)	$\sqrt{t}$ ($day^{\frac{1}{2}}$)	100% CO_2 DEPTH (μm)	5% CO_2 DEPTH (μm)	5% CO_2 +Cl^- DEPTH (μm)	AIR DEPTH (μm)	AIR +Cl^- DEPTH (μm)
13	3.61	COMPLETE	-	-	-	-
20	4.47		100	150	-	-
37	6.08			340	-	-
46	6.78		300	600	-	-
73	8.54		990	1480	-	-
108	10.39		1500	COMPLETE	-	-
160	12.65		COMPLETE		-	100
164	12.81				-	160
199	14.11				190	340
213	14.59				320	440
266	16.31				660	850
327	18.08				940	1280
441	21.00				1450	COMPLETE
458	21.40				COMPLETE	

APPENDIX 21 Calculation of carbonates and bicarbonates of the pore solution of carbonated cement pastes.

Example calculation of specimen B2 (table 5.2)

To titrate 1ml of solution down to pH 4 it required 18ml of 1M HNO_3

For bicarbonates we have:

$$HCO_3^- + H^+ \longrightarrow H_2CO_3$$

$$m=\frac{m'v'}{v}$$

where,

m = molarity of solution (HCO_3^-)
v = volume of solution
m'= molarity of acid
v'= volume of acid

$$m = \frac{1 \times 18}{1} = 18 \text{ mM/1 } HCO_3^-$$

For carbonates we have:

$$CO_3^{2-} + 2H^+ \longrightarrow 2HCO_3^-$$

$$2HCO_3^- + 2H^+ \longrightarrow 2H_2CO_3$$

ie two lots of acid are required to titrate CO_3^{--}

From ionization constants:

Primary ioniz. const. $\dfrac{[H^+][CO_3^{--}]}{[HCO_3^-]} = 5 \times 10^{-11}$

at pH 10.48 (table 5.2), $[H^+] = 3.31 \times 10^{-11}$ ($pH=-\log_{10}[H^+]$)

$$\frac{[CO_3^{2-}]}{[HCO_3^-]} = \frac{5 \times 10^{-11}}{3.31 \times 10^{-11}} = 1.51$$

If $y = CO_3^{2-}$ & $x = HCO_3^-$ then $y = 1.51x$ (1)

As twice as much acid is required for CO_3^{2-} we also have,

$$x + 2y = 18 \text{ (mM/1)(2)}$$

sub. (1) into (2):

$x + 3.02x = 18$ ie $4.02x = 18$ and $x = 4.4$

From (1) $y = 1.51 \times 4.4 = 6.6$

$HCO_3^- = 4$ mM/1 and $CO_3^{2-} = 7$ mM/1

APPENDIX 22

A. Calculation of the amount of CO_2 required to carbonate 1g of OPC-B' paste.(by wt of unhydrated cement)

Calculate the amount required for each of the main oxides separately:

CaO. $CaO + CO_2 \longrightarrow CaCO_3$

56.08g 44.00g

0.634g* 0.4974g

* Amount of CaO in 1g of cement (table 2.1a)

MgO. $MgO + CO_2 \longrightarrow MgCO_3$

40.32g 44g

0.012g 0.0131g

Na_2O. $Na_2O + CO_2 \longrightarrow Na_2CO_3$

61.96g 44g

0.004g 0.0028g

K_2O. $K_2O + CO_2 \longrightarrow K_2CO_3$

94.02g 44g

0.005g 0.0023g

Total CO_2 required for complete neutralization =

$= 0.4974 + 0.0131 + 0.0028 + 0.0023 = 0.5156g$

ie 1g of cement requires 0.52g CO_2 for neutralization of which 0.50g is required just by the CaO.

B. Calculation of the amount of acid required to neutralize 1g of cement paste.

Example for OPC-B':

Calculate the amount required for each of the main oxides seperately:

CaO. $CaO + 2HNO_3 \longrightarrow Ca(NO_3)_2 + H_2O$

56.08g 2 moles

0.634g 22.6 mM

MgO. $MgO + 2HNO_3 \longrightarrow Mg(NO_3)_2 + H_2O$

40.32g 2 moles

0.012g 0.6 mM

Na_2O. $Na_2O + 2HNO_3 \longrightarrow 2NaNO_3 + H_2O$

61.96g 2 moles

0.004g 0.1 mM

K_2O. $K_2O + 2HNO_3 \longrightarrow 2KNO_3 + H_2O$

94.02g 2 moles

0.005g 0.1 mM

Total acid = 22.6 + 0.6 + 0.1 + 0.1 = 23.4 mM

For 1M HNO_3 where 1000 ml of acid contain 1000mM

Total acid = 23.4 ml (required to neutralize 1g of cement by wt of unhydrated cement)

Need to calculate how much acid is required to neutralize 1g of hydrated cement.

From table 5.11 total water of OPC-B' cement =

= 0.245 + 0.197 = 0.442g

1g of cement = 1.442 g of hydrated cement

ie 1.442g hydrated cement requires 23.4 ml of acid

and 1g " " " 16.2 ml of acid

APPENDIX 23 Change of OH^- concentration and pH of 5g of hydrated cement with addition of 1M HNO_3 (mean of 4 values)

ml of 1M HNO_3	OH^- CONC.		pH	
	OPC-B'	SRPC	OPC-B'	SRPC
0	73.0	64.0	12.86	12.81
0.3	60.5	55.5	12.78	12.74
0.6	57.5	51.5	12.76	12.71
0.9	49.0	46.0	12.69	12.66
1.2	48.0	45.5	12.68	12.66
1.6	45.0	42.5	12.65	12.63
2.0	44.0	42.5	12.64	12.63
3	40.5	38.0	12.61	12.58
4	39.5	38.0	12.60	12.58
5	37.0	36.5	12.57	12.56
6	36.0	35.5	12.56	12.55
7	36.5	36.5	12.56	12.56
8	35.5	35.5	12.55	12.55
9	36.0	36.5	12.56	12.56
10	36.0	36.0	12.56	12.56
11	36.0	36.0	12.56	12.56
12	35.5	36.0	12.55	12.56
14	36.0	36.5	12.56	12.56
16	36.0	36.0	12.56	12.56
18	36.5	37.5	12.56	12.57
20	36.0	35.5	12.56	12.55
22	37.5	37.0	12.57	12.57
25	35.5	35.5	12.55	12.55
28	28.5	21.0	12.45	12.32
31	14.4	11.4	12.16	12.06
34	7.0	5.5	11.85	11.74
37	5.1	4.3	11.71	11.63
40	3.4	2.5	11.53	11.40
43	1.8	1.6	11.26	11.20
46	1.2	1.2	11.08	11.08
49	–	1.15	–	11.06
52	1.13	1.04	11.05	11.02
55	0.89	0.88	10.95	10.94
58	0.80	0.83	10.90	10.92
62	0.69	0.92	10.84	10.96
66	0.47	0.08	10.67	9.92
69	0.08	*	9.92	*
71	*		*	

* Complete neutralization as indicated by phenolphthalein.

ml of 1M HNO_3	OH^- CONC.		pH	
	OPC-B'/ 30% PFA	OPC-B'/ 65% BFS	OPC-B'/ 30% PFA	OPC-B'/ 65% BFS
0	78.5	59.0	12.89	12.77
0.3	74.5	57.5	12.87	12.76
0.6	67.0	54.0	12.83	12.73
0.9	54.5	48.0	12.74	12.68
1.2	53.5	47.5	12.73	12.68
1.6	52.5	43.0	12.72	12.63
2.0	46.5	37.0	12.67	12.57
3	37.5	23.5	12.57	12.37
4	33.5	19.5	12.53	12.29
5	24.0	13.5	12.38	12.13
6	17.0	11.0	12.23	12.04
7	12.0	9.0	12.08	11.95
8	9.0	7.5	11.95	11.88
9	6.9	6.5	11.84	11.81
10	6.5	6.0	11.81	11.78
11	5.0	5.5	11.70	11.74
12	4.5	5.4	11.65	11.73
13	4.0	4.9	11.60	11.69
14	3.9	4.5	11.59	11.65
16	2.5	2.8	11.40	11.45
18	1.6	2.2	11.20	11.34
20	1.5	2.0	11.18	11.30
22	1.5	1.9	11.18	11.28
25	1.0	1.4	11.0	11.15
28	#	0.97	#	10.99
31		0.57		10.76
34		0.51		10.71
37		0.33		10.52
40		0.28		10.45
43		0.20		10.30
46		0.03		9.48
47		*		*

PFA-based cements gellified.

* Complete neutralization as indicated by phenolphthalein.

APPENDIX 24 Calculation of Free $Ca(OH)_2$ in Hardened Cement Paste.

A. Actual amount of $Ca(OH)_2$ calculated from the "buffering" experiment (chapter 5 part II). Example calculation for OPC-B'.

Length of plateau at pH 12.6 in fig. 5.16 is 24.2 ml.

ie 5g of OPC-B' required 24.2 ml of 1M HNO_3 to neutralize the soluble $Ca(OH)_2$.

$\therefore$ 1g of OPC-B' required $\frac{24.2}{5}$ = 4.84 ml acid.

From the neutralization reaction:

$$Ca(OH)_2 + 2HNO_3 \longrightarrow Ca(NO_3)_2 + 2H_2O$$

74.08g 2000mM

As 1ml of acid contains 1mM, 4.84ml neutralize 0.179g of $Ca(OH)_2$.

Because the added acid always replaced the same amount of solution which was removed for analysis, an equal amount of sat. $Ca(OH)_2$ solution was removed during that period.

ie 24.2 ml of sat.$Ca(OH)_2$

Assume sat.$Ca(OH)_2$ = 36 mM/l

ie 1000 ml = 36 mM

24.2 ml = 0.87 mM $Ca(OH)_2$

for 1g = $\frac{0.87}{5}$ = 0.174 mM

Also at the end of the plateau there remains in the syringe 10 ml of solution which is approximately sat.$Ca(OH)_2$

as above, 10 ml = 0.36 mM $Ca(OH)_2$

and for 1 g = $\frac{0.36}{5}$ = 0.072 mM

1000 mM of $Ca(OH)_2$ = 74.08 g

(0.174 + 0.072) mM= 0.018 g

Total $Ca(OH)_2$ = 0.179 + 0.018 = 0.197 g

From table 5.11,

Weight of hydrated cement = 1 + We + Wn
= 1 + 0.245 + 0.197
= 1.442 g/g of ignited cement

since, 1g hydrated cement = 0.197 g $Ca(OH)_2$
then 1g ignited cement = 0.197 x 1.442
= 0.284 g $Ca(OH)_2$

B. Theoretical amount of $Ca(OH)_2$ in OPC-B'.

Reactions of C_3S & C_2S phases of OPC with water to form C-S-H gel and $Ca(OH)_2$ are as follows: [ref. 171]

For C_3S $2Ca_3SiO_5 + 6H_2O \longrightarrow Ca_3Si_2O_7.3H_2O + 3Ca(OH)_2$

For C_2S $2Ca_2SiO_4 + 4H_2O \longrightarrow Ca_{3.3}Si_2O_{7.3}.3.3H_2O +$
$+ 0.7\ Ca(OH)_2$

ie 456.8g C_3S gives 222.2g $Ca(OH)_2$

From table 2.1b,

0.434g C_3S gives 0.211g $Ca(OH)_2$

344.6g C_2S gives 51.9g $Ca(OH)_2$

0.252g C_2S gives 0.038g $Ca(OH)_2$

TOTAL $Ca(OH)_2$ = 0.211 + 0.038

ie 1g ignited cement = 0.249 g $Ca(OH)_2$

APPENDIX 25 Theoretical maximum amount of chloride that can be complexed by the C_3A phase of the SRPC paste.

Approximate formula for C_3A is:

$$3CaO.Al_2O_3.CaCl_2.10H_2O$$

By considering atomic weights,

270.2g C_3A binds 70.9g Cl^-

From table 2.1b SRPC contains 0.019g C_3A per g of cement

ie 0.019g C_3A binds 0.005g Cl^-

35.45g Cl^- = 1mole

ie 0.005g Cl^- = 0.141 mM

MAXIMUM AMOUNT OF Cl^- BOUND BY THE C_3A PHASE IN SRPC IS:

0.141 mM/g

REFERENCES

1) "The Durability of Reinforced Concrete Buildings"
National Building Studies Spec. Rep. No.25
(HMSO, London, 1956)

2) "The Durability of Steel in Concrete: Part I
Mechanism of Protection and Corrosion"
Building Research Establishment Digest no.263
(July 1982)

3) POPOVICS, S., SIMEONOV, Y, BOZHINOV, G. &
BAROVSKY, N.
"Durability of Reinforced Concrete in Sea-water"
Int. Conf. Corrosion of Reinforcements in concrete
Construction, A.P. Crane Ed., Soc. of Chem. Industry
(London 1983) pp 19-38.

4) CADY, P.D.
"Corrosion of Reinforcing Steel in Concrete - A general
overview of the problem"
Chloride Corrosion of Steel in Concrete, ASTM STP 629,
D.E. Tonini and S.W. Dean, Jr., Eds., (1977) pp 3-11.

5) MAYER, A.
"Investigations of the Carbonation of Concrete"
Supplementary Paper III-52, 5th International Symp.
Chemistry Cem., Proc., Part 3 (Tokyo 1968) pp 394-401

6) AKIBA, T., MINEGISHI, K. & SUDOH, G.
"Mechanisms and Kinetics on Neutralization of Concrete
in Sea-water"
7th Int. Symp. Chem. Cem., Vol. III (Paris 1980)
Communication VII-57 - VII-62.

7) TREADAWAY, K.W.J., MACMILLAN, G., HAWKINS, P. &
FONTENAY, C.
"The influence of concrete quality of carbonation in
Middle Eastern conditions - A preliminary study".
Corrosion of Reinforcements in Concrete Construction,
Proc., Soc. of Chem. Industry (London 1983) pp 101-118

8) HANSSON, C.M.
"Comments on electrochemical measurements of the rate
of corrosion of steel in concrete"
Cement and Concrete Res. 14, (1984) pp 574-584

9) HOLDEN, W.R., PAGE, C.L. & SHORT, N.R.
"The influence of chlorides and sulphates on durability of reinforcement in concrete".
Int. Conf. Corr. of Reinforcements in Concrete Construction, A.P. Crane Ed., Soc. of Chem. Industry (London 1983) pp 143-150.

10) British Standard Code of Practice, CP 110 part 1: 1972 (Ammended May 1977).

11) KILARESKI, W.P.
"Epoxy Coatings for corrosion protection of reinforcement steel"
Chloride Corrosion of Steel in Concrete, ASTM STP 629, D.E. Tonini and S.W. Dean, Jr., Eds., (1977) pp 82-88.

12) COOK, A.R. & RADTKE, S.F.
"Recent Research on galvanized steel for reinforcement of concrete". ibid pp 51-60.

13) TRFADAWAY, K.W.J., BROWN, B.L. & COX, R.N.
"Durability of galvanized steel in concrete"
Corrosion of Reinforcing Steel in Concrete, ASTM STP 713, D.E. Tonini and J.M. Gaidis, Eds., (1980) pp 102-131.

14) FOWLER, D.W., PAUL, D.R. AND YIMPRASERT, P.
"Corrosion protection of reinforcing provided by polymer-impregnated concrete".
Journal of the American Concrete Institute, Proc., 75, 53, (1978) pp 520-525.

15) KUKACKA, L.E.
"The use of concrete polymer materials for bridge deck applications".
Chloride Corrosion of Steel in Concrete, ASTM STP 629, D.E. Tonini and S.W. Dean, Jr., Eds., (1977) pp 100-109.

16) STEELE, G.W. and JUDY, J.M.
"Polymer-Modified Concretes in Bridge Deck Overlay Systems".
ibid pp 110-115

17) BLANCO, M.T., ANDRADE, C. AND MACIAS A.
"SEM study of the corrosion products of galvanized reinforcements immersed in solutions in the pH range 12.6 to 13.6"
British Corrosion Journal, 19, 1, (1984) pp 41-48.

18) SERGI, G., SHORT, N.R. AND PAGE, C.L.
"Corrosion of galvanized and galvannealed steel in solutions of pH 9.0-14.0"
Corrosion-NACE, 41, 11, (1985) pp 618-624.

19) UNZ, M.
"Performance of Galvanized reinforcement in calcium hydroxide solution".
Journal of the American Concrete Institute, Proc., 75, 13, (1978) pp 91-99.

20) DIAMOND, S.
"Cement paste microstructure"
Conf. on Hydraulic Cement Pastes: Their Structure and Properties, Proc., (Sheffield 1976) Cement and Concrete Association, Slough, pp 2-30.

21) LONGUET, P., BURGLEN, L. and ZELWER, A.
"La phase liquid du ciment hydraté".
Revue Matériaux de Construction et Travaux Publics, 676 (1973) pp 35-41

22) BARNEYBACK, R.S. Jr, and DIAMOND, S.
"Expression and analysis of pore fluids from hardened cement pastes and mortars".
Cement and Concrete Research 11, (1981) pp 279-285

23) SAMARAI, M.A.
"The disintegration of concrete containing sulphate-contaminated aggregates".
Magazine of Concrete Research 28, 96, (1976) pp 130-142.

24) MEHTA, P.K.
"Effect of cement composition on corrosion of reinforcing steel in concrete".
Chloride Corrosion of Steel in Concrete, ASTM STP 629, D.E. Tonini and S.W. Dean, Jr., Eds., (1977) pp 12-19.

25) Private communication with K.W.J. Treadaway, Building Research Establishment, Garston, Watford.

26) PAGE, C.L.
"Mechanism of Corrosion protection in reinforced concrete marine structures".
Nature 258, (1975) pp 514-515.

27) REGOURD, M.
"Structure and behaviour of slag portland cement hydrates".
7th Int. Conf. on the Chemistry of Cement, Proc., VOL III (Paris 1980) Communication III-2/10-III2/26

28) PAGE, C.L., SHORT, N.R. & EL TARRAS, A.
"Diffusion of chloride ions in hardened cement pastes"
Cement and Concrete Research 11, 3, (1981) pp 395-406.

29) NURSE, P.W.
"Slag Cements - chapter 13 - The Chemistry of Cements"
VOL 2, Editor, Taylor H.F.W,
Pub. Academic Press (1964) pp 37-67.

30) VOGEL, A.I.
"A text-book of quantitative inorganic analysis"
Third edition. Pub: Longmans, 1961. pp. 808-809

31) ibid. pp 742

32) LEA, F.M.
"The Chemistry of Cement and Concrete"
Third Edition. Pub: Edward Arnold, 1970. pp 270-279

33) BRITISH STANDARD 4550: part 2: section 13.2
"Loss-on-ignition"
(1970).

34) LAMBERT, P.
"The corrosion and passivation of steel in concrete"
PhD. Thesis, Aston University.
(1983)

35) BERMAN, H.A.
"Determination of chloride in hardened portland cement paste, mortar and concrete"
Journal of Materials, 7, 9 (1972) pp 330-335.

36) BRAGG, L.
"The crystalline state. Volume I. A general survey"
Pub: Bell, 1949.

37) TAYLOR, H.F.W. (Editor)
"The chemistry of cements" Volume 2. Appendix I.
Pub: Academic Press, 1964. pp 347-404.

38) WASHBURN, E.W.
"Porosity I. Purpose of investigation. II. Porosity and the mechanism of absorption"
Journal of the American Ceramic Society, 4 (1921)
pp 916-922.

39) WINSLOW, P.M. & DIAMOND, S.
"A Mercury Porosimetry Study of the Evolution of Porosity in Portland Cement" Journal of Materials, 5, 3, (1970) pp 564-585.

40) ANDRADE, C, GONZALEZ, J.A.
"Quantitative measurements of corrosion rate of reinforcing steels embedded in concrete using polarization resistance measurements"
Werkstoffe und Korrosion 29,(1978) pp 515-519.

41) GONZALEZ, J.A., ALGABA, S. AND ANDRADE, C.
"Corrosion of reinforcing bars in carbonated concrete"
British Corrosion Journal 15,3,(1980). pp 135-139.

42) GONZALEZ, J.A., ALONSO, C. AND ANDRADE, C.
"Corrosion rate of reinforcements during accelerated carbonation of mortar made with different types of cement" Int. Conf. Corrosion of Reinforcements in Concrete Construction, A.P. Crane, Ed., Soc. of Chem. Industry (London 1983) pp 159-174.

43) PAGE, C.L.& HAVDAHL, J. "Electrochemical monitoring of corrosion of steel in microsilica cement pastes" Matériaux et Constructions 18, 103, (1985) pp 41-47

44) STERN, M. & GEARY, A.L.
"A theoretical analysis of the shape of polarization curves"
J. of The Electrochemical Society, 104 (1957) pp 56-63

45) STERN, M.
"A method for determining corrosion rates from linear polarization data".
Corrosion- NACE, 14, 9 (1958) pp 60-64.

46) PETERSON, W.M. and SIEGERMAN, H.
"A microprocessor-based corrosion measurement system"
A.S.T.M. Special Technical Publication, 727 (1981) pp 390-406.

47) GONZALEZ, J.A., MOLINA, A., ESCUDERO, M.L., and ANDRADE C.
"Errors in the electrochemical evaluation of very small corrosion rates. Part I: Polarization resistance method applied to corrosion of steel in concrete"
Corrosion Science 25, 10, (1985) pp 917-930.

48) MANSFELD, F., KENDIG, M.W., and TSAI, S.
"Evaluation of Corrosion behaviour of coated metals with AC-impedance measurements"
Corrosion-NACE, 38, 9(1982). pp 478-485

49) DAWSON, J.L.
"Corrosion monitoring of steel in concrete"
Int. Conf. Corrosion of Reinforcements in Concrete Construction, A.P. Crane Ed., Soc. of Chem. Industry (London 1983) pp 175-191.

50) GONZALEZ, J.A., MOLINA, A., ESCUDERO, M.L., and ANDRADE, C.
"Errors in the electrochemical evaluation of very small corrosion rates. Part II: Other electrochemical techniques applied to corrosion of steel in concrete".
Corrosion Science 25, 7, (1985) pp 519-530

51) E.G. & G. PRINCETON APPLIED RESEARCH (USA)
"Basics of a.c. impedance measurements"
Application Note AC-1 (1984).

52) HLADKY, K., CALLOW, L.M., DAWSON, J.L.
"Corrosion rates from impedance measurements: An introduction".
British Corrosion Journal, 15, 1, (1980), pp 20-25.

53) ANDRADE, C., and CASTELO, V.
"Practical measurement of the AC impedance of steel bars embedded in concrete by means of a spectrum analyser (Fast Fourier Transform)".
British Corrosion Journal, 19, 2, (1984) pp 98-100.

54) KAY, E.A., FOOKES, P.G., & POLLOCK, D.J.
"Deterioration related to chloride ingress".
Concrete 15, 11, (1981) pp 22-28.

55) SORENSEN, B. & MAAHN, E.
"Penetration rate of chloride in marine concrete structures" Nordic Concrete Research 1,(1982) pp24.1 -24.8

56) HAUSMAN, D.A.
"Steel corrosion in concrete" Materials Protection 6,11, (1967) pp 19-23

57) TUUTTI, K.
"Corrosion of steel in concrete" Swedish Cement & Concrete Institute S-100 44-CBI Forskning Research fo. 4.82 Stockholm (1982).

58) GOUDA, V.K.
"Corrosion and corrosion inhibition of reinforcing steel - I. Immersed in alkaline solutions"
British Corrosion Journal, 5, (1970). pp 198-203.

59) GOUDA, V.K. & HALAKA, W.Y.
"Corrosion and corrosion inhibition of reinforcing steel - II. Embedded in concrete".
British Corrosion Journal, 5, (1970) pp 204-208.

60) PAGE, C.L. & TREADAWAY, K.W.
"Aspects of the electrochemistry of steel in concrete"
Nature 297, 5862 (1982) pp 109-115.

61) TRAETTEBERG, A.
"The Mechanism of chloride penetration in concrete"
Report by: Cement & Concrete Research Institute
Trondheim, Norway STF65 A77070 (1977)

62) MIDGLEY, H.G. & ILLSTON, J.M.
"Effect of chloride penetration on the properties of hardened cement pastes"
7th International Conf. on the Chemistry of Cement, Proc., VOL III, Paris (1980) Communication VII-101 -VII-103.

63) MIDGLEY, H.G. & ILLSTON, J.M.
"The penetration of chlorides into hardened cement pastes".
Cement & Concrete Research, 14, 4, (1984) pp 546-558.

64) OST, B. & MONFORE, G.E.
"Penetration of chloride into concrete"
Journal of the PCA research & Development Laboratories, 8, 1, (1966) pp 46-52

65) JOST, W.
"Diffusion of solids, liquids, gases"
Pub: Academic Press, 1952. pp163-164

66) SPINKS, J.W.T., BALDWIN, H.W. & THORVALDSON, T.
"Tracer Studies of Diffusion in set portland cement"
Canadian Journal of Technology, 30 (1952) pp 20-28

67) COLLEPARDI. M., MARCIALIS, A. & TURRIZIANI, R.
"The penetration of de-icing agents in cement pastes"
I1 Cemento 3, (1972) pp 143-149.

68) COLLEPARDI, M., MARCIALIS, A. & TURRIZIANI, R.
"The kinetics of penetration of chloride ions into the concrete"
I1 Cemento. 4, (1970) pp 157-163.

69) COLLEPARDI, M., MARCIALIS, A. & TURRIZIANI, R.
"Penetration of chloride ions into cement pastes and concretes"
Journal of the American Ceramic Society 55, 10 (1972) pp 534-535

70) BARRER, R.M.
"Diffusion in and through solids"
Pub: Cambridge University Press, 1951 pp 7-12

71) JOST, W.
"Diffusion in solids, liquids, gases"
Revised edition. Pub: Academic Press, 1960, pp 62.

72) ROBERTS, M.H.
"Effect of pretensioned wire in prestressed concrete"
Magazine of Concrete Research, 14, 42 (1962)
pp 143-154.

73) VERBECK, G.J.
"Mechanisms of corrosion of steel in concrete"
Corrosion of Metals in Concrete, SP-49, American
Concrete Institute, Detroit, (1975). pp 21-38.

74) VERBECK, G.J.
"Field and laboratory studies of the sulphate resistance of concrete"
Performance of Concrete, E.G. Swenson, Technical
Editor, Canadian Building Series no. 2, University
of Toronto Press, (1968). pp 113-124.

75) HANSSON, C.M., STRUNGE, H., MARKUSSEN, J.B & FRØLUND,T.
"The Effect of Cement type on the diffusion of chlorde"
To be published in Nordisk Betong.

76) HJORTH, L.
"Cement specifications for concrete exposed to chlorides and sulphates"
Presented at CANMET conference (Oct. 1984).

77) KONDO, R., SATAKE, M. & USHIYAMA, H.
"Diffusion of various ions in hardened portland cement"
Cement Association of Japan, 28th General Meeting,
Tokyo (1974) pp 41-43.

78) GOTO, S., & ROY, D.M.
"Diffusion of ions through hardened cement pastes"
Cement and Concrete Research, 11, 5, (1981) pp 751-757.

79) ATKINSON, A. & NICKERSON, A.K.
"The Diffusion of ions through water-saturated cement"
Journal of Materials Science, 19 (1984) pp 3068-3078

80) PARSONS, R.
"Handbook of Electrochemical Constants"
Pub: Butterworth, London (1959) p 79.

81) USHIYAMA, H. & GOTO, S.
"Diffusion of various ions in hardened portland cement paste"
The 6th International Congress on the Chemistry of Cement, Supplementary Paper, Section II,II-3,4,5, Moscow (1974) pp 331-337

82) UCHIKAWA, H., UCHIDA, S. & OGAWA, K.
"DIffusion of alkali ions in hardened cement paste containing slag or fly-ash".
Review of the 38th General Meeting of the Cement Association of Japan, 10, (1984) pp 56-59.

83) TAKAGI, T., GOTO. S. & DAIMON, M.
"Diffusion of I^- ion through hardened cement paste"
Review of the 38th General Meeting of the Cement Association of Japan, 14, (1984) pp 72-75.

84) SHAW, D.J.
"Introduction to colloid and surface chemistry"
Second Edition. Pub. Butterworths, 1970. pp 133-166

85) BAKKER, R.F.M.
"On the cause of increased resistance of concrete made from blast furnace cement to the alkali-silica reaction and to sulphate corrosion".
Doctoral Thesis- Maastricht, The Netherlands.
(June 1980). RWTH, Aachen, FRG.

86) EFES, Y.
"Effect of cements with varying content of granulated blast furnace slag on chloride diffusion in concrete"
Betonwerk+Fertigteil-Technik, Heft 4 (1980) pp 224-228, 5 pp 302-306 & 6 pp 365-368.

87) CRANK, J.
"The Mathematics of Diffusion" Second Edition, Pub: Clarendon Press Oxford, 1975. pp 32.

88) Ibid pp 254

89) TAYLOR, H.F.W.
"Hydrated calcium silicates. I. Compound formation of ordinary temperatures".
J. Chem. Soc. London, (1950) pp 3682-3690.

90) KALOUSEK, G.L.
"Application of differential thermal analysis in a study of the system lime-silica-water"
Proc. of the Third Int. Symp. on the Chemistry of Cement, London, 1952, (1954) pp 296-311.

91) BRUNAUER, S & GREENBERG, S.A.
"The hydration of tricalcium silicate and /3-dicalcium silicate at room temperature".
Proc. of the fourth Int. Symp. on the Chem. of Cem. Washinghton, Vol II (1960) pp 135-165.

92) TAYLOR, H.F.W.
"The Calcium Silicate Hydrates" - The Chemisty of Cements Vol. I chapter 5, Taylor, H.F.W. Editor, Academic Press 1964. pp 167-232.

93) ROY, D.M. & IDORN, G.M.
"Hydration, structure and properties of blast furnace slag cements, mortars and concrete".
Journal of the American Concrete Institute, Proc., 79, 43, (1982) pp 444-457.

94) BUTLER, F.G. MORGAN, S.R. & WALKER, E.J.
"Studies on the rate and extent of reaction between calcium hydroxide and pulverised fuel ash".
5th Int. Conf. on Alkali-Aggregate Reactions in concrete, Proc., (Cape Town 1981). National Building Research Institute, CSIR, Pretoria, 1981, 5252/38 pp 1-6.

95) LAMBERT, P., PAGE, C.L. & SHORT, N.R.
"Diffusion of chloride ions in hardened cement pastes containing pure cement minerals"
British Ceramic Society, Proc., The Chemistry of Chemically Related Properties of Cement, F.P. Glasser, ed., 35, (Sept. 1984) pp 267-276.

96) DAIMON, M., AKIBA, T. and KONDO, R.
"Through pore size distribution and kinetics of the carbonation reaction of portland cement mortars".
Journal of the American Ceramic Society, 54, 9, (1981), pp 423-428.

97) KLEMM, W.A., AND BERGER, R.L.
"Accelerated curing of cementitious systems by carbon dioxide".
Cement and Concrete Research, 2, 5, (1972) pp 567-576.

98) POWERS, T.C.
"A hypothesis on carbonation shrinkage"
Journal of the Portland Cement Association, (Research & Development Labs), 4, 2, (1962) pp 40-50.

99) SAUMAN, Z.
"Carbonization of porous concrete and its main binding components"
Cement and Concrete Research, 1, 6, (1971) pp 645-662.

100) SAUMAN, Z.
"Effect of CO_2 on porous Concrete"
Cement and Concrete Research, 2, 5, (1972). pp 541-549.

101) PAGE. C.L.
"Barriers to the prediction of service life of metallic materials".
Masters, L.W., Ed., Problems in Service Life Prediction of Building and Construction Materials, NATO advanced Science Institute series: Applied Sciences, Martinus Nijhoff, E.95, (1985) pp 59-74.

102) SCHUBERT, P. and EFES, Y.
"The carbonation behaviour of mortar and concrete with jet cement".
Carbonation of Concrete - RILEM International Symposium, Cement and Concrete Association, Theme 3, paper 5, (April 1976).

103) ALEKSEEV, S.N. and ROZENTAL, N.K.
"The rate of concrete carbonation"
Carbonation of Concrete - RILEM International Symposium, Cement and Concrete Association, Theme 3, paper 6 (April 1976)

104) SMOLCZYK, H.G.
"Written discussion - Carbonation of concrete"
5th International Symposium on the Chemistry of Cement Proc., Part III Vol III, (Tokyo 1968) - pp 369-382

105) SMOLCZYK, H.G.
"Oral discussion - Carbonation of concrete"
5th International Symposium on the Chemistry of Cement Proc., Part III Vol III, (Tokyo 1968). pp 382-383.

106) SMOLCZYK. H.G.
Physical and chemical phenomena of carbonation"

Carbonation of Concrete - RILEM International Symposium, Cement & Concrete Association, Theme 1 paper 1. (April 1976).

107) SMOLCZYK. H.G.
"Explorations to the German longtime - study on the rate of carbonation"
Carbonation of Concrete - RILEM International Symposium, Cement and Concrete Association, Theme 3 paper 2 (April 1976)

108) VERBECK, G.J. and HELMUTH, R.H.
"Principal paper - structures and physical properties of cement paste".
5th International Symposium of the Chemistry of Cement Vol III, Part III, proc., (Tokyo 1968) pp 1-13.

109) MILLS, R.H.
"Molecular sieve effect in concrete"
5th International Symposium of the Chemistry of Cement, Proc., Vol III, Supplementary Paper III-46 (Tokyo 1968) pp 74-85.

110) HAMADA, M.
"Principal paper - Neutralization (Carbonation) of concrete and corrosion of reinforcing steel".
5th International Symposium of the Chemistry of Cement Proc., Vol III, Properties of Cement & Concrete (Tokyo 1968) pp 343-369.

111) SKALNY, J.P. and BAJZA, A.
"Properties of cement pastes prepared by high pressure compaction"
Journal of the American Concrete Institure, Proc., 67 11, (1970) pp 221-227.

112) MANNS, W. and WESCHE, K.
"Variation in strength of mortars made of different cements due to carbonation".
5th International Symposium of the Chemistry of Cement, Proc., VOL III, Supplementary Paper III-16 (Tokyo 1968) pp 385-393.

113) ROZENTAL, N.K. and ALEKSEEV, S.N.
"Change in concrete porosity during carbonation"
Carbonation of Concrete - RILEM International Symposium; Cement & Concrete Association, Theme 2 paper 4 (April 1976)

114) PIHLAJAVAARA, S.E.
"Carbonation engineering properties and effects of carbonation on concrete structures - General Report"
Carbonation of Concrete - RILEM International Symposium, Cement and Concrete Association, Theme 4 paper 1 (April 1976).

115) KONDO, R., DAIMON, M. and AKIBA, T.
"Mechanisms and kinetics on carbonation of hardened cement".
5th International Symposium of the Chemistry of Cement Proc., VOL III, Supplementary paper III-116, (Tokyo 1968). pp 402-409.

116) PIHLAJAVAARA, S.E.
"Some results of the effect of carbonation on the porosity and pore size distribution of cement paste".
Matériaux et Construction, 1, 6, (1968) pp 521-526.

117) PIHLAJAVAARA, S.E. and PIHLMAN, E.
"Effects of carbonation on microstructural properties of cement stone".
Cement and Concrete Research, 4, 2, (1974) pp 149-154.

118) BERGER, R.L.
"Stabilization of silicate structures by carbonation"
Cement and Concrete Research, 9, 5, (1979) pp 649-651.

119) SAUMAN, Z. and LACH, V.
"Long term carbonization of the phases $3CaO.Al_2O_3.6H_2O$ and $3CaO.Al_2O_3.4H_2O$".
Cement and Concrete Research, 2, 4, (1972) pp 435-446.

120) SAUMAN, Z. and LACH, V.
"To the long term carbonation of binding components in cellular concretes".
Carbonation of Concrete - RILEM International Symposium, Cement and Concrete Association, Theme 6 paper 3, (April 1976).

121) COLE, W.F. and KROONE, B.
"Carbon dioxide in hydrated portland cement"
Journal of the American Concrete Institute, Proc., 56, 64, (1960) pp 1275-1295.

122) KRZYWOBLOCKA-LAUROW, R.
"Effect of increased curing temperature upon carbonation of concrete".
Carbonation of Concrete - RILEM International Symposium, Cement and Concrete Association, Theme 1, paper 6 (April 1976).

123) MATOUSEK, M.
"Carbonation of cellular concrete under the conditions in exposed structures".
Carbonation of Concrete - RILEM International Symposium, Cement and Concrete Association, Theme 6, paper 4, (April 1976).

124) RILEM DRAFT RECOMMENDATION CPC-18
"Measurement of hardened concrete carbonation depth"
Matériaux et Construction, 17, 102, (1984). pp 435-440.

125) VOGEL, A.I.
"Textbook of quantitative inorganic analysis"
4th Edition. Pub. Longmans (1978) pp 310-311.

126) RAMACHANDRAN, V.S.
"Applications of differential thermal analysis in cement chemistry".
Pub: Chemical Publishing Company, 1969.

127) LACH, L. and SAUMAN, Z.
"The determinaion of $CaCO_3$ modifications in the carbonated concrete".
Carbonation of Concrete - RILEM International Symposium, Cement and Concrete Association, Theme 1 paper 5 (April 1976).

128) PAGE, C.L., and VENNESLAND, Ø.
"Pore solution composition and chloride binding capacity of silica fume-cement pastes".
Matériaux et Constructions, 16, 91, (1983) pp 19-25.

129) MAYCOCK, J.N. & SKALNY, J.
"Carbonation of hydrated calcium silicates"
Cement and Concrete Research, 4, 1, (1974) pp 69-76.

130) SCHUBERT, B. & VON-BERG, W.
"The carbonation behaviour of mortars and concretes containing fly ash"
Carbonation of Concrete - RILEM Int. Symp.,
Cement & Concrete Assoc., Theme 3 paper 5 (April 1976).

131) FARMER, V.C.
"Infra-red spectroscopy of silicates and related compounds" The Chemistry of Cements, Taylor, H.F.W. Editor, Vol.2., Pub: Academic Press (1964) pp 289-309

132) RAMACHANDRAN, V.S.
"Applications of Differential thermal analysis in cement chemistry"
Pub: Chemical Publishing Company, (1969) pp 200.

133) MATTHEWS, J.D.
"Carbonation of ten-year-old concretes with and without added Pulverised-fuel-ash".
2nd Int. Conf. on Ash Technology and Marketing, Proc, Barbican Centre, (London 1984) Abstract Paper 398a.

134) CURRIE, R.J.
"Carbonation depths in structural-quality concrete: An assessment of evidence from investigations of structures and from other sources".
Building Research Establishment Report, (1986).

135) VENU, K., BALAKRISHNAN, K. and RAJAGOPALAN, K.S.
"A Potentiokinetic Polarization Study of the behaviour of steel in NaOH-NaCl System".
Corrosion Science, 5, (1965) pp 59-69.

136) OGUKA, K. and OHAMA, T.
"Pit formation in the cathodic polarization of passive iron III. Stimulation of pH initiation and uniform dissolution by Chelating Agents".
Corrosion, (NACE). 38, 8, (1982) pp 403-406.

137) PREECE, C.M., GRØNVOLD, F.O. and FRØLUND, T.
"The influence of cement type on the electrochemical behaviour of steel in concrete".
Proc. Corrosion of Reinforcements in Concrete Construction,Soc. of Chemical Industry London (June 1983) pp 393-417

138) HANSSON, C.M., FRØLUND, T. & MARKUSSEN, J.B.
"The effect of chloride cation type on the corrosion of steel in concrete by chloride salts"
Cement & Concrete Research, 15 (1985) pp 65-73.

139) ALVAREZ, M.G. & GALVELE, J.R.
"Mechanism of Passivity Breakdown of high purity Cadmium"
Journal Electrochemical Soc. 127, 6, (1980) pp 1235-1241.

140) GALVELE, J.R.
"Present state of Understanding of the Breakdown of Passivity and Repassivation".
Proc. Fourth Intern. Symp. on Passivity, Passivity of Metals, Editors Frankenthal, R.P. & Kruger, J. (1978). pp 285-327.

141) LECKIE, H.P. and UHLIG, H.H.
"Environmental Factors Affecting the Critical Potential of Pitting in 18-8 Stainless Steel".
J. Electrochemical Soc., 113, 12, (1966) pp1262-1267.

142) GALVELE, J.R.
"Transport Processes and the Mechanism of Pitting of Metals".
J. Electrochemical Soc., 123, 4, (1976) pp 464-474.

143) GALVELE, J.R.
"Transport Processes in Passivity Breakdown - II. Full Hydrolysis of the metal ions".
Corrosion Science, 21, 8, (1981) pp 551-579.

144) GRAVANO, S.M. & GALVELE, J.R.
"Transport Process in Passivity Breakdown III - Full Hydrolysis plus Ion Migration plus Buffers"
Corrosion Science, 24 (1984) pp 517-534.

145) PICKERING, H.W. and FRANKENTHAL, R.P.
"On the Mechanism of Localized Corrosion of Iron and Stainless Steel - I. Electrochemical Studies".
Journal Electrochemical Soc., 119, 10, (1972) pp 1297-1304.

146) DE WEXLER, S.B. & GALVELE, J.R.
"Anodic Behaviour of Aluminium Straining & a Mechanism for Pitting"
J. Electrochemical Soc., 121, 10, (1984) pp 1271-1276.

147) KEITELMAN, A.D., GRAVANO, S.M. & GALVELE, J.R.
"Localized Acidification as the Cause of Passivity Breakdown of High Purity Zinc".
Corrosion Science, 24 (1984) pp 535-545.

148) SEMINO, C.J. & GALVELE, J.R.
"Passivity Breakdown of high Purity Iron & AISI 4340 Steel in 0.5M NaCl solution".
Corrosion Science, 16 (1976) pp 297-306.

149) KEITELMAN, A.D. & GALVELE, J.R.
"Pitting & Pitting Inhibition of Iron in Sodium Sulphate Solutions".
Corrosion Science, 22, 8 (1982) pp739-751

150) DEHGHANIAN, C. & LOCKE, C.E.
"Electrochemical Behaviour of Steel in Concrete as a Result of Chloride Diffusion into Concrete: part 2". Corrosion - NACE, 38, 9, (1982) pp 494-499.

151) GILROY, D. & MAYNE, J.E.O.
"The De-aeration of Aqueous Solutions"
J. Applied Chemistry, 12 (1962) pp 382-384.

152) PAGE, C.L., SHORT, N.R. & HOLDEN, W.R.
"The Influence of Different Cements on Chloride Induced Corrosion of Reinforcing Steel".
Cement and Concrete Research, 16, 1, (1986) pp 79-86.

153) ANDRADE, C. & PAGE, C.L.
"Pore Solution Chemistry and Corrosion in Hydrated cement systems containing chloride salts: a study of cation specific effects".
British Corrosion Journal, 20, 4, (1985) pp 49-53.

154) MANSFELD, F., KENDIG, M.W. & TSAI, S.
"Recording and analysis of A.C. Impedance data for corrosion studies-II. Experimental approach and results". Corrosion-NACE. 38, 11, (1982) pp 570-580.

155) RAMACHANDRAN, V.S.
"Possible States of Chloride in the Hydration of Tricalcium Silicate in the Presence of Calcium Chloride" Materials and Structures 4, 19 (1971) pp 3-12.

156) RAMACHANDRAN, V.S.
"Calcium Chloride in Concrete"
Pub. Applied Science, London (1976) pp 57-59.

157) RAMACHANDRAN, V.S., SEELEY, R.L. & POLOMARK, G.M.
"Free and Combined Chloride in Hydrating Cement and Cement Components".
Materials and Structures, 17, 100 (1984) pp 285-289.

158) DIAMOND, S. & LOPEZ-FLORES, F.
"Fate of $CaCl_2$ dissolved in concrete mix water"
Journal American Ceramic Soc., 64 (1981) pp C162-164.

159) LAMBERT, P., PAGE, C.L. & SHORT, N.R.
"Pore Solution Chemistry of the Hydrated System Tricalcium Silicate/Sodium Chloride/Water"
Cement & Concrete Res., 15 (1985) pp 675-680.

160) SMOLCZYK, H.G.
"Chemical Reactions of Strong Chloride-Solutions with Concrete" 5th Int. Symp. Chem. Cem. Proc., VOL III, Suppl. Pap. III-31, (Tokyo 1968) pp 274-280.

161) BROWNE, R.D. & GEOGHEGAN, M.P.
"The Corrosion of marine structures: The present situation".
Symp. Corrosion of Steel Reinforcements in Concrete Construction, Proc., Society of Chemical Industy, London (1979) pp 79.

162) FORRESTER, J.A.
"Measurement of Carbonation" Carbonation of Concrete, RILEM Int. Symp., Cem. & Concr. Ass., Theme 2 paper 1 (April 1976).

163) KLIEGER, P.
"Effect of mixing and curing temperature on concrete strength"
Journal of the American Concrete Institute, Proc., 54 (1958) pp 1063-1081.

164) MATEOS, M.
"Heat Curing of Sand-Lime-Fly Ash Mixtures"
Materials Research & Standards (May 1964) pp 212-217.

165) NASSER, K.W. & MARZOUK, H.M.
"Properties of Mass Concretes Containing Fly Ash at High Temperatures" J. of the Amer. Concr. Inst. Proc., 76, 25, (1979) pp 537-550.

166) DALZIEL, J.A.
"The Effect of Curing Temperature on the Development of Strength of Mortar Containing Fly Ash"
7th Int. Conf. on the Chemistry of Cement, Proc., VOL III (Paris 1980), Communication IV-93-IV-97.

167) AL-KHALAF, M.N. & PAGE, C.L.
"Steel/Mortar Interfaces: Microstructural Features and Mode of Failure". Cem. & Concr. Res., 9, (1979) pp 197-208.

168) CHATFIELD, C.
"Statistics for technology"
Second Edition. pub: Chapman and Hall, 1978, pp 166-199.

169) HAYSLETT, H.T.
"Statistics made simple"
Revised edition, Pub: W.H. Allen & Co., 1968, pp 100-111.

170) ibid. pp 219.

171) TAYLOR, H.F.W.
"The Chemistry of cements" Vol. I ch. 7
Pub: Academic Press. 1964 pp 289.

172) SYKES J.M. & BALKWILL P.

"Simulating the pitting corrosion of steel reinforcement in concrete"
ASTM/NPL Conference on the Use of Synthetic Environments for Corrosion Testing, NPL (Teddington), Feb. 1986.